# How Well Do We Understand the Land-Ocean-Atmosphere Carbon Cycle?

**David Crisp[1], Han Dolman[2], Toste Tanhua[3], Galen A. McKinley[4], Judith Hauck[5], Ana Bastos[6], Stephen Sitch[7], Simon Eggleston[8], Valentin Aich[8]**

[1]Jet Propulsion Laboratory, California Institute of Technology, Pasadena, CA, USA.

[2] Royal NIOZ, Texel, Netherlands and Department of Earth Sciences, Vrije Universiteit Amsterdam, Amsterdam, The Netherlands.

[3]GEOMAR Helmholtz Centre for Ocean Research Kiel, Marine Biogeochemistry, Kiel, Germany.

[4]Columbia University and Lamont Doherty Earth Observatory, Palisades, NY, USA.

[5]Alfred-Wegener-Institut, Helmholtz-Zentrum für Polar und Meeresforschung, Bremerhaven, Germany.

[6]Max Planck Institute for Biogeochemistry Department Biogeochemical Integration, Jena, Germany

[7]College of Life and Environmental Sciences, University of Exeter, Exeter, EX4 4RJ, UK.

[8]Global Climate Observing System, World Meteorological Organization, Geneva, Switzerland.

Corresponding author: first and last name (David Crisp davidcri@gmail.com)

**Key Points:**

- Anthropogenic $CO_2$ emissions would have produced larger atmospheric increases if ocean and land sinks had not removed over half of this $CO_2$.
- Uptake by both ocean and land sinks increased in response to rising atmospheric $CO_2$ levels, maintaining the airborne fraction near 45%.
- Improved and sustained measurements and models are needed to track changes in sinks and enhance the scientific basis for carbon management.

## Abstract

Fossil fuel combustion, land use change and other human activities have increased the atmospheric carbon dioxide ($CO_2$) abundance by about 50% since the beginning of the industrial age. The atmospheric $CO_2$ growth rates would have been much larger if natural sinks in the land biosphere and ocean had not removed over half of this anthropogenic $CO_2$. As these $CO_2$ emissions grew, uptake by the ocean increased in response to increases in atmospheric $CO_2$ partial pressure ($pCO_2$). On land, gross primary production (GPP) also increased, but the dynamics of other key aspects of the land carbon cycle varied regionally. Over the past three decades, $CO_2$ uptake by intact tropical humid forests declined, but these changes are offset by increased uptake across mid- and high-latitudes. While there have been substantial improvements in our ability to study the carbon cycle, measurement and modeling gaps still limit our understanding of the processes driving its evolution. Continued ship-based observations combined with expanded deployments of autonomous platforms are needed to quantify ocean-atmosphere fluxes and interior ocean carbon storage on policy-relevant spatial and temporal scales. There is also an urgent need for more comprehensive measurements of stocks, fluxes and atmospheric $CO_2$ in humid tropical forests and across the Arctic and boreal regions, which are experiencing rapid change. Here, we review our understanding of the atmosphere, ocean, and land carbon cycles and their interactions, identify emerging measurement and modeling capabilities and gaps and the need for a sustainable, operational framework to ensure a scientific basis for carbon management.



## Plain Language Summary

Since the beginning of the industrial age in the mid-1700s, fossil fuel combustion, land use change and other human activities have increased the atmospheric carbon dioxide ($CO_2$) concentration to levels never seen before in human history. The atmospheric $CO_2$ growth rate would have been much larger if natural sinks in the ocean and on land carbon cycle had not removed over half of the $CO_2$ emitted by human activities. While the uptake of anthropogenic $CO_2$ by the ocean has increased with the increasing atmospheric $CO_2$ partial pressure, the land biosphere response has varied spatially and with time. Over the industrial age, $CO_2$ uptake by intact forests and other natural parts of the land biosphere has roughly balanced emissions from land use change. Since the 1990s, the tropical land sink has diminished while the high latitude land sink has increased. Here, we review our understanding of the natural carbon cycle and the processes controlling its response to human activities and climate change and identify measurement and knowledge gaps.


## 1 Introduction

Since the beginning of the industrial age, human activities have increased the atmospheric concentrations of carbon dioxide ($CO_2$) and other greenhouse gases (GHGs) to levels never before seen in human history. These large increases are driving climate change because $CO_2$ is an efficient greenhouse gas with atmospheric residence times spanning years to millennia (see Box 6.1 of Ciais et al., 2013). Bottom-up statistical inventories indicate that fossil fuel combustion, industry, agriculture, forestry, and other human activities are now adding more than 11.5 petagrams of carbon (Pg C) to the atmosphere each year (Friedlingstein et al., 2019; 2020; 2021). Direct measurements of $CO_2$ in the atmosphere and in air bubbles in ice cores (Etheridge et al., 1996) indicate that human activities have increased the globally averaged

atmospheric $CO_2$ dry air mole fraction from less than 277 parts per million (ppm) in 1750 (e.g., Joos and Spahni, 2008) to more than 412 ppm in 2020 (Dlugokencky et al., 2018; Rubino et al., 2019). Over half of this increase has been added since 1985 and over a quarter has been added since 2000.

These increases would be much larger if natural processes operating in the land and ocean had not removed over half of these anthropogenic $CO_2$ emissions. Carbon cycle measurements and modeling studies show that these anthropogenic $CO_2$ emissions are superimposed on an active natural carbon cycle that regulates $CO_2$ through photosynthesis and respiration on land and in the ocean (Beer et al., 2010), as well as temperature-driven solubility and carbonate chemistry coupled with the ocean circulation (Takahashi et al., 2002; 2009; Sabine et al., 2004; Gruber et al., 2019a). In pre-industrial times, these processes were roughly in balance, with the land biosphere and ocean emitting gross $CO_2$ fluxes of ~120 and ~90 Pg C $yr^{-1}$ into the atmosphere, respectively, then removing a comparable amount. Today, these natural fluxes have comparable amplitudes, but now, $CO_2$ "sinks" the land biosphere and ocean also remove about half of the anthropogenic $CO_2$ emissions, reducing the atmospheric $CO_2$ growth rate and mitigating climate change (Canadell et al., 2007; Raupach et al., 2008; Knorr 2009; Bennedsen et al., 2019, Friedlingstein et al., 2020).

While the fraction of the anthropogenic $CO_2$ that stays in the atmosphere (the "airborne fraction") has remained remarkably constant, at about 0.45 for the multi-year average for the past ~60 years (e.g., Ballantyne et al., 2012; Raupach et al., 2008; 2014; Bennedsen et al., 2019), it can change substantially from year to year (Francey et al., 1995; Keeling et al., 1995; Bousquet et al., 2000). In some years, the airborne fraction can be as high as 80%, while in others, it can be as low as 30% (Raupach et al., 2008; 2014). Some of the largest changes in this airborne fraction appear to be associated with changes in uptake of $CO_2$ by the land biosphere (the land sink) in response to large-scale temperature and precipitation anomalies, like those associated with major El Niño events or large volcanic aerosol injections into the stratosphere (Frölicher et al., 2011; 2013). The ocean sink also responds to El Niño events and large volcanic eruptions (Keeling et al., 2005; Eddebbar et al., 2019; McKinley et al., 2004; 2017; 2020), but has a smaller impact on the amplitude of variability in the airborne fraction. The relative roles of these and other processes reviewed here that link the land, ocean and atmospheric carbon cycles with the climate are less well understood, compromising our ability to predict how the atmospheric $CO_2$ growth rate might change as the carbon cycle responds to climate change (Ballantyne et al., 2012).

Over the past two decades, our understanding of the natural and anthropogenic contributions to the carbon cycle has grown steadily with the deployment of progressively more sophisticated ground-based, oceanic, airborne, and space-based measurement systems. These advances have been accompanied by the development of far more comprehensive diagnostic and prognostic carbon cycle modeling tools. For the ocean, measurements of vertical gradients in $pCO_2$ across the air-sea interface provide the best available estimates of ocean-atmosphere carbon fluxes on annual time-scales. Over land, flux towers provide estimates of carbon fluxes on local scales, while high-spatial-resolution space-based observations of solar induced chlorophyll fluorescence (SIF) and atmospheric $CO_2$ can be analyzed to constrain land carbon fluxes at regional scales and seasonal to interannual time scales (Heimann et al., 1998). On decadal time-scales, the storage of anthropogenic carbon in the interior ocean can be assessed by biogeochemical and tracer observations. On land, in situ carbon-13 ($\delta^{13}C$) measurements and

112 estimates of above-ground biomass derived from remote sensing observations provide similar
113 constraints on these time scales.

114 Both bottom-up stock and flux estimates and "top-down" atmospheric estimates are
115 providing key insights into the carbon cycle. Bottom-up methods use empirical or process-based
116 models to estimate fluxes, or to upscale in situ measurements of the time change of stocks or of
117 direct flux observations of the oceans (e.g., Sabine et al., 2004; Doney et al., 2004; Rödenbeck et
118 al., 2014; 2015; Gruber et al., 2019a; Landschützer, et al., 2013; Long et al., 2013; Hauck et al.,
119 2020; Carroll et al., 2020; Gregor et al., 2019; Watson et al., 2020) or land biosphere (Pan et al.,
120 2011; Sitch et al., 2015; Hubau et al., 2020; Piao et al., 2020a; Jung et al., 2020). "Top-down"
121 models use inverse methods to estimate the surface $CO_2$ fluxes from the land or ocean needed to
122 match the observed atmospheric or ocean $CO_2$ concentrations, within their uncertainties, in the
123 presence of the prevailing winds and ocean circulation (e.g., Enting et al., 1995; Mikaloff-
124 Fletcher et al., 2006; Jacobson et al., 2007; Khatiwala et al., 2009; Chevallier et al., 2010; 2019;
125 DeVries, 2014; Crowell et al., 2019; Wu et al., 2018; Nassar et al. 2021).

126 Both bottom-up and top-down methods benefit from remote sensing as well as in situ
127 data. For example, a bottom-up forest stock inventory might use in situ measurements to estimate
128 the above ground biomass from an ensemble of specific plots and then use remote sensing
129 measurements to upscale those measurements to larger areas. Similarly, a top-down approach
130 might combine in situ and remote sensing observations of atmospheric $CO_2$ along with models of
131 atmospheric transport to estimate regional-scale fluxes.

132 In practice, top-down and bottom-up methods are often combined. For example, top-
133 down inverse methods for estimating net biospheric exchange (NBE) often use prior biospheric
134 and fossil flux estimates derived from bottom-up methods (e.g., Crowell et al., 2019; Peiro et al.,
135 2021). They are also often compared to characterize processes or identify sources of uncertainty
136 (Kondo et al., 2020; Bastos et al. 2020). However, some caution is needed when comparing and
137 combing results from top-down and bottom-up methods because these approaches include
138 different processes and often use different definitions of stocks and fluxes (Ciais et al., 2022).

139 As the world embarks on efforts to monitor and control anthropogenic $CO_2$ emissions,
140 there is growing evidence that the natural carbon cycle is evolving in response to human
141 activities, severe weather, disturbances and climate change. If these changes affect the efficiency
142 of the land or ocean $CO_2$ sinks, they could impede or confuse efforts to monitor progress toward
143 emission reduction goals. An improved understanding of both the anthropogenic and natural
144 processes that control the emissions and removals of atmospheric $CO_2$ by the land biosphere and
145 ocean is critical to our ability to monitor and predict the rate of $CO_2$ increase in the atmosphere
146 and its impact on the climate.

147 Anthropogenic processes emitting $CO_2$ into the atmosphere are now routinely tracked in
148 the annual reports by the Global Carbon Project (e.g., Le Quéré et al., 2007; 2009; 2013; 2014;
149 2015a,b, 2016;2018 a,b; Friedlingstein et al., 2019; 2020; 2021) and in more focused reviews by
150 others (e.g., Andrew, 2019; 2020; Hong et al., 2021). Similarly, carbon-climate interactions on
151 long ("slow domain") and short ("fast domain") timescales, their representation in state-of-the-
152 art Earth System Models and their implications for climate change are described in J. Hansen et
153 al. (2013) and routinely reviewed in the IPCC reports. See, for example, Chapter 6 of IPCC AR5
154 (IPCC, 2014; Ciais et al., 2013) and the soon to be released IPCC AR6 reports (IPCC 2021).

Here, we begin with a brief review of the atmospheric carbon cycle, including the anthropogenic drivers. We then focus on the contemporary processes controlling the fluxes of $CO_2$ between the ocean and land carbon reservoirs and the atmosphere and their implications for the evolution of the ocean and land carbon sinks. We update earlier works (e.g., Ciais et al., 2014; Ballantyne, et al., 2015) by reviewing the mean state and emerging trends in carbon stocks and fluxes revealed by various approaches, including new observing capabilities and analysis techniques. Finally, we summarize critical measurement and modeling gaps that must be addressed to produce an effective system for monitoring the carbon cycle as it continues to respond to human activities and climate change.

## 2 A Note on Units

Because the bottom-up and top-down atmospheric, ocean and land carbon communities focus on different aspects of the carbon cycle, they have developed a diverse array of units to quantify stocks and fluxes of carbon and $CO_2$. For example, the land carbon community typically quantifies the mass of stocks and fluxes of carbon, the atmospheric remote sensing community typically measures and reports the column-averaged $CO_2$ dry air mole fraction, $XCO_2$, and the ocean community uses the partial pressure, $pCO_2$, fugacity, $fCO_2$, and the air-sea carbon flux. For the atmosphere, it is useful to note that one petagram of carbon (1 Pg C) yields 3.66 petagrams of $CO_2$ and that this is equivalent to a concentration change of ~ 2.124 ppm in the atmospheric $CO_2$ (e.g., Ballantyne et al., 2012; Friedlingstein et al., 2020). Table 1 summarizes these and other commonly used quantities and units used by the carbon cycle community and describes their relationships.

## 3 The Atmospheric Carbon Cycle

The atmosphere is the smallest, but most rapidly changing component of the global carbon cycle. It also serves as the primary medium for the exchange of carbon between the land biosphere, oceans and fossil reservoirs. The vast majority of the atmospheric carbon is in the form of $CO_2$. If we assume a total dry air mass of $5.1352 \times 10^{18}$ kg (Trenberth and Smith, 2005), a $CO_2$ dry air mole fraction of 412 ppm, a mean $CO_2$ molecular weight of 44.01 kg/kmole, and a mean atmospheric molecular weight of 28.97 kg/kmole, the total mass of $CO_2$ in the atmosphere was ~3214 Pg (~877 Pg C) in 2020. The next largest contributor to the atmospheric carbon reservoir is methane ($CH_4$), which is 220 times less abundant. For that reason, the atmospheric section of this carbon cycle review focuses on $CO_2$.

The largest net sources of atmospheric $CO_2$ are fossil fuel combustion, land use change and other human activities, which have added 700 ± 75 Pg C to the atmosphere between 1750 and 2019. Of that, 41 ± 11% has remained in the atmosphere (Friedlingstein et al., 2021). Because $CO_2$ has no significant photochemical sinks in the atmosphere, the remainder has been removed by natural sinks in the land biosphere and oceans. This section reviews our current understanding of the atmospheric carbon cycle, starting with observations, and then summarizing the insights contributed by top-down models and bottom-up inventories.

**Table 1.** Quantities and units commonly used to quantify stocks and fluxes by the atmosphere (white), ocean (blue) and land (yellow) carbon cycle communities.

| Quantity | Acronym | Typical units | Description |
|---|---|---|---|
| Carbon dioxide dry air mole fraction | $CO_2$ or $xCO_2$ | parts per million by volume (ppm) | Number of $CO_2$ molecules relative to each million ($10^6$) molecules of dry air. If $CO_2$ is assumed to be an ideal gas and its dry air mole fraction is increased by 1 ppm at constant temperature, the $CO_2$ partial pressure will increase by one micro atmosphere (μatm). |
| Column-averaged carbon dioxide dry air mole fraction | $XCO_2$ | ppm | A vertically-averaged quantity used by the atmospheric remote sensing community, derived from the ratio of the $CO_2$ column abundance and the dry air column abundance. The dry air column abundance is estimated from the measured molecular oxygen ($O_2$) column abundance (assuming an $O_2$ dry air mole fraction of 0.20955) or from surface pressure and humidity. |
| partial pressure of carbon dioxide | $pCO_2$ | μatm | At sea level, $pCO_2 = (P - pH_2O) \times xCO_2$, where P is the total atmospheric pressure and $pH_2O$ is the water vapor saturation vapor pressure (see Woolf et al., 2016). 1 μatm = $10^{-6}$ atmospheres = 0.10325 Pascals. |
| Carbon dioxide fugacity | $fCO_2$ | μatm | Effective partial pressure of $CO_2$ that has the same temperature and Gibbs free energy as the real gas. At the surface, $fCO_2 = xCO_2 \times \varphi_{CO2}$, where $\varphi_{CO2} \approx 0.0002$/K is the fugacity coefficient for $CO_2$ and K is the temperature in Kelvin. |
| Net Community Production | NCP | mol C $m^{-2}$ $yr^{-1}$ | The net carbon removed from the atmosphere by the ocean biological pump. |
| Dissolved Inorganic Carbon | DIC | μmol/kg | Total amount of inorganic carbon in water. |
| Carbon stock or stock change | | petagrams of carbon/year (Pg C $yr^{-1}$) | 1 Pg C = $10^{15}$ g C. 1 Pg C = $10^{12}$ kg C = $10^9$ tons of carbon = 1 Gt C. When oxidized to form $CO_2$, 1 Pg C = 3.664 Pg $CO_2$. |
| Gross Primary Production | GPP | Pg C $yr^{-1}$ | Total flux of carbon fixed through photosynthetic reduction of $CO_2$ by plants in an ecosystem. |
| Net Primary Production | NPP | Pg C $yr^{-1}$ | Net flux of organic carbon produced by plants in an ecosystem. NPP = GPP - $R_a$, where $R_a$ is autotrophic respiration by plants |
| Net Ecosystem Exchange or Net Ecosystem Production | NEE or NEP | Pg C $yr^{-1}$ | NPP - $R_h$, where $R_h$ is the carbon loss by heterotrophic (non-plant) respiration. NEE = -NEP but these terms are otherwise generally interchangeable, with NEE used more often to refer to fluxes measured in the atmosphere, while NEP is more often used for fluxes inferred from measurements of carbon stock changes. |
| Net Biospheric (Biome) Exchange | NBE | Pg C $yr^{-1}$ | Change in mass of carbon stocks after episodic carbon losses due to natural or anthropogenic disturbance. |
| Net Biome Productivity | NBP | Pg C $yr^{-1}$ | NEP minus disturbance emissions. |

### *3.1 Observations of Atmospheric $CO_2$*

Continuous measurements of atmospheric $CO_2$ were initiated in 1958 by Charles David Keeling of the Scripps Institution of Oceanography, when he established stations at Mauna Loa, Hawaii and the South Pole. Weekly flask samples and continuous measurements are now being returned by a global network that includes the U.S. National Oceanic and Atmospheric Administration (NOAA) Global Monitoring Laboratory (GML) Global Greenhouse Gas Reference Network (GGGRN) and other stations in their Carbon Cycle Greenhouse Gas (CCGG) Cooperative Global Air Sampling Network, the European Integrated Carbon Observation System (ICOS) network and other partners of the World Meteorological Organization Global Atmospheric Watch (WMO GAW) program (Figure 1).

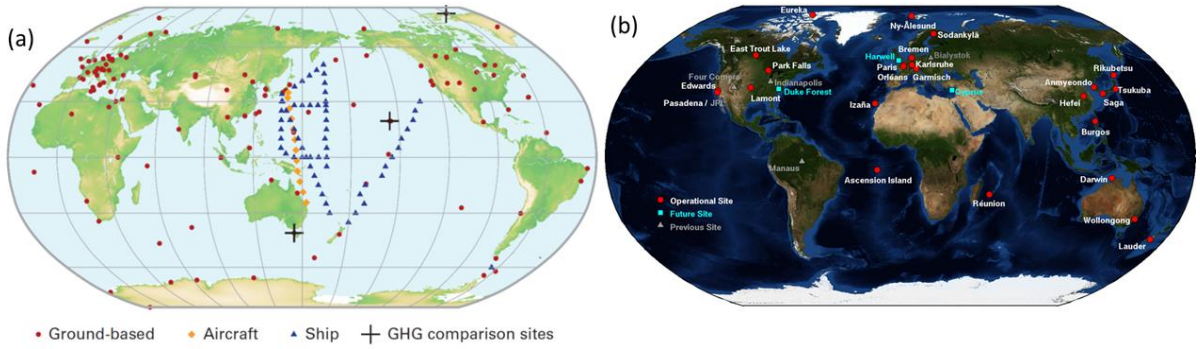


**Figure 1:** Spatial distribution of stations in the ground-based atmospheric $CO_2$ monitoring network. The vast majority of the stations are in North America and western Europe. (a) In situ $CO_2$ measurements are collected routinely at the WMO Global Atmospheric Watch Stations (from WMO Greenhouse Gas Bulletin, 25 Nov. 2019). (b) Solar-looking remote sensing observations of $CO_2$ are collected at Total Carbon Column Observing Network (TCCON) stations.

These in situ measurements provide the most accurate estimates of the $CO_2$ and $CH_4$ concentrations and their trends on global scales. The flask samples are also analyzed to quantify non-carbon greenhouse gases including nitrous oxide ($N_2O$), halocarbons, sulfur hexafluoride ($SF_6$), molecular hydrogen ($H_2$) and carbon isotopes including carbon-13 ($^{13}C$) and carbon-14 ($^{14}C$), which help to distinguish fossil fuel from biogenic contributions to the observed $CO_2$ trends.

More recently, these ground-based in situ networks have been joined by expanding networks of airborne in situ systems and ground-based remote sensing networks. NOAA routinely collects airborne profiles of $CO_2$ and other GHGs from 17 sites across North America using fixed-wing aircraft (see https://gml.noaa.gov/dv/data/). Vertical profiles of $CO_2$, $CH_4$ and other trace gases are also being returned by the balloon-borne AirCore systems (Karion et al., 2010; Baier et al., 2020), which are being deployed from an increasing number of sites. These research observations are now being augmented by GHG sensors deployed in the cargo holds of commercial aircraft as part of Japan's Comprehensive Observation Network for TRace gases by AIrLiner (CONTRAIL; Umezawa et al., 2018; Müller et al., 2021; data available at https://www.cger.nies.go.jp/contrail/protocol.html) program and Europe's In-service Aircraft for Global Observations (IAGOS; Clark et al., 2021; data available at https://www.iagos.org/iagos-data/) program. So far, GHG systems have been deployed on a small number of commercial

aircraft, but that number is expected to grow as the size and operational complexity of the sensor systems is reduced.

The atmospheric $CO_2$ content can also be monitored remotely by measuring the amount of sunlight that it absorbs as it traverses the atmosphere. The Total Carbon Column Observing Network (TCCON) exploits this approach from 27 stations in 14 countries spanning latitudes between Eureka, Canada (80.05°N) and Lauder, New Zealand (45.038°S; Figure 1b). Each station collects high-resolution spectra that are analyzed to yield estimates of the column-averaged dry air mole fractions of $CO_2$, $CH_4$, and other trace gases. These estimates are related to the WMO standard through comparisons with in situ measurements collected by over the stations by fixed-wing aircraft and AirCore instruments (Wunch et al., 2011).

One of the most important assets of the ground-based and airborne $CO_2$ measurement time series is their length, which now extends over 60 years at Mauna Loa and 40 years for the globe (Figure 2). The Mauna Loa measurements show that the atmospheric $CO_2$ dry air mole fraction has increased by about 100 ppm over this period, from less than 316 ppm in 1959 to more than 416 ppm in 2021. Over this period, the atmospheric growth rate increased from less than 1 ppm $yr^{-1}$ in the 1960s to more than 2.5 ppm $yr^{-1}$ during the 2010s, driven primarily by steadily increasing fossil fuel emissions (IPCC, 2014; Friedlingstein et al., 2021). In addition to this long-term trend, the growth rate also varies by up to 2 ppm from year to year. Because these variations occur in the context of much more uniformly increasing anthropogenic emissions, they are attributed to interannual changes in the anthropogenic $CO_2$ airborne fraction and thus the efficiency of the land and ocean $CO_2$ sinks (Keeling et al., 1989; 1995; Francey et al., 1995).

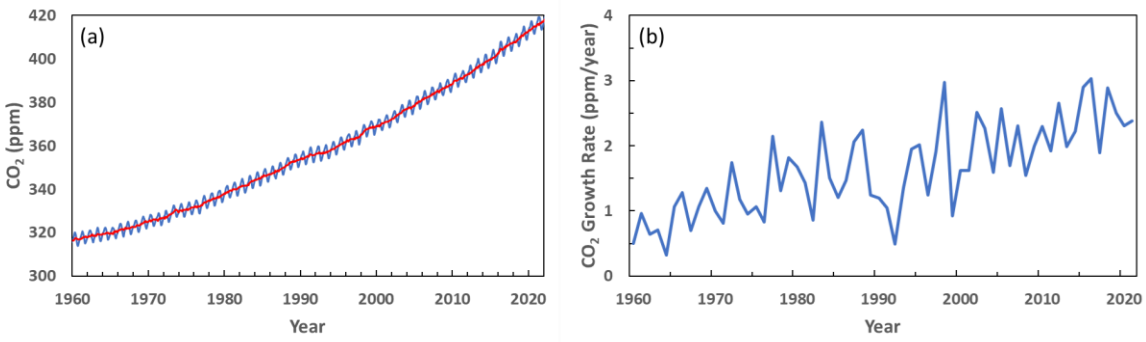


**Figure 2:** (a) Monthly mean $CO_2$ dry air mole fraction at Mauna Loa Observatory from 1960 to 2022 (blue line) and long-term trend (red line). (b) Annual growth rate in atmospheric $CO_2$ at Mauna Loa Observatory (data from NOAA GML, https://gml.noaa.gov/ccgg/trends/data.html).

During the first 30 years of this atmospheric $CO_2$ record, while there were still fewer than 10 stations regularly reporting data, innovative methods were already beginning to yield additional insights into the behavior of the land and ocean sinks. For example, Keeling et al. (1973; 1989; 1995) combined measurements of the atmospheric $CO_2$ growth rates from Mauna Loa and South Pole with $^{13}C/^{12}C$ ratios ($\delta^{13}C$) to assess the relative contributions to this variability from the land biosphere and ocean sinks. They found that the $CO_2$ growth rate anomalies were well correlated with atmospheric temperature increases during the warm phase of El Niño and decreases following the Pinatubo eruption. Their isotopic analysis suggested that

El Niño typically enhanced the efficiency of the ocean sink and decreased the uptake by the land sink. These early conclusions have been reinforced by more recent measurements and modeling studies (e.g., Bousquet et al., 2000; Canadell et al., 2007; Raupach et al., 2008; Bennedsen et al., 2019).

In addition to the global-scale perspectives, the ground-based record has provided new insights into regional-scale phenomena. For example, they not only provided the first evidence for the now well-known atmospheric $CO_2$ seasonal cycle (Keeling, 1960), they also provided the first evidence for long-term changes in the $CO_2$ seasonal cycle amplitude (SCA) across the northern hemisphere (Bacastow et al., 1985; Keeling et al., 1996). These results have also been reinforced by more recent experiments that exploit an expanded ground-based network and longer $CO_2$ data record (Graven et al., 2013; Byrne et al., 2018; 2020a; Liu et al., 2020a).

Recent advances in space-based remote sensing technologies are now providing new opportunities to dramatically improve the spatial and temporal coverage and resolution of atmospheric $CO_2$ observations. These space-based sensors collect high-resolution spectra of reflected sunlight within molecular oxygen ($O_2$) and $CO_2$ bands that can be analyzed to yield precise, spatially resolved estimates of $XCO_2$. The first space-based sensor to use this approach was the German-Dutch-Belgian SCanning Imaging Absorption spectroMeter for Atmospheric CartograpHY (SCIAMACHY) onboard the European Space Agency (ESA) Environmental Satellite (ENVISAT), which operated from 2002 to 2012. ENVISAT/SCIAMACHY was followed by Japan's Greenhouse gases Observing SATellite, GOSAT in 2009 (Kuze et al., 2009; 2016; Yoshida et al., 2011; ), and then by NASA's Orbiting Carbon Observatory-2 (OCO-2) in 2014 (Crisp et al., 2004; 2008, Eldering et al., 2017). OCO-2 returns about three million $XCO_2$ estimates over the sunlit hemisphere each month (Figure 3) with single sounding random errors of ~0.5 ppm and accuracies of ~1 ppm (Wunch et al., 2017; O'Dell et al., 2018; Müller et al., 2021). GOSAT and OCO-2 have recently been joined by their sister missions, GOSAT-2 (2018) and OCO-3 (2019), providing additional coverage and resolution.

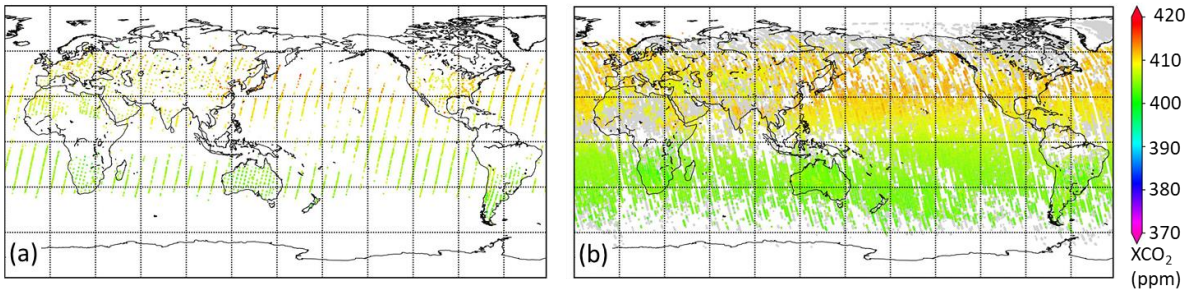


**Figure 3.** Monthly maps of $XCO_2$ estimates derived from (a) GOSAT and (b) OCO-2 measurements for April 2018. OCO-2 collects ~100 times as many samples each day as GOSAT, providing much greater data density. For both satellite products, the coverage at high latitudes varies with the availability of sunlight. Persistent optically-thick clouds and airborne dust (Sahara) limit the coverage (Images from the World Data Center for Greenhouse Gases, https://gaw.kishou.go.jp/satellite/file/0149-9011-1001-08-08-9999 ).

These data are now providing a record of the atmospheric $CO_2$ distribution with unprecedented detail, revealing trends in atmospheric $CO_2$ concentrations that are providing new insights into atmospheric sources and sinks. For example, each month, $XCO_2$ estimates derived

from OCO-2 observations using the Atmospheric $CO_2$ Observations from Space (ACOS) algorithm (O'Dell et al., 2018) provide a global maps of $CO_2$, reflecting the net effects of emissions, removals, and atmospheric transport. These maps provide snapshots of most robust features of the atmospheric carbon cycle. For example, during the early northern hemisphere (NH) spring, they reveal the relatively large (> 10 ppm) north-south gradient in $XCO_2$, driven by the $CO_2$ buildup across the NH during the winter, when photosynthetic uptake by the land biosphere is suppressed. The maps also indicate enhanced values over east Asia that might be associated with intense fossil fuel combustion.

While $CO_2$ time series and $XCO_2$ maps provide some direct insight into the sources and sinks of atmospheric $CO_2$, methods that account for atmospheric transport are needed to quantify $CO_2$ fluxes on sub-regional to continental scales. Atmospheric inverse systems address this need. Inverse systems designed to constrain fluxes on these scales typically incorporate a global chemical transport model that assimilates estimates of the atmospheric $CO_2$ dry air mole fraction with an optimization algorithm that derives estimates of the net surface $CO_2$ fluxes needed to match the observed $CO_2$ distribution to within its uncertainties in the presence of the imposed wind field (Enting et al., 1995; Bousquet et al., 2000; Enting 2002, Peters et al., 2005; Baker et al., 2006a). Studies of anthropogenic emissions from point sources or large urban areas typically employ simpler emission plume mass balance models (Nassar et al., 2017; 2021; Varon et al., 2018; Reuter et al., 2019) although some use more sophisticated inverse models with Eulerian (Ye et al., 2020; Lei et al., 2021) or Lagangian transport schemes (Wu et al., 2018). Both types of systems are summarized here.

## *3.2 Constraining $CO_2$ fluxes with Regional-scale Atmospheric Inverse Models*

Most inverse modeling systems use a form of Bayesian inference that adjusts surface fluxes to minimize a cost function, a mathematical expression that describes the mismatch between the observations and the simulated observations based on prior estimates of surface fluxes, accounting for their respective uncertainties (e.g., Enting, 2002). Commonly-used inverse methods include variational data assimilation (3-D and 4-D VAR), ensemble Kalman filter, and the Markov Chain Monte Carlo methods. These systems are typically initialized with "prior" $CO_2$ concentration and flux distributions derived from bottom-up inventories, climatologies and biogeochemical models. Most inverse modeling systems use precomputed (off-line) atmospheric winds fields from a meteorological reanalysis in a global, 3-dimensional chemical tracer transport models, such as the Goddard Earth Observing System (GEOS) Chemistry (GEOS-Chem) or Tracer Model 5 (TM5) (e.g., Crowell et al., 2019; Peiro et al., 2022).

### *3.2.1 Constraining Regional-scale $CO_2$ Sources and Sinks with Atmospheric Inverse Systems*

Historically, top-down estimates of $CO_2$ fluxes from atmospheric inverse systems have relied on *in situ* measurements collected by the surface network (Figure 1). To exploit this sparse network, $CO_2$ fluxes were derived for a small number of pre-defined continental and oceanic regions and anthropogenic emissions were prescribed from bottom-up inventories to diagnose the behavior of the ocean and land carbon cycles. For example, in early forward model studies, Tans et al. (1990) found that the observed pole-to-pole gradient in atmospheric $CO_2$ indicated the presence of a large land sink in the northern extratropics, a result that was confirmed by other studies (e.g., Ciais et al., 1995). Others used inverse models to study the variability of the airborne fraction and concluded that terrestrial carbon fluxes were roughly twice as variable as ocean fluxes during the 1980s and 1990s, and that tropical land ecosystems contributed the most

329 to this variability (Bousquet et al., 2000; Rödenbeck et al., 2003; Peylin et al., 2005). However,
330 there was significant disagreement in the relative contributions by the different ocean basins or
331 the land sinks in North America and Asia (e.g., Fan et al., 1998; King et al., 2015). These
332 differences were ascribed primarily to limitations in the observing network, the transport models
333 adopted and other differences in the inversion methods.

334 To make progress the latter two areas, large multi-model intercomparison projects, such
335 as the Atmospheric Carbon Cycle Inversion Intercomparison (TransCom 3; Gurney et al., 2002;
336 2003) and REgional Carbon Cycle Assessment and Processes (RECCAP) projects (Canadell et
337 al., 2011; Peylin et al., 2013) were launched. Early results from these projects confirmed that
338 model transport uncertainties were as large a source of error as the sampling uncertainties
339 introduced by the sparse $CO_2$ measurement network (Gurney et al., 2002; 2003) and that
340 transport errors had their largest impacts on northern latitudes (Baker et al., 2006b). More recent
341 multi-model intercomparison experiments constrained by in situ observations, alone, show
342 significant reductions in the spread of the model estimates when compared to independent
343 observations (Gaubert et al., 2019; Ciais et al., 2020a). However, these inverse model
344 experiments still do not have the spatial resolution needed to separately quantify natural and
345 anthropogenic emissions on regional scales or to constrain the relative contributions of the global
346 ocean and land sinks to better than ~1 Pg C $yr^{-1}$ (Jacobson et al., 2007; Chevallier et al., 2010;
347 Sarmiento et al., 2010; Tohjima et al., 2019; Kondo et al., 2020; Friedlingstein et al., 2021).

348 With their improved spatial resolution and temporal coverage, atmospheric $XCO_2$
349 estimates derived from space-based observations are now providing new opportunities to study
350 $CO_2$ emissions and uptake at policy-relevant spatial and temporal scales (e.g., Zhang et al., 2021;
351 Chevallier, 2021). $CO_2$ estimates retrieved from GOSAT and OCO-2 measurements clearly show
352 persistent positive anomalies associated with anthropogenic emissions over East Asia, Western
353 Europe and eastern North America (Hakkarainen et al., 2016; 2019; Wang et al., 2018). They
354 also show persistent positive anomalies over northern tropical Africa and northern tropical South
355 America.

356 When these space-based $XCO_2$ estimates are analyzed with flux inversion models (e.g.,
357 Maksyutov et al., 2013; Chevallier et al., 2019; Crowell, et al., 2019; Peiro et al., 2022), they
358 produce annual-averaged fluxes at sub-regional scales that reinforce and sometimes conflict with
359 those derived from bottom-up methods or inverse modeling methods constrained by in situ $CO_2$
360 measurements, alone. For example, there is generally good agreement between the NBE
361 estimates for northern hemisphere extratropical land derived using inverse methods constrained
362 in situ and OCO-2 v9 $XCO_2$ estimates (Peiro et al., 2022; Zhang et al., 2021). However, both in
363 situ and space-based inverse modeling results indicate a substantially larger summertime
364 seasonal drawdown than the prior, which was constrained by bottom-up results from dynamic
365 global vegetation models (DGVMs). Over tropical land, NBE estimates from ensembles of
366 inverse models constrained by space-based measurements are both more positive and have a
367 smaller spread across the ensemble than those constrained only by in situ measurements from the
368 sparse tropical network or ensembles of DGVMs (Palmer et al., 2019; Crowell, et al., 2019;
369 Peiro et al., 2022). These differences are explored in greater detail in Section 5.

370 Over the ocean, results from atmospheric inversions constrained by in situ and space-
371 based observations are less conclusive. For example, Chevallier et al. (2019) find that inversions
372 constrained by ACOS/GOSAT $XCO_2$ estimates reduce the ocean sink by ~0.5 Pg C $yr^{-1}$ in 2015,
373 relative to a prior constrained by ocean $pCO_2$ estimates (Landschützer et al., 2017), a result that

is consistent with the onset of the strong 2015-2016 El Niño. However, when ACOS/OCO-2 version 9 (v9) $XCO_2$ ocean glint estimates are used to constrain inverse models, a known ~1 ppm negative bias in this product, produces an unrealistically large (3.75 Pg C $yr^{-1}$) ocean sink during that period (Peiro et al., 2022), while methods constrained by ocean $pCO_2$ indicate an ocean sink between 2 and 3 Pg C $yr^{-1}$ during the 2010s' (Friedlingstein et al., 2019; 2020; 2021). Because of this, the OCO-2 v9 ocean glint observations have been excluded from most inverse model studies. This ocean glint bias was reduced by over 90% in the v10 ACOS/OCO-2 $XCO_2$ product (Müller et al., 2021), but there is still little evidence that space-based $XCO_2$ estimates can provide useful constraints on the ocean sink.

Atmospheric inverse models are also being used to constrain anthropogenic $CO_2$ emissions and removals (Chevallier, 2021; Deng et al., 2021; Hwang et al., 2021; Petrescu et al., 2021). On regional scales, estimates of $CO_2$ emissions and removals derived from atmospheric measurements of $XCO_2$ are not as source specific as the traditional bottom-up statistical methods used to compile national inventories, which infer $CO_2$ emissions from fuel use (e.g., Andrew 2020), land use change (e.g., Houghton and Nassikas, 2017) and other human activities. However, they complement those methods by providing an integral constraint on the total amount of $CO_2$ added to or removed from the atmosphere by all natural and anthropogenic processes. They can also be used to identify and track rapidly-evolving emission hotspots that are often missed in the bottom-up statistical inventories. As these tools are integrated into a more comprehensive carbon management system, they could also help carbon managers to assess the effectiveness of their carbon management strategies, and help to identify emerging emission reduction opportunities.

The current ground-based, airborne and space-based $CO_2$ measurement and modeling capabilities do not yet provide the resolution and coverage needed to estimate net emissions for all countries. In addition, ongoing concerns about the accuracy of the space-based estimates also compromise the reliability of these top-down products as an independent Monitoring and Verification System (MVS) for evaluating national inventory reports (Janssens-Maenhout et al., 2020). The current atmospheric $CO_2$ measurements and inverse modeling systems are not adequate to clearly distinguish the contributions of fossil fuel sources from land and ocean sources and sinks of $CO_2$ on regional scales (Ciais et al., 2020b; Chevallier, 2021).

However, atmospheric inverse systems are improving rapidly. Existing systems clearly illustrate many of the strengths and weaknesses of top-down methods for inventory development and assessment. To demonstrate these capabilities, pilot, national-scale flux inversion efforts focus on the largest countries. Most of these studies prescribe fossil fuel $CO_2$ emissions from a bottom-up emissions inventory and hold these as fixed, and then optimize the terrestrial and ocean carbon fluxes to match the spatial and temporal fluctuations in the observations within their uncertainties (e.g., Chevallier, 2021; Deng et al., 2021). Ongoing efforts to expand the ground-based and space-based atmospheric measurement and inverse modeling capabilities are expected to mitigate this limitation to some extent through the use of proxies, such as nitrogen dioxide ($NO_2$), carbon monoxide (CO), and $^{14}C$ to distinguish fossil fuel emissions from biomass burning (e.g., Heymann et al., 2017; Reuter et al., 2019; Hakkarainen et al., 2021). Others are combining $CO_2$ observations with observations of carbonyl sulfide, OCS (Remaud et al., 2022) or SIF (Liu et al., 2017; Palmer et al. 2019; Yin et al., 2020) to discriminate the relative roles relative roles of photosynthesis and respiration.

### *3.2.2 Constraining Atmospheric $CO_2$ emissions from Local Sources*

On smaller scales, space-based $XCO_2$ estimates are being combined with ground-based and airborne measurements to quantify $CO_2$ emissions from large urban areas (Hedelius et al., 2018; Wu et al., 2018; Wu et al., 2020) and individual power plants (e.g., Nassar et al., 2017; 2021; Reuter et al., 2019; Hakkarainen et al., 2021). Space-based sensors do not yet have the coverage needed to track all local sources, but they do provide opportunities to assess the precision that could be delivered by future space-based instruments. For example, Nassar et al. (2017; 2021) used OCO-2 $XCO_2$ estimates to quantify emissions from individual coal-fired power plants (Figure 4). They combine these estimates with wind speed and direction from ERA-5 (Hersbach et al., 2020) and MERRA-2 (Molod et al., 2015) in a simple Gaussian plume model to estimate the fluxes. They find emission rates of about 98 kilotons per day (kT $day^{-1}$), which compare well with the reported value on that day of 103 kT $day^{-1}$. OCO-2 $XCO_2$ observations are also being combined with $NO_2$ observations from the Copernicus Sentinel 5 Precursor TROPOMI instrument to track and quantify $CO_2$ emission plumes tens of km downwind of large powerplants (Reuter et al., 2019; Hakkarainen et al., 2021).

Other studies have focused on top-down estimates of emissions from large urban areas, which are responsible for ~70% of all anthropogenic $CO_2$ emissions. For example, Hedelius et al. (2018) estimate the net $CO_2$, $CH_4$, and CO flux from the Los Angeles South Coast Air Basin (So-CAB) using an inversion system that couples TCCON and OCO-2 observations with the Hybrid Single Particle Lagrangian Integrated Trajectory (HYSPLIT) model and the Open-source Data Inventory for Anthropogenic $CO_2$ (ODIAC). TCCON $XCO_2$ measurements indicate that the net $CO_2$ flux from the So-CAB is $104 \pm 26$ megaton of $CO_2$ per year ($MtCO_2$ $yr^{-1}$) for the study period of July 2013–August 2016. A slightly higher estimate of $120 \pm 30$ $MtCO_2$ $yr^{-1}$ is obtained using OCO-2 data. These $CO_2$ emission estimates are slightly lower than those from previous work. In another study, Wu et al. (2020) analyzed OCO-2 $XCO_2$ data with an advanced version of the Stochastic Time-Inverted Lagrangian Transport model, XSTILT, to quantify per capita $CO_2$ emissions from 20 major urban areas. In general, they find that cities with greater population density have lower per capita emissions, which is consistent with earlier bottom-up estimates. However, they find that cities with heavy power industries or greater affluence stand out with higher per capita emissions. These studies suggest that space-based measurements could eventually play a significant role in emissions monitoring efforts.

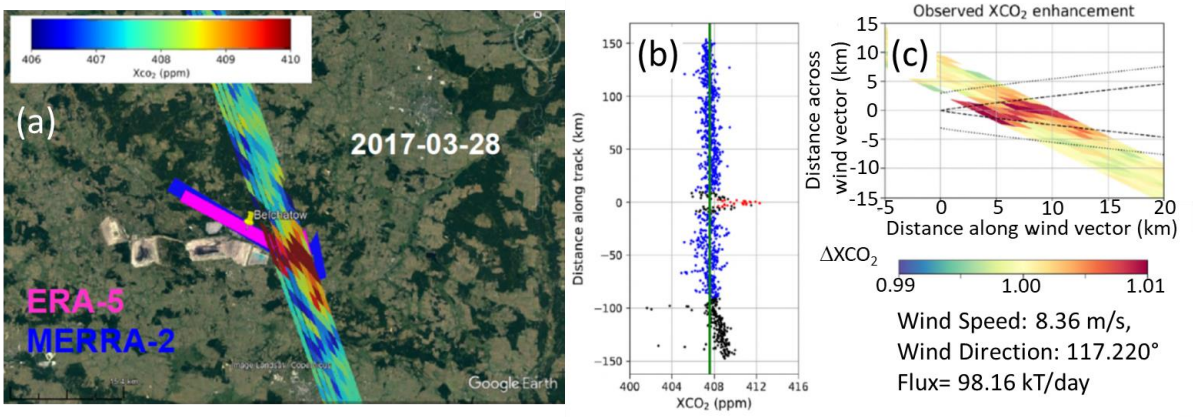


**Figure 4.** (a) OCO-2 flight track over the Bełchatów power station (Poland) on 28 March 2017, showing enhanced $XCO_2$ (red) downwind of the station. (b) $XCO_2$ values along ground track, showing a ~4 ppm enhancement downwind. (c) Gaussian plume model used to estimate the fluxes (adapted from Nassar et al., 2021).

The principal challenge of the space-based measurements is the need for unprecedented levels of precision and accuracy. While intense local sources, such as large coal-fired power plants or large urban areas can increase the near-surface $CO_2$ concentrations by more than 10%, these variations decay rapidly with altitude, such that they rarely yield $XCO_2$ variations larger than 1-2 ppm (0.25 to 0.5%) on the spatial scale of a satellite footprint (1 to 100 $km^2$). Natural sinks of $CO_2$, such as forests or ocean basins, are characterized by weak, spatially extensive, local fluxes and thus produce even smaller changes in $XCO_2$, which place much greater demands on measurement precision and accuracy.

To ensure that these space-based $XCO_2$ estimates meet these demanding requirements, they are routinely validated through comparisons with co-incident, ground-based remote sensing estimates of $XCO_2$ derived from TCCON observations, which provide a transfer standard to the WMO in situ standard (Wunch et al., 2011; 2017). Using this approach, the current state of the art for space-based $XCO_2$ estimates is single-sounding random errors and biases between 0.5 and 1 ppm (Hedelius et al., 2017; O'Dell et al., 2018; Kiel et al., 2019; Müller et al., 2021). This is adequate to track regional scale changes in surface sources and sinks as small as those produced by the COVID-19 lockdowns (Weir et al., 2021), but not yet adequate to constrain relative roles of the ocean and land biospheric sinks to much better than 1 Pg C $yr^{-1}$.

These new measurement capabilities are also driving the development of atmospheric inverse systems, spawning a new series of multi-model intercomparison experiments that use only ground-based and airborne in situ observations, space-based measurements, or both (Houweling et al., 2015; Chevallier et al., 2019; Crowell et al., 2019; Kondo et al., 2020; Ciais et al., 2020a; 2022; Peiro et al., 2022). These experiments are providing new insights into the relative roles of $CO_2$ measurement accuracy, atmospheric transport (Schuh et al., 2019; Gaubert et al., 2019; Torres et al., 2019) and other aspects of the model setup (Peiro et al., 2022). These efforts are expected to improve both the spatial resolution and accuracy of these methods and to help reconcile their results with bottom-up methods (Kondo et al., 2020; Ciais et al., 2022).

### *3.3 Bottom-up Estimates of Anthropogenic Contributions to the Atmospheric Carbon Cycle*

$CO_2$ emissions from fossil fuel combustion in the energy sector constitute the largest direct anthropogenic contribution to the global carbon cycle (Andrew, 2020; Friedlingstein et al., 2021). Emissions of $CO_2$ and other GHGs from land use and land use change (LUC) on managed lands are the second largest contribution, accounting for almost one quarter of all anthropogenic GHG emissions (Houghton, 2003; Smith et al., 2014; Houghton and Nassikas, 2017). These emissions originate primarily from deforestation and forest degradation, but also include contributions from agricultural land, livestock, forest management, and secondary forest regrowth. This section summarizes the approaches used to track the emissions and removals of $CO_2$ by these and other human activities and quantifies their current values and uncertainties.

#### *3.3.1 Anthropogenic $CO_2$ emissions inventories for regulation and commerce*

Atmospheric GHG emissions from fossil fuel use (Andrew, 2020) and cement production (Andrew, 2019) are currently being tracked by the regulatory, commercial and scientific communities. National regulatory organizations such as the U.S. Environmental Protection Agency (EPA), Japan's Ministry of the Environment (MOE) and the European Union's European Environment Agency (EEA) compile statistics for regulating and reporting national emissions to other government agencies or organizations such as the United Nations Framework Convention on Climate Change (UNFCCC). These inventories are compiled using best practices recommended in the Intergovernmental Panel on Climate Change (IPCC 2006; 2019) Guidelines for National Greenhouse Gas Inventories, which require reports of annual emissions by sources and removals by sinks in specific sectors and categories. For example, fossil fuel combustion is tracked in in the energy sector while those from managed lands are tracked in the agriculture, forestry and other land use (AFOLU) sector. Net emissions and removals in each category of each sector are approximated either by multiplying the measured *activity data* (i.e., number of liters of oil burned) by an assumed *emission factor* (number of kilograms $CO_2$ emitted per liter of oil) or by sampling carbon stock changes directly, and summing the results to yield totals.

Additional information about GHG emissions associated with the extraction, transport and use of fossil fuels is compiled by several organizations. For example, the International Energy Agency (IEA) originally compiled fossil fuel statistics to avoid disruptions in the world's oil supplies, but now provides annual reports on a range of technologies to support sustainable energy development (IEA 2020). Commercial organizations, such as British Petroleum, produce inventories to track trends in energy markets (BP 2020). Those from national organizations, such as the U.S. Energy Information Administration (EIA), serve a similar purpose, tracking short-term and long-term trends in supply and demand globally to support the energy industry.

Similarly, to track emissions from LUC, international organizations such as the United Nations Food and Agriculture Organization (FAO) collect and disseminate global information on AFOLU. Several methods are used to track fluxes from LUC. For example, statistical data on land cover area collected by FAO are used in so-called bookkeeping models that prescribe carbon changes in biomass and soil pools over time and their resulting fluxes to the atmosphere (Hansis et al., 2015, Houghton and Nassikas, 2017). For tracking historical LUC, a map of historical land use is required such as LUH2-GCB2020 (Hurtt et al., 2020; see also Friedlingstein et al., 2020; Chini et al., 2021). Using this information, it is also possible to estimate fluxes from land-use change using the new generation of dynamic global vegetation models (DGVMs). Another approach uses satellite remote sensing data to determine the amount of land cover change (LCC) and to associate emission losses with LCC by applying emission factors or

detailed biogeochemical models, e.g., emissions from fires associated with deforestation and forest degradation (van der Werf et al., 2017). Finally, at the national level, LCC emissions are compiled and delivered to the UNFCCC by country level organizations such as the U.S. EPA, Japan's MOE and the European Union's EEA. These LCC estimates often differ from those derived by the carbon cycle community because they include different processes and quantities (Grassi et al., 2018; Ciais et al., 2022; Chevallier 2021).

### *3.3.2 Inventories of anthropogenic $CO_2$ supporting carbon cycle research*

Scientific inventories, such as those compiled by the Carbon Dioxide Information Analysis Center (CDIAC; Boden et al., 2017) and the annual reports compiled by the Global Carbon Project (GCP), combine information from all of these sources to support scientific investigations and modeling of the energy and carbon cycles as well as other applications. The science community has also produced high resolution gridded inventories such as the Emissions Database for Global Atmospheric Research, EDGAR (Janssens-Maehout et al., 2019), Open-source Data Inventory for Anthropogenic $CO_2$, ODIAC (Oda et al., 2018), and Hestia (Gurney et al., 2019). These inventories use other data (population, night lights, etc.) to disaggregate national-scale emissions from fossil fuel combustion, industry, LUC and other processes to support carbon cycle investigations on spatial scales spanning individual urban areas to countries. These gridded inventories also provide more actionable information on anthropogenic $CO_2$ emissions for policy makers working on urban to sub-national scales.

One limitation of these inventories is that there is typically a year or more lag in their availability. Motivated by reports of large reductions in fossil fuel use during the initial COVID-19 lockdowns in 2020, several groups began investigating the feasibility and utility of near-real-time (NRT) emission inventories based on proxy data. Le Quéré et al. (2020) derived daily, national estimates of emission changes based on a three-level Confinement Index that was based on historical relationships between confinement and activity data from six categories of the energy sector (power, industry, surface transport, public, and residential). They report that daily global $CO_2$ emissions decreased by 17% by early April 2020, compared to 2019 values. Liu et al. (2020b) created the near-real-time Carbon Monitor (https://carbonmonitor.org/) inventory by combining data from a variety sources including hourly datasets of electrical power use from 31 countries, daily vehicle traffic data from 416 cities, daily global passenger aircraft flights, and other sources. They found emission reductions similar to those reported Le Quéré et al., but with somewhat larger variability. These NRT inventories are not as complete or accurate as the more conventional scientific inventories, but are useful for tracking rapid changes in emissions associated with energy use.

The Global Carbon Project compiles the Global Carbon Budget (GCB) annually (LeQuéré et al., 2009; 2013; 2014; 2015a,b; 2016; 2018a,b; Friedlingstein et al., 2019; 2020; 2021) These papers document global impalancebudgets of anthropogenic carbon fluxes for five key components: atmosphere, fossil fuel emissions, LUC, uptake by the terrestrial biosphere ("land sink") and uptake by the ocean ("ocean sink"). The net land carbon balance represents the difference between the fluxes from land-use change (i.e., deforestation, degradation, secondary forest regrowth, forestry and crop management) and the natural land carbon sink. Decadal mean emissions from fossil fuel use and cement production increased from $7.7 \pm 0.4$ Pg C $yr^{-1}$ in 2000-2010 to 9.5 Pg C $yr^{-1}$ for 2011-2020 with a peak of $9.9 \pm 0.5$ Pg C $yr^{-1}$ in 2019. Over this same period, land use change emissions increased from $1.4 \pm 0.7$ Pg C $yr^{-1}$ to $1.6 \pm 0.7$ Pg C $yr^{-1}$.

In 2020, fossil fuel emissions decreased to 9.5 ± 0.5 Pg C $yr^{-1}$ due to lockdowns and other measures adopted in response to the COVID-19 pandemic, but are projected to rebound to values around those from 2019 in 2021 (Friedlingstein et al., 2021). LUC emissions decreased slightly from 1.2 ± 0.7 Pg C $yr^{-1}$ in the decade, 2000-2010, to 1.1 ± 0.7 Pg C $yr^{-1}$ in the decade, 2011-2020. The ocean and land sinks increased during the same time from 2.2 to 2.8 ± 0.4 Pg C $yr^{-1}$ and 2.6 to 3.1 Pg C $yr^{-1}$ respectively (Friedlingstein et al., 2021). The anthropogenic land and ocean sinks are defined as their responses to the direct effects of increasing atmospheric $CO_2$ and indirect effects associated with climate change.

### *3.3.3 Tracking Uncertainties in Anthropogenic $CO_2$ Inventories*

In addition to these flux estimates, the GCBs document uncertainties, expressed as one standard deviation around the mean. Figure 5 shows the relative error of these estimates (uncertainty/mean) as they progress through the years for the 2008–2019 budgets. The estimates refer to each individual year for which the budget was prepared. As such, they indicate the progression in understanding of the uncertainties in the budget at that time (as opposed to an *a posteriori* analysis of the uncertainties of all years in a similar manner).

The relatively low, stable uncertainties associated with both the fossil fuel emissions and atmospheric $CO_2$ concentrations result from two factors (Ballantyne et al., 2012). The first is the precision of the atmospheric in situ $CO_2$ measurements and efficient mixing of $CO_2$ throughout the atmosphere, although analytical errors and sampling bias do play a role. Second, while fossil fuel combustion is the primary source of anthropogenic $CO_2$ emissions, the relative error on this contribution is small (~11%, e.g., Quilcaille et al., 2018) because the fossil fuel industry provides reliable numbers on their sales, which are well correlated with the amount of fossil fuel burned. The largest relative errors are associated with LUC emissions. Compared to the early period, 2000-2010, the relative error for this component has not substantially decreased, nor has the mean value substantially changed.

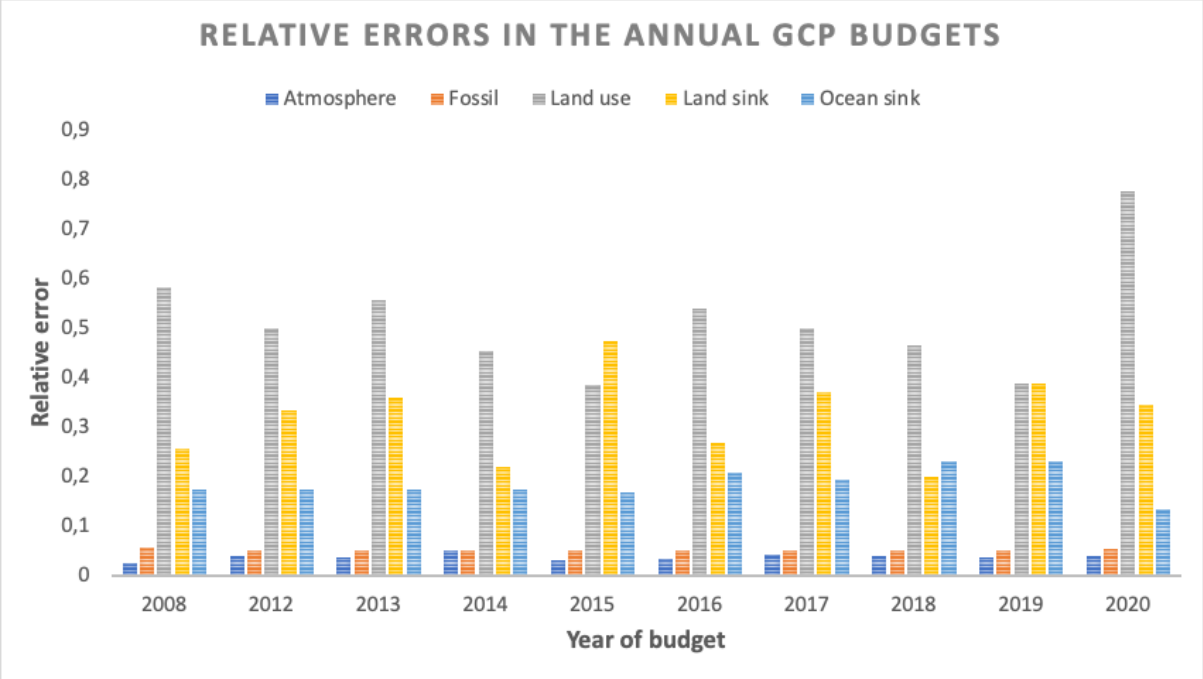


**Figure 5**. Relative error (1 standard deviation uncertainty / mean) for the Global Carbon Budget estimates since 2000. Numbers are taken for the individual year(s) reported each year from Canadell et al. (2007), LeQuéré et al. (2009) and LeQuéré et al. (2013-2018) and Friedlingstein et al. (2019-2021) and refer to the annual estimates.

In the 2015 GCB (LeQuéré et al., 2016) and before, the land sink was calculated as a residual, as described in Eq. 1:

$$land\ sink = emissions\ (fossil\ fuel\ and\ LUC) - atmospheric\ growth\ rate - ocean\ sink \quad (1)$$

Since 2017 (year 2016), the GCB has estimated LUC directly from bookkeeping models (Hansis et al., 2015; Gasser et al., 2020; Houghton and Nassikas, 2017). Uncertainties in these estimates are derived from the spread of these models and that of an ensemble of DGVMs (Friedlingstein et al., 2021).

At the same time, a normalization of the ocean sink estimate from models to a data-based estimate from the 1990s (Denman et al., 2007) was also discontinued. This normalization had previously been applied to ensure that the land sink estimate from the budget residual had a realistic mean value. This change in methodology led to a smaller mean 1990s ocean sink, and thus slightly increased the estimate of the relative uncertainty from 17% in 2015 to 19% in 2016. The ocean sink uncertainty had also varied between 17 and 19% for the years 2006 to 2015. In Friedlingstein et al., (2021), the ocean sink is derived from models and observation-based products and the uncertainty was re-assessed based on a combination of ensemble standard deviation and propagation of known uncertainties in the calculations.

With the advent of a direct estimate of the land sink from DGVMs, the GCP can now assess the degree to which the overall global carbon budget can be closed, i.e., the difference between the sum of the fluxes and the atmospheric accumulation. A budget imbalance represents a measure of our imperfect understanding of the carbon cycle and uncertainty in related measurements. Over decadal scales, the budget imbalance is close to zero, but with substantial interannual to semi-decadal variability, possibly relating to the response of natural sinks to climate variability. The budget imbalance was estimated at -0.3 Pg C for the decade 2011-2020, or approximately 10% of the magnitude of the land and ocean sinks (Friedlingstein et al., 2019, 2020; 2021). This budget imbalance and its associated uncertainties illustrates the limitations to our understanding of global annual mean fluxes at the interannual time scale.

## 4 The Ocean Carbon Cycle

The ocean holds a large natural reservoir of carbon that exchanges with the atmosphere on time-scales of decades up to hundreds of thousands of years. Superimposed upon the cycling of this natural reservoir, the increasing atmospheric $CO_2$ partial pressure is causing the ocean to absorb a significant fraction of anthropogenic carbon emissions. Due to the natural carbon cycle of the ocean, 39,000 Pg C is stored in the ocean, which amounts to ~90% of the carbon contained in the combined land, ocean and atmosphere domains (Bolin et al., 1983; Sundquist 1993; Sabine and Tanhua, 2010). The natural carbon cycle is driven by ocean circulation, seasonal heating and cooling, and biological processes (Figure 6, left).

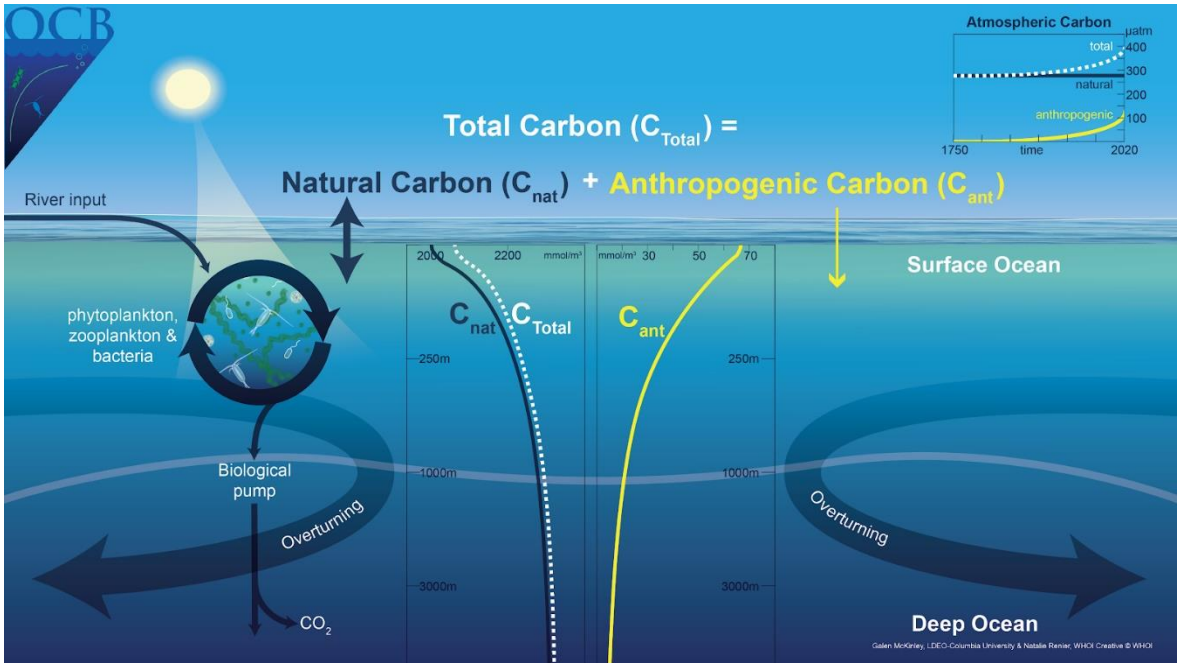


**Figure 6**. The total carbon cycle in the ocean ($C_{Total}$) is the sum of the natural carbon cycle ($C_{nat}$) and the anthropogenic carbon cycle ($C_{ant}$). The natural carbon cycle is quantitatively dominant, as shown in the observed data (GLODAPv2, Olsen et al., 2016) plotted in the center, and includes contributions from biological activity and the large-scale circulation of the ocean. Overlain is the uptake of additional carbon due to anthropogenic emissions to the atmosphere that occurs in the present ocean as atmospheric $pCO_2$ continues to rise. The air-sea flux associated with $C_{Total}$ is $F_{net}$ (see text).

The ocean carbon budget can be quantified as the storage of inorganic and organic carbon in the ocean, the fluxes of carbon across the air-sea interface, river input, and a small term for sedimentation. The natural carbon inventory is very large compared to the anthropogenic component and is believed to have been near a long-term steady state in preindustrial times, such that there was zero net flux to the global ocean of natural carbon ($F_{nat}$), i.e., there was a balance between riverine input, sedimentation rates and air-sea flux. The anthropogenic uptake flux ($F_{ant}$) is the additional ocean uptake due to the direct effect of increasing atmospheric $CO_2$ mixing ratio and occurs as a perturbation to the vigorous natural cycle (Figure 6, right), with the column inventory of anthropogenic carbon ($C_{ant}$) from the latest data-based estimates mapped in Figure 7 (bottom).

The increase in natural carbon ($C_{nat}$) from surface to depth (Figure 6) is largely due to the biological carbon pump (BCP) (Sarmiento and Gruber, 2006). If the BCP did not operate, the atmospheric $CO_2$ mixing ratio would be around 200 ppm higher (Maier-Reimer et al., 1996). During the last glacial maximum, changes in the efficiency of the BCP may have played an important role in lowering atmospheric $CO_2$ (Galbraith and Skinner, 2020; Sigman et al., 2010). Biological feedbacks may accompany anthropogenic climate change (Sabine & Tanhua, 2010, Hauck et al., 2015, Moore et al., 2018), but there is significant spread in model projections (Laufkötter et al., 2015, 2016; Frölicher et al., 2016). To date, observed time-series are too short to provide evidence for long-term biologically-driven trends in the ocean carbon cycle (Henson et al., 2016). Thus, the ocean carbon sink for anthropogenic carbon over the industrial era is currently understood as a physical and chemical process. In Figure 6, the contemporary (or 'net') air-sea $CO_2$ flux ($F_{net}$) is the sum of $F_{nat}$ and $F_{ant}$. $C_{Total}$ is the carbon concentration corresponding to $F_{net}$. Global maps of $pCO_2$, the $CO_2$ flux and the interior ocean inventory of anthropogenic carbon ($C_{ant}$) are shown in Figure 7.

The ocean surface layer carbon content equilibrates with the atmosphere on time-scales of months. The ocean continually removes $C_{ant}$ from the atmosphere because the ocean circulation transports $C_{ant}$-laden waters away from the surface layer and into the ocean interior, while the water that returns to the surface tends to have low $C_{ant}$ content. Thus, the ocean circulation is essential to continued $CO_2$ uptake. At the global scale, the ocean mixes from surface to depth relatively slowly, on timescales of 1000 years. Thus, 75% of all anthropogenic carbon attributable to the industrial age remains in the upper 1000 m (Gruber et al., 2019a). Because carbon is highly soluble and exists as DIC in ocean water, the fundamental limit on the rate of anthropogenic carbon uptake by the ocean is the rate of exchange between surface and the deep ocean across the mixed layer depth and, ultimately, the large scale overturning circulation; these processes determine how fast intermediate and deep waters with $C_{ant}$ uptake capacity are exposed to the surface.

Since the beginning of the industrial era, the ocean has been the primary cumulative $C_{ant}$ sink (Friedlingstein et al., 2019; 2020), although there are large regional differences in the magnitude and sign of the flux (Figure 7, middle panel). Looking forward, the behavior of the ocean carbon sink is expected to play a critical role in determining how much anthropogenic carbon remains in the atmosphere (Randerson et al., 2015, Zickfeld et al., 2016, Schwinger and Tjiputra, 2018, Ridge and McKinley, 2021).

The following sections describe the approaches used to study the ocean carbon sink. A mechanistic understanding of this sink is essential for diagnosing its state and for making reliable future predictions. This requires quantification of air-sea fluxes at higher spatial and temporal resolution than is available from interior data alone. Air-sea fluxes on monthly to decadal timescales are quantified using surface ocean observations and ocean models of varying

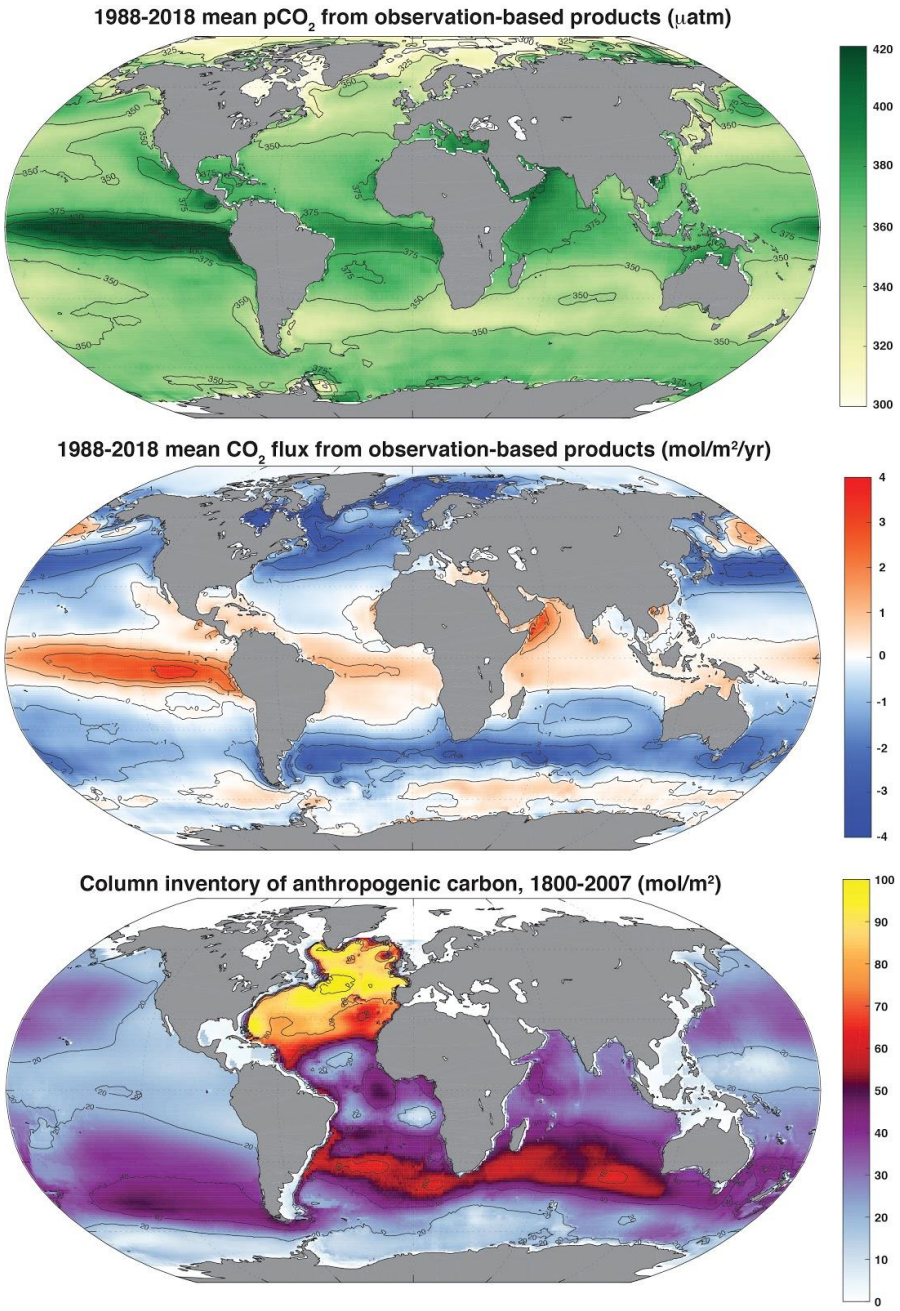


**Figure 7.** Surface ocean $pCO_2$ (top); and air-sea $CO_2$ flux ($F_{net}$), positive flux to the atmosphere (middle), 1988-2018, mean of 6 observation-based products (Fay et al., 2021); column inventory of anthropogenic carbon ($C_{ant}$, bottom), 1800-2007 (Sabine et al., 2004, Gruber et al., 2019a).

complexity. Agreement between independent estimates for mean fluxes and temporal variability indicates growing confidence in global-scale mechanistic understanding. Yet, uncertainties remain and must be resolved to support better predictions for future ocean carbon sink and to allow for reduced diagnostic uncertainty for the global carbon cycle as it evolves. Substantial advances in observing systems, quantification of land-to-ocean fluxes of carbon, and models of ocean circulation and biogeochemistry are needed to reduce these uncertainties. In addition, as nations implement substantial reductions in carbon emissions, the near-term response of the ocean carbon sink to reduced atmospheric $CO_2$ growth rates must be accurately diagnosed and mechanistically explained.

### *4.1 Bottom-up Estimates of Anthropogenic Carbon Accumulation in the Ocean from Interior Observations*

Based on a bottom-up accounting method using interior ocean data, Gruber et al. (2019a) find a total ocean $C_{ant}$ accumulation of 152 ± 20 Pg C for the industrial era through 2007. By combining evidence from top-down and bottom-up approaches, Khatiwala et al. (2013) find an inventory of 160 ± 26 Pg C in 2010. Consistent with previous inventories (Sabine et al., 2004), these studies find that the ocean has cumulatively absorbed excess carbon equivalent to 45% of industrial-era fossil fuel emissions until 2010, or 30% of the total anthropogenic emissions, including land use change. The column inventory of ocean $C_{ant}$ accumulation from Sabine et al. (2004) and Gruber et al. (2019a) is shown in Figure 7 (bottom).

The amount of $C_{ant}$ estimated for 2010 (160 ± 26 Pg C) represents only about ~0.4% of the ocean carbon stock, indicating the significant challenge of directly observing the temporal change in carbon stock over time. Direct measurements are only possible in areas with rapid change in dissolved inorganic carbon (DIC; e.g., Tanhua and Keeling, 2012). Instead, it is more practical to infer ocean storage of $C_{ant}$ against the large natural background, and then to calculate the change in storage over time.

A few different methods have been used to estimate the storage of $C_{ant}$, either based on observations of biogeochemistry variables, or by transient tracers (see Sabine and Tanhua (2010) for a review). On a global scale, different methods converge within the uncertainties, but significant differences persist regionally (e.g., Waugh et al., 2006, Khatiwala et al., 2009). Multivariate techniques (e.g., Friis et al., 2005, Clement and Gruber, 2018) can be used to disentangle variability and calculate decadal-scale trends. A global estimate of the storage of anthropogenic carbon finds an increase of 34 ± 4 Pg C between 1994 and 2007 (Gruber et al., 2019a), indicating a mean $F_{ant}$ uptake of -2.6 ± 0.3 Pg C (negative flux into the ocean) annually over this time frame. This relatively accurate (~12%) estimate provides an important benchmark for the ocean's role in sequestering anthropogenic carbon, and acts as a direct constraint on the net magnitude of the land flux, given low uncertainty on fossil fuel emissions and atmospheric carbon accumulation. The magnitude of the uptake implies that the ocean is continuing to take up anthropogenic carbon at a rate proportional to anthropogenic carbon emissions.

Critical elements to the success of global estimates of anthropogenic carbon stocks and changes in carbon storage are ship-based hydrographic sampling that collects carbon-relevant interior ocean data (Sloyan et al., 2019) and the GLODAP data product (Key et al., 2004; Olsen et al., 2020), which collates these interior data after extensive quality control (Tanhua et al., 2010). These data are required to quantify small changes over a large background. This data

product is now being released on an annual basis and the GLODAPv2.2021 version contains data from over 1.2 million water samples collected during 989 cruises (Lauvset et al., 2021).

### *4.2 Bottom-up Estimates of Ocean-Atmosphere $CO_2$ Fluxes from Observations of Surface Ocean $pCO_2$*

In order to understand the ocean carbon sink on annual to interannual timescales relevant to climate change policy, more frequent estimates of the sink are required than those produced from decadal timescale interior ocean observations. These data come from observations of $pCO_2$, and are used to estimate net air-sea $CO_2$ fluxes ($F_{net}$). The reported variable is surface ocean fugacity of $CO_2$ ($fCO_2$) which equals the partial pressure of $CO_2$ corrected for the non-ideal behavior of the gas (Pfeil et al., 2013). The fugacity of $CO_2$ is 0.3-0.4% smaller than the partial pressure of $CO_2$ (Zeebe and Wolf-Gladrow, 2001). However, the air-sea gradient, $\Delta pCO_2$ or $\Delta fCO_2$, are essentially the same as the correction of the non-ideal gas behavior applies to both the ocean and atmospheric $CO_2$. For simplicity, we use the terminology $pCO_2$ to refer to these data for the remainder of this paper. Over the past decade, the number of publicly available observations of $pCO_2$ has increased rapidly from 6 million in the first release of the Surface Ocean $CO_2$ Atlas (SOCAT) database (Pfeil et al., 2013, Bakker et al., 2014; 2016; 2020) in 2011 to 30 million in 2021 (www.socat.info). These observations and their automated organization into a consistent database have enabled scientists to create a variety of new observationally-based estimates of the ocean carbon sink that use co-located data from satellite (sea surface temperature, height, and chlorophyll) or from climatologies of in situ data (sea surface salinity and mixed layer depth) to drive upper ocean extrapolation techniques and machine-learning algorithms so as to fill the observational gaps (Rödenbeck et al., 2014; 2015, Landschützer et al., 2013; 2014; 2020; Denvil-Sommer et al., 2019, Gregor et al., 2019; Gloege et al., 2021).

As the SOCAT database provides $pCO_2$ data for only ~2% of all months and 1° x 1° locations across the surface ocean from 1982 to present, a significant amount of extrapolation is needed to create full-coverage fields at monthly intervals. Nonetheless, comparisons of the extrapolated, observationally-based products to independent data indicate relatively low bias and convergence of the independent estimates (Gregor et al., 2019). Root mean square errors (RMSE) range from 10 to 35 µatm. The fact that bias and RMSE comparisons are largely consistent across the variety of approaches suggests that it is data sparsity rather than extrapolation methodology that is now a fundamental limitation on further error reduction (Gregor et al., 2019). Additional tests of the machine-learning based extrapolation approaches using an Earth System Model testbed indicate that the techniques are able to reconstruct from sparse data with low bias and show skill for the amplitude and timing of seasonality across the global ocean. However, higher and lower frequency variations are more poorly represented because of inadequate sampling on these timescales (Gloege et al., 2021, Stamell et al., 2020). Several challenges remain in using these data, including the uneven distribution of data over time, methodological differences in the calculation of air-sea flux from $pCO_2$ (Fay et al., 2021, Woolf et al., 2019, Zavarsky and Marandino, 2019), and the potential need for adjustments to $pCO_2$ data to account for near-surface temperature and salinity gradients (Watson et al., 2020).

Despite the significant extrapolation and remaining uncertainties, it is a major advance for ocean carbon cycle science to have spatially-resolved, data-based estimates of air-sea $CO_2$ fluxes on monthly timescales. This allows for new investigation into the magnitudes and mechanisms of interannual and decadal variability in the ocean carbon sink, and a key point of

comparison to ocean models that were previously the only basis for this analysis. Models are discussed in the next section, and results are compared in the following.

### *4.3 Bottom-Up Estimates of Ocean-Atmosphere $CO_2$ Fluxes from Ocean Models*

Global ocean biogeochemical hindcast models estimate interior ocean carbon cycling and, from this, air-sea $CO_2$ fluxes. Models simulate the carbon distribution in the ocean due to the influences of currents, water mass formation and mixing, and biological processes. The bottleneck for ocean carbon uptake in the models, as in the real world, is the carbon transport across the mixed layer depth and its redistribution to greater depths via the overturning circulation. As a result, the models' carbon uptake is sensitive to simulated physics (Doney et al., 2004; Goris et al., 2018; Huber and Zanna, 2017). Models can also provide air-sea flux estimates prior to the 1990s when surface $pCO_2$ observations were rare.

Models are routinely evaluated against observations or observation-derived estimates that characterize the physical and biogeochemical state of the ocean for the last several decades (Doney et al., 2004; Schourup-Kristensen et al., 2014; Aumont et al., 2015; Schwinger et al., 2016; Stock et al., 2020; Séférian et al., 2020; Fay and McKinley, 2021). For the suite of models used in the GCP, comparison of $pCO_2$ at locations observed by SOCAT reveals the models' ability to capture variability and trends on annual (RMSE <10 μatm) and decadal timescales (RMSE <10 μatm). However, large model-data mismatches on the seasonal timescale also exist (RMSE of 20–80 μatm; Hauck et al., 2020).

Despite the overall concurrence with $pCO_2$ observations on annual and decadal timescales, model and data-based estimates of the ocean carbon sink started to diverge from each other since around 2002, particularly in the Southern Ocean (Hauck et al., 2020), reinforcing the need for evaluation of models in addition to that of data-products (section 4.2). As one way forward, Fay and McKinley (2021) evaluate the spatial distribution of modelled mean fluxes against an ensemble of these products adjusted by lateral fluxes from rivers, $F_{nat,riv}$. They find that few models fall within 3 standard deviations of the product spread for each of five large regions that together cover the globe. The regional differences are to a large extent governed by the natural carbon fluxes and this metric therefore identifies models with the balance between physical and biological processes that is most consistent with observations.

Another approach evaluates models using the global anthropogenic carbon accumulation, thus assessing the global balance between atmospheric $pCO_2$ growth and global surface-to-deep ventilation instead of regional processes. Using simulations mimicking the anthropogenic carbon accumulation ($F_{ant,ss}$), Friedlingstein et al. (2021) compare the simulated ocean interior anthropogenic DIC inventory for 1994-2007 to the estimate of Gruber et al. (2019a). This reveals an underestimation of anthropogenic carbon uptake by the majority of the models on the order of 20% for the ensemble average. However, uncertainties on the interior estimates are also significant, and other interior estimates are lower for 1994-2007 by about 10% (DeVries, 2014). More models might fall within the constraint if both interior estimates were considered. Nonetheless, atmospheric inversions that take advantage of the constraint provided by the atmospheric $CO_2$ observation network also suggest that some models underestimate the sink (Friedlingstein et al., 2021). This conclusion is further supported by a recent estimate of the ocean sink from observed $O_2/N_2$ (Tohjima et al., 2019) and the models' low 1990s estimate compared to the best estimate from different methodologies (Denman et al., 2007).

These are first efforts to exploit an array of observations to quantitatively assess regional and seasonal air-sea flux patterns in models, going beyond the typical discussion of spatial bias patterns (e.g., Séférian et al., 2020). A larger array of targeted metrics including seasonal cycles, trends and the interior ocean carbon inventory needs to be developed. Model development priorities include efforts to improve the regional and sub-regional distribution of mean fluxes and temporal variability from the seasonal cycle to the multi-decadal trend.

Global ocean biogeochemical models were the sole basis for quantifying the ocean sink in the GCB until 2020 (section 3). For example, for 2019, the GCB finds that the ocean sink accounted for 22% of 2019 anthropogenic $CO_2$ emissions (Friedlingstein et al., 2020). Models have also shed light on processes behind observed variability such as the weakening of the Southern Ocean carbon sink in response to increased westerlies (LeQuéré et al., 2007), and to explore the role of stationary Rossby waves in subduction of anthropogenic carbon (Langlais et al., 2017). As a component of Earth System Models, ocean models are the single tool for future projections. In the future, the rate of the ocean carbon sink will be largely determined by anthropogenic emissions, but ocean chemistry and physics will also play a significant role. On timescales from decadal to centennial, models project a decreased rate of uptake by the ocean carbon sink relative to the atmospheric $pCO_2$ concentration due to the fact that most of anthropogenic carbon already absorbed is in the near-surface ocean, and reduced buffer capacity (Schwinger et al., 2014, Randerson et al., 2015, Zickfeld et al., 2016, Schwinger and Tjiputra, 2018, Ridge and McKinley 2021).

### *4.4 Reconciling Air-Sea Flux Estimates from Different Methods*

We must accurately quantify the ocean sink and understand its underlying mechanisms to diagnose its ongoing evolution and improve projections of future change. The best measure of our current understanding is the degree to which the above-mentioned independent estimates of the present-day sink's magnitude agree. We discuss the degree of agreement in this section, where a negative flux refers to a flux from atmosphere to ocean, and we discuss mechanistic understanding in the next section.

Surface ocean carbon observations indicate the net air-sea flux of carbon into the ocean (implicitly including riverine outgassing), $F_{net}$, is ~ -1.6 Pg C $yr^{-1}$, while analysis of interior measurements yields estimates of the anthropogenic uptake and storage, $F_{ant}$, is ~ -2.6 Pg C $yr^{-1}$, over the period, 1994 to 2007. Dynamic hindcast models used in the GCB, typically estimate the total of anthropogenic perturbations, that is the sum of anthropogenic uptake ($F_{ant}$) and anthropogenic climate change induced natural carbon fluxes ($F_{nat,\,ns}$). Closure terms of significant net magnitude (~1 Pg C $yr^{-1}$) are required to bridge the gap between $F_{net}$ and $F_{ant}$.

To reconcile flux estimates from $pCO_2$-based data products with ocean models and estimates from interior data, an adjustment due to the riverine input of natural carbon that outgasses from the ocean ($F_{nat,riv}$) must be applied (Sarmiento and Sundquist, 1992; Aumont et al., 2001; Lacroix et al., 2020). This adjustment is needed because these fluxes are not included in ocean models, but exist in the real world. Unfortunately, high quality direct estimates of $F_{nat,riv}$ do not exist, so the closure between surface flux estimates of $F_{net}$ and $F_{ant}$ remains a significant uncertainty. Lacking better evidence, values typically used are between 0.45 and 0.78 Pg C $yr^{-1}$ (Jacobson et al., 2007, Resplandy et al., 2018), with large uncertainties. Recent work using stable carbon isotopes suggest an even larger efflux of 1.2 Pg C $yr^{-1}$ to the atmosphere from coastal margin inputs, also considering submarine groundwater discharge (Kwon et al., 2021).

Anthropogenic changes to the riverine input of carbon are an additional closure term not usually considered with no temporally-resolved estimates available and one estimate for 2000-2010 suggesting it to be small (0.1 Pg C $yr^{-1}$, Regnier et al., 2013; Bauer et al., 2013). No estimates on anthropogenic changes to the outgassing of the riverine carbon in the ocean are yet available.

Climate change may already be having an effect on the natural carbon cycle fluxes ($F_{nat,ns}$), although the magnitude of this non-steady state component is still uncertain. The first estimates of $F_{nat,ns}$ came from one model for the period 1981-2007 (Le Quéré et al., 2010) and from a back-of-the-envelope calculation for the period 1994-2007 (Gruber et al., 2019a), suggesting a reduction of $F_{ant}$ by 10 to 15%. Gruber et al. (2019a) estimate $F_{nat, ns}$ by assuming that the accumulation of anthropogenic carbon in the ocean follows a linear scaling with the atmospheric load. However, this assumption is known to hold only when the atmospheric growth is strictly exponential, which has not been the case (Raupach et al., 2014, Ridge and McKinley, 2021), and thus the resulting estimate of +0.38 Pg C $yr^{-1}$ is likely an upper-bound. Another approach for estimating $F_{nat, ns}$ is to use ocean models that represent the natural carbon cycle, and to make a reasonable assumption that the total carbon cycle response to climate variability is dominated by the natural component. With this assumption, models indicate for 1994-2007, $F_{nat, ns}$ = +0.06 to +0.31 Pg C $yr^{-1}$ (DeVries et al., 2019; McKinley et al., 2020) and for the recent decade, 2011-2020, $F_{nat, ns}$ = +0.12±0.07 Pg C $yr^{-1}$, equivalent to a 5% reduction of the ocean sink due to climate change (Friedlingstein et al., 2021). Better quantification of this term is clearly needed as well as a mechanistic understanding of the processes at play. Le Quéré et al. (2010) identified wind and temperature changes to be the dominant drivers behind this response, but the degree to which this is model dependent has not yet been investigated.

Estimates of the magnitude of the ocean sink relative to emissions vary between 23% and 48% in the literature (Friedlingstein et al., 2020; Khatiwala et al., 2013; Sabine et al., 2004). These seemingly contradicting numbers result from differences in the way the ocean sink is compared to different components of the emissions (Table 2). Quantitatively, the most important choice is the denominator used. For studies of the interior ocean cumulative ocean sink, the denominator typically used is the anthropogenic fossil emissions, resulting in an ocean sink of 44% for the industrial era through 2010 (Khatiwala et al., 2013), and 48% for the industrial era through 1994 (Sabine et al., 2004). GCB estimates, however, compare the ocean sink to total anthropogenic $CO_2$ emissions, which also include emissions to the atmosphere from land-use change. Over the industrial era, GCB estimates that the ocean has absorbed 171 Pg C, while the cumulative fossil fuel emission is 446 Pg C and LUC is 238 Pg C. The ocean has thus absorbed 38% of the cumulative fossil fuel emissions, or 25% of the total anthropogenic emissions. For the period 2010-2019, GCB estimates a smaller percentage for the ocean sink, 23% of total anthropogenic emissions (Friedlingstein et al., 2020). A second difference between the estimates is that the GCB's approach also includes climate perturbation effects ($F_{nat,ns} + F_{ant,ns}$), which reduces the magnitude of the ocean sink. Table 2 further illustrates the role of the chosen time-period in the various estimates with general agreement between GCB and interior ocean estimates when considering the spread in emission numbers used. For estimates stretching back to 1800 or before, the time-series extending to more recent years have a smaller proportion of the ocean sink relative to the fossil-fuel emissions, whereas the ratio relative to total emissions is more stable.

**Table 2.** Comparison of estimates of the relative magnitude of the ocean sink to emissions, ordered from shortest times-series to longest. GCB numbers are taken from Friedlingstein et al (2021). GCB fossil fuel emissions include the cement carbonation sink. GCB land-use change emissions are taken from annual time-series, plus 30 Pg C $yr^{-1}$ for the period 1750-1850 (Friedlingstein et al., 2021), and half of that number for the period 1800-1850. The same uncertainties are used for GCB estimates recomputed for 1750-2010 and 1800-1994 as for 1750-2020.

| Source of Estimate | Time range | Cumulative fossil emissions (Pg C) | Cumulative land-use change emissions (Pg C) | Cumulative ocean sink (Pg C) | Ocean sink relative to fossil emissions | Ocean sink relative to total anthropogenic emissions |
|---|---|---|---|---|---|---|
| GCB (Friedlingstein et al., 2021) | 2011-2020 | $95 \pm 5$ | $11 \pm 7$ | $28 \pm 4$ | 29% | 26% |
| Sabine et al. (2004) | 1800-1994 | $244 \pm 20$ | 100-180 | $118 \pm 19$ | 48% | 28-34% |
| GCB | 1800-1994 | $245 \pm 25$ | $185 \pm 75$ | $114 \pm 35$ | 47% | 27% |
| Khatiwala et al. (2013) | 1750-2010 | ~350 | $180 \pm 50$ | $155 \pm 30$ | 44% | 29% |
| GCB | 1750-2010 | $363 \pm 25$ | $220 \pm 75$ | $151 \pm 35$ | 42% | 26% |
| GCB | 1750-2020 | $458 \pm 25$ | $232 \pm 75$ | $179 \pm 35$ | 39% | 26% |

The choice to compare studies of interior ocean accumulation to fossil fuel emissions is motivated by the fact that these numbers are cumulative over the industrial era, and over this time, the land use source and land sink have been in approximate balance. Thus, this approach circumvents the large uncertainties associated with separate estimates of land-use change emissions and the land sink. The GCB's approach, on the other hand, acknowledges that fossil fuel and land-use change emissions add to the total atmospheric $CO_2$ mixing ratio, and that ocean and land carbon sinks respond to this increasing total. This is reinforced by the more stable ratio of the ocean carbon sink relative to total $CO_2$ emissions rather than the contribution from fossil fuel emissions, alone (Table 2).

### *4.5 Recent Evidence for Decadal Variability of the Ocean Carbon Sink*

In the mid-2000s, studies using ocean hindcast models suggested a slowing of the ocean carbon sink from the mid-1990s and attributed this change to processes in the Southern Ocean (Lovenduski et al., 2007; 2008; Le Quéré et al., 2007). In the following decade, the release of both the LDEO $pCO_2$ database (Takahashi et al., 2009) and the development of the international SOCAT database (Pfeil et al., 2013; Bakker et al., 2014; 2016; 2020) allowed for new analyses of trends in air-sea $CO_2$ fluxes directly from observations (Le Quéré et al., 2009; McKinley et al.,

2011; Fay and McKinley, 2013; Xue et al., 2018). Additionally, a variety of extrapolations of these data to global monthly coverage were developed (Rödenbeck et al., 2015), and a recovery of the ocean carbon sink following the low near the year 2000 was noted (Fay and McKinley, 2013; Landschützer et al., 2015; DeVries et al., 2017; Gruber et al., 2019b).

The Southern Ocean was generally identified as a significant regional driver of these mid-1990s to mid-2000s trends. A number of studies agreed that the stagnation of the Southern Ocean carbon sink in the 90s was related to a trend towards a more positive Southern Annular Mode (SAM) index associated with stronger westerly winds leading to more upwelling of natural carbon and hence dampened net air-to sea $CO_2$ flux (Le Quéré et al., 2007; Lovenduski et al., 2007; Lenton and Matear, 2007; Hauck et al., 2013).

Increasing nutrient concentrations in surface waters of all sectors of the Southern Ocean are consistent with a strengthened upwelling during the late 1990s (Iida et al., 2013; Ayers and Strutton, 2013; Hoppema et al., 2015; Pardo et al., 2017; Panassa et al., 2018). However, the same driving mechanisms cannot explain the reinvigoration of the sink in the 2000s, as the trends towards a more positive SAM and stronger winds in the 2000s continued. Asymmetric changes in atmospheric circulation (Landschützer et al., 2015), a weaker upper ocean overturning circulation (DeVries et al., 2017) and regional wind variability (Keppler and Landschützer, 2019) were proposed as possible explanations, but no consensus was reached on the driving mechanisms of the reinvigoration. Several studies concluded that ocean models were substantially underestimating the magnitude of decadal variability in the ocean carbon sink (De Vries et al., 2019; Gruber et al., 2019b).

In the last few years, more observation-based estimates have become available (Denvil-Sommer et al., 2019, Gregor et al., 2019), and now the size of the ensemble of observation-based estimates and of hindcast models is more comparable. With similar size ensembles for both observation-based and hindcast models, estimates of decadal variability are more similar in magnitude and phase, and not as large as the initial observation-based products had suggested (McKinley et al., 2020; Hauck et al., 2020). Both the ensemble of hindcast models and observation-based products indicate a larger ocean carbon sink in the early 1990s, then a slowing of the sink through about 2000, and then a strong and steady recovery through 2018 (Figure 8). In both the products and models, flux variability is largely homogenous across the globe outside the equatorial Pacific (McKinley et al., 2020).

By representing the surface ocean as a single abiotic box that exchanges water with the deep ocean at a constant rate, McKinley et al. (2020) are able to reproduce the variability of the ocean carbon sink with two external forcings (Figure 8). The two external forcings are the observed atmospheric $pCO_2$ and the forced change in upper ocean temperature due to the eruptions of large volcanoes (1982 El Chichon; 1991 Mt Pinatubo). This result emerges because the globally-averaged air to sea $pCO_2$ gradient - the fundamental driver of the flux - is only 6-10 µatm, and thus anomalies in the atmospheric growth rate of a few µatm over several years can rapidly modify the global air-sea gradient. Large volcanic eruptions, such as Mt Pinatubo in 1991, cause a rapid surface ocean cooling, which increases solubility and creates an uptake pulse (Church et al., 2005; Eddebbar et al., 2019). Then, as the ocean warms from this rapid cooling, solubility is lowered, and there is excess DIC in the upper ocean relative to what would have occurred without the eruption. These two effects contribute to a reduced growth rate of the sink for 5-7 years beyond the eruption (Figure 8).

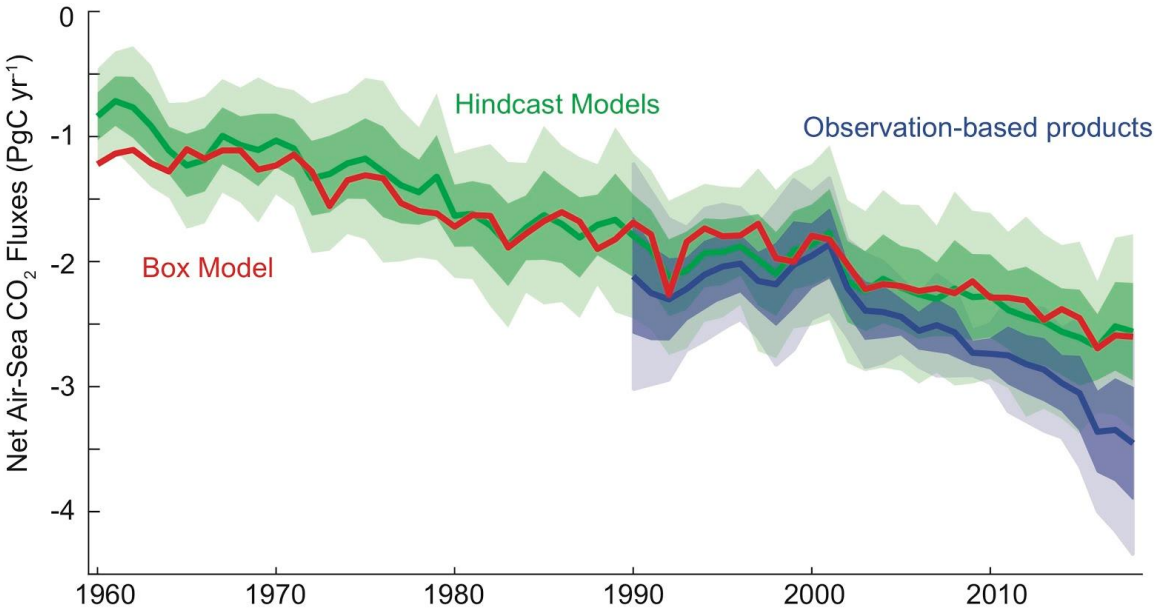


**Figure 8.** Air-sea $CO_2$ flux of carbon ($F_{ant}$ + $F_{nat,ns}$) from observationally-based products (blue), hindcast models (green) and upper ocean diagnostic box model (red); negative flux into the ocean. Global ensemble means (bold), with 1 sigma and 2 sigma of individual members (shading). Hindcast ocean models from Global Carbon Budget 2020 (Friedlingstein et al., 2020). Observationally-based product $pCO_2$ fields have missing ocean areas filled with a full-coverage climatology (Landschützer et al., 2020) and air-sea flux calculated as average of 3 wind reanalyses (CCMP, ERA5, JRA55) with a quadratic parameterization (Wanninkhof 2014, Fay et al., 2021); to this $F_{net}$ estimate, $F_{nat,riv}$ = 0.62 Pg C $yr^{-1}$ (Jacobson et al., 2007, Resplandy et al., 2018) is added. The upper ocean diagnostic box model (McKinley et al., 2020) is forced with observed atmospheric $pCO_2$ and surface ocean temperature changes forced by the eruptions of three large volcanoes of this period (1963 Agung, 1982 El Chichon, and 1991 Mt. Pinatubo; Eddebbar et al., 2019).

This model of McKinley et al. (2020) is simple, considering a global surface ocean of 200 m depth that is uniformly impacted by atmospheric $pCO_2$ and upper ocean heat content anomalies forced by large volcanos. Yet, it can reproduce the ocean carbon uptake that occurs in the ensemble mean of much more complex models and observation-based products. What does this mean? It can be interpreted simply as Henry's Law operating at the global scale, wherein the partial pressure in the water is moving toward equilibration with the partial pressure in the air. Since the atmospheric $pCO_2$ continues to increase, the ocean continues to adjust toward equilibrium. McKinley et al. (2020) demonstrate that the ocean carbon sink temporal variability today is likely dominated by the external forcing from slight variations in the atmospheric $pCO_2$ growth rate. This perspective is consistent with recent analysis that shows heat uptake and interior redistribution in the ocean is far more sensitive to the details of the ocean circulation than is the pattern and magnitude of carbon uptake and storage (Bronselaer and Zanna, 2020). Ultimately, the mechanisms driving interannual to decadal timescale variability remains a topic of debate, and the focus of a significant research effort by the ocean carbon cycle community.

Observation-based products and hindcast models differ in the strength of sink increase since around 2002 (Figure 8). The growth rate of the ocean sink since 2010 is uncertain by a factor of three. Observation-based products indicate that the sink has increased by 0.9 Pg C $yr^{-1}$ between 2010 and 2020 whereas models only simulate an increase of 0.3 Pg C $yr^{-1}$ (Friedlingstein et al. 2021). This discrepancy is unresolved despite its importance for the near-term predictions of the remaining carbon budget and climate targets. Observation-based products may overestimate decadal variability of the ocean sink, consistent with too large a trend for these years (Gloege et al., 2021). Watson et al (2020) evidenced that the uncertainty of the sink estimate is generally a factor two higher at both ends of the time-series, independent of temporal and spatial data coverage, making the trend over the final one to two decades more uncertain.

Some models, however, underestimate the accumulation of anthropogenic carbon in the ocean interior for 1994-2007 (section 4.3; Friedlingstein et al., 2021), although the rate used as the basis for comparison (Gruber et al., 2019a) is on the high end of existing estimates (DeVries, 2014). If one assumes a steady state rate of anthropogenic carbon accumulation, an underestimated mean uptake rate for 1994-2007 would also imply an underestimated mean rate for 2002 to present. One possible explanation for this is that too little carbon is transported out of the mixed layer, which leads to a too strong increase in the buffer factor and hence to a reduction of ocean carbon uptake. Analysis of CMIP5 models in the Atlantic reveals that models that better represent current interior carbon storage have larger present-day and future carbon uptake (Goris et al., 2018). Biases in simulated ocean ventilation were identified as one process that affects ocean heat uptake (Bronselaer and Zanna, 2020) and to be the dominant cause of underestimated historical trends in modeled ocean oxygen decrease (Buchanan and Tagliabue, 2021). If ocean ventilation is too slow, models should underestimate the rate of the ocean carbon sink, and potentially also the sink's rate of change. It is also possible that variability in the ocean ventilation (DeVries et al., 2017) somewhat decouples the 1994-2007 rate of anthropogenic accumulation and ocean sink trends since 2002.

### *4.6 Advancing Understanding of the Current and Future Ocean Carbon Sink*

To quantify the global carbon cycle, the constraint provided by the relatively low-uncertainty estimates for decadal anthropogenic carbon accumulation must be maintained. To better quantify fluxes on monthly to decadal timescales, increased observations of surface $pCO_2$ and higher fidelity models are needed. In order to be prepared to support climate management efforts in the near-term, the likely behavior of the ocean sink under emissions mitigation must receive increased attention.

Observations of ocean interior carbon require measurements with high accuracy and precision due to the small perturbations on a large background signal. For example, in 2010, the $C_{ant}$ content was ~160 Pg C out of a total inorganic carbon content of ~39,000 Pg C. For the surface ocean flux estimates, the high spatiotemporal variability in $pCO_2$ and a low average deviation from air-sea equilibrium concentration needed to drive the observed net flux, i.e., a net flux of ~2.5 Pg C $yr^{-1}$ over a gross flux of ~90 Pg C $yr^{-1}$, indicates that accuracy and data coverage are possibly the most important components of the observing system. There is a seasonal bias in the observing system, with fewer observations being made in winter at high latitudes. This is particularly important for observations of surface fluxes, which tend to be high in winter, but less so for the interior ocean observations where seasonality tends to be low below the winter mixed layer.

### *4.6.1 Expanding Autonomous Observations*

Although ship-based observations remain a central resource for the ocean carbon observing system, these are expensive and tend to be seasonally biased. Driven by these demands, there is a continuous development of sensors for inorganic carbon system measurements with at least some of these attributes: increased precision and accuracy, lower power consumption and lower instrument drift (Johnson et al., 2016; Sabine et al., 2020; Seelmann et al., 2019; Sutton et al., 2014). Similarly, there is a continuous development of autonomous platforms capable of carrying sensors for ocean carbon. These include moorings (Sutton et al., 2014), profiling floats (e.g., BGC Argo, Claustre et al., 2020), underwater gliders (Rudnick, 2016, Sutton et al., 2021), and autonomous surface vehicles powered by wind or waves (Sabine et al., 2020). These developments are rapidly changing the capability to monitor ocean carbon with higher spatial and temporal resolution. For instance, observations from Biogeochemical (BGC) Argos floats enable the calculation of surface $pCO_2$ (from pH and alkalinity estimates) with reasonable accuracy and precision, ~11 µatm (Takeshita et al., 2018; Williams et al., 2017). Although not as good as the 2 µatm target for the ship-based observations, this system has shown potential to fill spatiotemporal gaps in the observations, with important implications for the carbon flux estimates. For example, Bushinsky et al. (2019) report on significantly lower uptake of carbon in the Southern Ocean by including winter time $pCO_2$ from BGC-Argo floats using a neural network interpolation. Uncrewed Surface Vehicles (USVs) directly measure $pCO_2$ with an uncertainty of 2 µatm, which is comparable to ship-based observations The strong winter outgassing observed by floats in 2015-2016 was not detected by USVs in 2019, illustrating how these novel techniques can progress research on interannual variability (Sutton et al., 2021).

### *4.6.2 Improving Constraints on Carbonate Chemistry*

Although individual components of the ocean carbon observing system have high technical readiness levels, the new capabilities have not yet been integrated with existing, well-tested technologies to provide an observing system that can quantify ocean carbon uptake to within 10%. One critical need is an improved understanding of the ocean inorganic carbon system. There are four measurable inorganic carbon variables in the ocean - total alkalinity (TA), total dissolved inorganic carbon (DIC), pH and $fCO_2$. By measuring two out of those, the complete inorganic carbon system can, in theory, be calculated. Small errors in the dissociation constants, the boron-salinity ratio, and small contributions to the total alkalinity from unknown bases, can cause significant discrepancies in directly measured and calculated carbon variables (Fong and Dickson, 2019, Takeshita et al., 2020). A recent study by Álvarez et al. (2020) shows that inconsistencies between calculated and measured pH have decreased during the last decade, and they conclude that improved standard operating procedures for measurements and calculation of pH are urgently needed. An improved understanding of these issues is essential to fully utilize data from, for instance, BGC Argo floats equipped with pH sensors.

### *4.6.3 Ensuring Quality Control and Timely Data Delivery*

As noted above, the anthropogenic perturbation in the global ocean is more than an order of magnitude smaller than the background natural state. Thus, to track the changing anthropogenic carbon uptake by the ocean, very high standards for accuracy and precision of inorganic carbon system data must be maintained. New autonomous technologies offer great promise for expanding the observing system, but cannot be incorporated into the observing system if this substantially increases overall uncertainties. For the foreseeable future, ship-based

measurements will continue to be required to calibrate and validate autonomous observations. Cross-over evaluations should occur both with deployment and post-deployment (Fay et al., 2018). At the same time, ocean carbon data must be ingested into public databases or products (e.g., SOCAT, GLODAP) in a timely manner that supports annual diagnoses of the ocean carbon sink. It is essential that these data be carefully quality controlled. As the timescales at which the user community requires these diagnoses become shorter, these data will need to be available more quickly. One key component of this integration into scientific products is certified reference materials (CRMs). CRMs are critical because they allow for consistent observations across independent laboratories, which is essential for the development of high-quality global datasets. Currently, a single laboratory is the source for these materials and a plan for a long-term future source remains unclear (Catherman, 2021).

Similarly, better observational constraints on ocean carbon perturbations can be gained from stable carbon isotope observations. The ocean inorganic carbon pool is lightening due to the uptake of $CO_2$ originating from the burning of $^{13}C$-depleted fossil fuel carbon, a phenomenon also known as the oceanic $^{13}C$ Suess effect. By observing this temporal development, estimates of the anthropogenic carbon fraction of DIC are possible. Recent improvements in observations are making this approach attractive (e.g., Becker et al., 2012, Cheng et al., 2019, Cheng et al., 2021).

#### *4.6.4 Quantifying Closure Terms to Link Estimates of Surface Flux and Interior $C_{ant}$ Accumulation*

In order to reduce uncertainties in the global and regional ocean carbon cycle, we need to understand how interior-based estimates of $F_{ant}$ and surface flux estimates of $F_{net}$ are quantitatively linked. An important barrier to this is the significant magnitude and high uncertainty in current estimates for natural fluxes of carbon in rivers ($F_{nat,riv}$) and interannual variability in the natural carbon cycle ($F_{nat,\ ns}$). More observations of these two quantities are needed to improve our understanding and reduce the uncertainties.

#### *4.6.5 Constraining Mechanisms of Surface Flux Variability*

Recent work has identified the important role of external forcing from atmospheric $pCO_2$ and volcanoes in driving ensemble-mean estimates of recent variability of the ocean carbon sink, but individual models and individual observation-based products deviate from the mean of the ensembles (Hauck et al., 2020, McKinley et al., 2020). These deviations are due to different methods for simulating the ocean circulation and biology in each individual ensemble member. We do not yet understand which of these individual estimates best represent the real ocean. To understand the actual total variability of the real ocean carbon sink (total = forced + internal), we need to select the observation-based products and models of highest fidelity. More stringent application of observational constraints (Fay and McKinley, 2021; Friedlingstein et al., 2021) would facilitate weighting of the models for global budgeting, focused analysis of the mechanisms driving variability in the highest-fidelity models and guidance for improving others.

Another approach for combining observations and models is through data-assimilation that constrains the model ocean state and fluxes using observations, and closes data gaps by model dynamics rather than extrapolation. While assimilation applications so far have not provided annually updated global ocean sink estimates with full spatial and temporal resolution (e.g., Mikaloff Fletcher et al., 2006; DeVries, 2014; Verdy and Mazloff, 2017;

DeVries et al., 2019), the first spatially and temporally resolved global data-assimilated models are starting to become available (Carroll et al., 2020).

#### *4.6.6 Tracking the Magnitude of Trends in the Ocean Carbon Sink Since 2002*

The current divergence of ocean sink trends in observation-based products and models has implications for closure of the global carbon budget and remaining allowable emissions and the feasibility of internationally agreed climate targets. These trends may be methodological or may illustrate a fundamental knowledge gap in how the ocean sink responds to rising atmospheric $CO_2$ levels and the natural and anthropogenic physical changes occurring in the ocean. There are indications that observation-based products may overestimate decadal timescale trends (Gloege et al., 2021) and also that models may underestimate this trend (Goris et al., 2018) due to biases in ocean ventilation (Bronselaer and Zanna, 2020, Buchanan and Tagliabue, 2021). Understanding this deviation, and fixing potential methodological issues in both approaches is necessary to more accurately track the evolution of the ocean carbon sink.

#### *4.6.7 Quantifying the Impact of Interactions Between the Natural Carbon Cycle and Climate*

Climate change induced modifications of the ocean, such as ocean acidification, warming and ecosystem composition could significantly influence the transport of particulate and dissolved organic carbon from the surface to the interior ocean, i.e., the “biological pump”. The efficiency of this transport is a key factor regulating the atmospheric $CO_2$ mixing ratio and is thought to play a role in regulating glacial / deglacial atmospheric $CO_2$ (e.g., Galbraith and Skinner, 2020). For instance, Marsay et al. (2015) suggest that a warmer ocean might lead to reduced sequestration of $CO_2$ by the biological pump. Complex interactions in the marine ecosystem will affect carbon export in a changing climate in ways that are difficult to predict and currently inadequately quantified (Laufkötter et al., 2015, 2016, Frölicher et al., 2016). In a recent work, Claustre et al. (2021) provide a research framework to improve the understanding of the oceans' biological carbon pump.

#### *4.6.8 Tracking the Future Ocean Sink Under Scenarios of Emission Mitigation*

On centennial timescales under high emissions scenarios, slowing of the overturning circulation and reduced buffer capacity will significantly reduce the rate of ocean carbon uptake (Randerson et al., 2015, Ridge and McKinley, 2020; 2021). But how will the ocean sink evolve under the increasingly more likely scenario of substantial emissions mitigation (Hausfather and Peters, 2020)? Given that the long-term growth and interannual variability of the ocean sink observed to date is driven by the exponential growth of atmospheric $pCO_2$ (Joos et al., 1996, Raupach et al., 2014, McKinley et al., 2020, Ridge and McKinley, 2021), the ocean sink is expected to slow in response to reduced growth rates of atmospheric $pCO_2$. In effect, the anthropogenic carbon trapped in the near-surface ocean will begin to equilibrate with the atmosphere and the sink will be significantly reduced in response to the mitigation of emissions. This will occur simply due a change in the growth of atmospheric $pCO_2$ - no change in the ocean circulation or buffer capacity is required (Ridge and McKinley, 2021). Slowing of the ocean sink will further offset the effect of reduced emissions. This will reduce the apparent effectiveness of mitigation actions in limiting climate warming (Jones et al., 2016). Despite a slowed rate of the sink, the largest share of cumulative emissions will be taken up by the ocean and land sink if a low emissions trajectory is followed (IPCC, 2021).

Though a series of idealized studies have established the general fact that the ocean sink will be reduced with mitigation (Joos et al., 1996, Raupach et al., 2014, Zickfeld et al., 2016,

Schwinger and Tjiputra, 2018, MacDougall et al., 2020, Ridge and McKinley, 2021), the spatially and temporally resolved response of the ocean sink to emission mitigation has received little attention. Thus, we do not know how rapidly the ocean sink will slow, nor where surface flux changes will be most substantial. We do not know what will be required from our monitoring systems to detect these changes.

Current uncertainties in ocean models suggest that, despite the fact that the current ensemble of models largely agrees as to the recent evolution of the sink (Figure 8), there may be substantial divergence in feedback strength and ocean sink response to emission mitigation. Since the majority of the anthropogenic carbon is held in the ocean's thermocline (Gruber et al., 2019a), the circulation here is critical to the ocean sink's near-term response to mitigation (Iudicone et al., 2016; Rodgers et al., 2020; Ridge and McKinley, 2020). There is substantial spread in the regional distribution of ocean carbon uptake in current models (McKinley et al., 2016, Hauck et al., 2020; Fay and McKinley 2021), and major differences in representations of seasonality (Mongwe et al., 2018), which illustrates knowledge gaps with respect to physical and biological processes and their representations in models. In addition, circulation in these critical upper-ocean regions is not consistently represented in state-of-the-art models (Bronselaer and Zanna, 2020). Uncertainties in the response of the ocean sink to emissions mitigation strategies need to be assessed, and then they need to be reduced by model development efforts and verified by observations, so that robust projections can be made. Especially in these first decades of climate management via emission mitigation, there will be great public interest in how emission cuts are changing atmospheric $CO_2$. Scientists need to be prepared to explain ocean carbon sink changes as they occur.

## 5 The Terrestrial Carbon Cycle

The terrestrial carbon cycle is characterized by large, spatially heterogeneous fluxes from anthropogenic activity and natural processes dominated by biospheric activity at daily, seasonal through interannual and multidecadal time-scales. Its primary stocks and fluxes are illustrated in Figure 9 and summarized in Table 3. The largest carbon stocks are held in aboveground biomass and soils in tropical and high latitude forests, respectively, with total stocks in vegetation and soils of 450-650 Pg C and 1500-2400 Pg C, respectively (Ciais et al., 2013; Scharlemann et al., 2014). As noted in Section 3, excluding fossil fuel combustion and other industrial activities (Section 3), the largest components of the net global land-atmosphere $CO_2$ fluxes are from land-use change and management and a sink in the terrestrial biosphere (Friedlingstein et al., 2021).

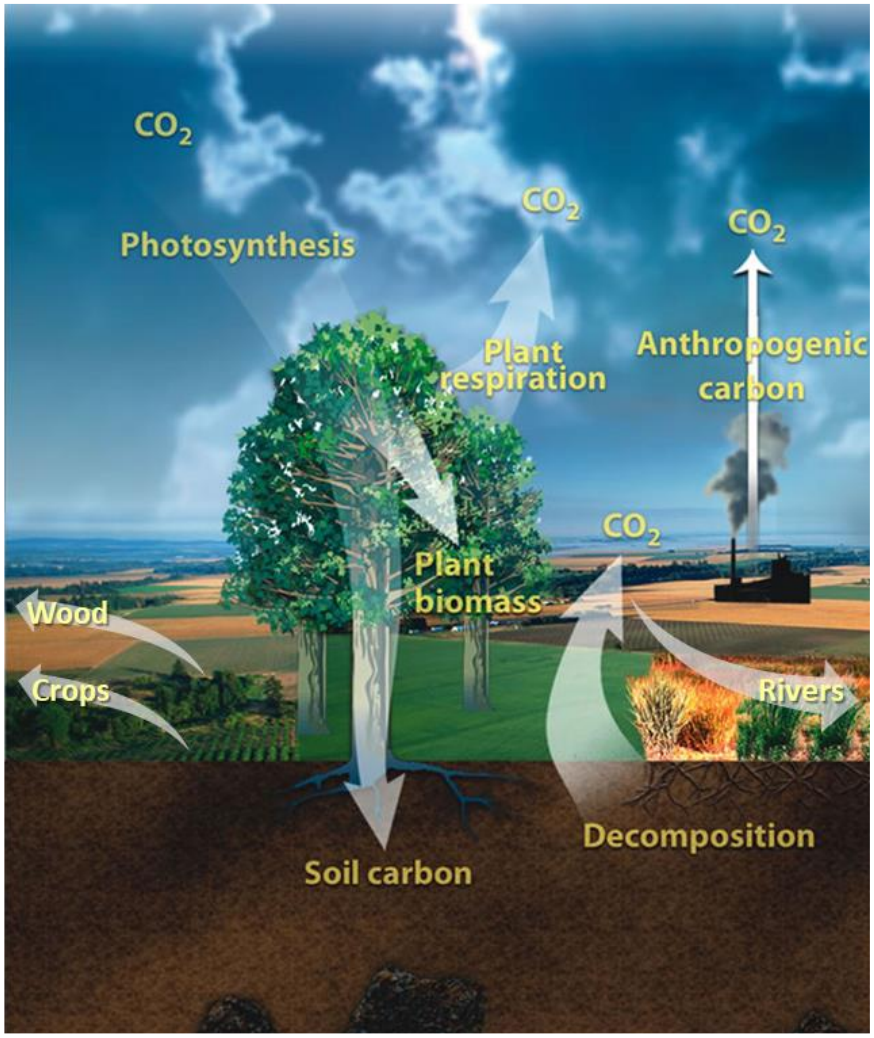


**Figure 9.** The land carbon cycle, showing the primary fluxes and reservoirs. The amplitudes of the primary land-atmosphere fluxes (white arrows), are listed in Table 3. "Lateral" land carbon fluxes such as land-to-ocean transfer of carbon by rivers and the import/export of harvested wood and agricultural products are also shown. (Adapted from U.S. Department of Energy Genomic Science program - https://genomicscience.energy.gov).

### *5.1 Processes Controlling Net Ecosystem Production*

The net land carbon balance is determined primarily by the balance of $CO_2$ uptake through photosynthesis (GPP) and release by autotrophic respiration ($R_a$), litter and soil organic matter decomposition (soil heterotrophic respiration, *SHR*). It also includes smaller contributions such as source/sink dynamics from fires and other disturbances ($F_{dist}$), emissions from crop product consumption and grazing ($F_{crop}$, $F_{grazing}$), wood product decay ($F_{wood}$), outgassing from water bodies and lateral exports such as DIC/DOC ($F_{nat,riv}$) and trade of crop and wood products ($F_{trade}$). These quantities are related to Net Biome Productivity (NEP) in Eqs. 2-4.

$$NBP = GPP - R_a - SHR - F_{dist} - F_{crop} - F_{grazing} - F_{wood} - F_{nat,riv} - F_{trade} - F_{others}\ , \qquad (2)$$

$$NPP = GPP - R_a \,, \quad (3)$$

$$TER = R_a + SHR \,. \quad (4)$$

Another commonly-used quantity, the Net Ecosystem Production (NEP), is similar to NBP on large ecosystem scales, but attempts to separate out carbon fluxes due to episodic disturbances (Schulze and Heimann 1998, Chapin et al., 2006). Additional fluxes of carbon in the form of carbon monoxide (CO), methane ($CH_4$) or biogenic volatile compounds are included in $F_{others}$. Ciais et al. (2022) estimate these contributions as 0.3, 0.43, and 0.75 Pg C $yr^{-1}$, respectively. These terms smaller than those included here and not considered further.

**Table 3.** Contemporary land carbon fluxes. (Note: numbers without uncertainties are assumed to have uncertainties comparable to their stated values.)

| Quantity | Flux (P C $yr^{-1}$) | Reference |
|---|---|---|
| Gross Primary Production (GPP) | 115 to 190 | Cai and Prentice (2020) |
| Net Primary Production (NPP) | ~50 (44 to 57) | Ciais, Yao et al. (2020) |
| Autotrophic Respiration ($R_a$) | ~64 ± 12 | Ito (2020) |
| Soil Heterotrophic Respiration (SHR) | 39 (33 to 46) | Ciais, Yao et al. (2020) |
| Outgassing by Rivers, Lakes and Estuaries | 0.8 to 2.3 | Ciais, Yao et al. (2020) |
| Fires | 1.6 | Ciais, Yao et al. (2020) |
| Consumption of Harvested Crops | 1.5 | Ciais, Yao et al. (2020) |
| Land Use Change (LUC) | 1.1 | Ciais, Yao et al. (2020) |
| Grazing | 1.0 | Ciais, Yao et al. (2020) |
| Biogenic Reduced Carbon | 0.8 | Ciais, Yao et al. (2020) |
| Decay and Burning of Wood Products | 0.7 | Ciais, Yao et al. (2020) |

Land carbon stocks and fluxes, and thus the natural land sink, are affected by increases in atmospheric $CO_2$ as well as changes in nitrogen deposition, land use change (LUC) and the response of ecosystems to climate variability since the beginning of the industrial age. Elevated atmospheric $CO_2$ mixing ratios directly stimulate plant productivity through $CO_2$ fertilization and enhancements in plant water use efficiency in arid regions (Schimel et al., 2015; Gonsamo et al., 2021). These factors, combined with its contributions to warming at high latitudes, contribute to longer growing seasons. The magnitude of these effects is debated (Walker et al., 2021), underscoring remaining uncertainties in empirical understanding and modelling (Medlyn et al., 2015).

In the current paradigm for nutrient control on productivity, high-latitude ecosystems are potentially nitrogen limited. This reflects the young age of soils post glaciation, since nitrogen sourced through biological nitrogen fixation from the atmosphere and cold environments limit nutrient mineralization. In contrast, the tropics are more likely to be phosphorus limited as they typically have older and often highly weathered soils (phosphorus being sourced from bedrock;

see Vitousek et al., 2010). In terms of climate constraints on primary productivity, tropical systems are often characterized by distinct wet and dry seasons, and are water and/or radiation limited, the latter due to clouds (over moist tropical forests), whereas mid- and high-latitudes are typically temperature and light limited, except semi-arid and drylands, which are typically water limited (Nemani et al., 2003).

The net carbon balance can be determined by bottom-up methods, such as biomass and soil inventories and process-based models (e.g., DGVMs). Two biomass-based, bottom-up approaches are considered in this review: 1) stock change (difference between carbon stocks over a period of time) 2) gain/loss method (annual gains and losses in biomass carbon). The net carbon balance can also be inferred from top-down methods that infer net land-atmosphere $CO_2$ fluxes by analyzing spatially-and temporally-resolved measurements of $CO_2$ concentrations using atmospheric inverse models. Top-down atmospheric inversions provide spatially-explicit and temporally continuous estimates of the surface (land and ocean) fluxes that are consistent with $CO_2$ concentration measurements and ensure mass-balance, but require the choice of an atmospheric transport model, assumptions about uncertainties and depend on the priors used when the observational network is too sparse (Kaminski and Heimann, 2001). The extent to which the top-down and bottom-up estimates of the net carbon balance agree provides a measure of our understanding of the carbon cycle. Results from both approaches are summarized in the following sections. Here, we focus on contemporary fluxes, covering the past three decades (1990 – 2020), broadly aligning with the availability of global satellite remote-sensing data, although exact time periods will differ among individual studies reported.

### *5.2 Bottom-up Inventories of Net Ecosystem Exchange*

$CO_2$ emissions or uptake by natural ecosystems, including those associated with deforestation, reforestation, disturbance, or land management are usually expressed in terms of the Net Ecosystem Exchange, NEE = - NEP. Bottom-up methods estimate NEE based on information about (i) the area affected by a given process, (ii) the corresponding carbon stock per unit area (and its trends) and (iii) the fraction of carbon exchanged with the atmosphere due to the observed change (e.g., Hubau et al., 2020). In practice, all three of these properties are challenging to quantify accurately (e.g., Saatchi et al., 2011; Ramankutty et al., 2007; Pearson et al., 2017, Xu et al., 2021), but all have benefited from new in situ and remote sensing measurement techniques and more advanced bottom-up modeling techniques.

The areal extent of land use and land cover change (LULCC) associated with human activities and natural processes are typically tracked using the bookkeeping methods and remote sensing observations summarized in Section 3.3. Recent advances in the remote sensing methods are summarized in Section 5.4. Estimates of the carbon stock per unit area are derived by combining above ground and below ground biomass and soil carbon. Until recently, estimates of all three quantities relied primarily on in situ measurements collected from a limited number of dedicated research plots at regular intervals (e.g., Pan et al., 2011). Soil carbon inventories still rely exclusively on in situ measurements, which are often characterized by limited spatial coverage and infrequent (decadal) repeat intervals (Scharlemann et al., 2014; Ciais et al., 2014). However, recent advances in microwave and lidar remote sensing technologies have provided dramatic improvements in above ground biomass measurements (see Section 5.4.2).

Alternately, NEE can also be estimated from direct measurement of $CO_2$ fluxes between the surface and the atmosphere using networks of eddy covariance flux towers, such as those

deployed by FLUXNET (Baldocchi et al., 2001). The global network of eddy covariance sites has grown substantially over the past 25 years, with some records spanning that full period. These data provide unique constraints on the $CO_2$ fluxes from a broad range of vegetation types, climate regions and disturbance types. Eddy flux data have been combined with other

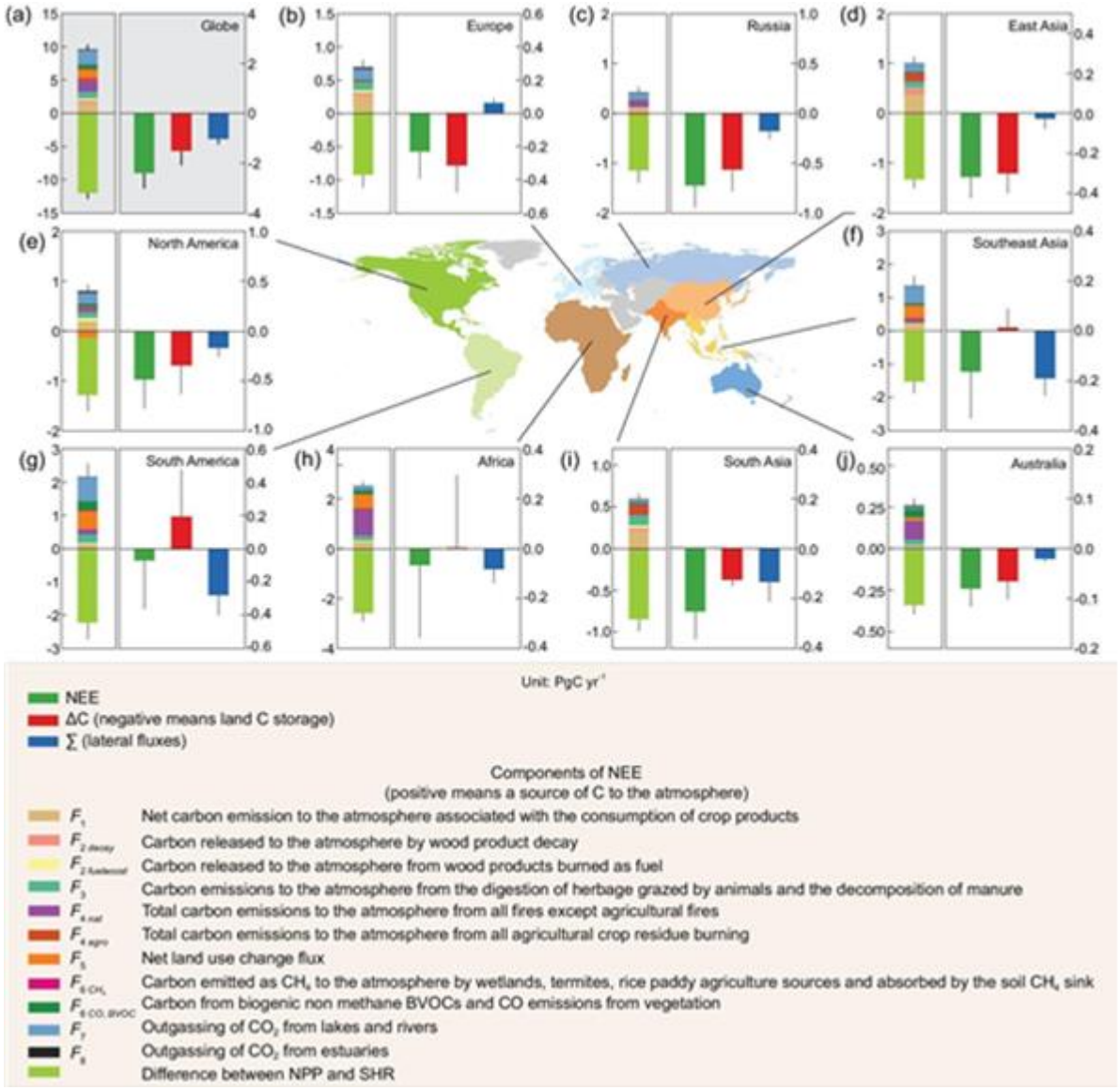


**Figure 10.** Contributions to net ecosystem exchange (NEE, as defined in Ciais, Yao et al., 2020, which corresponds to the definition of NBP in Eq. 2) at continental scales from bottom-up inventories, compiled by RECCAP2. All major flux components included in their definition of NEE are shown in the left sub-panel of each plot. The right sub-panels summarize NEE (green bars), the carbon-storage change, ΔC (red bars) and the combined lateral fluxes from trade and riverine-carbon export to the ocean, Ftrade + Fnat,riv (blue bars) for different regions of the globe for the

climatological data to provide insights into the processes acting across these domains and their changes over time. Over the past two decades, the eddy flux network has expanded to span the globe, but still has large gaps, particularly in the tropics and at high latitudes, and each flux tower

characterizes the fluxes within a limited spatial footprint. Because of this, efforts to upscale results from local to regional or global scales are often associated with large uncertainties in the magnitude of the land $CO_2$ sink and especially its interannual variability (Baldocchi, 2003; Jung et al., 2009; Beer et al., 2010; Xiao et al., 2012; Keenan and Williams, 2018; Jung et al., 2020).

Figure 10 shows the net carbon balance expressed as NEE across continents, drawn from a comparison of bottom-up methods employed in the REgional Carbon Cycle Assessment and Processes-2 (RECCAP2) project (Ciais et al., 2020a). Here, NEE is defined by subtracting lateral carbon fluxes ($F_{nat,riv}$, $F_{trade}$) from the total net land carbon stock change, $\Delta C$. In Europe, Russia and East Asia, the lateral fluxes tend to be small, and NEE almost equals the change in carbon stocks as observed from inventories. Overall, Ciais et al. (2020a) find a global sink of -2.2 ± 0.6 Pg C $yr^{-1}$, which is comparable to the independent estimate obtained by the DGVMs used in the GCB (Friedlingstein et al., 2021) of -2.7 ± 0.6 Pg C $yr^{-1}$. The results from bottom-up estimates in Ciais et al. (2020a) are also roughly consistent with results from an ensemble of atmospheric inversions (Peylin et al., 2013), which estimate a global net land sink of -1.32 ± 0.39 Pg C $yr^{-1}$, with a sink of -2.18 ± 0.53 Pg C $yr^{-1}$ in the northern hemisphere but a highly uncertain source of 0.91 ± 0.93 Pg C $yr^{-1}$ in the tropics (estimated as a sink by Ciais et al., 2020a). These net sink estimates are not consistent with a sum of the mean values of GPP, Ra, SHR listed in Table 3, but are allowed within the range of uncertainties on these variables quoted there (see discussion in Ciais et al. 2020a).

### *5.3 Bottom-up Estimates of Gross $CO_2$ fluxes from land ecosystems – GPP, $R_a$ and SHR*

To understand variability and trends in NEE, the component fluxes (Eq. 2) must be quantified. Gross primary productivity (GPP) reflects the total uptake of carbon through photosynthesis and is an essential variable to understand the carbon cycle. Up to 40% of the carbon in the atmosphere passes through leaf stomata annually, and approximately 16% (120 Pg C $yr^{-1}$) is assimilated in vegetation (GPP) (Ciais et al., 1997). Some of this carbon is used for plant functioning and growth, and the remainder is released back to the atmosphere through respiration. GPP minus autotrophic respiration (Ra) equals Net Primary Production (NPP) and this is further reduced by soil heterotrophic respiration and disturbances.

An analysis of direct flux observation made by a network of eddy covariance towers yielded estimates of the global GPP near 123 Pg C $yr^{-1}$ (Beer et al., 2010). Roughly one third of this (40.8 Pg C $yr^{-1}$) is produced in the tropical forests, and one quarter (31.3 Pg C $yr^{-1}$) in the tropical savannas, making the tropics by far the largest contributor to global GPP. Temperate and boreal forests are estimated to have a GPP of only 9.9 Pg C $yr^{-1}$ and 8.3 Pg C $yr^{-1}$, respectively. When integrated over the globe, croplands contributes an estimated 14.8 Pg C $yr^{-1}$ to GPP.

An alternate analysis using oxygen isotopes (Welp et al., 2011), suggests that this value of Global GPP may be too low and would be closer to 150 -175 Pg C $yr^{-1}$. However, Anav et al. (2015) argue that Welp et al. used a limited number of observations and a simple model that included gross photosynthesis, but neglected photorespiration by land plants. They note that plants immediately respire away 20-40% of the carbon fixed by photosynthesis. When photorespiration is included, they note that these GPP values are more in line with those obtained from other methods. Table 4 presents a comparison of several GPP estimates. Noteworthy features include the large range, and the fact that the more recent estimates using SIF suggest a rather higher global total than the earlier estimates (see also Campbell et al., 2017).

**Table 4.** Comparisons of published contemporary (1990-2020) GPP Estimates.

| Estimate (Pg C $yr^{-1}$) | Method | Reference |
|---|---|---|
| 140 | MODIS, SIF, Fluxnet | Joiner et al. (2018) |
| 150-175 | isotopes | Welp et al. (2011) |
| 123±8 | Fluxnet +RS | Beer et al. (2010) |
| 108-130 | FLUXNET, RS, other | Jung et al., 2020 |
| 115-190 | TRENDY models | Cai and Prentice (2020) |
| 167 ±5 | SIF, model assimilation | Norton et al. (2019) |
| 166 ±10 | SIF | MacBean et al. (2018) |
| 120 ±30 | Isotopes | Liang et al. (2017) |
| 131–163 | NIRv | Badgley et al. (2019) |

More recent methods that combine flux tower data with remote sensing data in machine learning algorithms to produce upscaled fluxes (see Jung et al., 2020) yield global GPP estimates that agree well with those obtained from other methods, while providing insights into the processes controlling the carbon cycle of the land biosphere and their changes over time, particularly in the temperate Northern latitudes. Using radar derived estimates of biomass and soil carbon data from the harmonized world soil database and other sources combined with flux estimates of the global product of Beer et al. (2010), Carvalhais et al. (2014) calculated residence times of carbon. They found that the sensitivity of the residence time to soil moisture and temperature did not agree with the sensitivity of a set of DGVMs, while the overall pattern of increasing residence time at higher latitudes was reproduced. The following sections summarize recent results from bottom-up inventories that combine plot-based in situ measurements and remote sensing observations to constrain carbon uptake and emissions from the land biosphere.

Global autotrophic respiration, $R_a$, is estimated at 64 ±12 Pg C $yr^{-1}$ (Ito, 2020). This term is also called “maintenance respiration” and consists mainly of dark respiration. Precise determination of $R_a$ is difficult as it also involves a substantial below ground component, and is expected to vary with biome and climate. Estimates of NPP (GPP – $R_a$), are generally assumed to be of the order of 50% of GPP (i.e., Ito, 2020).

Estimates of soil (heterotrophic) respiration (SHR) associated with the decomposition of organic matter are even more challenging to constrain at regional to global scales. To estimate SHR, Ciais et al. (2020a) combined independent estimates of NPP, NEE and the last seven processes listed in Table 3 from a series of bottom-up inventories and observation-based datasets. They find a value of 39 Pg C $yr^{-1}$ with an interquartile range of 33-46 Pg C $yr^{-1}$. This estimate is lower than those conventionally assumed, but agrees with recent large-scale estimates based on site soil respiration measurements (Jian et al., 2021).

### *5.4 Advances in Remote Sensing of Primary Productivity and Biomass*

Since the launch of LandSat 1 in 1972, carbon cycle scientists have used a variety of optical and near infrared remote sensing observations to characterize plant productivity. One of the earliest indicators was the Normalized Difference Vegetation Index (NDVI), which is defined as the difference between the observed radiances within near-infrared (NIR) and red channels divided by their sum. NDVI and other vegetation indices such as Leaf Area Index (LAI; Zhu et al. 2013) or fraction of Absorbed Photosynthetically Active Radiation (fAPAR; Myneni et al., 2015) have been used as proxies for vegetation activity and photosynthesis. Such indices have also been used as proxies for fAPAR in semi-empirical light-use efficiency models, and combined with estimates of photosynthetically active radiation (PAR) (Zhao and Running, 2010; Smith et al., 2015) or more complex radiative transfer models (Jiang and Ryu, 2016) to estimate GPP. More recently, NDVI has been joined by other optical and near infrared indicators such as the Near Infrared Reflectance of Vegetation, NIRv, and SIF. Recent results derived from these indicators are summarized in this section.

#### *5.4.1 Remote Sensing proxies for Photosynthesis and GPP*

SIF provides a closer proxy for photosynthesis than NDVI. As plants absorb sunlight to perform photosynthesis, a fraction of that light (< 2%) is re-emitted at longer NIR wavelengths (fluorescence), which can be detected in the cores of strong solar Fraunhofer lines or in the molecular oxygen ($O_2$) A- and B-bands by high resolution space-based spectrometers (Meroni et al., 2009; Frankenberg et al., 2014; Guan et al., 2016; Sun et al., 2018).

SIF is a rapidly-responding indicator that shows strong linear relationships with GPP at site-scale and thus has been adopted as a functional proxy for photosynthesis and GPP. The availability of global SIF datasets from space-based sensors, such as GOME-2, GOSAT, OCO-2 and TROPOMI (Figure 11) have substantially expanded the use of this product in studies of the terrestrial carbon cycle. SIF-based estimates of global GPP are beginning to converge, but still differ, ranging from $166 \pm 10$ Pg C $yr^{-1}$ (Table 3). While SIF provides robust estimates of spatial distribution and seasonality of GPP, the strong relationship between SIF and GPP is largely explained by their common dependence on APAR (Mohammed et al., 2019), so that SIF might not be a good proxy for photosynthesis when down regulation occurs under stress conditions (Wohlfahrt et al., 2018; Marrs et al., 2020). SIF is now being combined with other vegetation indices and climate properties in diagnostic process models (e.g., Bacour et al. 2019; Bloom et al. 2020) to provide additional insight into NBE and GPP on regional-scales.

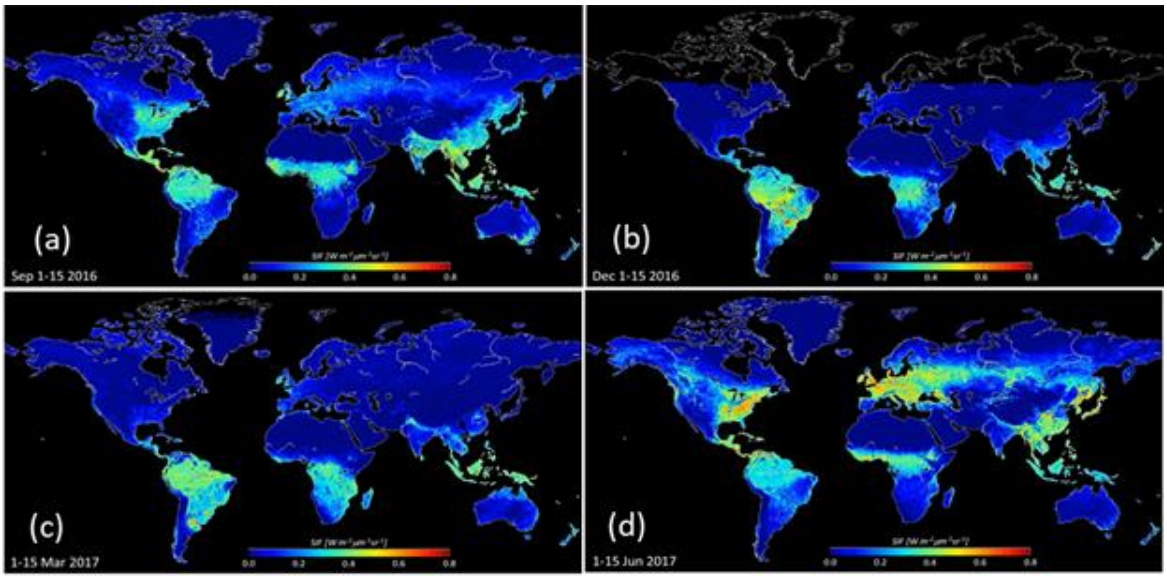


**Figure 11.** OCO-2 observations of SIF for (a) 1-15 September 2016; (b) 1-15 December 2016; (c) 1-15 March 2017, and (d) 1-15 June 2017. Blue indicates low SIF and therefore low photosynthetic activity. The warmer colors indicate higher SIF and higher photosynthetic activity (Ying Sun, Personal communication,2018).

Recently, the NIRv (the product of NIR reflectance by NDVI) has been proposed as an alternative method to estimate GPP that overcomes some of the challenges of other indices and that shows high correlation with SIF. Using NIRv, Badgley et al. (2017) estimate global GPP to be 131-163Pg C $yr^{-1}$, in line with upper estimates of other studies and in line with isotope-based estimates by Welp et al. (2011) and Liang et al. (2017) (Table 4).

### *5.4.2 Advances in Measurements of Above Ground Biomass*

Vegetation optical depth (VOD) retrievals from satellite-based passive microwave instruments are sensitive to vegetation cover and water content (e.g., Liu et al., 2015). Passive microwave measurements have the advantage of not being affected by cloud cover, a common problem with other remote-sensing datasets. High frequency microwave measurements have been used to analyze seasonality and trends in vegetation (Barichivich et al., 2013) and to derive estimates above-ground biomass (AGB) based on empirical relationships between AGB and VOD (e.g., Liu et al., 2011; 2015).

Merging VOD data from multiple space-based microwave sensors, Liu et al. (2015) produced a global survey of AGB based on two decades of observations for both forests and non-forest biomes. They estimate a global average AGB of ~362 Pg C (310 – 422 Pg C) between 1998-2002, of which, 65% was in forests and 17% was in savannahs. Spawn et al. (2020) used satellite products of biomass with land cover with machine learning techniques to produce estimates of global AGB, and link this to below ground carbon density information. These estimates yield a total living terrestrial biomass of 409 Pg C, composed of an AGB of 287 Pg C and a below ground biomass carbon density of 122 Pg C (Figure 12).

Since 2010, the European Space Agency's Soil Moisture and Ocean Salinity (SMOS) measurements of lower frequency L-band microwave radiation at multiple angles have been used

to simultaneously obtain information about soil-moisture and vegetation structure, which are not fully attenuated at high biomass (Konings et al., 2017). Changes in peak VOD between years can be used to infer biomass changes, albeit at coarse (~25 km) spatial resolution (Brandt et al., 2018, Qin et al., 2021). VOD has also been used to derive GPP fluxes (Teubner et al., 2018).

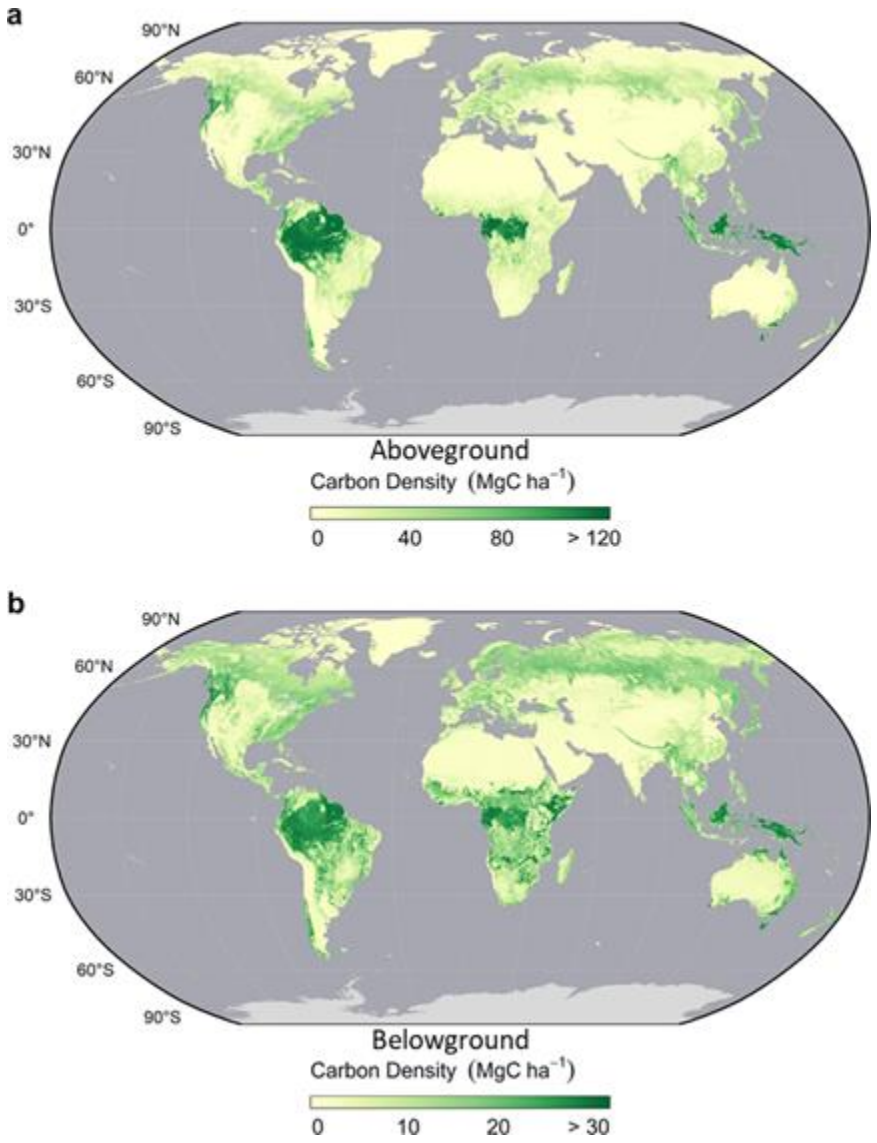


**Figure 12.** Maps of above and belowground living biomass carbon densities. (a) Aboveground biomass carbon density (AGBC) and (b) belowground biomass carbon density (BGBC). Maps have been aggregated at 5 km spatial resolution (Spawn et al., 2020).

The increasing availability of above-ground biomass estimates derived from light detection and ranging (Lidar) and radio detection and ranging (radar) sensors on airborne and space-based platforms are now providing improved spatial coverage and temporal sampling frequency (Xu et al., 2021). The availability of high-resolution space-based remote sensing observations from sensors such as LandSat Operational Land Imager (OLI), Moderate Resolution Spectroradiometer (MODIS) and Sentinel-2 Multi-Spectral Instrument (MSI) have

facilitated improved estimates of the land cover changes (Lamarche et al., 2017) and of burned areas (Chuvieco et al., 2016), and detection of changes in biomass to monitor forest carbon losses and gains (Hansen et al., 2013b). When combined with AGB estimates from VOD, these allow quantifying and attributing changes in biomass to human vs. natural sources (Harris et al., 2016; 2021), as discussed in Sections 5.7 and 5.8.

### *5.5 Progress in Modelling Forest Land Use Change*

For several decades, estimates of emissions from land-use change by the research community were based primarily on a book-keeping model using a stock-change approach (Houghton and Nassikas 2017). This approach combines information on forest area and deforestation rates from the FAO Forest Resource Assessment (FRA) and other sources. Carbon fluxes are based on country-level surveys of vegetation and soil carbon density for different forest ecosystems and response curves for temporal carbon dynamics following disturbance and recovery, e.g., legacy fluxes and regrowth. More recently, satellite-based biomass data are being used in book-keeping approaches (e.g., Rosan et al., 2021) to more accurately reflect spatial variation in carbon stocks, and implicitly include the influence of environmental factors.

Process-based models offer an alternate, complementary approach to estimate land-use emissions. The first generation of DGVMs have been extensively used in land carbon-cycle research (Sitch et al., 2015). They typically build upon a detailed representation of leaf photosynthesis coupled to a water balance scheme and simulate gross fluxes, GPP, $R_a$, NPP, and carbon stocks in vegetation and soils. A new generation of DGVMs include more biological processes. These include nutrient cycling (N and now P), and more comprehensive representations of vegetation demography (Smith et al., 2001; Argles et al., 2020) with explicit representation of mortality, plant succession and temporal development of age/size classes, and explicit disturbance (e.g., fire-enabled DGVMs, Rabin et al., 2017). This enables comprehensive assessments of the impact of land management on the carbon cycle (e.g., forest growth and harvest), and separates effects of environmental and human drivers on the land carbon sink (Houghton et al., 2012). McGuire et al. (2001) pioneered the use of DGVMs in factorial experiment design to enable attribution of the land carbon sink to processes, $CO_2$, Climate and Land Use and Land Cover Change (LULCC) over the $20^{th}$ century.

A similar protocol is adopted for the DGVMs in the annual GCB assessment (Friedlingstein et al., 2021). The DGVM land-use flux is calculated as the difference between two simulations (1700 to present-day): the first (S2) with varying observed historical $CO_2$ and climate but fixed pre-industrial LU and a second (S3) with all three varying ($CO_2$, climate and LUC). However, the natural vegetation in S2 is affected by temporal changes in environmental factors (e.g., $CO_2$ fertilization) - not included in static carbon density maps employed by book-keeping models. One would expect an additional carbon sink in forests relative to faster-turnover cultivated systems, which would be lost with deforestation; this foregone sink is referred to as the Loss of Additional Sink Capacity (Gitz and Ciais, 2003, Sitch et al., 2005; Gasser et al., 2020; Pongratz et al., 2014). Obermeier et al. (2021) has attempted to reconcile these methodological differences between the DGVM approach employed in GCB and book-keeping models.

More recent DGVMs updates capture more land-use change related processes, e.g., shifting cultivation (gross land-cover transitions), grazing/crop harvest and cropland management and wood harvest. Results including these newly incorporated processes suggest a substantial underestimation in land-use emissions in earlier DGVMs, with implications for the magnitude of the natural land sink, given that the net land sink is constrained (Arneth et al., 2017). Recent attempts to reconcile DGVMs estimates with country reporting of anthropogenic forest $CO_2$ sinks address conceptual differences in definitions of anthropogenic land fluxes between DGVMs (used in IPCC) and national GHG Inventories (Grassi et al., 2018).

### *5.6 Net Ecosystem Exchange from Atmospheric Measurements and Inverse Models*

As noted in Section 3, top-down atmospheric inverse models have been used to study the land carbon cycle for more than 40 years. Early in this period, when there were only a few dozen ground-based stations, these flux inversions focused on continental to regional scales, with uncertainty increasing for smaller scales (Kaminski and Heimann, 2001; Chevallier et al., 2010). As the ground-based and airborne in situ network has expanded, its data have been used support flux estimates at regional scales for well-sampled regions, such as Europe (Monteil et al., 2020; Petrescu et al., 2021).

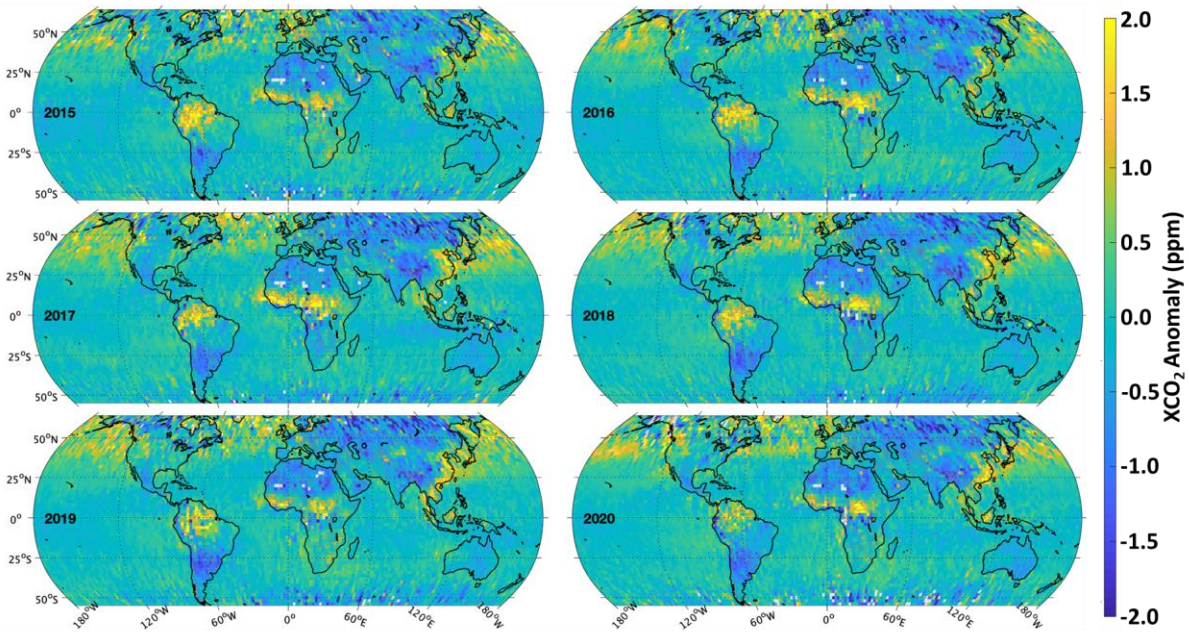


**Figure 13.** Maps of annually-averaged $XCO_2$ anomalies derived from OCO-2 $XCO_2$ estimates from 2015 - 2020. Positive anomalies (yellow) indicate regions that have $XCO_2$ values that are persistently higher than their surroundings while negative anomalies (blue) indicate regions where $XCO_2$ is lower than in the surrounding areas. (Updated from Hakkarainen et al., 2019 with the OCO-2 v10 product).

Space-based remote sensing estimates of $XCO_2$ have dramatically improved the spatial and temporal resolution and coverage of the atmospheric $CO_2$ field, enabling studies at much finer spatial and temporal scales. For example, Hakkarainen et al. (2016; 2019) processed OCO-2 $XCO_2$ observations to filter out the annual growth rate and seasonal cycle to yield maps of

temporally-persistent spatial anomalies (Figure 13). Here, positive $XCO_2$ anomalies are associated with persistent sources while negative $XCO_2$ anomalies are interpreted as persistent sinks. When averaged over the annual cycle, tropical land regions, including the Amazon, north equatorial Africa, and equatorial Asia have positive $XCO_2$ anomalies while, mid- and high-latitude land regions of Asia, North and South America have negative $XCO_2$ anomalies. The positive anomalies in east Asia and western Europe include contributions from intense fossil fuel combustion, biomass burning or other human activities. The positive anomalies over the north Pacific and Atlantic Oceans are just downwind of persistent $CO_2$ sources in east Asia and North America, respectively, indicating the effects of transport rather than local sources.

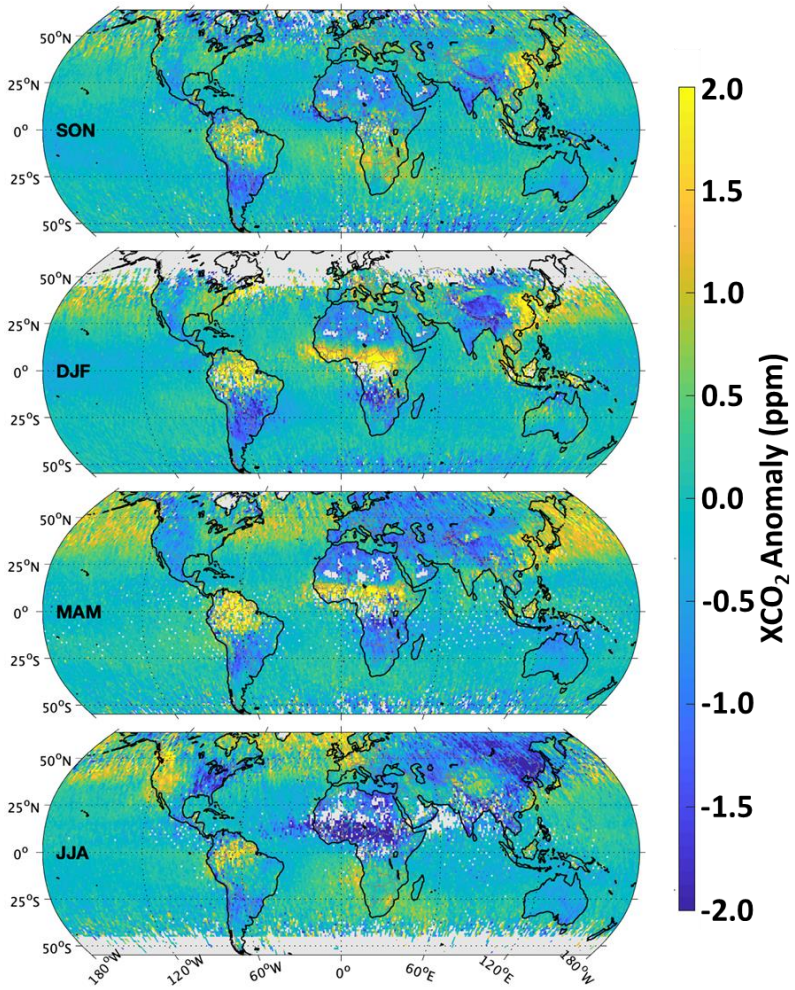


**Figure 14.** Maps of seasonally-averaged $XCO_2$ anomalies derived from OCO-2 $XCO_2$ estimates from 2015 – 2020, including September-October-November (SON), December-January-February (DJF), March-April-May (MAM) and June-July August (JJA). (Updated from Hakkarainen et al., 2019 with the OCO-2 v10 product).

Seasonally averaged maps (Figure 14) show that the $XCO_2$ anomalies over north equatorial Africa transition from negative values during June-August to positive values from December-May. In contrast, the Amazon appears to exhibit mostly positive $XCO_2$ anomalies throughout the year during this period. Strong negative $XCO_2$ anomalies over mid- and high

latitudes in the northern hemisphere in JJA are associated with strong uptake by the land biosphere. These negative anomalies even extend across heavily-industrialized east Asia during this season, as biospheric uptake temporarily balances anthropogenic emissions. The variations across North America are also noteworthy, with the western regions showing positive anomalies during JJA, while the mid-west and eastern United States shows strong negative anomalies. While none of these features are especially surprising, this is the first time that we have been able to quantify the atmospheric $CO_2$ distribution on sub-regional scales over the entire globe on seasonal to annual time scales.

These space-based $XCO_2$ estimates are being combined with ground-based and airborne in situ $CO_2$ measurements and analyzed with atmospheric inverse modeling systems to quantify sub-regional to continental changes in the land biosphere. Early efforts exploited the global coverage provided by GOSAT to constrain regional-scale $CO_2$ flux estimates. These investigations demonstrated the value of the improved coverage provided by the GOSAT data for reducing flux uncertainties, particularly in the tropics, where there are few in situ observations (e.g., Maksyutov et al., 2013; Deng et al., 2016; Byrne et al., 2020b). However, other inverse modeling showed large differences between top-down and bottom-up flux estimates in some regions, revealing limitations of this approach (e.g., Kondo et al., 2015; Reuter et al., 2014). For example, an unrealistically large sink in Europe (Reuter et al., 2014; Kaminski et al., 2017) has been ascribed to biases in the seasonal coverage (Houweling et al., 2015) and/or in the $XCO_2$ estimates themselves (Scholze et al., 2019).

As the accuracy, resolution and coverage of the atmospheric $CO_2$ measurements and inverse modeling systems have improved, the spread between the global land flux estimates from these top-down methods has decreased from > 3 Pg C $yr^{-1}$ to ~1 Pg C $yr^{-1}$ (i.e., Kondo et al., 2020). Significant improvements have been achieved on regional scales as well (Zhang et al., 2021). An ensemble of six inverse models constrained by in situ data used in the 2020 GCB (Friedlingstein et al., 2021) indicates that the Northern extratropics (>30°N) were indeed the main contributor to the global NEE land sink between 2010 and 2019, with a amplitude of -2.9±0.6 Pg C $yr^{-1}$. This is slightly stronger than the northern extra-tropical land sink derived from DGVMs, -2.3±0.6 Pg C $yr^{-1}$. On shorter time scales, an ensemble of nine inverse models constrained by OCO-2 v9 data (Peiro et al., 2022) indicates that the northern extratropical land sink increased from -2.5 to -3±0.25 Pg C $yr^{-1}$ between 2015-2016 and then decreased to -2±0.25 Pg C $yr^{-1}$ in 2017 and to -1.75±0.25 Pg C $yr^{-1}$ in 2018. When this ensemble is constrained by in situ data, the results from 2015-2016 are the same, but the sink increases to -2.75 Pg C $yr^{-1}$ in 2017 and returns to -2.5±.25 in 2018. The source of the $CO_2$ data used to constrain the inverse models explains some of the remaining differences between the top-down and bottom-up results.

Meanwhile, recent inverse modeling intercomparisons indicate that tropical land is not a significant net sink for atmospheric $CO_2$ (Gaubert et al., 2019; Palmer et al., 2019; Crowell et al., 2019; Friedlingstein et al., 2021; Peiro et al., 2022). Gaubert et al. (2019) find near neutral tropical uptake for 2009-2011, but note that given reported emissions from deforestation, this result indicates substantial uptake by intact tropical forests. Friedlingstein et al. (2020) also use an inverse model ensemble constrained by in situ data and find that tropical land was roughly in total carbon balance between 2010 and 2019.

Inverse model ensembles constrained by space-based $XCO_2$ estimates indicate that the tropics are now a net source of $CO_2$ as the $XCO_2$ anomaly maps (Figures 13, 14) suggest. For example, Peiro et al. (2022) find that tropical land was strong source (1.0 to 2.0 Pg C $yr^{-1}$) during

the 2015-2016 El Niño, supporting earlier results by Crowell et al (2019) and Palmer et al. (2019), but then returned to near neutral conditions (-0.5 to 0.5 Pg C $yr^{-1}$) in 2017 and 2018. These results support other recent studies that attribute these net emissions to deforestation, forest degradation, drought and other factors (i.e., Aragão et al., 2018; Wigernon et al., 2020; Qin et al., 2021, Gatti et al., 2014; 2021). However, given the sparseness of the tropical in situ $CO_2$ network and the shortness of the satellite $XCO_2$ data records, it is too soon to determine whether this represents a slow recovery from the intense 2015-2016 El Niño, or if tropical land has permanently transitioned from a net sink to a net source of $CO_2$.

A key set of quantities that explain some of the bias between the top-down and bottom-up estimates are the lateral fluxes of carbon, which are implicitly included in net land-atmosphere fluxes by inversions, but not in those estimated by DGVMs (Ciais, Yao et al., 2020; Ciais et al., 2022). When adjusted for lateral fluxes, the top-down and bottom-up estimates show good agreement on the long-term average land sink, but still show disagreements in the regional partitioning and inter-annual variability of the land sink (Bastos et al., 2020). Several processes contribute to the challenges in constraining the land-sink: large uncertainty in the regional partitioning of fluxes between individual inversions, the representation of land-use change and management in DGVMs, and the ability of DGVMs to simulate responses to disturbances and extreme events such as droughts or fires (Friedlingstein et al., 2020; Bastos et al., 2020).

However, flux inversions provide an integrated estimate of the net surface fluxes, including contributions from fossil fuel burning, land-use change and management, disturbances, $CO_2$ outgassing, etc. This makes attribution of inverse model-based fluxes to specific sectors (e.g., separating between natural and anthropogenic fluxes or fossil fuel and LUC contributions) challenging, especially given the high uncertainty associated with some of these terms. One approach for addressing this limitation combines geostatistical inverse models with MERRA-2 estimates of air and soil temperature, precipitation, soil moisture, humidity, PAR and other variables to identify the processes driving interannual variability (IAV) in the observed $CO_2$ fluxes (Chen et al., 2021a, b). Their results from OCO-2 observations indicate that the tropical grassland biome, including grasslands, savanna, and agricultural lands, contribute as much to IAV as the tropical forests and that temperature and precipitation produce comparable contributions to IAV. This supports the conclusion of Ahlström et al. (2015), but Chen et al. (2021b) note that these results contradict those from most the DGVMs included in the TRENDY project (Sitch et al., 2015; Friedlingstein, et al., 2019; 2020; Piao et al., 2020b).

### *5.7 Long-term Trends in the Land Sink*

Multiple lines of evidence support an increasing sink in the terrestrial biosphere. In innovative studies using atmospheric $CO_2$ and $\delta^{13}C$ measurements, Keeling et al. (1989) pointed out an increase in the retention of $CO_2$ emitted from fossil fuel combustion, which they attributed to an increasing sink in the terrestrial biosphere. These results have been supported by subsequent updates (Keeling et al., 2001) and additional studies using different approaches (McGuire et al., 2001; Khatiwala et al., 2009; Ballantyne et al., 2012; Le Quéré et al., 2009; 2013; 2018a,b; Friedlingstein et al., 2019; 2020; 2021). While the existence of an increasing global land sink is undisputed (Friedlingstein et al., 2020, Fernández-Martínez et al., 2019), the location and drivers of the inferred increase in the past decades remain a matter of debate (Casperson et al., 2000; McGuire et al., 2001, Pacala et al., 2001; Nabuurs et al., 2013; Piao et al., 2009). These include the fertilization effects of elevated $CO_2$ (McGuire et al., 2001),

increased nitrogen deposition in northern latitudes (Fernández-Martínez et al., 2019), agricultural intensification (Zeng et al., 2014), lengthening of the growing seasons in the northern hemisphere and/or vegetation expansion (Forkel et al., 2019) and forest expansion (Casperson et al., 2000) and management (Nabuurs et al., 2013; Erb et al., 2018). Disentangling the compound effects of $CO_2$ fertilization, i.e., the increased rate of photosynthesis resulting from increased levels of $CO_2$ in the atmosphere, and increased temperature and drought, is, however, challenging. Here, we discuss the observational evidence for some of these effects.

The global AGB dataset compiled from microwave VOD measurements by Liu et al. (2015) indicate no statistically significant global trend in AGB (-0.07 Pg C $yr^{-1}$) from 1993-2012. However, they do show large losses over tropical forests (-0.26 Pg C $yr^{-1}$) that were offset by net gains (0.13 Pg C $yr^{-1}$) over temperate and boreal forests. More recently, Xu et al. (2021) used forest inventory plots, airborne laser scanning (ALS) data and satellite lidar inventories of forest height to estimate global AGB and adopted allometric relationships to derive below ground carbon stocks. They conclude that globally, woody carbon stocks are increasing at 0.23 ± 0.09 Pg C $yr^{-1}$. Regions with carbon gains are located in western conifer and boreal forests of North America, tropical forests in Africa, subtropical forests in eastern China, and the boreal forests of eastern Siberia. Tropical forest and subtropical dry forest and savannah lands gained carbon at a rate of 0.09 ±0.04 Pg C $yr^{-1}$. Temperate and boreal forests had accumulation at rates of 0.10 ±0.03 and 0.04±0.02 Pg C $yr^{-1}$.

Satellite observations collected since the 1980s indicate a significant global increase in the area covered by green vegetation, or "greening" (IPCC, 2014; Zhu et al., 2016; Piao et al., 2020b; Cortés et al., 2021). Zhu et al., (2016) used long-term satellite observations of LAI to study this greening trend from 1982-2009. They report a persistent, widespread greening over 25-50% of the global vegetated area. In a more recent study, Piao et al. (2020b) use a combination of vegetation indices (NDVI, LAI, EVI, and NIRv) to quantify global greening between the early 1980s and 2018. They conclude that globally, ~34% of vegetated land shows signs of greening over this period (Figure 15). They also note significant greening over China and India, which they attribute primarily to afforestation and agricultural intensification.

Both studies also note that a small fraction (3 – 4%) of vegetated land experienced browning (less greening) between 1982 and 2014. Piao et al. (2020b) note that there is considerable debate about the relative roles of greenness and brownness over the Amazon due to saturation effects in dense vegetation and contamination by clouds and aerosols. However, they conclude that about 5% of the area has experienced browning, which they attribute to drought, heat stress and human activities, but concede that the relative roles of these processes are not well resolved by these data. In the Arctic, browning is seen over ~3% of the land area, with North American boreal forests exhibiting browning areas nearly 20 times larger than the Eurasian boreal forests (Piao et al., 2020b).

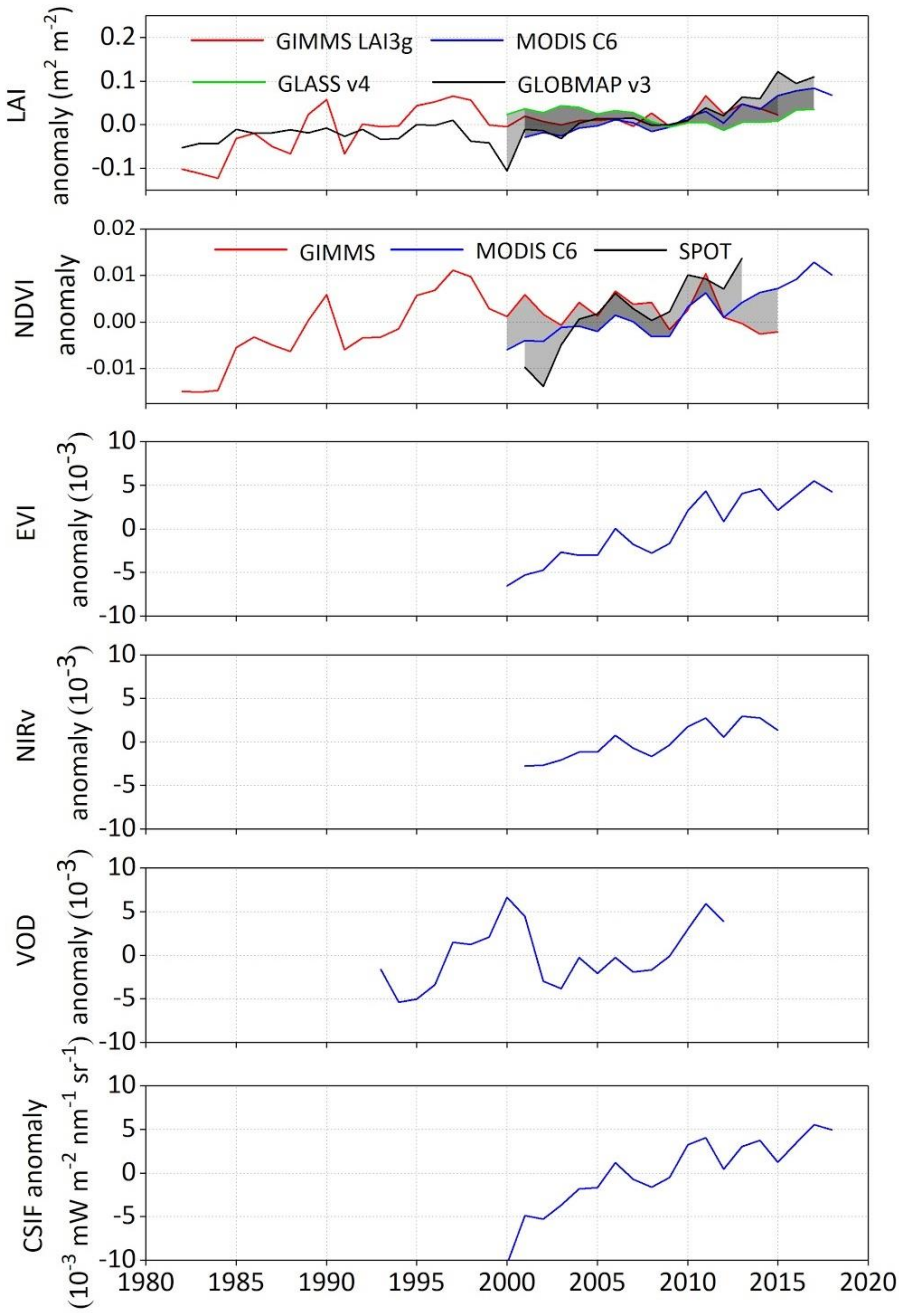


**Figure 15.** Changes in satellite- derived global vegetation indices, including anomalies in the normalized difference vegetation index (NDVI), Enhanced Vegetation Index (EVI), near-infrared reflectance of vegetation (NIRv), vegetation optical depth (VOD) and contiguous solar- induced fluorescence (CSIF) (Data: Piao et al., 2020b.)

At mid- and high-latitudes, bottom-up and top-down models constrained by space-based remote sensing measurements largely reinforce the in situ results, showing a long term increase in the $CO_2$ seasonal cycle amplitude (SCA) and indicate that mid-latitude and boreal forests are strong net sinks of $CO_2$ (Keeling et al., 1996; Graven et al., 2013; Jeong et al., 2018; Byrne et al., 2018; 2020a; Piao et al., 2020b; Liu et al., 2020a). It is important to note that estimates derived

using the stock change approach still differ by as much as a factor of two or three in the rates quoted above (Xu et al., 2021, see their Table 2). With increasing data availability, new satellites (e.g., BIOMASS expected to launch in 2023, and the GEDI instrument on board of the ISS) are expected to reduce uncertainties and increase consistency in the global estimates.

Based on the results presented above, two things can be stated with relative certainty: (1) in the tropics, LUC approximately balances the land sink (Grace et al., 2014, Gatti et al., 2021) and (2) in the northern extratropics, a sink exists that is still growing. The mechanisms driving these long term trends are explored in the following two sub-sections.

### *5.7.1 Mechanisms Driving Long-Term Trends in the Tropical Land Sink*

Long-term changes in the land sink are typically attributed to $CO_2$ fertilization, secular trends in nutrient and water availability, temperature changes, disturbance or other factors, but the relative roles of these processes are often challenging to diagnose because they often work in concert (e.g., Bastos et al., 2019: Piao et al., 2020a; Hubau et al., 2020; Liu et al., 2020a; Gampe et al., 2021). All of these factors have been considered in studies of long term trends in the tropical forest sink. For example, Hubau et al. (2020) assess the carbon sink in intact African and Amazon forests (Figure 16) and conclude that while the African sink strength showed no trend (0.66 Mg C $ha^{-1}$ $yr^{-1}$), the Amazon forest sink slowed down –0.034 Mg C $ha^{-1}$ $yr^{-2}$ between 1983 and 2010, citing Brienen et al. (2015). The results presented in Figure 16 show that this trend has persisted. Hubau et al. (2020) attribute the downward trend in sink strength by intact forests primarily to higher temperature and droughts, leading to increased tree mortality. DGVMs simulate strong $CO_2$-induced sinks in moist tropical forests, counterbalanced by a negative effect of climate change and variability. An improved representation of mortality processes is needed in DGVMs, particularly those relating to drought response.

Other studies have focused on the differing impacts of increasing temperature on photosynthesis and heterotrophic respiration in the tropics. For example, Doughty and Goulden (2008) show that on short time scales, the efficiency of photosynthesis decreases beyond a critical temperature, while that of heterotrophic respiration continues to increase. Mau et al. (2018) suggest that many species of tropical trees may be especially sensitive to these effects. Possible evidence for this behavior was recently obtained by Duffy et al. (2021) using FLUXNET data, albeit with the caveat that $CO_2$ effects on GPP were not considered in their temporal extrapolation. Meanwhile, process-based models provide conflicting insights into the role of plant physiological processes including plant thermal responses and acclimation (McGuire et al., 2001; Friedlingstein et al., 2006; Booth et al., 2012, Mercado et al., 2018). There is also little consensus on how these changes will progress on longer time scales, when heterotrophic carbon limitation on microbial decomposition may also start playing a role (Soong et al., 2019).

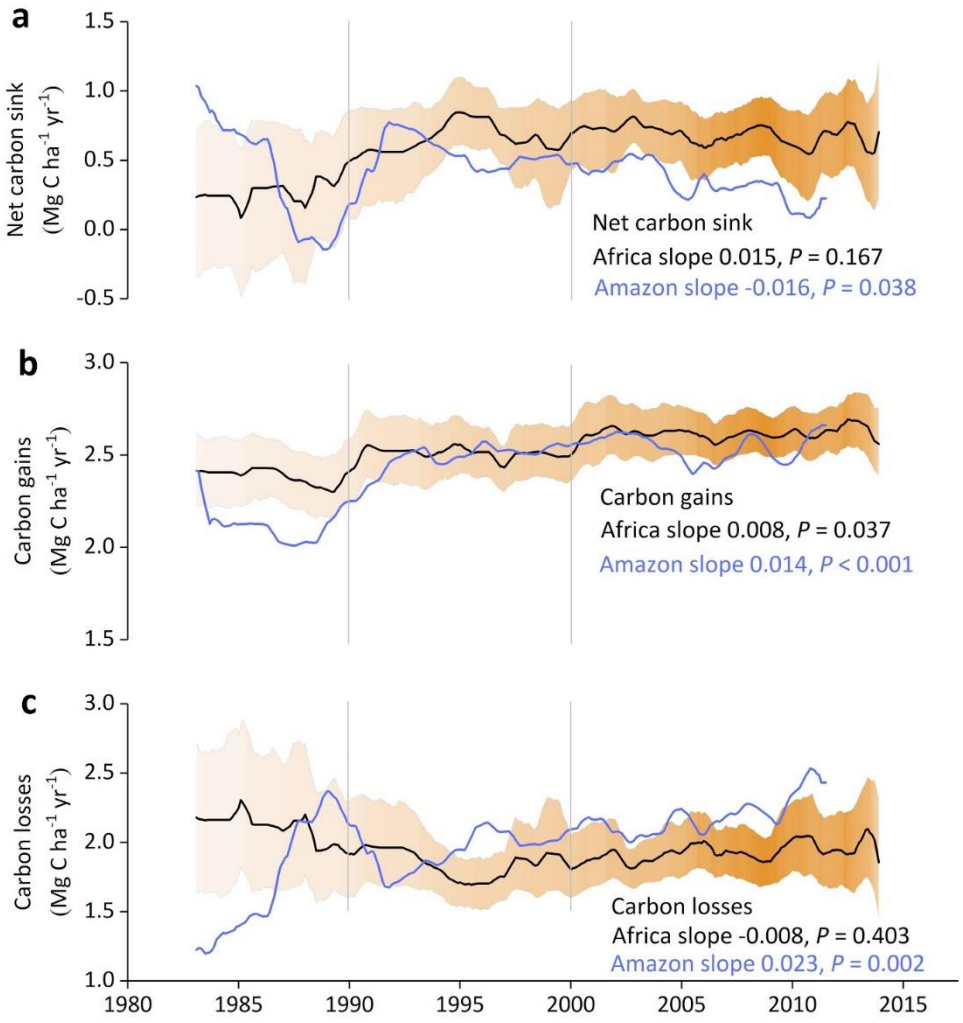


**Figure 16.** Time series of carbon dynamics from structurally-intact old-growth tropical forests in Africa and Amazonia from 1985 through 2015 (Data: Hubau et al., 2020). Note, the net carbon sink in Panel, a, refers to the net of two processes, carbon gains (productivity) and carbon losses (mortality), over intact tropical forests only. To obtain a net carbon sink estimate for the whole-region to compare with atmospheric measurements and inversions (e.g., Gatti et al., 2021), in addition to the intact forest sink, fluxes associated with disturbance (deforestation, degradation through fire and selective logging), secondary forest regrowth and land-use fluxes (fluxes over crop and pasture), must be considered.

### *5.7.2 Mechanisms Driving Long-term Trends in the Extratropical Land Sink*

In the extratropics, studies have focused on identifying the mechanisms responsible for the changes in greening, seasonal cycle amplitude (SCA) and net $CO_2$ uptake across the high-latitude northern forests since at least the 1960s. Unlike the tropics, where heat-related increases in respiration and water stress are key growth limiters, here, the forests have adequate water, but their growth is thought to be limited primary by low light levels, low summer temperatures and short growing seasons (Song et al., 2018). Therefore, vegetation cover and phenology changes in response to warming trends and the effects elevated $CO_2$ have been identified as the likely

drivers of increase in SCA (Graven et al., 2013; Forkel et al., 2019; Piao et al., 2017). At mid-latitudes, Zhu et al. (2016) and Piao et al. (2020b) analyzed their greenness time series with ensembles of DGVMs to identify the primary drivers of the observed increases. Both studies conclude that $CO_2$ fertilization is the primary driver of global greening since the 1980s. However, they concede that other processes dominate on regional scales. For example, Piao et al. (2020b) attribute the enhanced greening over China and India primarily to afforestation and agricultural intensification.

To explain the mechanisms behind the enhanced SCA at higher northern latitudes, Keenan and Riley (2018) used observations of fAPAR collected between 1982 and 2012 to characterize the relationship between maximum annual foliage cover and summer warmth index. They attribute these changes to the recent warming (reduced spatial extent of temperature limitation) rather than $CO_2$ fertilization. In another observation-based study, Liu et al. (2020a) analyzed data from a variety of sources to determine the extent to which temperature changes alone could account for the long-term trends in SCA and $CO_2$ uptake of high latitude northern forests. They analyze space-based observations of SIF and $XCO_2$ from OCO-2 to estimate monthly mean GPP and NEE, respectively, at 4°×5° resolution for 2015-2017 and derive total ecosystem respiration, TER, as the difference between NEE and GPP. They fit simple exponential functions to the observed temperature dependence of GPP/PAR and TER and then hindcast spatially-resolved, monthly mean estimates of these variables to produce a time series spanning 1960 to 2014. They find that growing season mean temperature (GSMT) is the dominant driver of fPAR and GPP, explaining 70% of the observed spatial and temporal variability at latitudes between 50N and 75N over this time period, accounting for a 60% to 70% of the observed ~20% growth in SCA.

While these results support the conclusions of Keenan and Riley (2018), they appear to contradict the studies by Zhu et al. (2016) and Piao et al. (2020b), which analyzed greenness time series with ensembles of DGVMs to identify the primary drivers of the observed greening trends. Both studies conclude that $CO_2$ fertilization is the primary driver of global greening since the 1980s. Other studies based on atmospheric data and biogeochemical models have also pointed out a key role of $CO_2$ fertilization in SCA trends (Forkel et al., 2019; Thomas et al., 2016 Bastos et al., 2019; Piao et al., 2017).

A noteworthy difference between the observation-based studies and the model-based studies is the relationship between SCA and temperature adopted at high northern latitudes. While Keenan and Riley (2018) and Liu et al. (2020a) found that fPAR, NEE, and SCA are positively correlated with temperature at 50N-75N, model-based studies (e.g., Bastos et al., 2019) find a negative relationship between SCA and temperature during the growing season at latitudes > 40N, which they attribute to moisture deficits and fires. This would be consistent with browning trends at high latitudes, attributed to disturbances such as fires, harvesting and insect defoliation (Beck and Goetz, 2011, Cortés et al., 2021). Regional differences across the arctic and boreal regions might also play a role. For example, North American boreal forests exhibit browning areas nearly 20 times larger than the Eurasian boreal forests (Harris et al., 2016; Piao et al., 2020b). Large-scale fire disturbances and insect infestation such as those from the bark beetle (Hlásny et al., 2021) have also been seen in browning areas in temperate regions in the past decade. Peñuelas et al. (2017) identified recent signs of a slow-down of SCA increase at Barrow, pointing to a limitation of the positive effect of temperature in stimulating northern hemisphere $CO_2$ uptake, possibly due to increasingly negative impacts of weather extremes and

disturbances. This lack of consensus on the relative roles of temperature, $CO_2$ fertilization and disturbance at high latitudes must be resolved, given their implications for the future evolution of this rapidly changing part of the land carbon cycle.

## *5.8 Patterns and Drivers of Interannual Variability in the Land Sink*

In spite of the steady increase in fossil fuel $CO_2$ emissions over recent decades, the annual growth rate in atmospheric $CO_2$ varies markedly from year to year (Ballantyne et al., 2012; Piao et al., 2020a). The global growth rate of atmospheric $CO_2$ positively correlates with temperature. This relationship has been used to diagnose and constrain the future climate-carbon cycle feedback (Cox et al., 2013). The strong positive correlation between atmospheric growth rate and tropical temperature has been a conundrum, since the dynamics in tropical ecosystems are thought to be primarily driven by variations in moisture, i.e., dry season length and severity. Indeed, Jung et al. (2017) argue that at the local scale, the tropical carbon cycle is driven by moisture but at larger spatially scales the moisture signal is lost due to compensatory water effects (essentially there is greater spatial variability in moisture and thus regional signals counterbalance) leaving the temperature signal, which is more spatially coherent at the larger spatial scales.

Humphrey et al. (2018) challenged this conclusion showing a strong relationship between atmospheric $CO_2$ growth rate and observed changes in terrestrial water storage. Disentangling the land response to variation in temperature and water is complicated, for a variety of reasons. For example, soil-moisture-atmosphere feedbacks modify temperature and humidity, which impact vapor pressure deficit (VPD), which drive plant stomata opening and closure. Yuan et al. (2019) found that an increase in VPD reduces global vegetation growth, while Liu et al. (2020a) suggest that soil moisture dominates dryness-related stress on global productivity, using SIF as a proxy. Finally, Humphrey et al. (2021) clarified the picture, showing how global NEE variability is driven by temperature and VPD effects controlled by soil moisture.

### *5.8.1 The Role of Climate Variability in the Interannual Variations of the Land Sink*

Large interannual variations in global NBE are attributed to modes of climate variability, e.g., the impacts of the El Niño Southern Oscillation (ENSO) in tropical and southern regions (Figure 17). Two other modes of coupled ocean-atmosphere variability in addition to ENSO influence land-atmosphere $CO_2$ fluxes over the globe. The Pacific Decadal Oscillation (PDO) impacts tropical regions and extratropical North and South American regions. The Atlantic Multidecadal Oscillation (AMO) influences $CO_2$ fluxes in Eurasia, northern North-America, and is an important influence in the Sahel and sub-tropical South American regions (Bastos et al., 2017; Zhu et al., 2017). These three modes of climate variability are thought to explain inter-annual variability (IAV) in $CO_2$ fluxes over more than 50% of the land surface (Zhu et al., 2017). Other processes, such as global cooling following large volcanic eruptions also contribute to IAV (e.g., Lucht et al., 2002; Angert et al., 2004).

In the Northern extratropics, regional modes of atmospheric variability also play a role in IAV in $CO_2$ fluxes. Dannenberg et al. (2018) showed that two leading modes of north Pacific variability controlled the onset of growing seasons over large regions in North America: the West-Pacific and the Pacific-North American patterns. In the Southern Hemisphere, in addition to ENSO, two other modes influence land carbon uptake: the Indian Ocean Dipole (IOD: Marchant et al., 2006) and the Southern Annular Mode (SAM; Marshall, 2003). Positive phases of IOD have been associated with reduced GPP and increased bushfires in Australia, and

increased productivity in South Africa (Cai et al., 2009, Wang et al., 2021). Cleverly et al. (2016) have shown that periods when synchrony between ENSO, the IOD and the SAM occur, they were associated with carbon cycle extremes in Australia.

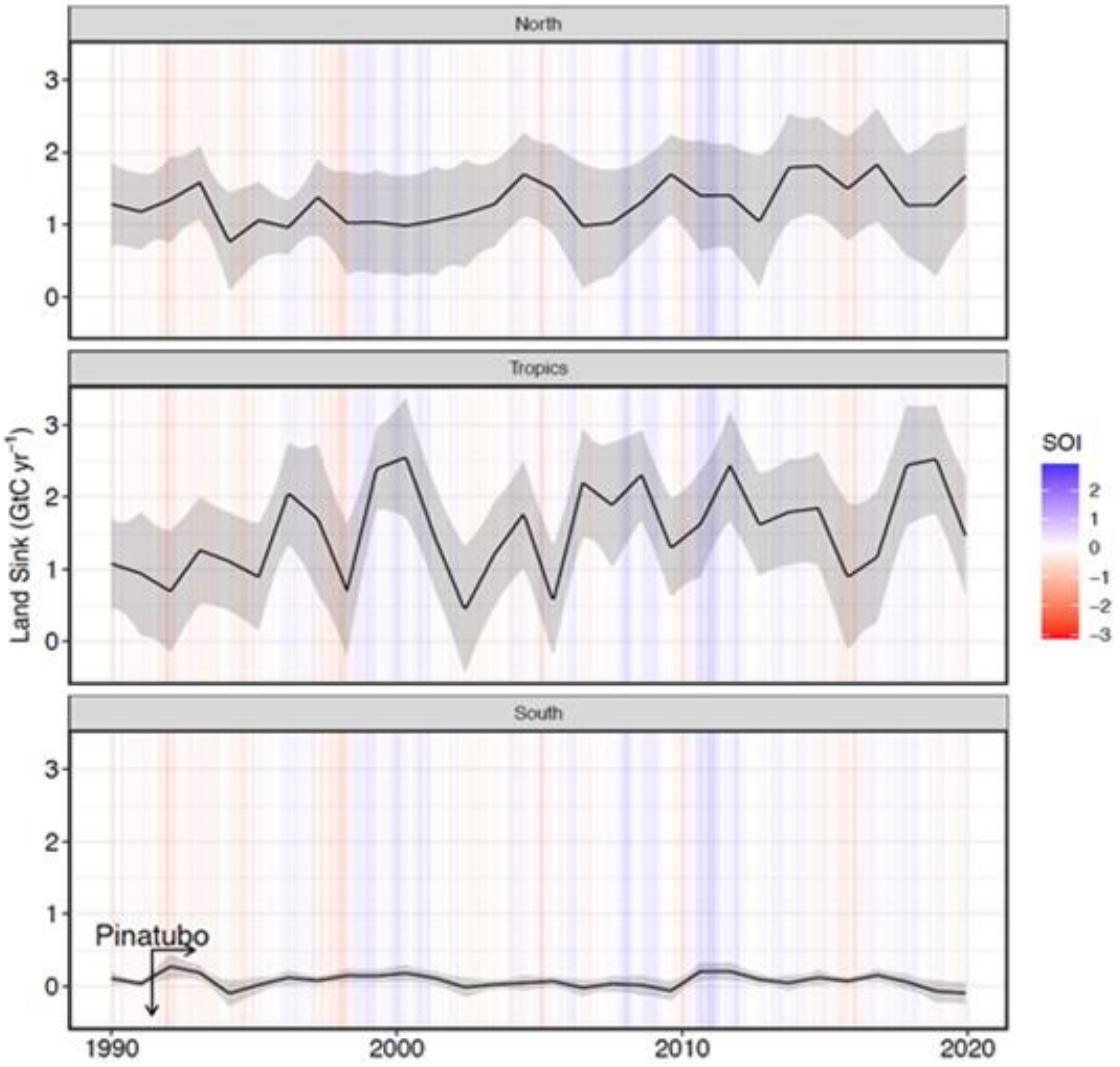


**Figure 17.** The multi-model mean land sink as derived from 14 TRENDY DGVMs for three regions and Southern Oscillation Index (SOI) between 1990 and 2020. The grey band represents 1 standard deviation. The Mount Pinatubo eruption in June 1991 in the Philippines is indicated with a vertical arrow with a horizontal arrow showing the duration of its effect on regional and global climate.

Extreme weather and climate conditions and associated disturbances are important contributors to the regional land carbon cycle (Reichstein et al., 2013; Zscheischler et al., 2014). While a few extremes have been found to explain 78% of IAV in GPP, they only accounted for 8-22% of IAV in NEE (Zscheischler et al., 2014). In their study, Zscheischler et al. (2014) indicate that drought is the most common driver of negative extremes in GPP (>50% of the

events), followed by fires (20-30% of events). There is also evidence for an increasing impact of warm droughts on northern ecosystem productivity in recent decades (Gampe et al., 2021).

Drought is a primary driver of reductions in photosynthesis and enhanced tree mortality through hydraulic failure (Rowland et al., 2015). Major droughts in recent years have been associated to strong reductions in regional GPP and net carbon uptake (Ma et al., 2016; Wolf et al., 2016; Peters et al., 2020), in some cases even turning ecosystems from sinks to sources of $CO_2$ (Ciais et al., 2005; van der Laan-Luijkx et al., 2015). In addition to direct impacts, droughts further contribute to subsequent disturbances, e.g., by increasing fire risk or insect outbreaks, and can lead to lagged tree mortality and consequent carbon losses (Anderegg et al., 2015).

Globally, fires constitute a major flux of carbon to the atmosphere (1.3-3.0 Pg C $yr^{-1}$, van der Werf et al., 2017), which is followed by regrowth sinks in the subsequent years. Even though fires can have both natural and human (e.g., deforestation, degradation and management ) drivers, hot and dry conditions increase fire risk through increased fuel flammability. Therefore, all else being equal (i.e., human drivers), hot and dry periods, such as El Niño years, are associated with higher burnt area and $CO_2$ emissions, e.g., the massive burning associated in part with the 1997 El Niño over equatorial Asia. An increase in "mega- or extreme-" wildfires and associated large carbon emissions are anticipated with continued warming (Bowman et al., 2017; 2021; van der Velde et al., 2021).

### *5.8.2 ENSO as a Dominant Driver to Interannual Variability*

El Niño is a climate mode associated with coupled atmosphere-ocean dynamics, originating in the tropical Pacific basin, with a frequency of between 2 and 7 years (McPhaden et al., 2006, p.200). At the onset of El Niño (ENSO "warm-phase"), the trade-winds weaken, reducing the upwelling along the western coast of South America, allowing the pool of warm surface water and associated convection and rainfall to move eastwards towards the central Pacific. South East Asia and eastern Australia experience a large reduction in precipitation and increased warming, and teleconnections lead to reductions in precipitation over Amazonia and east Africa (Diaz et al., 2001). Because ENSO usually peaks during the wet seasons over tropical continents, this reduced rainfall leads to longer and more severe dry seasons, decreasing photosynthesis and reducing plant carbon uptake by tropical forests.

In contrast, La Niña (ENSO "cold phase") is associated with stronger than usual trade winds and wetter, cooler conditions that promote enhanced land carbon uptake over Equatorial Asia and Amazonia. The TRENDs in land carbon cYcle (TRENDY; Sitch et al., 2015) results for the tropical latitude band ($30^oN$-$30^oS$) in Figure 10 illustrate the impact of El Niño and La Niña on the land carbon uptake. Because tropical forests usually account for ~50% of the global NPP by terrestrial ecosystems, these impacts are reflected in the global growth rate of atmospheric $CO_2$. However, there is some evidence for an asymmetry in land response to ENSO (Cadule et al., 2010), whereby rainforests are less responsive to increased precipitation during La Niña than water deficit during El Niño. In addition to the asymmetry between El Niño and La Niña events, two types of ENSO can be distinguished: the "East Pacific", described above, and the "central Pacific" type, where the warm SST pool is shifted to the central Pacific region (Kao and Yu, 2009). Central Pacific El Niño events have been associated with even stronger responses by the land carbon cycle (Dannenberg et al., 2021).

ENSO is also the dominant mode of interannual variability in air-sea $CO_2$ fluxes (Feely et al., 1999; McKinley et al., 2004; 2017; Chatterjee et al., 2017). With the El Niño phase,

upwelling of high-DIC waters in the eastern equatorial Pacific is reduced, lowering surface ocean $pCO_2$. At the same time, reduced wind speeds slow gas exchange. The net effect is to substantially reduce eastern equatorial Pacific $CO_2$ outgassing. In the La Niña phase, upwelling is enhanced and outgassing is increased. The magnitude of these variations is up to +-0.5 Pg C $yr^{-1}$, and the type of ENSO event is a significant modulator of the flux (Liao et al., 2020). The effect on atmospheric $CO_2$ concentration from the ocean from ENSO is thus the opposite from that from land, with a greater ocean sink during El Niño and a lesser ocean sink during La Niña.

In addition to the tropical regions, ENSO is known to influence IAV in land $CO_2$ fluxes in some extratropical regions, especially semi-arid regions in the Southern Hemisphere such as Australia, South Africa and parts of Southern South America (Poulter et al., 2014; Bastos et al., 2013). Indeed, tropical drylands are now thought to contribute about equally or more to IAV in the global carbon cycle as humid tropical biomes (Ahlström et al., 2015; Piao et al., 2020a). These ecosystems are characterized by lower biomass and productivity than forests. Nevertheless, their vast spatial area allows them to be important to the global carbon cycle. Extra-tropical ecosystems are estimated to contribute up to 30% to global land sink IAV (Piao et al., 2020a).

While it is difficult to show the impact of climate extremes such as a strong El Niño using in situ inventory data alone, bottom-up inventories of AGB stocks compiled from microwave remote sensing observations provide a temporally denser record of such impacts. For example, contrary to the conclusions of Hubau et al. (2020), who found negligible change in the African forest, Wigneron et al. (2020) show that there was a strong “legacy effect” after the 2015-2016 El Niño event in both African and Amazonian forests, extending the duration of the response in both regions (0.9 and 0.5 Pg C loss in 2014-2017 respectively). For the overall tropics, Fan et al. (2019) use VOD data from microwave sensors to show how changes in the AGB of the forests of tropical Africa and tropical Asia contributed strongly to the IAV in $CO_2$ growth rates, but concluded that AGB in semi-arid biomes dominated the IAV in these growth rates.

### *5.8.3 The Best Observed ENSO Ever - the 2015-2016 El Niño*

The record-setting 2015-2016 El Niño was the first large ENSO event for which atmospheric $CO_2$ and SIF estimates were available at high spatial and temporal resolution from space based platforms. This data-rich perspective provided a more comprehensive description of the impacts of climate perturbations on the exchange of carbon between land and ocean reservoirs and the atmosphere on regional scales. Chatterjee et al. (2017) compared $XCO_2$ estimates derived from Orbiting Carbon Observatory-2 (OCO-2) observations over the central and eastern tropical Pacific basin to an $XCO_2$ climatology of this region based on observations from the Greenhouse gases Observing SATellite (GOSAT). Between March and July 2015, these comparisons reveal a 0.5 ppm decrease in $XCO_2$ that is attributed to reductions in outgassing in the tropical Pacific Ocean (Chatterjee et al., 2017). By September of 2015, these reduced $XCO_2$ values were replaced by 0.5 to 2 ppm increases in $XCO_2$ that were attributed to reduced uptake and increased emissions of $CO_2$ by tropical forests in South America, Africa and tropical Asia (Liu et al., 2017; Heymann et al., 2017; Palmer et al., 2019; Crowell et al., 2019; Figure 18).

Observations of SIF provided similar insights. Koren et al. (2018) find that SIF was strongly suppressed in late 2015 over tropical areas with anomalously high temperatures and reduced soil moisture. Their observations show that SIF fell below its climatological range starting from the end of the 2015 dry season (October), but returned to normal levels by February

2016 when atmospheric conditions returned to normal. Importantly, the impacts of the El Niño were not uniform across the Amazon basin.

Additional insight into the tropical land carbon cycle's response to the 2015-2016 El Niño was gained by comparing coincident observations of $XCO_2$ anomalies and SIF (Liu et al., 2017). Specifically, the largest positive $CO_2$ anomalies derived from the space-based $XCO_2$ estimates are seen in regions where SIF observations indicate the highest photosynthetic activity (Figure 11). This suggests that in spite of significant growth, tropical forests are now emitting more $CO_2$ than they absorb, when integrated over the annual cycle. This may be due to human activities, such as deforestation and forest degradation or climate related factors such as temperature-dependent respiration increases, drought stress, fires, and other processes.

Liu et al. (2017) find that the pan-tropical biosphere released an additional 2.5 ± 0.34 Pg C into the atmosphere, or about 78% of the global total emissions of $CO_2$ from the land biosphere during the 2015-2016 El Niño compared with the 2011 La Niña year. These values are substantially larger than those inferred from ensembles of bottom-up land surface models or inverse models constrained the sparse in situ network alone (Bastos et al., 2018; Crowell et al., 2019). Liu et al. find that emissions originated throughout the tropics with 0.91 ± 0.24, 0.85 ± 0.21, and 0.60 ± 0.31 Pg C from tropical South America, tropical Africa, and tropical Asia, respectively. Although the enhanced emissions from these three regions were comparable, *different* processes appeared to dominate in each region. Fire emissions dominated over tropical Asia. Both increased respiration and fires associated with historically high temperatures dominated over tropical Africa. Increased atmospheric $CO_2$ mixing ratios over the Amazon in 2015-2016 were attributed to GPP reductions associated with drought. These results support the hypothesis that El Niño related increases in $CO_2$ growth rates are primarily due to tropical land carbon fluxes, but they show that specific mechanisms can differ from continent to continent.

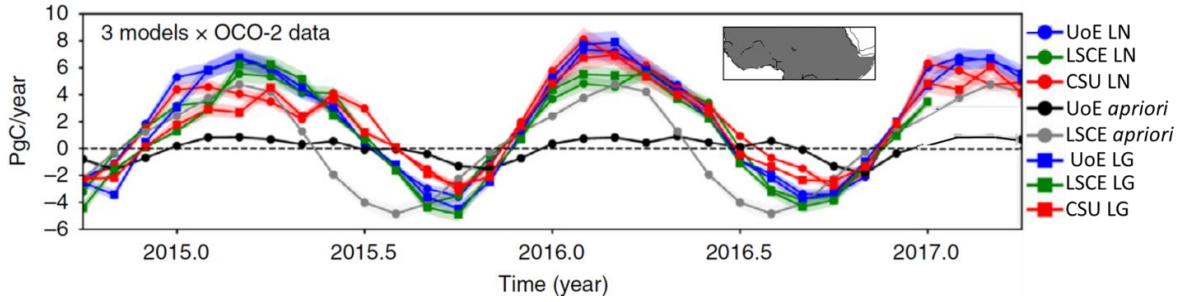


**Figure 18.** $CO_2$ fluxes from tropical northern Africa inferred from the University of Edinburgh (UoE), LSCE and Colorado State University (CSU) models constrained by in situ $CO_2$ measurements as well as $XCO_2$ data from GOSAT and OCO-2. Positive fluxes indicate $CO_2$ emissions from the land surface to the atmosphere. LN and LG denote OCO-2 $XCO_2$ measurements taken using nadir and glint observing modes, respectively. The geographical region is shown in the inset. Fluxes inferred from OCO-2 data have larger amplitudes and a larger seasonal cycle than those from in situ data (Adapted from Palmer et al., 2019).

Palmer et al. (2019) and Crowell et al. (2019) use ensembles of models to analyze in situ $CO_2$ measurements along with $XCO_2$ and SIF observations from GOSAT and OCO-2 (Figure 18). Like Liu et al., in 2015–2016, they find that the largest $CO_2$ emissions were over western

Ethiopia and western tropical Africa, where there are large soil organic carbon stores and substantial LUC. While the amplitude of the $XCO_2$ anomalies that produced these sources may have been overestimated in the early OCO-2 $XCO_2$ products used in this investigation (version 7), they clearly reveal an important source of emissions from the tropical carbon budget that is largely missing from in carbon flux inverse models constrained by *in situ* measurements alone.

It is interesting to compare the terrestrial carbon cycle's response to the two largest recent El Niño events in 1997 and 2015/16. Large fire emissions in equatorial Asia were responsible for ~1 Pg C $yr^{-1}$ emissions in 1997 (i.e., Page et al., 2002), yet far smaller fire emissions were estimated in 2015/16. This is largely due to the timing of the El Niño in relation to the dry season (i.e., in 2015/16 the El Niño was about 1 month later). El Niño events are associated with reductions in GPP in Amazonia and a lagged increase in respiration (Braswell et al., 1997). This is likely related to the lagged mortality associated with forest degradation, and thus respiration from the larger necromass pool. More generally, forest degradation is becoming a larger carbon source than deforestation, with highest ground-level forest fires associated with drought years.

As the 2015-2016 El Niño transitioned to a weak La Niña in 2017 and then to more neutral conditions in 2018, OCO-2 $XCO_2$ estimates indicate that tropical forests, once thought to be significant net sinks of $CO_2$ (Pan et al., 2011; Sellers et al., 2018) may now be net sources (Palmer et al., 2019; Crowell et al., 2019; Peiro et al., 2022). The atmospheric inversions support the inferences from $XCO_2$ anomaly maps (Hakkarainen et al., 2016; 2019; Figures 13, 14) which show positive $XCO_2$ anomalies over tropical forests with amplitudes of 1-2 ppm above the background since 2015. For the Amazon, both the spatial extent of the positive anomaly and the amplitude of the inferred source were greater during the 2015–2016 El Niño (~0.5 Pg C $yr^{-1}$) than in later years (0.1-0.2 P C $yr^{-1}$), but both indicate that this region has been a net source from season to season and from year to year since 2015. These conclusions are consistent with results inferred from in situ $CO_2$ profiles described by Gatti et al. (2021), which indicate that the Amazon has been a source of $CO_2$, rather than a sink since 2010.

Positive $XCO_2$ anomalies over topical Africa and Southeast Asia are seen on annual time scales (Figures 13). However, tropical African fluxes are negative during June-July-August (Figure 18), indicating that this region becomes a weak sink during that season (Palmer et al., 2019). These conclusions are supported by some satellite-based aboveground biomass studies (Baccini et al., 2017; Wigneron et al., 2020), but are inconsistent with plot-based studies (Pan et al., 2011; Hubau et al., 2020), which conclude that tropical forests are absorbing less $CO_2$, but are still a net sink of carbon.

### *5.9 Observations Needed to Advance Understanding of Trends in the Land Carbon Sink*

The overall picture that emerges from recent observations of AGB stocks is that the classical sinks in the tropical humid forests are slowly losing strength, with these changes amplified by deforestation. In extra-tropical areas, greening has taken place due to afforestation, increased agriculture and longer growing seasons. In some parts of the Arctic and boreal regions, browning, i.e., a loss of vegetation activity, is increasing. These trends provide the fragile background for a still slowly increasing land uptake. The underlying causes for these increases are complex and consist of interacting processes of $CO_2$ fertilization, nutrient and water availability compounded by variability and secular changes in climate. On top of this, the impact of human activities including deforestation, afforestation and intensifying agriculture are additional complications.

This myriad of interacting processes complicates predictions of the future trajectory of the terrestrial sink in a warming climate. Until now, the sink has grown in harmony with increased fossil fuel emissions with the result that the airborne fraction has remained remarkably constant over the past 60 years or so. Theoretical and empirical evidence, such as that summarized in this paper, suggests that the sink may stop growing at some point in the future as water and nutrient shortages will start to impede increased growth.

### *5.9.1 Linking Stocks and Fluxes with Bottom-up Measurements and DGVMs*

One factor that has impeded progress in the analysis of trends inferred from AGB stocks is they are not well represented in the current generation of DGVMs. For example, Sitch et al. (2015) use an ensemble of nine DGVMs to study global and regional processes and trends in the land sink for a period extending from 1990 - 2009. They conclude that for this period, the global land sink is increasing, led by $CO_2$ fertilization of plant production, with the largest increases seen in the natural ecosystems of the tropics. They find no significant trend in northern land regions. More recent studies with updated versions of DGVMs now estimate increasing trends in the Northern Hemisphere land sink, although with large spread across models (Ciais et al., 2019; Fernández-Martinez et al., 2019) and regional mismatches with observation-based estimated (Bastos et al., 2020).

Fortunately, advances in bottom-up observation capabilities and modeling tools are coming on line to facilitate more comprehensive and responsive monitoring and analysis of the land carbon cycle. Ground-based estimates of stocks and fluxes will continue to provide the most accurate and site-specific information. However, remote sensing observations from airborne and space-based active and passive sensors and modeling tools will play an increasingly important role for upscaling these results to yield useful constraints on regional to global scales. While new space-based datasets provide an increasingly diverse set of measurements to monitor the land-surface with high spatial and temporal resolution, long-term in situ datasets still provide crucial information to properly constrain patterns and drivers of long-term trends and inter-annual to decadal variability.

### *5.9.2 Space-based Estimates of Fluxes and Stocks*

Xiao et al. (2019) review the evolution of remote sensing observations of terrestrial carbon stocks over the past 50 years, spanning the electromagnetic spectrum from the visible, infrared, and microwave. They then review the methods being used to analyze the observations to yield quantitative estimates of carbon stocks and fluxes, including vegetation indices, SIF, light use efficiency models, DGVMs, as well as data driven (including machine learning) techniques. Xiao et al. discuss the use of these data and analysis techniques to quantify the impacts of disturbances and to quantify uncertainties in carbon stock estimates, noting advances achieved by integrating in situ and remote sensing observations into progressively more advanced, process-based carbon cycle models. Looking forward, they predict substantial improvements in our ability to track AGB stocks through the use of merged datasets, such as the NASA Harmonized LandSat and Sentinel 2 (HLS) products, ultra-high resolution imaging products from QuickBird, IKONOS, and UAVs, lidar measurements from GEDI, future active microwave products from NASA's NISAR (Rosen et al., 2016), TanDEM-L and BIOMASS missions (Quegan et al., 2019).

While in situ and space-based measurements of AGB play a critical role in efforts to monitor trends in managed and natural forests, they do not have the sensitivity needed for

monitoring the rapid turnover of carbon stocks in croplands and grasslands, where the biomass changes are spatially extensive, but below the detection limits of these measurements. Until recently, high resolution imaging observations and moderate resolution estimates of vegetation indices provided the primary tools for scaling up plot-based observations to national and continental scales. Recently, these capabilities have been augmented by space-based observations of SIF. SIF relates the emission of excess radiative energy from the photosynthesis process of leaves at two wavelengths (685 nm and 740 nm) to photosynthesis or GPP. Estimates of SIF from GOME, GOME2, GOSAT, OCO-2 and TROPOMI are increasingly being used to monitor crop and grassland productivity and for crop yield prediction (Guan et al., 2017; He et al., 2020; Peng et al., 2020; Parazoo et al., 2020; Qiu et al., 2020; Yin et al., 2020). Future SIF observations from the ESA FLuorescence EXplorer (FLEX), Japan's GOSAT-GW, NASA's GeoCarb, and the Copernicus CO2M missions promise substantial improvements in resolution.

Space-based observations of $XCO_2$ and SIF are being combined with observations of vegetation indices (LAI, NDVI, NIRv), VOD and other environmental properties to provide new insights into the high latitude terrestrial carbon cycle. Unlike for the tropics, top-down estimates of $CO_2$ fluxes derived from space-based observations of $XCO_2$ anomalies over northern temperate and boreal forests tend to reinforce the conclusions from other observations and modeling studies. During the northern hemisphere summer, negative $XCO_2$ anomalies (JJA in Figure 14) and large positive SIF emissions (Figure 11d) prevail across most of this region. NBE estimates from flux inversion experiments constrained by space-based $XCO_2$ data (Figure 19) show negative NBE in regions where models constrained by satellite-derived reflectance and SIF data (e.g., Figure 11 and Joiner et al., 2018) show moderately strong GPP (Liu et al., 2020a). These satellite-derived NBE estimates therefore indicate that northern forests have continued to act as significant net $CO_2$ sinks as the $CO_2$ seasonal cycle amplitude has grown in response to warming.

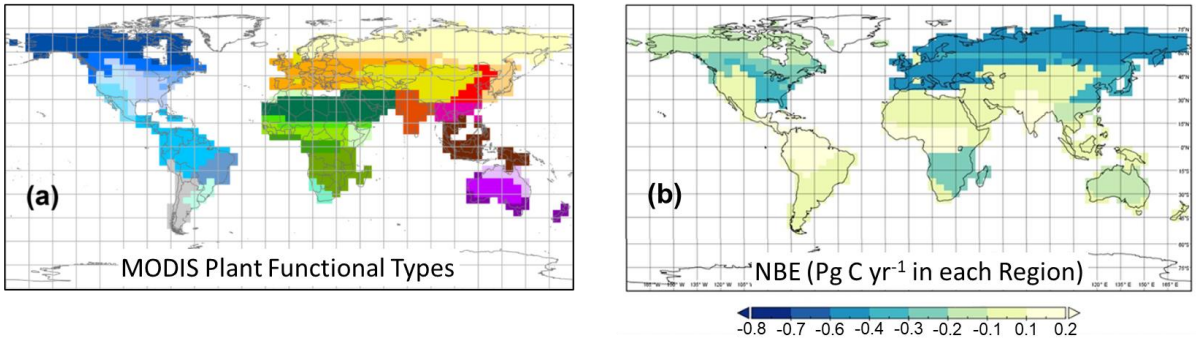


**Figure 19.** (a) Regional mask based on MODIS International Geosphere-Biosphere Programme (IGBP) plant functional types (see Liu et al., 2020a for a more complete description) (B) Net Biospheric Exchange (NBE) from $XCO_2$ and SIF, expressed in Pg C $yr^{-1}$ from each region shown in panel (a) for 2010-2018. Negative NBE indicates sinks while positive values indicate sources. (adapted from Liu et al., 2020a).

Observations of $XCO_2$ and SIF also provide unique opportunities to study the relationships between the land and atmospheric carbon cycles and the hydrological cycle. Yin et al. (2020) combine SIF with atmospheric $CO_2$ observations to quantify the effects of large-scale flooding on cropland carbon sequestration. Widespread flooding during spring and early summer

of 2019 delayed crop planting across the U.S. Midwest. As a result, satellite observations of SIF from OCO-2 and the TROPOspheric Monitoring Instrument (TROPOMI) reveal a delay of 16 days in the seasonal increase of photosynthetic activity relative to 2018, along with a 15% lower peak photosynthesis. Yin et al. find that the 2019 anomaly produced an estimated GPP reduction of -0.21 Pg C in June and July that was partially compensated in August and September with a +0.14 Pg C increase. The growing season integral corresponds to a 4% reduction in cropland GPP for the Midwest, but a 3% increase for areas where cropland occupies less than 10% of the land. Using an atmospheric transport model, they show that a decline of ~0.1 Pg C in the net carbon uptake in June and July is consistent with observed ~10 ppm $CO_2$ enhancements in the midday boundary layer from the Atmospheric Carbon and Transport - America (ACT-America) aircraft and the ~1 ppm increases in $XCO_2$ seen by OCO-2.

In another study, Gonsamo et al. (2019) combined OCO-2 SIF observations with soil moisture (SM) observations from NASA's Soil Moisture Active Passive (SMAP) mission to study the impact of environmental limiting factors on terrestrial ecosystem productivity of drylands and croplands. For drylands (dry sub-humid, semi-arid, and arid zones) and the majority of croplands, soil water content is typically low and topsoil moisture is critical for plant growth. As expected, SMAP SM retrievals show positive daily relationships with OCO-2 SIF for drylands and croplands of the tropics and Australia, where SM is limiting plant growth and concurrent data records are sufficient to make statistical inferences. Negative relationships between SIF and SM were observed in forested areas of mid-latitude dry sub humid zones with high average annual SM. In these regions, SIF showed a positive relationship with air temperature. They find strong evidence that the OCO-2 SIF is accurately capturing monthly SMAP SM dynamics, particularly for regions with distinct seasonality of rainfall such as Sub-Saharan North Africa, Indian subcontinent, and southern Africa.

Other advances in remote-sensing capabilities are expected to accelerate progress in monitoring, verification and understanding of temporal changes in biomass and productivity. Until very recently, the remote-sensing community has pioneered static biomass maps, based on a composite of products and field-truthing, or inferred biomass change from products like VOD. Now, with new missions and sensors, e.g., GEDI and BIOMASS, the community is at the cusp of direct monitoring biomass change at scale for the first time. This information in combination with monitoring of productivity directly and land cover change, will revolutionize research on the land carbon cycle.

To fully exploit these new measurements to describe long term trends in the terrestrial carbon cycle, the in situ and remote sensing measurements must be reconciled so that their climate data records can be combined to increase their spatial and temporal resolution and coverage. The protocol for cross-validating aboveground biomass products described by Duncanson et al. (2019) and the effort by the Forest Observation Initiative to develop a global in situ forest biomass databases for validating remote sensing observations (Schepaschenko et al., 2018) are positive steps in this direction.

While the current generation of DGVMs and other terrestrial biosphere models are evolving rapidly and providing important insights into the processes driving the land carbon cycle, these modeling tools are still yielding widely diverging results the uptake of $CO_2$ by the land biosphere and its trends (e.g., Fisher et al., 2014; Sitch et al., 2015; Keenan and Williams, 2018; Parazoo et al., 2020). These limitations have raised concerns about their use in $CO_2$ emission inventory development activities (Grassi et al., 2018; Petrescu et al., 2020). Pioneering

model intercomparison efforts such as the Carbon-Land Model Intercomparison Project (C-Lamp; Randerson et al., 2009) are being followed up by the International Land Model Benchmarking (ILAMB) project (see https://www.ilamb.org/) to address these concerns and accelerate the development of these critical tools.

## 6 Discussion

When integrated over the industrial age, the land sink associated with intact forests and other natural parts of the terrestrial biosphere has roughly balanced sources associated with LUC while the ocean has been a cumulative net sink of anthropogenic carbon emissions (Friedlingstein et al., 2021). Since 1958, when continuous atmospheric $CO_2$ measurements have been available, $CO_2$ emissions from fossil fuel combustion have increased by about a factor of four, from less than 2.5 Pg C $yr^{-1}$ to almost 10 Pg C $yr^{-1}$ in 2019. During this period, the land sink grew as well, absorbing a near constant fraction of the anthropogenic emissions (~30%). Together, sinks in ocean and on land have absorbed enough anthropogenic $CO_2$ to limit the fraction that has remained in the atmosphere to a remarkably constant value around 45% (Raupach et al., 2014). This implies that, to first order, the uptake by the ocean and land sinks has increased proportionally with the emissions (Friedlingstein et al., 2021).

There has been debate as to whether increases in the airborne fraction since 1958, i.e., declines in sink efficiency, are already observable (Canadell et al., 2007; Knorr 2009; Gloor et al., 2010; Raupach et al., 2014). Even if an increasing airborne fraction is not yet detectable, process-level understanding and regional trends indicate that the airborne fraction should increase as climate change progresses (Raupach et al., 2014; Canadell et al., 2021). While the exact timing and magnitude of changes in the land and ocean sinks remains unclear, the likelihood is high that substantial climate-carbon feedbacks will occur during this century. Any upward change in the airborne fraction, or reduction in sink capacity, will decrease the allowable fossil carbon that can still be burned without violating the temperature targets specified in the Paris Agreement.

For the ocean, despite remaining uncertainties and missing closure terms, distinct methodologies for quantifying the ocean uptake of anthropogenic $CO_2$ agree that the sink has increased over the industrial era, including in recent decades. Since the uptake of atmospheric $CO_2$ on annual to decadal time scales is primarily controlled by the $pCO_2$ gradient at its surface, the carbon sink is expected to grow as long as near-exponential growth of atmospheric $pCO_2$ continues. However, if anthropogenic emissions are reduced, atmospheric $pCO_2$ will grow more slowly, and thus there will be a reduced ocean carbon sink even if the ocean circulation and chemical buffer capacity do not change (Ridge and McKinley, 2021). To understand these likely changes, it is essential that ocean carbon studies start to focus more attention on the near-term response to emission mitigation scenarios (Hausfather and Peters, 2020). If emissions are not mitigated, current climate models suggest that by the middle to late 21st century, a slowing ocean overturning rate and reduced chemical capacity in the ocean will reduce the rate of growth in the global ocean sink (Randerson et al., 2015).

To develop an integrated ocean carbon observing system that can track the evolution of the ocean sink on the annual to interannual timescales most relevant to climate change policy, we need to sustain existing and continue to develop improved observation systems for the surface and interior ocean. Ocean carbon instruments deployed on autonomous platforms are revolutionizing the spatial and temporal resolution and coverage of ocean carbon measurements,

but reduced uncertainties in the carbonate constants are needed to fully exploit these data. High-quality shipboard observations will continue to be required. We also need improved ocean hindcast models and better understanding of uncertainties in observation-based data products derived through statistical extrapolation of sparse surface ocean $pCO_2$ data in order to track the real-time evolution of the ocean carbon sink and its decadal trend reliably.

For the land carbon cycle, the current state, trends and near-future evolution is less clear. Classical sinks in the tropical humid forest sinks are slowly losing their strength and these changes are amplified by the losses associated with deforestation, forest degradation and extreme climate events. In the extratropics, multiple data sources support the existence of an increasing terrestrial sink, driven by $CO_2$ fertilization, afforestation, agricultural intensification and other factors. Across the Arctic and boreal regions, which are experiencing roughly twice the average rate of global warming, most regions have seen significant increases in GPP, NBE and SCA since the 1960s due to higher growing season temperatures and other factors. However, a small fraction of this region is seeing reduced NBE that is attributed to increases in fire disturbances, drought stress, and insect infestation. Both improved observations and models are needed to track these changes as the carbon cycle continues to respond to human activities and climate change.

Space-based remote sensing observations are helping to revolutionize our ability to monitor the response of the global carbon cycle to anthropogenic forcing and a changing climate. In the ocean, sea surface temperature and chlorophyll are critical to process-based and machine learning extrapolations of sparse $pCO_2$ data to global coverage. From a bottom-up perspective, microwave and lidar measurements are providing higher spatial and temporal resolution estimates of AGB stocks. SIF measurements are providing a more responsive estimate of light use efficiency and $CO_2$ uptake by plants. From a top-down perspective, space-based remote sensing estimates of $XCO_2$ are complementing ground-based and aircraft in situ measurements with much greater spatial and temporal resolution and coverage.

These space-based measurements can reinforce or contradict conclusions about the land carbon cycle inferred from ground-based in situ measurements, painting a somewhat controversial picture of the evolution of the land carbon cycle. For example, in the tropics, both space-based microwave estimates of AGB (Wigneron et al., 2020) and top-down atmospheric inverse models constrained by space-based estimates of $XCO_2$ (Liu et al., 2017; 2020; Palmer et al., 2019; Crowell et al., 2019; Gatti et al., 2021) indicate that the humid tropical forests did not fully recover from the 2015-2016 El Niño, and have transitioned from net sinks to net sources of $CO_2$. More generally, the space-based measurements are also providing more information about rapid changes in the land carbon cycle associated with severe weather, such as droughts (Gonsamo et al., 2019; Castro et al., 2020) and floods (Yin et al., 2020). They are also beginning to provide estimates of $CO_2$ emissions from fossil fuel combustion and other human activities (Hakkarainen et al., 2016; 2019; Wang et al., 2018; Hedelius et al., 2018; Wu et al., 2018; 2020; Reuter et al., 2019).

In spite of these advances, the reliability of the space-based remote sensing results are still a subject of substantial debate within the land carbon cycle community. This is especially true for the tropics, where $CO_2$ fluxes derived from the space-based $XCO_2$ estimates differ in both sign and magnitude from the results of earlier flux inversion experiments constrained by bottom-up stock or flux estimates or ground-based in situ measurements of atmospheric $CO_2$. This apparent inconsistency suggests one of three possibilities. First, the space-based $XCO_2$

estimates might still include biases that compromise the accuracy of the top-down flux estimates. Recent efforts to validate the space-based $XCO_2$ estimates using measurements from TCCON and other standards (Wunch et al., 2017) indicate biases with amplitudes less than one third as large as the observed tropical $XCO_2$ anomalies. However, there are few TCCON stations or other validation capabilities in the tropics. Second, fluxes constrained by surface in situ measurements, alone, may tell an incomplete story of the land carbon cycle in sparsely sampled regions. The spatial resolution and coverage provided by surface in situ measurements of carbon stocks, fluxes, or atmospheric $CO_2$ are still very limited, especially in the tropics and boreal regions, where the largest flux differences are seen. Both top-down and bottom-up methods may yield unreliable results where there are few measurements. Third, flux estimates based on the much denser space-based $XCO_2$ measurements may be tracking changes in the natural carbon cycle on time and space scales too short to be resolved by the in situ measurements of stocks or $CO_2$ concentrations. A tropical land carbon monitoring system with even greater spatial and temporal coverage is needed to track these changes as the these areas continue to respond to human activity and climate change.

While these space-based observations and top-down inverse models are providing new insights into this system, they have also revealed measurement gaps and modeling limitations that must be addressed to develop a true global carbon monitoring system that can track changes in both natural and anthropogenic sources and sinks of $CO_2$ on policy relevant time and space scales. For example, space-based remote sensing observations of atmospheric $CO_2$ and land and ocean surface properties can expand the coverage and resolution of surface-based in situ measurements. However, passive remote sensing observations are largely precluded in persistently cloudy regions such as tropical rain forests, or mid- and high-latitude forests during the fall, winter and spring. These regions are often centers of action in the carbon cycle, but are also among the most challenging to observe systematically with surface-based in situ measurement systems. Similarly, remote sensing observations provide little insight into the carbon budget of the interior ocean, but here networks of autonomous in situ sensors have great potential to greatly expand opportunities for gathering critical ocean carbon data. Like remote sensing observations, their data typically has larger uncertainties and biases than conventional shipboard in situ measurements. Thus, a robust ocean carbon observing system will require continued shipboard observations for calibration and validation.

These perspectives reinforce the continuing need to maintain and expand the ground-based, ship-based and airborne $CO_2$ measurement networks. These networks fill three critical needs. First, as noted above, in situ measurements are needed to complement the coverage provided by remote sensing observations in persistently cloudy regions. In addition, because the air-sea flux of $CO_2$ is determined mainly by the $pCO_2$ gradient between the ocean surface layer and the atmospheric surface boundary layer, in situ vertical profiles of near-surface atmospheric $CO_2$ concentrations are critical for validating flux estimates over the ocean. Second, because surface and airborne in situ and surface remote sensing observations are more accurate than space-based remote sensing measurements, these data are critical for validating the space-based remote sensing measurements. Finally, while atmospheric $CO_2$ and $CH_4$ can now be measured from space with the accuracies needed to quantify surface fluxes, other critical greenhouse gases ($N_2O$, CFCs, HCFCs, $SF_6$ etc.) can only be measured to adequate accuracy with ground-based and airborne sensors. Other species that are useful for distinguishing fossil fuel from biospheric $CO_2$ emissions, such as carbon-14 ($^{14}C$) can also only be measured in situ (Miller et al., 2012; 2020).

To address these needs, national agencies such as the U.S. National Oceanic and Atmospheric Administration (NOAA), Japan's National Institute for Environmental Studies (NIES) and European organizations, including the European Space Agency (ESA), Copernicus, Integrated Carbon Observation System (ICOS) and IAGOS, are working with WMO Global Atmospheric Watch (GAW) and the Global Climate Observing System and the Global Ocean Observing System (GCOS, GOOS) to coordinate and expand the deployment of ground-based, ocean and airborne in situ sensors. While the number of ground-based and airborne $CO_2$ monitoring stations has grown slowly over the past decade, new measurement capabilities are coming on line that promise substantial increases in coverage. The up-looking remote sensing measurements being collected by the TCCON spectrometers are being complemented by measurements from smaller, less costly, and more portable Bruker EM27/SUN systems. These spectrometers are now being deployed as networks in urban settings (Hedelius et al., 2018) and in remote locations (Frey et al., 2019). In situ vertical profiles of $CO_2$, $CH_4$ and other gases are now being collected at altitudes as high as 25 km by AirCore instruments deployed on low-cost weather balloons (Karion et al., 2010; Baier et al., 2020). Additional in situ profiles and upper tropospheric measurements are now being made by commercial aircraft in Japan's Comprehensive Observation Network for Trace gases by Airliner (CONTRAIL) and Europe's In-service Aircraft for a Global Observing System (IAGOS).

The world's space agencies are actively working to coordinate ambitious plans for an expanded space-based remote sensing capability that supports atmospheric $CO_2$ measurements, high resolution maps of land surface type and biomass and ocean biological productivity. These efforts are being led by the Committee on Earth Observation Satellites (CEOS) and Coordination Group on Meteorological Satellites (CGMS) through their Joint Working Group on Climate (WGClimate) Greenhouse Gas Task team. The modeling systems needed to ingest and analyze the data collected by these expanding measurement systems are also advancing. However, efforts to coordinate carbon cycle modeling efforts are receiving less attention from the carbon cycle science community and their stakeholders.

## 7 Conclusions

Fossil fuel use, LUC and other human activities are now adding more than 10 petagrams of carbon to the atmosphere each year. These emissions have increased the atmospheric $CO_2$ mixing ratio by almost 50% since the beginning of the industrial age and would have produced much larger changes if natural sinks in the land biosphere and ocean had not removed over half of this anthropogenic $CO_2$. As the world embarks on efforts to monitor and control $CO_2$ emissions, there is growing evidence that the natural carbon cycle is evolving in response to human activities, severe weather, disturbances and climate change.

Our understanding of the carbon cycle and its response to natural and anthropogenic forcing has grown steadily over the past two decades as more advanced carbon cycle measurement systems have been deployed and their results have been analyzed with more sophisticated top-down atmospheric $CO_2$ flux inversions as well as bottom-up diagnostic and prognostic carbon cycle models. These measurements and models reveal a strongly coupled, dynamic system that responds on daily, to seasonal, to interannual time scales across spatial scales spanning individual fields, forest plots or coal-fired power plants on land or individual eddies in the ocean to entire continents or ocean basins.

On decadal or longer time scales, measurements of changes in carbon stocks in the ocean and on land provide a reliable integral constraint on fluxes of $CO_2$ to the atmosphere. These measurements show that while the ocean and terrestrial biosphere now absorb comparable amounts of anthropogenic $CO_2$, LUC emissions have roughly balanced the terrestrial sink over the industrial era and the ocean has provided the primary cumulative net sink of anthropogenic carbon. Over this period, the $CO_2$ uptake by the ocean has increased as the atmospheric $CO_2$ partial pressure ($pCO_2$) has increased nearly exponentially and the ocean overturning has continually circulated from depth to surface, thus exposing pristine deep waters to the anthropogenically-perturbed atmosphere. However, additional study is needed to reconcile diverging estimates of the decadal trend of the ocean sink. For the land carbon cycle, the emerging picture is regionally dependent. Over the past three decades, the uptake of $CO_2$ by intact tropical humid forests appears to be declining. These reductions in the tropical land sink are offset by net increases across mid- and high-latitudes associated with $CO_2$ fertilization, afforestation, the agricultural green revolution, and longer growing seasons associated with climate change.

Direct measurements and model-derived estimates of $CO_2$ fluxes at the Earth's surface provide additional insight into variability on seasonal to decadal timescales. Surface ocean $pCO_2$ measurements and ocean models indicate that the global ocean carbon sink did not grow significantly over the 1990s, but then grew steadily since 2000, a pattern that can be explained, to first order, by the changing growth rate of atmospheric $pCO_2$. This implies that a rapid decline of the ocean sink can be expected when atmospheric levels are reduced through emission reductions. The evolution of the land sink is more difficult to predict given its ongoing declines in strength in tropical regions and enhancements in strength across the extratropics, both strongly driven by human activities and climate change.

While these observations and models are providing new insights into the carbon cycle, they are also revealing measurement gaps and modeling limitations that will have to be addressed to diagnose its current state and predict its evolution. In particular, they reinforce the urgent need for more comprehensive measurements of stocks, fluxes and atmospheric $CO_2$ concentrations in humid tropical forests and at high latitudes, which appear to be experiencing rapid changes. This requires expanded ground-based and airborne measurement capabilities, because these regions are intrinsically difficult to monitor with emerging remote sensing techniques due to persistent cloud cover and limited sunlight at high latitudes during the winter. Similarly, existing uncertainties in the measurements and the physical and biological processes controlling air-sea $CO_2$ fluxes on seasonal to decadal time scales support the need for continued ship-based observations combined with expanded deployments of autonomous platforms with next-generation sensors to quantify ocean-atmosphere fluxes with increased accuracy and greater spatial and temporal resolution. These updates, combined with ongoing advances in space-based remote sensing and modeling capabilities are essential elements of the global carbon monitoring system that is critically needed to diagnose ongoing trends in the emissions and uptake of $CO_2$ by the land biosphere and oceans and to predict their evolution as the climate evolves.

## 8 Open Research

This is a review of other published work. No new data has been created or archived specifically for this manuscript. Original data are available through the citations listed here. Figures have been redrawn to avoid copyright conflicts.

## 9 Acknowledgments

Some of the work presented here was performed at the Jet Propulsion Laboratory, California Institute of Technology under contract to the National Aeronautics and Space Administration (NASA). Government sponsorship acknowledged. Figure 6 was designed by GAM and Natalie Renier, WHOI Creative, with funding from Ocean Carbon & Biogeochemistry (OCB) Project Office that has support from the US National Science Foundation (NSF) and NSF, NASA. We thank Amanda Fay for assistance with Figures 7 and 8. GAM acknowledges support from NSF OCE-1948624 and US National Oceanic and Atmospheric Administration (NA20OAR4310340). HD was supported by the European Commission, Horizon 2020 Framework Programme (VERIFY, grant no. 776810, COCO2 grant no. 958927) and the Netherlands Earth System Science Centre (NESSC), financially supported by the Ministry of Education, Culture and Science (OCW) (grant 024.002.001). JH acknowledges funding from the Initiative and Networking Fund of the Helmholtz Association (Helmholtz Young Investigator Group Marine Carbon and Ecosystem Feedbacks in the Earth System, MarESys), Grant Number: VH- NG-1301. TT acknowledges support from the EU H2020 framework program (EuroSea, grant no. 862626). AB acknowledges funding by the European Space Agency Climate Change Initiative ESA-CCI RECCAP2 project (ESRIN/ 4000123002/18/I-NB). The writing of this paper was initiated at the GCOS joint panel meeting in Marrakech, 18-22 March, 2019. We thank Mike O'Sullivan for the provision of Figure 17 and the TRENDY consortium modelers for use of the multi-model mean ensemble. We also wish to acknowledge the tremendous value of the products produced annually the Global Carbon Project.

## 10 References

Ahlström, A., Raupach, M. R., Schurgers, G., Smith, B., Arneth, A., Jung, M., Reichstein, M., Canadell, J. G., Friedlingstein, P., Jain, A. K., and Kato, E. (2015). The dominant role of semi-arid ecosystems in the trend and variability of the land $CO_2$ sink, *Science*, **348**, 895–899. doi: 10.1126/science.aaa1668

Álvarez, M., Fajar, N. M., Carter, B. R., Guallart, E. F., Pérez, F. F., Woosley, R. J. and Murata, A. (2020). Global Ocean Spectrophotometric pH Assessment: Consistent Inconsistencies. *Environmental Science and Technology,* **54**, 10977-10988. doi:10.1021/acs.est.9b06932

Anav, A., Friedlingstein, P., Beer, C., Ciais, P., Harper, A., Jones, C., Murray-Tortarolo, G., Papale, D., Parazoo, N. C., Peylin, P., Piao, S., Sitch, S., Viovy, N., Wiltshire, A. and Zhao, M. (2015). Spatiotemporal patterns of terrestrial gross primary production: A review. *Rev. Geophys.*, **53**, 785–818. doi:10.1002/2015RG000483

Anderegg, W. R. L., Hicke, J. A., Fisher, R. A., Allen, C. D., Aukema, J., Bentz, B., Hood, S., Lichstein, J. W., Macalady, A. K., McDowell, N., Pan, Y., Raffa, K., Sala, A., Shaw, J. D., Stephenson, N. L., Tague, C. and Zeppel, M. (2015). Tree mortality from drought, insects, and their interactions in a changing climate. *New Phytologist*, **208**: 674-683. doi:10.1111/nph.13477

Andrew, R. M. (2019). Global $CO_2$ emissions from cement production, 1928–2018. *Earth System Science Data*, **11**, 1675–1710. doi: 10.5194/essd-11-1675-2019

Andrew, R. M. (2020). A comparison of estimates of global carbon dioxide emissions from fossil carbon sources. *Earth System Science Data,* **12**, 1437–1465. doi:10.5194/essd-12-1437-2020

2296 Angert, A., Biraud, S., Bonfils, C., Buermann, W. & Fung, I. (2004). $CO_2$ seasonality indicates
2297 origins of post-Pinatubo sink. *Geophys Res Lett*ers, **31**, L11103. doi:
2298 10.1029/2004GL019760
2299 Aragão, L. E. O. C., Anderson, L. O., Fonseca, M. G., Rosan, T. M., Vedovato, L. B., Wagner, F.
2300 H., Silva, C. V. J., Silva Junior, C. H. L., Arai, E., Aguiar, A. P. Barlow, J., Berenguer, E.,
2301 Deeter, M. N., Domingues, L. G., Gatti, L., Gloor, M., Malhi, Y., Marengo, J. A., Miller, J.
2302 B., Phillips, O., L., and Saatchi, S. (2018). 21st Century drought-related fires counteract the
2303 decline of Amazon deforestation carbon emissions. *Nature Communications*, **9**, 536. doi:
2304 10.1038/s41467-017-02771-y
2305 Argles, A. P. K., Moore, J. R., Huntingford, C., Wiltshire, A. J., Harper, A. B., Jones, C. D., and
2306 Cox, P. M. (2020). Robust Ecosystem Demography (RED version 1.0): a parsimonious
2307 approach to modelling vegetation dynamics in Earth system models, *Geoscientific Model*
2308 *Development*, **13**, 4067–4089. doi:10.5194/gmd-13-4067-2020
2309 Arneth, A., Sitch, S., Pongratz, J., Stocker, B. D., Ciais, P., Poulter, B., Bayer, A. D., Bondeau,
2310 A., Calle, L., Chini, L. P., Grasser, T., Fader, M, Friedlingstein, P., Kato, E., Li, W.,
2311 Lindeskog, M., Nabel, J. E. M. S., Pugh, T. A. M., Robertson, E., Viovy, N., Yue, C. and
2312 Zaehle, S. (2017). Historical carbon dioxide emissions caused by land-use changes are
2313 possibly larger than assumed, *Nature Geoscience*, **10**, 79-84. doi: 10.1038/NGEO2882.
2314 Aumont, O., Orr, J. C., Monfray, P., Ludwig, W., Amiotte-Suchet, P. and Probst, J. -L. (2001).
2315 Riverine-driven interhemispheric transport of carbon. *Global Biogeochemical Cycles.* **15**,
2316 393–405. doi:10.1029/1999GB001238
2317 Aumont, O., Ethé, C., Tagliabue, A., Bopp, L. and Gehlen, M. (2015). PISCES-v2: An ocean
2318 biogeochemical model for carbon and ecosystem studies. *Geoscientific Model Development*,
2319 **8**, 2465–2513. doi:10.5194/gmd-8-2465-2015
2320 Ayers, J.M. and Strutton, P.G. (2013). Nutrient variability in Subantarctic Mode Waters forced by
2321 the Southern Annular Mode and ENSO: Subantarctic mode water nutrients. *Geophysical*
2322 *Research Letters,* **40**, 3419–3423. doi:10.1002/grl.50638
2323 Bacastow, R. B., Keeling, C. D., and Whorf, T. P. (1985). Seasonal amplitude increase in
2324 atmospheric $CO_2$ concentration at Mauna Loa, Hawaii, 1959–1982. *Journal of Geophysical*
2325 *Research: Atmospheres*, **90**, 10529– 10540.
2326 Baccini, A., Walker, W., Carvalho, L., Farini, M., Sulla-Menashe, D. and Houghton, R. A.
2327 (2017). Tropical forests are a net carbon source based on aboveground measurements of
2328 gain and loss. *Science.* **358**, 230–234. doi:10.1126/science.aam5962
2329 Bacour, C., Maignan, F., MacBean, N., Porcar-Castell, A., Flexas, J., Frankenberg, C., Peylin, P.,
2330 Chevallier, F., Vuichard, N., and Bastrikov, V. (2019). Improving estimates of Gross
2331 Primary Productivity by assimilating solar-induced fluorescence satellite retrievals in a
2332 terrestrial biosphere model using a process-based SIF model, *Journal of Geophysical.*
2333 *Research-Biogeosciences*, **124**, 3281–3306
2334 Badgley G., Field C. B., Berry J. A. (2017). Canopy near-infrared reflectance and terrestrial
2335 photosynthesis. *Science Advances*, **3**, e1602244. doi: 10.1126/sciadv.1602244. PMID:
2336 28345046; PMCID: PMC5362170
2337 Badgley, G. Anderegg, L. D. L., Berry, J. A., and Field, C. B. (2019). Terrestrial gross primary
2338 production: Using NIRV to scale from site to globe. *Global Change Biology*, **25**, 3731-
2339 3740. doi: 10.1111/gcb.14729

Baier, B., Sweeney, C., Wolter, S., Newberger, T. and Higgs, J. (2020). 2017-2018 Full-Column Greenhouse Gas Sampling Field Campaign Report. DOE/SC-ARM-19-014

Baker, D. F., Doney, S. C., and Schimel, D. S. (2006a). Variational data assimilation for atmospheric $CO_2$, *Tellus, B*, 359–365. doi: 10.1111/j.1600-0889.2006.00218.x

Baker, D. F., Law, R. M., Gurney, K. R., Rayner, P., Peylin, P., Denning, A. S., Bousquet, P., Bruhwiler, L., Chen, Y. H., Ciais, P., Fung, I. Y., Heimann, M., John, J., Maki, T., Maksyutov, S., Masarie, K., Prather, M., Pak, B., Taguchi, S., and Zhu, Z. (2006b). TransCom 3 inversion intercomparison: Impact of transport model errors on the interannual variability of regional $CO_2$ fluxes, 1988-2003. *Global Biogeochem. Cycles*, **20**, 01 [GB1002]. doi:10.1029/2004GB002439

Bakker, D. C. E., Pfeil, B., Smith, K., Hankin, S., Olsen, A., Alin, S. R., Cosca, C., Harasawa, S., Kozyr, A., Nojiri, Y., O'Brien, K. M., Schuster, U., Telszewski, M., Tilbrook, B., Wada, C., Akl, J., Barbero, L., Bates, N. R., Boutin, J., Bozec, Y., Cai, W.-J., Castle, R. D., Chavez, F. P., Chen, L., Chierici, M., Currie, K., de Baar, H. J. W., Evans, W., Feely, R. A., Fransson, A., Gao, Z., Hales, B., Hardman-Mountford, N. J., Hoppema, M., Huang, W.-J., Hunt, C. W., Huss, B., Ichikawa, T., Johannessen, T., Jones, E. M., Jones, S. D., Jutterström, S., Kitidis, V., Körtzinger, A., Landschützer, P., Lauvset, S. K., Lefévre, N., Manke, A. B., Mathis, J. T., Merlivat, L., Metzl, N., Murata, A., Newberger, T., Omar, A. M., Ono, T., Park, G.-H., Paterson, K., Pierrot, D., Ríos, A. F., Sabine, C. L., Saito, S., Salisbury, J., Sarma, V. V. S. S., Schlitzer, R., Sieger, R., Skjelvan, I., Steinhoff, T., Sullivan, K. F., Sun, H., Sutton, A. J., Suzuki, T., Sweeney, C., Takahashi, T., Tjiputra, J., Tsurushima, N., van Heuven, S. M. A. C., Vandemark, D., Vlahos, P., Wallace, D. W. R., Wanninkhof, R. and Watson, A. J. (2014). An update to the Surface Ocean $CO_2$ Atlas (SOCAT version 2). *Earth System Science Data,* **6**, 69-90. doi:10.5194/essd-6-69-2014

Bakker, D. C. E., Pfeil, B., Landa, C. S., Metzl, N., O'Brien, K. M., Olsen, A., Smith, K., Cosca, C., Harasawa, S., Jones, S. D., Nakaoka, S. I., Nojiri, Y., Schuster, U., Steinhoff, T., Sweeney, C., Takahashi, T., Tilbrook, B., Wada, C., Wanninkhof, R., Alin, S. R., Balestrini, C. F., Barbero, L., Bates, N. R., Bianchi, A. A., Bonou, F., Boutin, J., Bozec, Y., Burger, E. F., Cai, W. J., Castle, R. D., Chen, L., Chierici, M., Currie, K., Evans, W., Featherstone, C., Feely, R. A., Fransson, A., Goyet, C., Greenwood, N., Gregor, L., Hankin, S., Hardman-Mountford, N. J., Harlay, J., Hauck, J., Hoppema, M., Humphreys, M. P., Hunt, C. W., Huss, B., Ibanhez, J. S. P., Johannessen, T., Keeling, R., Kitidis, V., Kortzinger, A., Kozyr, A., Krasakopoulou, E., Kuwata, A., Landschutzer, P., Lauvset, S. K., Lefevre, N., Lo Monaco, C., Manke, A., Mathis, J. T., Merlivat, L., Millero, F. J., Monteiro, P. M. S., Munro, D. R., Murata, A., Newberger, T., Omar, A. M., Ono, T., Paterson, K., Pearce, D., Pierrot, D., Robbins, L. L., Saito, S., Salisbury, J., Schlitzer, R., Schneider, B., Schweitzer, R., Sieger, R., Skjelvan, I., Sullivan, K. F., Sutherland, S. C., Sutton, A. J., Tadokoro, K., Telszewski, M., Tuma, M., van Heuven, S. M. A. C., Vandemark, D., Ward, B., Watson, A. J. and Xu, S. (2016). A multi-decade record of high-quality $fCO_2$ data in version 3 of the Surface Ocean $CO_2$ Atlas (SOCAT). *Earth System Science Data*, **8**, 383-413. doi:10.5194/essd-8-383-2016

Bakker, D. C. E., Alin, S. R., Bates, N., Becker, M., Castaño-Primo, R., Cosca, C. E., Cronin, M., Kadono, K., Kozyr, A., Lauvset, S. K., Metzl, N., Munro, D. R., Nakaoka, S., O'Brien, K. M., Ólafsson, J., Olsen, A., Pfeil, B., Pierrot, D., Smith, K., Sutton, A. J., Takahashi, T., Tilbrook, B., Wanninkhof, R., Andersson, A., Atamanchuk, D., Benoit-Cattin, A., Bott, R., Burger, E. F., Cai, W.-J., Cantoni, C., Collins, A., Corredor, J. E., Cronin, M. F., Cross, J. N, Currie, K. I., De Carlo, E. H., DeGrandpre, M. D., Dietrich, C., Emerson, S., Enright, M. P.,

Evans, W., Feely, R. A., García-Ibáñez, M. I., Gkritzalis, T., Glockzin, M., Hales, B., Hartman, S. E., Hashida, G., Herndon, J., Howden, S. D., Humphreys, M. P., Hunt, C. W., Jones, S. D., Kim, S., Kitidis, V., Landa, C. S, Landschützer, P., Lebon, G. T., Lefèvre, N., Lo Monaco, C., Luchetta, A., Maenner Jones, S., Manke, A. B., Manzello, D., Mears, P., Mickett, J., Monacci, N. M., Morell, J. M., Musielewicz, S., Newberger, T., Newton, J., Noakes, S., Noh, J.-H., Nojiri, Y., Ohman, M., Ólafsdóttir, S., Omar, A. M., Ono, T., Osborne, J., Plueddemann, A. J., Rehder, G., Sabine, C. L, Salisbury, J. E., Schlitzer, R., Send, U., Skjelvan, I., Sparnocchia, S., Steinhoff, T., Sullivan, K. F., Sutherland, S. C., Sweeney, C., Tadokoro, K., Tanhua, T., Telszewski, M., Tomlinson, M., Tribollet, A., Trull, T., Vandemark, D., Wada, C., Wallace, D. W. R., Weller, R. A., and Woosley, R. J. (2020). Surface Ocean $CO_2$ Atlas Database Version 2020 (SOCATv2020) (NCEI Accession 0210711), NOAA National Centers for Environmental Information. doi:10.25921/4xkx-ss49

Baldocchi, D., Falge, E., Gu, L., Olson, R., Hollinger, D., Running, S. W., Anthoni, P., Bernhofer, C., Davis, K. J., Evans, R., Fuentes, J., Goldstein, A., Katul, G., Law, B., Lee, X., Malhi, Y., Meyers, T., Munger, W., Oechel, W., Paw, U. K. T., Pilegaard, K., Schmid, H. P., Valentini, R., Verma, S., Vesala, T., Wilson, K. and Wofsy, S. (2001). FLUXNET: A new tool to study the temporal and spatial variability of ecosystem-scale carbon dioxide, water vapor, and energy flux densities. *Bull. Amer. Meteor. Soc.*, **82**, 2415–2434. doi:10.1175/1520-0477

Baldocchi D. D. (2003). Assessing the eddy covariance technique for evaluating carbon dioxide exchange rates of ecosystems: past, present and future. *Global Change Biology*, **9**, 479–492. doi:10.1046/j.1365-2486.2003.00629.x

Ballantyne, A. P., Alden, C. B., Miller, J. B., Tans, P. P. and White, J. W. C. (2012). Increase in observed net carbon dioxide uptake by land and oceans during the past 50 years. *Nature*, **488**, 70–72. doi:10.1038/nature11299

Ballantyne, A. P., Andres, R., Houghton, R., Stocker, B. D., Wanninkhof, R., Anderegg, W., Cooper, L. A., DeGrandpre, M., Tans, P. P., Miller, J. B., Alden, C., and White, J. W. C. (2015). Audit of the global carbon budget: estimate errors and their impact on uptake uncertainty, *Biogeosciences*, **12**, 2565–2584. doi: 10.5194/bg-12-2565-2015.

Barichivich, J., Briffa, K.R., Myneni, R.B., Osborn T.J., Melvin, T.M., Ciais, P., Piao, S., Tucker, C. (2013). Large-scale variations in the vegetation growing season and annual cycle of atmospheric $CO_2$ at high northern latitudes from 1950 to 2011. *Global Change. Biology*, 19,3167-3183. doi:10.1111/gcb.12283

Bastos, A., Running, S. W., Gouveia, C., and Trigo, R. M. (2013). The global NPP dependence on ENSO: La Niña and the extraordinary year of 2011. *Journal of Geophysical Research: Biogeosciences*, 118, 1247-1255. doi: 10.1002/jgrg.20100

Bastos, A., Ciais, P., Park, T., Zscheischler, J., Yue, C., Barichivich, J., Myneni, R. B., Peng, S., Piao, S., and Zhu, Z. (2017). Was the extreme Northern Hemisphere greening in 2015 predictable? *Environmental Research Letters*, **12**, 044016. doi: 10.1088/1748-9326/aa67b5

Bastos, A., Friedlingstein, P., Sitch, S., Chen, C., Mialon, A., Wigneron, J.-P., Arora, V. K., Briggs, P. R., Canadell, J. G., and Ciais, P. (2018). Impact of the 2015/2016 El Niño on the terrestrial carbon cycle constrained by bottom-up and top-down approaches, *Philosophical Transactions of the Royal Society London B*., **373**, 1760. doi: 10.1098/rstb.2017.0304

Bastos, A., Ciais, P., Chevallier, F., Rödenbeck, C., Ballantyne, A. P., Maignan, F., Yin, Y., Fernández-Martínez, M., Friedlingstein, P., Peñuelas, J., Piao, S. L., Sitch, S., Smith, W. K.,

Wang, X., Zhu, Z., Haverd, V., Kato, E., Jain, A. K., Lienert, S., Lombardozzi, D., Nabel, J. E. M. S., Peylin, P., Poulter, B., and Zhu, D. (2019). Contrasting effects of $CO_2$ fertilization, land-use change and warming on seasonal amplitude of Northern Hemisphere $CO_2$ exchange, *Atmospheric Chemistry and Physics*, **19**, 12361–12375, https://doi.org/10.5194/acp-19-12361-2019.

Bastos, A., O'Sullivan, M., Ciais, P., Makowski, D., Sitch, S., Friedlingstein, P., Chevallier, F., Rödenbeck, C., Pongratz, J., Luijkx, I. T., Patra, P. K., Peylin, P., Canadell, J. G., Lauerwald, R., Li, W., Smith, N. E., Peters, W., Goll, D. S., Jain, A.K., Kato, E., Lienert, S., Lombardozzi, D. L., Haverd V., Nabel, J. E. M. S., Poulter, B., Tian, H., Walker, A. P. and Zaehle, S. (2020). Sources of uncertainty in regional and global terrestrial $CO_2$ exchange estimates. *Global Biogeochemical Cycles*, **34**, e2019GB006393. doi: 10.1029/2019GB006393

Bauer, J. E., Cai, W. -J., Raymond, P. A., Bianchi, T. S., Hopkinson, C. S., and Regnier, P. A. G. (2013). The changing carbon cycle of the coastal ocean. *Nature* **504**, 61-70. doi: 10.1038/nature12857

Beck, S. A. and Goetz, S. J. (2011). Satellite observations of high northern latitude vegetation productivity changes between 1982 and 2008: ecological variability and regional differences. *Environmental Research Letters*, **6**, 045501. doi:10.1088/1748-9326/6/4/045501

Becker, M., Andersen, N., Fiedler, B., Fietzek, P., Körtzinger, A., Steinhoff, T., and Friedrichs, G. (2012). Using cavity ringdown spectroscopy for continuous monitoring of $\delta^{13}C(CO_2)$ and $fCO_2$ in the surface ocean. *Limnology and Oceanography: Methods,* **10**, 752-766. doi:10.4319/lom.2012.10.752

Beer, C., Reichstein, M., Tomelleri, E., Ciais, P., Jung, M., Carvalhais, N., Rödenbeck, C., Arain, M. A., Baldocchi, D., Bonan, G., B., Bondeau, A., Cescatti, A., Lasslop,G., Lindroth, A., Lomas, M., Luyssaert, S., Margolis, H., Oleson, K. W., Roupsard, O., Veenendaal, E., Viovy, N., Williams, C., Woodward, F., I. and Papale, D. (2010). Terrestrial gross carbon dioxide uptake: global distribution and covariation with climate. *Science,* **329**, 834–838. doi:10.1126/science.1184984

Bennedsen, M., Hildebrand, E. and Koopman, S. (2019). Trend analysis of the airborne fraction and sink rate of anthropogenically released $CO_2$. *Biogeosciences*, **16**, 3651–3663. doi:10.5194/bg-16-3651-2019

Bloom, A. A., Bowman, K. W., Liu, J., Konings, A. G., Worden, J. R., Parazoo, N. C., Meyer, V., Reager, J. T., Worden, H. M., Jiang, Z., Quetin, G. R., Smallman, T. L., Exbrayat, J.-F., Yin, Y., Saatchi, S. S., Williams, M., and Schimel, D. S. (2020). Lagged effects regulate the inter-annual variability of the tropical carbon balance, Biogeosciences, 17, 6393–6422, 2020. doi: 10.5194/bg-17-6393-2020

Boden T. A., Marland G. and Andres R. J. (2017). Global, Regional, and National Fossil-Fuel $CO_2$ Emissions. Carbon Dioxide Information Analysis Center, Oak Ridge National Laboratory, U.S. Department of Energy, Oak Ridge, Tenn., U.S.A. doi:10.3334/CDIAC/00001_V2017

Bolin, B., Björkström, A., Holmén, K. and Moore, B. (1983). The simultaneous use of tracers for ocean circulation studies. *Tellus B*, **35B**, 206–236. doi:10.1111/j.1600-0889.1983.tb00025.x

Bronselaer, B., and Zanna, L. (2020). Heat and carbon coupling reveals ocean warming due to circulation changes. *Nature*, 584, 227-233. doi: 10.1038/s41586-020-2573-5

Booth, B. B. B., C. D. Jones, M. Collins, I. J. Totterdell, P. M. Cox, S. Sitch, C. Huntingford, R. Betts, G. R. Harris, and J. Lloyd. (2012). High sensitivity of future global warming to land carbon cycle processes, *Environmental Research Letters,* **7**, 024002. doi: 10.1088/1748-9326/7/2/024002

Bousquet, P., Peylin, P., Ciais, P., Le Quéré, C., Friedlingstein, P., and Tans, P. (2000). Regional Changes in Carbon Dioxide Fluxes of Land and Oceans Since 1980. *Science*, **290**,1342-1346. doi: 10.1126/science.290.5495.1342

Bowman, D. M. J. S., Williamson, G. J., Abatzoglou, J. T., Kolden, C. A., Cochrane, M. A. and Smith, A. M. S. (2017). Human exposure and sensitivity to globally extreme wildfire events. *Nature Ecology and Evolution*, **1**, 0058. doi: 10.1038/s41559-016-0058

Bowman, D. M. J. S., Williamson, G. J., Price, O. F., Ndalila, M. N., and Bradstock, R. A. (2021). Australian forests, megafires and the risk of dwindling carbon stocks. *Plant Cell & Environment,* **44**, 347–355. doi: 10.1111/pce.13916

BP Statistical Review of World Energy 2020. available at https://www.bp.com/en/global/corporate/energy-economics/statistical-review-of-world-energy/co2-emissions.html, last access 30 November 2021.

Brandt, M., Wigneron, J.-P., Chave, J., Tagesson, T., Peñuelas, J., Ciais, P., Rasmussen, K., Tian, F., Mbow, C., Al-Yaari, A., Rodriguez-Fernandez, N., Schurgers, G., Zhang, W., Chang, J., Kerr, Y., Verger, A., Tucker, C., Mialon, A., Rasmussen, L., Fan, L., and Fensholt, R. (2018). Satellite passive microwaves reveal recent climate-induced carbon losses in African drylands. *Nature Ecology and Evolution,* **2**, 827–835. doi: 10.1038/s41559-018-0530-6

Braswell, B. H., Schimel, D. S., Linder, E., and Moore, B. (1997). The Response of Global Terrestrial Ecosystems to Interannual Temperature Variability, *Science*, **278**, 870-873. doi: 10.1126/science.278.5339.870

Brienen, R. J.W., Phillips, O. L., Feldpausch, T. R., Gloor, E., Baker, T. R., Lloyd, J., Lopez-Gonzalez, G., Monteagudo-Mendoza, A., Malhi, Y., Lewis, S. L., Vásquez Martinez, R., Alexiades, M., Álvarez Dávila, E., Alvarez-Loayza, P., Andrade, A., Aragão, L. E. O. C., Araujo-Murakami, A., Arets, E. J. M. M., Arroyo, L., Aymard, C. A. G., Bánki, O.S., Baraloto, C., Barroso, J., Bonal, D., Boot, R. G. A., Camargo, J. L. C., Castilho, C. V., Chama, V., Chao, K. J., Chave, J., Comiskey, J. A., Cornejo Valverde, F., da Costa, L., de Oliveira, E. A., Di Fiore, A., Erwin, T. L., Fauset, S., Forsthofer, M., Galbraith, D. R., Grahame, E. S., Groot, N., Hérault, B., Higuchi, N., Honorio Coronado, E. N., Keeling, H., Killeen, T. J., Laurance, W. F., Laurance, S., Licona, J., Magnussen, W. E., Marimon, B. S., Marimon-Junior, B. H., Mendoza, C., Neill, D. A., Nogueira, E. M., Núñez, P., Pallqui Camacho, N. C., Parada, A., Pardo-Molina, G., Peacock, J., Peña-Claros, M., Pickavance, G. C., Pitman, N. C. A., Poorter, L., Prieto, A., Quesada C. A., Ramírez, F., Ramírez-Angulo, H., Restrepo, Z., Roopsind, A., Rudas, A., Salomão, R. P., Schwarz, M., Silva, N., Silva-Espejo, J. E., Silveira, M., Stropp, J., Talbot, J., ter Steege, H., Teran-Aguilar, J., Terborgh, J., Thomas-Caesar, R., Toledo, M., Torello-Raventos, M., Umetsu, R. K., van der Heijden, G. M. F., van der Hout, P., Guimarães, Vieira I. C., Vieira, S. A., Vilanova, E., Vos, V. A. and Zagt, R. J. (2015). Long-term decline of the Amazon carbon sink. *Nature,* **519**, 344-348. doi: 10.1038/nature14283

Bronselaer,B., and Zanna, L. (2020), Heat and carbon coupling reveals ocean warming due to circulation changes. *Nature,* **584**, 227–233. doi:10.1038/s41586-020-2573-5

Buchanan, P. J., and Tagliabue, A. (2021). The Regional Importance of Oxygen Demand and Supply for Historical Ocean Oxygen Trends. *Geophysical Research Letters*, **48**, e2021GL094797. doi: 10.1029/2021GL094797

Bushinsky, S. M., Landschützer, P., Rödenbeck, C., Gray, A. R., Baker, D., Mazloff, M. R., Resplandy, L., Johnson, K. S., and Sarmiento, J. L. (2019). Reassessing Southern Ocean air-sea $CO_2$ flux estimates with the addition of biogeochemical float observations. *Global Biogeochemical Cycles*, **33**, 1370-1388, doi:10.1029/2019GB006176

Byrne, B., Wunch, D., Jones, D. B. A., Strong, K., Deng, F., Baker, I., Köhler, P., Frankenberg, C., Joiner, J., Arora, V. K., Badawy, B., Harper, A. B., Warneke, T., Petri, C., Kivi, R. and Roehl, C. M. (2018). Evaluating GPP and respiration estimates over northern midlatitude ecosystems using solar-induced fluorescence and atmospheric $CO_2$ measurements. *Journal of Geophysical Research: Biogeosciences*, **123**, 2976–2997. doi:10.1029/2018JG004472

Byrne, B., Liu, J., Lee, M., Baker, I., Bowman, K. W., Deutscher, N. M., Feist, D. G., Griffith D. W. T., Iraci, L. T., Kiel, M., Kimball, J. S., Miller, C. E., Morino, I., Parazoo, N. C., Petri, C., Roehl, C. M., Sha, M. K., Strong, K., Velazco, V. A., Wennberg, P. O. and Wunch, D. (2020a). Improved constraints on northern extratropical $CO_2$ fluxes obtained by combining surface-based and space-based atmospheric $CO_2$ measurements. *Journal of Geophysical Research: Atmospheres*, **125**, e2019JD032029. doi:10.1029/2019JD032029

Byrne, B., Liu, J., Lee, M., Baker, I., Bowman, K. W., Deutscher, N. M., Feist, D. G., Griffith D. W. T., Iraci, L. T., Kiel, M., Kimball, J. S., Miller, C. E., Morino, I., Parazoo, N. C., Petri, C., Roehl, C. M., Sha, M. K., Strong, K., Velazco, V. A., Wennberg, P. O., and Wunch, D. (2020b). Improved constraints on northern extratropical $CO_2$ fluxes obtained by combining surface-based and space-based atmospheric $CO_2$ measurements. *Journal of Geophysical Research: Atmospheres*, **125**, e2019JD032029. doi: 10.1029/2019JD032029

Cadule P., Friedlingstein P., Bopp L., Sitch, S., Jones, C. D., Ciais, P., Piao, S. L., and Peylin, P. (2010). Benchmarking coupled climate-carbon models against long-term atmospheric CO2 measurements. *Global Biogeochemical Cycles*, **24**, GB2016. doi: 10.1029/2009gb003556

Cai, W., Cowan, T., and Raupach, M. (2009), Positive Indian Ocean Dipole events precondition southeast Australia bushfires, *Geophysical Research Letters*, **36**, L19710, doi: 10.1029/2009GL039902

Cai, W., and Prentice, I. C. (2020). Recent trends in gross primary production and their drivers: analysis and modelling at flux-site and global scales. Environmental Research Letters, 15, 124050. doi: 10.1088/1748-9326/abc64e

Campbell, J. E., Berry, J. A., Seibt, U., Smith, S. J., Montzka, S. A., Launois, T., Belviso, S., Bopp, L., and Laine, M. (2017). Large historical growth in global terrestrial gross primary production, Nature, 544, 84–87. doi: 10.1038/nature22030

Canadell, J. G., Le Quéré, C., Raupach, M. R., Field, C. B., Buitenhuis, E., Ciais, P., Conway, T. J., Gilett, N. P., Houghton, J. T. and Marland, G. (2007). Contributions to accelerating atmospheric $CO_2$ growth from economic activity, carbon intensity, and efficiency of natural sinks. *Proceedings of the National Academy of Sciences, USA*, **104**, 18,866 – 18,870. doi:10.1073/ pnas.0702737104

Canadell, J. G., Ciais, P., Gurney, K., Le Quéré, C., Piao, S., Raupach, M. R., and Sabine, C. L. (2011). An International Effort to Quantify Regional Carbon Fluxes, *Eos Transactions AGU*, **92**, 81–82. doi: 10.1029/2011EO100001

2564 Canadell, J. G., Monteiro, P. M. S., Costa, M. H., Cotrim da Cunha, L., Cox, P. M., Eliseev, A.V.,
2565 Henson, S., Ishii, M., Jaccard, S., Koven, C., Lohila, A., Patra, P. K., Piao, S., Rogelj, J.,
2566 Syampungani, S., Zaehle, S., and Zickfeld, K.: Global Carbon and other Biogeochemical
2567 Cycles and Feedbacks. In: Climate Change 2021: The Physical Science Basis. Contribution
2568 of Working Group I to the Sixth Assessment Report of the Intergovernmental Panel on
2569 Climate Change [Masson-Delmotte, V., P. Zhai, A. Pirani, S. L. Connors, C. Péan, S. Berger,
2570 N. Caud, Y. Chen, L. Goldfarb, M. I. Gomis, M. Huang, K. Leitzell, E. Lonnoy, J.B.R.
2571 Matthews, T. K. Maycock, T. Waterfield, O. Yelekçi, R. Yu and B. Zhou (eds.)]. Cambridge
2572 University Press. In Press., 2021.

2573 Carroll, D., Menemenlis, D., Adkins, J. F., Bowman, K. W., Brix, H., Dutkiewicz, S., Fenty, I.,
2574 Gierach, M. M., Hill, C., Jahn, O., Landschützer, P., Lauderdale, J. M., Liu, J., Manizza, M.,
2575 Naviaux, J. D., Rödenbeck, C., Schimel, D. S., Van der Stocken, T. and Zhang, H. (2020).
2576 The ECCO-Darwin data-assimilative global ocean biogeochemistry model: Estimates of
2577 seasonal to multi-decadal surface ocean $pCO_2$ and air-sea $CO_2$ flux. *Journal of Advances in*
2578 *Modeling Earth Systems*, **12**, e2019MS001888. doi:10.1029/2019MS001888

2579 Carvalhais, N., Forkel, M., Khomik, M., Bellarby, J., Jung, M., Migliavacca, M. Mu, M.,
2580 Saatchi, S., Santoro, M., Thurner, M., Weber, U., Ahrens, B., Beer, C., Cescatti, A.,
2581 Randerson, J. T. and Reichstein, M. (2014). Global covariation of carbon turnover times
2582 with climate in terrestrial ecosystems. *Nature*, **514**, 213-217. doi:10.1038/nature13731

2583 Casperson, J. P., S. W. Pacala, J. C. Jenkins, G. C. Hurtt, P. R. Moorcroft, and R. A. Birdsey
2584 (2000). Contributions of land use history to carbon accumulation in U.S. Forests. *Science*,
2585 **290**, 1148-1151. doi: 10.1126/science.290.5494.1148

2586 Castro, A. O., Chen, J., Zang, C. S., Shekhar, A., Jimenez, J. C., Bhattacharjee, S., Kindu, M.,
2587 Morales, V. H. and Ramming, A. (2020). OCO-2 Solar-Induced Chlorophyll Fluorescence
2588 Variability across Ecoregions of the Amazon Basin and the Extreme Drought Effects of El
2589 Nino (2015-2016), *Remote Sensing*, **12**, 1202. doi:10.3390/rs12071202

2590 Catherman, C. (2021). Ocean scientists confront a critical bottleneck, *Science*, **374** (6563), doi:
2591 10.1126/science.acx9218

2592 Chapin, F. S., Woodwell, G. M., Randerson, J. T., Rastetter, E. B., Lovett, G. M., Baldocchi, D.
2593 D., Clark, D. A., Harmon, M. E., Schimel, D. S., Valentini, R., Wirth, C., Aber, J. D., Cole,
2594 J. J., Goulden, M. L., Harden, J. W., Heimann, M., Howarth, R. W., Matson, P. A., McGuire,
2595 A. D., Melillo, J. M., Mooney, H. A., Neff, J. C., Houghton, R. A., Pace, M. L., Ryan, M.
2596 G., Running, S. W., Sala, O. E., Schlesinger, W. H. and Schulze, E. D. (2006). Reconciling
2597 carbon-cycle concepts, terminology, and methods. *Ecosystems*, **9**, 1041-1050. doi:
2598 10.1007/s10021-005-0105-7

2599 Chatterjee, A., Gierach, M. M., Sutton, A. J., Feely, R. A., Crisp, D., Eldering, A., Gunson, M.
2600 R., O'Dell, C. W., Stephens, B. B. and Schimel, D. S. (2017). Influence of El Niño on
2601 atmospheric $CO_2$ over the tropical Pacific Ocean: Findings from NASA's OCO-2 mission.
2602 *Science,* **358**, eaam5776. doi:10.1126/science.aam5776

2603 Chen, Z., Huntzinger, D. N., Liu, J. Piao, S., Wang, X. Sitch, S., Friedlingstein, P., Anthoni, P.,
2604 Arneth, A., Bastrikov, V., Goll, D. S., Haverd, V., Jain, A. K., Joetzjer, E., Kato, E., Lienert,
2605 S., Lombardozzi, D. L., McGuire, P. C., Melton, J. R., Nabel, J. E. M. S., Pongratz, J.,
2606 Poulter, B., Tian, H., Wiltshire, A., J., and Miller, S. (2021a). Five years of variability in the
2607 global carbon cycle: comparing an estimate from the Orbiting Carbon Observatory-2 and

process-based models. *Environmental Research Letters*, **16**, 054041. doi: 10.1088/1748-9326/abfac1

Chen, Z., Liu, J., Henze, D. K., Huntzinger, D. N., Wells, K. C., Sitch, S., Friedlingstein, P., Joetzjer, E., Bastrikov, V., Goll, D. S., Haverd, V., Jain, A. K., Kato, E., Lienert, S., Lombardozzi, D. L., McGuire, P. C., Melton, J. R., Nabel, J. E. M. S., Poulter, B., Tian, H., Wiltshire, A. J., Zaehle, S., and Miller, S. M. (2021b). Linking global terrestrial $CO_2$ fluxes and environmental drivers: inferences from the Orbiting Carbon Observatory 2 satellite and terrestrial biospheric models. *Atmospheric Chemistry and Physics*, **21**, 6663–6680. doi:10.5194/acp-21-6663-2021

Cheng, L., Normandeau, C., Bowden, R., Doucett, R., Gallagher, B., Gillikin, D.P., Kumamoto, Y., Mckay, J.L., Middlestead, P., Ninnemann, U., Nothaft, D., Dubinina, E.O., Quay, P., Reverdin, G., Shirai, K., Mørkved, P.T., Theiling, B.P., Van Geldern, R., and Wallace, D.W.R. (2019). An international intercomparison of stable carbon isotope composition measurements of dissolved inorganic carbon in seawater. *Limnology and Oceanography: Methods,* **17**, 200-209. doi: 10.1002/lom3.10300

Cheng, L., Normandeau, C., Cai, W.-J., Wallace D.W.R. (2021). Shipboard measurement of DIC and $\delta^{13}$C-DIC on discrete seawater samples using Cavity Ring-Down Spectroscopy: system testing and performance during three research cruises in the North Atlantic. *Isotopes in Environmental and Health Studies,* In revision, [preprint]

Chevallier, F., Ciais, P., Conway, T. J., Aalto, T., Anderson, B. E., Bousquet, P., Brunke, E. G., Ciattaglia, L., Esaki, Y., Frohlich, M., Gomez, A. J., Gomez-Pelaez, A. J., Haszpra, L., Krummel, P., Langenfelds, R., Leuenberger, M., Machida, T., Maignan, F., Matsueda, H., Morgui, J. A., Mukai, H., Nakazawa, T., Peylin, P., Ramonet, M., Rivier, L., Sawa, Y., Schmidt, M., Steele, P., Vay, S. A., Vermeulen, A. T., Wofsy, S. and Worthy, D. (2010). $CO_2$ surface fluxes at grid point scale estimated from a global 21-year reanalysis of atmospheric measurements. *Journal of Geophysical Research: Atmospheres*, **115**, D21307. doi:10.1029/2010JD013887

Chevallier, F., Remaud, M. O'Dell, C. W., Baker, D., Peylin, P. and Cozic, A. (2019). Objective evaluation of surface and satellite driven $CO_2$ atmospheric inversion. *Atmospheric Chemistry and Physics*, **19**, 14233–14251. doi:10.5194/acp-19-14233-2019

Chevallier, F. (2021). Fluxes of carbon dioxide from managed ecosystems estimated by national inventories compared to atmospheric inverse modeling. *Geophysical Research Letters*, **48**, e2021GL093565. doi: 10.1029/2021GL093565

Chini, L., Hurtt, G., Sahajpal, R., Frolking, S., Goldewijk, K. K., Sitch, S., Ganzenmüller, R., Ma, L., Ott, L., Pongratz, J., and Poulter, B. (2021). Land-use harmonization datasets for annual global carbon budgets, *Earth System Science Data*, **13**, 4175–4189. doi: 10.5194/essd-13-4175-2021

Church, J. A., White, N. J., Arblaster, J. M. (2005). Significant decadal-scale impact of volcanic eruptions on sea level and ocean heat content. *Nature*, **438**, 74–77. doi:10.1038/nature04237

Chuvieco, E., Yue, C., Heil, A., Mouillot, F., Alonso-Canas, I., Padilla, M., Pereira, J.M.C., Oom, D., Tansey, K. (2016) A new global burned area product for climate assessment of fire impacts. *Global Ecology and Biogeography*, 25, 619-629. doi:10.1111/geb.12440

Ciais, P., Tans, P. P., Trolier, M., White, J. W. C., and Francey, R. J. (1995). A Large Northern Hemisphere Terrestrial $CO_2$ Sink Indicated by the $^{13}C/^{12}C$ Ratio of Atmospheric $CO_2$. *Science*, **269**, 1098-1102. doi: 10.1126/science.269.5227.1098

Ciais, P., Tans, P. P., Denning, A. S., Francey, R. J., Trolier, M., Meijer, A. J., White, J. W. C, Berry, J. A., Randall, D. A., Collatz, G. J., Sellers, P. J., Monfray, P., and Heimann, M. (1997). A three-dimensional synthesis study of $\delta^{18}O$ in atmospheric $CO_2$ 2. Simulations with the TM2 transport model. *Journal of Geophysical Research*, **102**, 5873-5883. doi: 10.1029/96JD02361

Ciais, P., Reichstein, M., Viovy, N., Granier, A., Ogee, J., Allard, V., Aubinet, M., Buchmann, N., Bernhofer, C., Carrara, A., Chevallier, F., De Noblet, N., Friend, A. D., Friedlingstein, P., Grunwald, T., Heinesch, B., Keronen, P., Knohl, A., Drinner, G., Loustau, D., Manca, G., Matteucci, G., Miglietta, F., Ourcival, J. M., Papale, D., Pilegaard, K., Rambal, S., Seufert, G., Soussana, J. F., Sanz, M. J., Schulze, E. D., Vesala, T. and Valentini, R. (2005). Europe-wide reduction in primary productivity caused by the heat and drought in 2003. *Nature,* **437**, 529–533. doi: 10.1038/nature03972

Ciais, P., Sabine, C., Bala, G., Bopp, L., Brovkin, V., Canadell, J., Chhabra, A., DeFries, R., Galloway, J., Heimann, M., Jones, C., Le Quere, C., Myneni, R.B., Piao, S. and Thornton, P. (2013). Carbon and Other Biogeochemical Cycles. In: Climate Change 2013: The Physical Science Basis. Contribution of Working Group I to the Fifth Assessment Report of the Intergovernmental Panel on Climate Change [Stocker, T.F., D. Qin, G.-K. Plattner, M. Tignor, S.K. Allen, J. Boschung, A. Nauels, Y. Xia, V. Bex and P.M. Midgley (eds.)]. Cambridge University Press, Cambridge, United Kingdom and New York, NY, USA.

Ciais, P., Dolman, A. J., Bombelli, A., Duren, R., Peregon, A., Rayner, P. J., Miller, C., Gobron, N., Kinderman, G., Marland, G., Gruber, N., Chevallier, F., Andres, R. J., Balsamo, G., Bopp, L., Bréon, F.-M., Broquet, G., Dargaville, R., Battin, T. J., Borges, A., Bovensmann, H., Buchwitz, M., Butler, J., Canadell, J. G., Cook, R. B., DeFries, R., Engelen, R., Gurney, K. R., Heinze, C., Heimann, M., Held, A., Henry, M., Law, B., Luyssaert, S., Miller, J., Moriyama, T., Moulin, C., Myneni, R. B., Nussli, C., Obersteiner, M., Ojima, D., Pan, Y., Paris, J.-D., Piao, S. L., Poulter, B., Plummer, S., Quegan, S., Raymond, P., Reichstein, M., Rivier, L., Sabine, C., Schimel, D., Tarasova, O., Valentini, R., Wang, R., van der Werf, G., Wickland, D., Williams, M. and Zehner, C. (2014). Current systematic carbon-cycle observations and the need for implementing a policy-relevant carbon observing system, *Biogeosciences*, **11**, 3547–3602. doi:10.5194/bg-11-3547-2014

Ciais, P., Tan, J., Wang, X., Roedenbeck, C., Chevallier, F., Piao, S.-L., Broquet, G., Le Quéré, C., Canadell, J. G., Peng, S., Poulter, B., Liu, Z., and Tans, P. (2019). Five decades of northern land carbon uptake revealed by the interhemispheric $CO_2$ gradient. *Nature*, **568**, 221-225. doi: 10.1038/s41586-019-1078-6

Ciais, P., Yao, Y., Gasser, T., Baccini, A., Wang, Y., Lauerwald, R., Peng, S., Bastos, A., Li, W., Raymnd, P. A., Canadell, J. G., Peters, G. P., Andres, R. J., Chang, J., Yue, C., Dolman, A. J., Haverd, V., Hartman, J., Laruelle, G., Konings, A. G., King, A. W., Liu, Y., Luyssaert, S., Maignan, F., Patra, P. K., Peregon, A., Regnier, P., Pongratz, J., Poulter, B., Shvidenko, A., Valentini, R., Wang, R., Broquet, G., Yin, Y., Zscheischler, J., Guenet, B., Goll, D., S., Ballantyne, A.-P., Yang, H., Qiu, C. and Zhu, D. (2020a). Empirical estimates of regional carbon budgets imply reduced global soil heterotrophic respiration. *National Science Review*, **0**, nwaa145,1-14. doi:10.1093/nsr/nwaa145

Ciais, P. Wang, Y., Andrew, R. M., Bréon, F. M., Chevallier, F., Broquet, G., Nabuurs, G. J., Peters, G. P., McGrath, M. J., Meng, W., Zheng, B. and Tao, S. (2020b). Biofuel burning and human respiration bias on satellite estimates of fossil fuel $CO_2$ emissions. *Environmental Research Letters*, **15**, 074036. doi:10.1088/1748-9326/ab7835

2699 Ciais, P., Bastos, A., Chevallier, F., Lauerwald, R., Poulter, B., Canadell, P., Hugelius, G.,
2700 Jackson, R. B., Jain, A., Jones, M., Kondo, M., Luijkx, I. T., Patra, P. K., Peters, W.,
2701 Pongratz, J., Petrescu, A. M., R., Piao, S., Qiu, C., Von Randow, C., Regnier, P., Saunois,
2702 M., Scholes, R., Shvidenko, A., Tian, H., Yang, H., Wang, X., and Zheng, B
2703 (2022). Definitions and methods to estimate regional land carbon fluxes for the second
2704 phase of the REgional Carbon Cycle Assessment and Processes Project (RECCAP-2).
2705 *Geoscientific Model Development*, **15**, 1289-1316. doi: 10.5194/gmd-15-1289-2022
2706 Clark, H., Bennouna, Y., Tsivlidou, M., Wolff, P., Sauvage, B., Barret, B., Le Flochmoën, E.,
2707 Blot, R., Boulanger, D., Cousin, J.-M., Nédélec, P., Petzold, A., and Thouret, V. (2021). The
2708 effects of the COVID-19 lockdowns on the composition of the troposphere as seen by In-
2709 service Aircraft for a Global Observing System (IAGOS) at Frankfurt, *Atmospheric*
2710 *Chemistry and Physics*, **21**, 16237–16256. doi: 10.5194/acp-21-16237-2021
2711 Claustre, H., Johnson, K. S., and Takeshita, Y. (2020). Observing the global ocean with
2712 Biogeochemical-Argo, *Annual Review of Marine Science*, **12**, 23-48. doi:10.1146/annurev-
2713 marine-010419-010956
2714 Claustre, H., Legendre, L., Boyde, P.W., and Levy, M. (2021). The Oceans' Biological Carbon
2715 Pumps: Framework for a Research Observational Community Approach. *Frontiers in*
2716 *Marine Science, Ocean Observation*, **8**, 780052. doi: 10.3389/fmars.2021.780052
2717 Clement, D., and Gruber, N. (2018). The eMLR(C*) Method to determine decadal changes in the
2718 global ocean storage of anthropogenic $CO_2$. *Global Biogeochemical Cycles,* **32**, 654-679.
2719 doi:10.1002/2017gb005819
2720 Cleverly, J., Eamus, D., Luo, Q., Coupe, N. R., Kljun, N., Ma, X., Ewenz, C., Li, L., Yu, Q. and
2721 Huete, A. (2016). The importance of interacting climate modes on Australia's contribution
2722 to global carbon cycle extremes. *Scientific Reports,* **6**, 23113. doi: 10.1038/srep23113
2723 Cortés, J., Mahecha, M. D., Reichstein, M., Myneni, R. B., Chen, C., and Brenning, A. (2021).
2724 Where are global vegetation greening and browning trends significant? *Geophysical*
2725 *Research Letters*, *48*, e2020GL091496. doi:10.1029/2020GL091496
2726 Cox, P. M., Pearson, D., Booth, B. B., Friedlingstein, P., Huntingford, C., Jones, C. D., and Luke,
2727 C. M. (2013). Sensitivity of tropical carbon to climate change constrained by carbon dioxide
2728 variability, *Nature*, **494**, 341–344. doi: 10.1038/nature11882
2729 Crisp, D., Atlas, R. M., Bréon, F.-B., Brown, L. R., Burrows, J. P., Ciais, P., Connor, B.J., Doney,
2730 S. C., Fung, I. Y., Jacob, D. J., Miller, C. E., O'Brien, D., Pawson, S., Randerson, J. T.,
2731 Rayner, P., Salawitch, R. J., Sander, S. P., Sen, B., Stephens, G. L., Tans, P. P., Toon, G. C.,
2732 Wennberg, P. O., Wofsy, S. C., Yung, Y. L., Kuang, Z., Chudasama, B., Sprague, G., Weiss,
2733 B., Pollock, R., Kenyon, D., Schroll, S. (2004). The Orbiting Carbon Observatory (OCO)
2734 mission. *Advances in Space Research*, **34**, 700–709, doi: 10.1016/j.asr.2003.08.062
2735 Crisp, D., Miller, C. E., and DeCola, P. L. (2008). NASA Orbiting Carbon Observatory:
2736 measuring the column averaged carbon dioxide mole fraction from space. *Journal of*
2737 *Applied Remote Sensing*, **2**, 023508; doi: 10.1117/1.2898457
2738 Crowell, S., Baker, D., Schuh, A., Basu, S., Jacobson, A., Chevallier, F., Liu, J., Deng, F., Feng,
2739 L., McKain, K., Chatterjee, A., Miller, J., Stephens, B., Eldering, A., Crisp, D., Schimel, D.,
2740 Nassar, R., O'Dell. C., Oda, T., Sweeney, C., Palmer, P., and Jones, D. (2019). The 2015-
2741 2016 carbon cycle as seen from OCO-2 and the global in situ network. *Atmospheric*
2742 *Chemistry and Physics*, **19**, 7347–7376. doi:10.5194/acp-19-7347-2019

2743 Dannenberg, M. P., Wise, E. K., Janko, M., Hwang, T., and Smith_W. K. (2018). Atmospheric
2744 teleconnection influence on North American land surface phenology. *Environmental*
2745 *Research Letters*, **13**, 034029. doi: 10.1088/1748-9326/aaa85a/meta
2746 Dannenberg, M. P., Smith, W. K., Zhang, Y., Song, C., Huntzinger, D. N., and Moore, D. J. P.
2747 (2021). Large-Scale Reductions in Terrestrial Carbon Uptake Following Central Pacific El
2748 Niño, *Geophysical Research Letters*, **48**, e2020GL092367. doi: 10.1029/2020GL092367
2749 Deng, F., D. B. A. Jones, C. W. O'Dell, R. Nassar, and N. C. Parazoo (2016). Combining GOSAT
2750 $XCO_2$ observations over land and ocean to improve regional $CO_2$ flux estimates, Journal of
2751 *Geophysical Research Atmospheres*, **121**, 1896–1913. doi:10.1002/2015JD024157.
2752 Deng, Z., Ciais, P., Tzompa-Sosa, Z. A., Saunois, M., Qiu, C., Tan, C., Sun, T., Ke, P., Cui, Y.,
2753 Tanaka, K., Lin, X., Thompson, R. L., Tian, H., Yao, Y., Huang, Y., Lauerwald, R., Jain, A.
2754 K., Xu, X., Bastos, A., Sitch, S., Palmer, P. I., Lauvaux, T., d'Aspremont, A., Giron, C.,
2755 Benoit, A., Poulter, B., Chang, J., Petrescu, A. M. R., Davis, S. J., Liu, Z., Grassi, G.,
2756 Albergel, C., and Chevallier, F. (2021). Comparing national greenhouse gas budgets
2757 reported in UNFCCC inventories against atmospheric inversions, *Earth System Science*
2758 *Data Discuss.* [preprint]. doi:10.5194/essd-2021-235
2759 Denman, K. L., Brasseur, G., Chidthaisong, A., Ciais, P., Cox, P. M., Dickinson, R. E.,
2760 Hauglustaine, D., Heinze, C., Holland, E., Jacob, D., Lohmann, U., Ramachandran, S., Leite
2761 da Silva Dias, P., Wofsy, S. C., and Zhang, X. (2007). Couplings Between Changes in the
2762 Climate System and Biogeochemistry, in: Climate Change 2007: *The Physical Science*
2763 *Basis.* Contribution of Working Group I to the Fourth Assessment Report of the
2764 Intergovernmental Panel on Climate Change, edited by: Solomon, S., Qin, D., Manning, M.,
2765 Marquis, M., Averyt, K., Tignor, M. M. B., Miller, H. L., and Chen, Z. L., Cambridge
2766 University Press, Cambridge, UK and New York, USA, 499–587.
2767 Denvil-Sommer, A., M. Gehlen, M. Vrac, and C. Mejia (2019). LSCE-FFNN-v1: A two-step
2768 neural network model for the reconstruction of surface ocean $pCO_2$ over the global ocean.
2769 *Geoscientific Model Development*, **12**, 2091–2105. doi:10.5194/gmd-12-2091-2019
2770 DeVries, T. (2014). The oceanic anthropogenic $CO_2$ sink: Storage, air-sea fluxes, and transports
2771 over the industrial era, *Global Biogeochemical Cycles*, **28**, 631–647.
2772 doi:10.1002/2013GB004739
2773 DeVries, T., Holzer, M. and Primeau, F. (2017). Recent increase in oceanic carbon uptake driven
2774 by weaker upper-ocean overturning. *Nature,* **542**, 215–218. doi:10.1038/nature21068
2775 DeVries, T., Le Quéré, C., Andrews, O., Berthet, S., Hauck, J., Ilyina, T., Landschützer, P.,
2776 Lenton, A., Lima, I. D., Nowicki, M., Schwinger, J., Séférian, R. (2019). Decadal trends in
2777 the ocean carbon sink. *Proceedings of the National Academy of Sciences,* **116**, 11646-11651.
2778 doi:10.1073/pnas.1900371116
2779 Diaz, H. F., Hoerling, M. P. and Eischeid, J. K. (2001). ENSO variability, teleconnections and
2780 climate change, *Int. J. Climatol*., **21**, 1845–1862. doi: 10.1002/joc.631
2781 Dlugokencky, E. J., Hall, B.D., Montzka, S.A., Dutton, G., Muhle, J. and Elkins, J.W. (2018).
2782 Long-lived greenhouse gases [in "State of the Climate in 2017"]. *Bulletin of the American*
2783 *Meteorological Society*, **99**, S46-S48. doi:10.1175/2018BAMSStateoftheClimate.1
2784 Doney S.C., Lindsay, K., Caldeira, K., Campin, J.-M., Drange, H., Dutay, J. C., Follows, M.,
2785 Gao, Y., Gnanadesikan, A., Gruber, N., Ishida, A., Joos, F., Madec, G., Maier-Reimer, E.,
2786 Marshall, J. C., Matear, R. J., Monfray, P., Mouchet, A., Najjar, R., Orr, J. C., Plattner, G.-
2787 K., Sarmiento, J., Schlitzer, R., Slater, R., Totterdell, I. J., Weirig, M. F., Yamanaka, Y.

and Yool, A. (2004). Evaluating global ocean carbon models: The importance of realistic physics. *Global Biogeochemical Cycles,* **18** (3), GB3017. doi:10.1029/2003GB002150

Doughty, C. E. and Goulden, M. L. (2008). Are tropical forests near a high temperature threshold? *Journal of Geophysical Research: Biogeosciences,* **113**, G00B07. doi:10.1029/2007JG000632

Duffy, K., A., Schwalm, C. R., Arcus, V. L., Koch, G. W., Liang, L. L. and Schipper, L. A. (2021). How close are we to the temperature tipping point of the terrestrial biosphere? *Science Advances*, **7**, eaay1052. doi: 10.1126/sciadv.aay1052

Duncanson, L., Armston, J., Disney, M., Avitabile, V., Barbier, N., Calders, K., Carter, S., Chave, J., Herold, M., Crowther, T. W., Falkowski, M., Kellner, J. R., Labrière, N., Lucas, R., MacBean, N., McRoberts, R. E., Meyer, V., Naesset, E., Nickeson, J. E., Paul, K. I., Phillips, O. L., Réjou-Méchain, M., Román, M., Roxburgh, S., Saatchi, S., Schepaschenko, D., Scipal, K., Siqueira, P. R., Whitehurst, A. and Williams, M. (2019). The importance of consistent global forest aboveground biomass product Validation. *Surveys in Geophysics,* **40**, 979–999. doi: 10.1007/s10712-019-09538-8

Eddebbar, Y. A., Rodgers, K. B., Long, M. C., Subramanian, A. C., Xie S.-P. and Keeling, R. F. (2019). El Niño-like physical and biogeochemical ocean response to tropical eruptions. *Journal of Climate*, **32**, JCLI–D–18–0458.1, doi:10.1175/JCLI-D-18-0458.1

Eldering, A.,Wennberg, P. O., Crisp, D., Schimel, D., Gunson, M. R., Chatterjee, A., Liu J., Schwandner, Y. Sun, C.W. O'Dell, C. Frankenberg, T. Taylor, B. Fisher, G.B. Osterman, D. Wunch, F., Hakkarainen, J. and Tamminen, J. **(**2017). The Orbiting Carbon Observatory-2 early science investigations of regional carbon dioxide fluxes. *Science*, **358**, eaam5745. doi:10.1126/science.aam5745

Enting, I.G., Trudinger, C.M. and Francey, R.J. (1995). A synthesis inversion of the concentration and $\delta^{13}C$ atmospheric $CO_2$. *Tellus*, **47B**, 35-52. doi:10.1034/j.1600-0889.47.issue1.5.x

Enting, I. G. (2002). Inverse Problems in Atmospheric Constituent Transport, Cambridge University Press, Cambridge, doi: 10.1017/CBO9780511535741

Erb, K. H., Kastner, T., Plutzar, C., Bais, A. L. S., Carvalhais, N., Fetzel, T., Gingrich, S., Haberl, H., Lauk, C., Niedertscheider, M., Pongratz, J., Thurner, M. and Luyussaert, S. (2018). Unexpectedly large impact of forest management and grazing on global vegetation biomass. *Nature,* **553**, 73–76. doi: 10.1038/nature25138

Etheridge, D. M., Steele, L. P., Langenfelds, R. L. and Francey (1996). Natural and anthropogenic changes in atmospheric $CO_2$ over the last 1000 years from air in Antarctic ice and firn. Journal of Geophysical Research, 101, 4115-4128. doi: 10.1029/95JD03410

Fan, S., Gloor, M., Mahlman, J., Pacala, S., Sarmiento, J., Takahashi, T., and Tans, P. (1998). A Large Terrestrial Carbon Sink in North America Implied by Atmospheric and Oceanic Carbon Dioxide Data and Models. *Science*, **282**, 442-446. doi: 10.1126/science.282.5388.442

Fan, L., Wigneron, J.-P., Ciais, P., Chave, J., Brandt, M., Fensholt, R., Saatchi, S. S. Bastos, A., Al-Yaari, A., Hufkens, K., Qin, Y., Xiao, X., Chen, C., Myneni, R. B., Rernandez-Moran, R., Mialon, A., Rodriguez-Fernandez, N. J., Kerr, Y., Tian, F. and Peñuelas, J. (2019). Satellite-observed pantropical carbon dynamics. *Nature Plants,* **5**, 944–951. doi:10.1038/s41477-019-0478-9

2832 Fay, A. R. and McKinley, G. A. (2013). Global trends in surface ocean $pCO_2$ from in situ data.
2833 *Global Biogeochemical Cycles*, **27**, 541–557. doi:10.1002/gbc.20051
2834 Fay, A. R., Lovenduski, N. S., McKinley, G. A., Munro, D. R., Sweeney, C., Gray, A. R.,
2835 Landschützer, P., Stephens, B. B., Takahashi, T. and Williams, N. (2018). Utilizing the
2836 Drake Passage Time-series to understand variability and change in subpolar Southern Ocean
2837 $pCO_2$. *Biogeosciences*, **15**, 3841–3855. doi:10.5194/bg-15-3841-2018
2838 Fay, A.R., Gregor, L., Landschützer, P. McKinley, G.A., Gruber, N., Gehlen, M., Iida, Y.,
2839 Laruelle, G. G., Rödenbeck, C. and Zeng J. (2021). Harmonization of global surface ocean
2840 $pCO_2$ mapped products and their flux calculations; an improved estimate of the ocean
2841 carbon sink. *Earth System Science Data*, doi: 10.5194/essd-2021-16 [preprint]
2842 Fay, A. R., and McKinley, G. A. (2021). Observed regional fluxes to constrain modeled estimates
2843 of the ocean carbon sink. *Geophysical Research Letters*, **48**, e2021GL095325. doi:
2844 10.1029/2021GL095325
2845 Feely, R. A., Wanninkhof, R., Takahashi, T., and, Tans P. (1999). Influence of El Niño on the
2846 equatorial Pacific contribution of atmospheric $CO_2$ accumulation, *Nature*, **398**, 597–601.
2847 doi: 10.1038/19273
2848 Fernández-Martínez, M., Sardans, J., Chevallier, F., Ciais, P., Obersteiner, M., Vicca, S.,
2849 Canadell, J. G., Bastos, A., Friedlingstein, P., Sitch, S., Piao, S. L., Janssens_I. A.
2850 and Peñuelas, J. (2019). Global trends in carbon sinks and their relationships with $CO_2$ and
2851 temperature. *Nature Climate Change,* **9**, 73–79. doi: 10.1038/s41558-018-0367-7
2852 Fisher, J. B., Huntzinger, D. N., Schwalm, C. R. and Sitch, S. (2014). Modeling the terrestrial
2853 biosphere. *Annual Review of Environment and Resources*, **39**, 91–123. doi:10.1146/annurev-
2854 environ-012913-093456
2855 Fong, M. B. and Dickson, A. G. (2019). Insights from GO-SHIP hydrography data into the
2856 thermodynamic consistency of $CO_2$ system measurements in seawater. *Marine Chemistry*,
2857 **211**, 52-63. doi:10.1016/j.marchem.2019.03.006
2858 Forkel, M., Drüke, M., Thurner, M., Dorigo, W., Schaphoff, S., Thonicke, K., von Bloh, W., and
2859 Carvalhais, N. (2019) Constraining modelled global vegetation dynamics and carbon
2860 turnover using multiple satellite observations. *Scientific Reports*, **9**, 18757.
2861 doi:10.1038/s41598-019-55187-7
2862 Francey, R., Tans, P., Allison, C. E., Enting, I. G., White, J. W., C. and Trolier, M. (1995).
2863 Changes in oceanic and terrestrial carbon uptake since 1982. *Nature* **373,** 326–330. doi:
2864 10.1038/373326a0
2865 Frankenberg, C., O'Dell, C., Berry, J., Guanter, L., Joiner, J., Köhler, P., Pollock, R. and Taylor,
2866 T. E. (2014). Prospects for chlorophyll fluorescence remote sensing from the orbiting
2867 carbon observatory-2. *Remote Sensing of Environment*, **147**, 1–12. doi:
2868 10.1016/j.rse.2014.02.007. ISSN 0034–4257
2869 Frey, M., Sha, M. K., Hase, F., Kiel, M., Blumenstock, T., Harig, R., Surawicz, G., Deutscher, N.
2870 M., Shiomi, K., Franklin, J. E., Bösch, H., Chen, J., Grutter, M., Ohyama, H., Sun, Y., Butz,
2871 A., Mengistu Tsidu, G., Ene, D., Wunch, D., Cao, Z., Garcia, O., Ramonet, M., Vogel, F.
2872 and Orphal, J. (2019). Building the COllaborative Carbon Column Observing Network
2873 (COCCON): long-term stability and ensemble performance of the EM27/SUN Fourier
2874 transform spectrometer. *Atmospheric Measurement Technologies*, **12**, 1513–1530. doi:
2875 10.5194/amt-12-1513-2019

Friedlingstein, P., Cox, P., Betts, R., Bopp, L., von Bloh, W., Brovkin, V., Cadule, P., Doney, S., Eby, M., Fung, I., Bala, G., John, J., Jones, C., Joos, F., Kato, T., Kawamiya, M., Koor, W., Lindsay, D., Matthews, H. D., Raddatz, T., Rayner, P., Reick, C., Roekner, E., Schnitzler, D.-G., Schnur, R., Strassmann, K., Weaver, A., J., Yoshikawa, C., and Zeng, N. (2006). Climate–Carbon Cycle Feedback Analysis: Results from the $C^4$MIP Model Intercomparison. *Journal of Climate*, **19**, 3337-3353. doi: 10.1175/JCLI3800.1

Friedlingstein, P., Jones, M. W., O'Sullivan, M., Andrew, R. M., Hauck, J., Peters, G. P., Peters, W., Pongratz, J., Sitch, S., Le Quéré, C., Bakker, D. C. E., Canadell, J. G., Ciais, P., Jackson, R. B., Anthoni, P., Barbero, L., Bastos, A., Bastrikov, V., Becker, M., Bopp, L., Buitenhuis, E., Chandra, N., Chevallier, F., Chini, L. P., Currie, K. I., Feely, R. A., Gehlen, M., Gilfillan, D., Gkritzalis, T., Goll, D. S., Gruber, N., Gutekunst, S., Harris, I., Haverd, V., Houghton, R. A., Hurtt, G., Ilyina, T., Jain, A. K., Joetzjer, E., Kaplan, J. O., Kato, E., Klein Goldewijk, K., Korsbakken, J. I., Landschützer, P., Lauvset, S. K., Lefèvre, N., Lenton, A., Lienert, S., Lombardozzi, D., Marland, G., McGuire, P. C., Melton, J. R., Metzl, N., Munro, D. R., Nabel, J. E. M. S., Nakaoka, S.-I., Neill, C., Omar, A. M., Ono, T., Peregon, A., Pierrot, D., Poulter, B., Rehder, G., Resplandy, L., Robertson, E., Rödenbeck, C., Séférian, R., Schwinger, J., Smith, N., Tans, P. P., Tian, H., Tilbrook, B., Tubiello, F. N., van der Werf, G. R., Wiltshire, A. J. and Zaehle, S. (2019). Global Carbon Budget 2019. *Earth System Science Data*, **11**, 1783–1838. doi:10.5194/essd-11-1783-2019

Friedlingstein, P., O'Sullivan, M., Jones, M. W., Andrew, R. M., Hauck, J., Olsen, A., Peters, G. P., Peters, W., Pongratz, J., Sitch, S., Le Quéré, C., Canadell, J. G., Ciais, P., Jackson, R. B., Alin, S., Aragão, L. E. O. C., Arneth, A., Arora, V., Bates, N. R., Becker, M., Benoit-Cattin, A., Bittig, H. C., Bopp, L., Bultan, S., Chandra, N., Chevallier, F., Chini, L. P., Evans, W., Florentie, L., Forster, P. M., Gasser, T., Gehlen, M., Gilfillan, D., Gkritzalis, T., Gregor, L., Gruber, N., Harris, I., Hartung, K., Haverd, V., Houghton, R. A., Ilyina, T., Jain, A. K., Joetzjer, E., Kadono, K., Kato, E., Kitidis, V., Korsbakken, J. I., Landschützer, P., Lefèvre, N., Lenton, A., Lienert, S., Liu, Z., Lombardozzi, D., Marland, G., Metzl, N., Munro, D. R., Nabel, J. E. M. S., Nakaoka, S.-I., Niwa, Y., O'Brien, K., Ono, T., Palmer, P. I., Pierrot, D., Poulter, B., Resplandy, L., Robertson, E., Rödenbeck, C., Schwinger, J., Séférian, R., Skjelvan, I., Smith, A. J. P., Sutton, A. J., Tanhua, T., Tans, P. P., Tian, H., Tilbrook, B., van der Werf, G., Vuichard, N., Walker, A. P., Wanninkhof, R., Watson, A. J., Willis, D., Wiltshire, A. J., Yuan, W., Yue, X. and Zaehle, S. (2020). Global Carbon Budget 2020. *Earth System Science Data*, **12**, 3269–3340. doi:10.5194/essd-12-3269-2020

Friedlingstein, P., Jones, M. W., O'Sullivan, M., Andrew, R. M., Bakker, D. C. E., Hauck, J., Le Quéré, C., Peters, G. P., Peters, W., Pongratz, J., Sitch, S., Canadell, J. G., Ciais, P., Jackson, R. B., Alin, S. R., Anthoni, P., Bates, N. R., Becker, M., Bellouin, N., Bopp, L., Chau, T. T. T., Chevallier, F., Chini, L. P., Cronin, M., Currie, K. I., Decharme, B., Djeutchouang, L., Dou, X., Evans, W., Feely, R. A., Feng, L., Gasser, T., Gilfillan, D., Gkritzalis, T., Grassi, G., Gregor, L., Gruber, N., Gürses, Ö., Harris, I., Houghton, R. A., Hurtt, G. C., Iida, Y., Ilyina, T., Luijkx, I. T., Jain, A. K., Jones, S. D., Kato, E., Kennedy, D., Klein Goldewijk, K., Knauer, J., Korsbakken, J. I., Körtzinger, A., Landschützer, P., Lauvset, S. K., Lefèvre, N., Lienert, S., Liu, J., Marland, G., McGuire, P. C., Melton, J. R., Munro, D. R., Nabel, J. E. M. S., Nakaoka, S.-I., Niwa, Y., Ono, T., Pierrot, D., Poulter, B., Rehder, G., Resplandy, L., Robertson, E., Rödenbeck, C., Rosan, T. M., Schwinger, J., Schwingshackl, C., Séférian, R., Sutton, A. J., Sweeney, C., Tanhua, T., Tans, P. P., Tian, H., Tilbrook, B., Tubiello, F., van der Werf, G., Vuichard, N., Wada, C., Wanninkhof, R., Watson, A., Willis, D., Wiltshire,

A. J., Yuan, W., Yue, C., Yue, X., Zaehle, S., and Zeng, J. (2021). Global Carbon Budget 2021, Earth System Science Data Discuss. [preprint], doi: 10.5194/essd-2021-386, in review, 2021.

Friis, K., Körtzinger, A., Pätsch, J. and Wallace, D. W. R. (2005). On the temporal increase of anthropogenic $CO_2$ in the subpolar North Atlantic. *Deep-Sea Research.* **52**, 681-698. doi:10.1016/j.dsr.2004.11.017

Frölicher, T. L., Joos, F. and Raible, C. C. (2011). Sensitivity of atmospheric $CO_2$ and climate to explosive volcanic eruptions. *Biogeosciences*, **8**, 2317–2339. doi: 10.5194/bg-8-2317-2011

Frölicher, T. L., Joos, F., Raible, C. C. and Sarmiento, J. L. (2013). Atmospheric $CO_2$ response to volcanic eruptions: The role of ENSO, season, and variability. *Global Biogeochemical Cycles*, **27**, 239-251. doi:10.1002/gbc.20028

Frölicher, T.L., Rodgers, K. B., Stock, C. A., Cheung, W. W. L. (2016). Sources of uncertainties in 21st century projections of potential ocean ecosystem stressors: Uncertainties in stressor projections. *Global Biogeochemical Cycles,* **30**, 1224–1243. doi:10.1002/2015GB005338

Galbraith, E. D. and Skinner, L. C. (2020). The biological pump during the last glacial maximum. *Annual Reviews of Marine Science* **12**, 559–586. doi:10.1146/annurev-marine-010419-010906

Gampe, D., Zscheischler, J., Reichstein, M., O'Sullivan, M., Smith, W. K., Sitch, S. and Buermann, W. (2021). Increasing impact of warm droughts on northern ecosystem productivity over recent decades. *Nature Climate Change*, **11**, 772–779. doi: 10.1038/s41558-021-01112-8

Gasser, T., Crepin, L., Quilcaille, Y., Houghton, R. A., Ciais, P., and Obersteiner, M. (2020). Historical $CO_2$ emissions from land use and land cover change and their uncertainty, *Biogeosciences*, **17**, 4075–4101. doi: 10.5194/bg-17-4075-202

Gatti, L.V., Gloor, M., Miller, J. B., Doughty, C. E., Malhi, Y., Domingues, L. G., Basso, L. S., Martinewski, A., Correia, C. S., Borges, V. F., Freitas, S., Braz, R., Anderson, L. O., Rocha, H., Grace, J., Phillips, O. L. and Lloyd, J. (2014). Drought sensitivity of Amazonian carbon balance revealed by atmospheric measurements. *Nature*, **506**, 76-80. doi:10.1038/nature12957

Gatti, L, V., Basso, L., S., Miller, J., B., Gloor, M., Domingues, L. G., Cassol, H. L. G., Tejada, G., Arango, L. E. O. C. Nobre, C., Peters, W., Marani, L., Arai, E., Sanches, A. H., Correa, S. M., Anderson, L., von Randow, C., Correia, C. S. C., Crispim, S., P., and Neves, R. A. L. (2021). Amazonia as a carbon source linked to deforestation and climate change. *Nature*, **595**, 388-393. doi: 10.1038/s41586-021-03629-6

Gaubert, B., Stephens, B. B., Basu, S., Chevallier, F., Deng, F., Kort, E. A., Patra, P. K., Peters, W., Rödenbeck, C., Saeki, T., Schimel, D., Van der Laan-Luijx, I., Wofsy, S., Yin, Y. (2019). Global atmospheric $CO_2$ inverse models converging on neutral tropical land exchange, but disagreeing on fossil fuel and atmospheric growth rate. *Biogeosciences*, **16**, 117–134. doi: 10.5194/bg-16-117-2019

Gitz, V. and Ciais, P. (2003) Amplifying effects of land-use change on future atmospheric $CO_2$ levels. Global Biogeochemical Cycles, 17, 1024. doi: 10.1029/2002GB001963

Gloege, L., McKinley, G. A., Landschützer, P., Fay, A., Frölicher, T., Fyfe, J. C., Illyina, T., Jones, S.D., Lovenduski, N. S., Rödenbeck, C., Rodgers K. B., Schlunegger, S. and Takano, Y. (2021). Quantifying errors in observationally-based estimates of ocean carbon sink

variability. *Global Biogeochemical Cycles,* **35**, e2020GB006788. doi: 10.1029/2020GB006788

Gloege, L., Yan, M., Zheng, T., & McKinley, G. A. (2022). Improved quantification of ocean carbon uptake by using machine learning to merge global models and pCO 2 data. Journal of Advances in Modeling Earth Systems, 14, e2021MS002620. doi: 10.1029/2021MS002620

Gloor, M., Sarmiento, J. L. and Gruber, N. (2010). What can be learned about carbon cycle climate feedbacks from the $CO_2$ airborne fraction? *Atmospheric Chemistry and Physics,* **10**, 7739–7751. doi: 10.5194/acp-10-7739-2010

Gonsamo, A., Chen, J. M., He, L., Sun, Y., Rogers, C. and Liu, J. (2019). Exploring SMAP and OCO-2 observations to monitor soil moisture control on photosynthetic activity of global drylands and croplands, *Remote Sensing of Environment*, **232**, 111314. doi:10.1016/j.rse.2019.111314

Gonsamo, A., Ciais, P., Miralles, D. G., Sitch, S., Dorigo, W., Lombardozzi, D., Friedlingstein, P., Nabel, J. E. M. S., Goll, D. S., O'Sullivan, M., Arneth, A., Anthoni, P., Jain, A. K., Wiltshire, A., Peylin, P. and Cescatti, A. (2021). Greening drylands despite warming consistent with carbon dioxide fertilization effect. *Glob Change Biol*, **27**, 3336-3349. doi: 10.1111/gcb.15658

Goris, N., Tjiputra, J. F., Olsen, A., Schwinger, J., Lauvset S. K. and Jeansson E. (2018). Constraining projection-based estimates of the future North Atlantic carbon uptake. *Journal of Climate*, **31**, 3959–3978, doi:10.1175/JCLI-D-17-0564.1

Grace, J., Mitchard, E., and Gloor, E. (2014). Perturbations in the carbon budget of the tropics. *Global Change Biology*, **20**, 3238–3255. doi: 10.1111/gcb.12600

Grassi, G., House, J., Kurz, W. A., Cescatti, A., Houghton, R. A., Peters, G. P., Sanz, M. J., Viñas, R. A., Alkama, R., Arneth, A., Bondeau, A., Dentener, F., Fader, M., Federici, S., Friedlingstein, P., Jain, A. K., Kato, E., Koven, C. D., Lee, D., Nabel, J. E. M. S., Nassikas, A. A., Perugini, L., Rossi, S., Sitch, S., Viovy, N., Wiltshire, A. and Zaehle, S. (2018). Reconciling global-model estimates and country reporting of anthropogenic forest $CO_2$ sinks. *Nature Climate Change*, **8**, 914–920. doi: 10.1038/s41558-018-0283-x

Graven, H. D., Keeling, R. F., Piper, S. C., Patra, P. K., Stephens, B. B., Wofsy, S. C., Welp, L. R., Sweeney, C. and Tans, P. P. (2013). Enhanced seasonal exchange of $CO_2$ by northern ecosystems since 1960, *Science*, **341**, 1085–1089. doi:10.1126/science.1239207

Gregor, L., Lebehot, A. D. Kok, S. and Scheel Monteiro, P. M. (2019). A comparative assessment of the uncertainties of global surface-ocean $CO_2$ estimates using a machine learning ensemble (CSIR-ML6 version 2019a); have we hit the wall? *Geoscientific Model Development*, **12**, 5113–5136. doi:10.5194/gmd-12-5113-2019

Gruber, N., Clement, D., Carter, B.R., Feely, R.A., Van Heuven, S., Hoppema, M., Ishii, M., Key, R.M., Kozyr, A., Lauvset, S.K., Lo Monaco, C., Mathis, J.T., Murata, A., Olsen, A., Perez, F.F., Sabine, C.L., Tanhua, T., and Wanninkhof, R. (2019a). The oceanic sink for anthropogenic $CO_2$ from 1994 to 2007. *Science,* **363**, 1193-1199. doi:10.1126/science.aau5153

Gruber, N., Landschützer, P., and Lovendusk, N. S. (2019b). The variable Southern Ocean carbon sink. *Annual Reviews of Marine Sci*ence, **11**, 159–186. doi:10.1146/annurev-marine-121916-063407

3010 Guan, K., Berry, J. A., Zhang, Y., Joiner, J., Guanter, L., Badgley, G. and Lobell, D. B. (2016).
3011 Improving the monitoring of crop productivity using spaceborne solar-induced
3012 fluorescence. *Global Change Biology*, **22**, 716–726. doi:10.1111/gcb.13136
3013 Guan, K., Wu, J., Kimball, J. S., Anderson, M. C., Frolking, S., Li, B., Hain, C. R. and Lobell, D.
3014 B. (2017). The shared and unique values of optical, fluorescence, thermal and microwave
3015 satellite data for estimating large-scale crop yields. *Remote Sensing of Environment*, **199**,
3016 333–349. doi:10.1016/j.rse.2017.06.043
3017 Gurney, K. R., Law, R. M., Denning, A. S., Rayner, P. J., Baker, D., Bousquet, P., Bruhwiler, L.,
3018 Chen, Y.-H., Ciais, P., Fan, S., Fung, I. Y., Gloor, M., Heimann, M., Higuchi, K., John, J.,
3019 Maki, T., Maksyutov, S., Masarie, K., Peylin, P., Prather, M., Pak, B. C., Randerson, J.,
3020 Sarmiento, J., Taguchi, S., Takahashi, T., and Yuen, C.-W. (2002). Towards robust regional
3021 estimates of $CO_2$ sources and sinks using atmospheric transport models, *Nature*, **415**, 626–
3022 630. doi: 10.1038/415626a
3023 Gurney, K. R., Law, R. M., Denning, A. S., Rayner, P. J., Baker, D., Bousquet, P., Bruhwiler, L.,
3024 Chen, Y.-H., Ciais, P., Fan, S., Fung, I. Y., Gloor, M., Heimann, M., Higuchi, K., John, J.,
3025 Kowalczyk, E., Maki, T., Maksyutov, S., Peylin, P., Prather, M., Pak, B. C., Sarmiento, J.,
3026 Taguchi, S., Takahashi, T., and Yuen, C.-W. (2003). TransCom 3 CO2 inversion
3027 intercomparison: 1. Annual mean control results and sensitivity to transport and prior flux
3028 information, *Tellus B,* **55**, 555–579. doi: 10.3402/tellusb.v55i2.16728
3029 Gurney, K. R., Liang, J., O'Keeffe, D., Patarasuk, R., Hutchins, M., Huang, J., Rao, P. and Song,
3030 Y. (2019). Comparison of global downscaled versus bottom-up fossil fuel $CO_2$ emissions at
3031 the urban scale in four U.S. urban areas. *Journal of Geophysical Research: Atmospheres*,
3032 **124**, 2823--2840. doi:10.1029/2018JD028859
3033 Hakkarainen, J., Ialongo, I. and Tamminen, J. (2016). Direct space-based observations of
3034 anthropogenic $CO_2$ emission areas from OCO-2. *Geophysical Research Letters,* **43**, 11,400–
3035 11,406. doi:10.1002/2016GL070885
3036 Hakkarainen, J., Ialongo, I., Maksyutov, S., and Crisp, D. (2019). Analysis of Four Years of
3037 Global $XCO_2$ Anomalies as Seen by Orbiting Carbon Observatory-2, *Remote Sensing*, **11**,
3038 850. doi:10.3390/rs11070850
3039 Hakkarainen, J., Szelag, M. E., Ialongo, I., Retscher, C., Oda, T. and Crisp, D. (2021). Analyzing
3040 nitrogen oxides to carbon dioxide emission ratios from space: A case study of Matimba
3041 Power Station in South Africa. *Atmospheric Environment*, **10**, 100110. doi:
3042 10.1016/j.aeaoa.2021.100110
3043 Hansen, J., Sato, M., Russell, G. and Kharecha, P., (2013). Climate sensitivity, sea level and
3044 atmospheric carbon dioxide, *Philosophical Transactions of the Royal Society. A*., **371**,
3045 20120294. doi: 10.1098/rsta.2012.0294
3046 Hansen, M. C., Potapov, P. V., Moore, R., Hancher, M., Turubanova, S. A., Tyukavina, A., Thau,
3047 D., Stehman, S. V., Goetz, S. J., Loveland, T. R., Kommareddy, A., Egorov, A., Chini, L.,
3048 Justice, C. O., and Townshend, J. R. G. (2013b). High-Resolution Global Maps of 21st-
3049 Century Forest Cover Change. *Science*, **342**, 850–53. doi: 10.1126/science.1244693.
3050 Hansis, E., Davis, S. J. and Pongratz, J. (2015). Relevance of methodological choices for
3051 accounting of land use change carbon fluxes. *Global Biogeochemical Cycles*, **29**, 1230–
3052 1246. doi:10.1002/2014GB004997
3053 Harris, N. L., Hagen, S. C., Saatchi, S. S., Pearson, T. R. H., Woodall, C. W., Domke, G. M.,
3054 Braswell, B. H., Walters, B. F., Brown, S., Salas, W., Fore, A., and Yu, Y. (2016). Attribution

of net carbon change by disturbance type across forest lands of the conterminous United States. *Carbon Balance and Management*, **11**, 24. doi: 10.1186/s13021-016-0066-5

Harris, N. L., Gibbs, D. A., Baccini, A., Birdsey, R. A., de Bruin, S., Farina, M., Fatoyinbo, L., Hansen, M. C., Herold, M., Houghton, R. A., Potapov, P. V., Suarez, D. R., Roman-Cuesta, R. M., Saatchi,S., S., Slay, C. M., Turubanova, S., A., and Tyukavina, A. (2021). Global maps of twenty-first century forest carbon fluxes. *Nature Climate Change,* **11**, 234–240. doi:10.1038/s41558-020-00976-6

Hauck, J., Völker, C., Wang, T., Hoppema, M., Losch, M. and Wolf-Gladrow, D.A. (2013). Seasonally different carbon flux changes in the Southern Ocean in response to the southern annular mode. *Global Biogeochemical Cycles,* **27**, 1236–1245. doi:10.1002/2013GB004600

Hauck, J., Völker, C., Wolf-Gladrow, D. A., Laufkötter, C., Vogt, M., Aumont, O., Bopp, L., Buitenhuis, E. T., Doney, S. C., Dunne, J., Gruber, N., Hashioka, T., John, J., Le Quéré, C., Lima, I. D., Nakano, H., Séférian, R. and Totterdell, I. (2015). On the Southern Ocean $CO_2$ uptake and the role of the biological carbon pump in the 21st century. *Global Biogeochemical Cycles,* **29**, 1451–1470. doi:10.1002/2015GB005140

Hauck, J., Zeising, M., Le Quéré, C., Gruber, N., Bakker, D. C. E., Bopp, L., Chau, T. T. T., Gürses, Ö., Ilyina, T., Landschützer, P., Lenton, A., Resplandy, L., Rödenbeck, C., Schwinger, J. and Séférian, R. (2020). Consistency and challenges in the ocean carbon sink estimate for the Global Carbon Budget. *Frontiers in Marine Science,* **7**, 571720. doi:10.3389/fmars.2020.571720

Hausfather, Z. and Peters, G. P. (2020). Emissions - the "business as usual" story is misleading. *Nature*, **577**, 618–620, doi:10.1038/d41586-020-00177-3

He, L., Magney, T., Dutta, D., Yin, Y., Köhler, P., Grossmann, K., Stutz, J., Dold, C., Hatfield, J., Guan, K., Peng, B. and Frankenberg, C. (2020). From the ground to space: Using solar-induced chlorophyll fluorescence to estimate crop productivity. *Geophysical Research Letters*, **47**, e2020GL087474. doi:10.1029/2020GL087474

Hedelius, J. K., Feng, S., Roehl, C. M., Wunch, D., Hillyard, P. W., Podolske, J. R., Iraci, L. T., Patarasuk, R., Roa, P., O'Keeffe, D., Gurney, K. R., Lauvaux, T., and Wennberg, P. O. (2017). Emissions and topographic effects on column $CO_2$ ($XCO_2$) variations, with a focus on the Southern California Megacity. *Journal of Geophysical Research, Atmospheres,* **122**, 7200–7215, doi:10.1002/2017JD026455

Hedelius, J. K., Liu, J., Oda, T., Maksyutov, S., Roehl, C. M., Iraci, L., Podolske, J., Hillyard, P., Liang, J., Gurney, K., Wunch, D. and Wennberg P. (2018). Southern California megacity $CO_2$, $CH_4$, and CO flux estimates using ground- and space-based remote sensing and a Lagrangian model, *Atmospheric Chemistry and Physics,* **18**, 16271-16291. doi:10.5194/acp-18-16271-2018

Heimann, M., Esser, G., Haxeltine, A., Kaduk, J., Kicklighter, D. W., Knorr, W., Kohlmaier, G. H., McGuire, A. D., Melillo, J., Moore III, B., Otto, R. D., Prentice, I. C., Sauf, W., A. Schloss, Sitch, S., Wittenberg, U., Wurth, G. (1998). Evaluation of terrestrial carbon cycle models through simulations of the seasonal cycle of atmospheric $CO_2$: First results of a model intercomparison study. *Global Biogeochemical Cycles*, 12., 1, p 1-24. doi: 10.1029/97GB01936

Henson, S. A., Beaulieu, C. and Lampitt, R. (2016). Observing climate change trends in ocean biogeochemistry: when and where. *Global Change Biology,* **22**, 1561–1571. doi:10.1111/gcb.13152

3100 Hersbach, H., Bell. B., Berrisford, P., Hirahara, S., Horányi, A., Muñoz-Sabater, J., Nicolas, J.,
3101 Peubey, C., Radu, R., Schepers, D., Simmons, A., Soci. C., Abdalla, S., Abellan, X.,
3102 Balsamo G., Bechtold, P., Biavati, G., Bidlot, J., Bonavita, M., De Chiara, G., Dahlgren, P.,
3103 Dee, D., Diamantakis, M., Dragani, R., Flemming, J., Forbes, R., Fuentes, M., Geer A.,
3104 Haimberger L., Healy, S., Hogan, R. J., Hólm, E., Janisková, M., Keeley, S., Laloyaux, P.,
3105 Lopez, P., Radnoti, G., de Rosnay, P., Rozum, I., Vamborg, F., Villaume, S. and Thépaut J.-
3106 N. (2020). The ERA5 Global Reanalysis. *Quarterly Journal of the Royal Meteorological*
3107 *Society*, **146**, 1999-2049. doi: https://doi.org/10.1002/qj.3803

3108 Heymann, J., Reuter, M., Buchwitx, M., Schneising, O., Bovensmann, H., Burrows, J. P.,
3109 Massart, S., Kaiser, J. W., and Crisp, D. (2017). $CO_2$ emission of Indonesian fires in 2015
3110 estimated from satellite-derived atmospheric $CO_2$ concentrations. *Geophysical Research*
3111 *Lett*ers, **44**, 1537-1544. doi: 10.1002/2016GL072042

3112 Hlásny, T., Zimová, S., Merganičová, K., Štěpánek, P., Modlinger, R., and Turčáni, M. (2021).
3113 Devastating outbreak of bark beetles in the Czech Republic: Drivers, impacts, and
3114 management implications, *Forest Ecology and Management*, **490**,119075, doi:
3115 10.1016/j.foreco.2021.119075

3116 Hong, C., Burney, J. A., Pongratz, J., Nabel., J. E. M. S., Mueller, N. D., Jackson, R. B., and
3117 Davis, S. J. (2021). Global and regional drivers of land-use emissions in 1961–2017.
3118 *Nature*, **589**, 554-561. doi: 10.1038/s41586-020-03138-y

3119 Hoppema, M., Bakker, K., van Heuven, S. M. A. C., van Ooijen, J. C. and de Baar, H. J. W.
3120 (2015). Distributions, trends and inter-annual variability of nutrients along a repeat section
3121 through the Weddell Sea (1996–2011). *Marine Chemistry,* **177**, 545–553.
3122 doi:10.1016/j.marchem.2015.08.007

3123 Houghton, R. A. (2003). Revised estimates of the annual net flux of carbon to the atmosphere
3124 from changes in land use and land management 1850–2000. *Tellus*, **55B**, 378–390.
3125 doi:10.1034/j.1600-0889.2003.01450.x

3126 Houghton, R. A., House, J. I., Pongratz, J., van der Werf, G. R., DeFries, R. S., Hansen, M. C.,
3127 Le Quéré, C., and Ramankutty, N. (2012). Carbon emissions from land use and land-cover
3128 change, *Biogeosciences*, **9**, 5125–5142, doi: 10.5194/bg-9-5125-2012

3129 Houghton, R. A. and Nassikas, A. A. (2017). Global and regional fluxes of carbon from land use
3130 and land cover change 1850–2015. *Global Biogeochemical Cycles*, **31**, 456–472.
3131 doi:10.1002/2016GB005546

3132 Houweling, S., Baker, D., Basu, S., Boesch, H., Butz, A., Chevallier, F., Deng, F., Dlugokencky,
3133 E. J., Feng, L., Ganshin, A., Hasekamp, O., Jones, D., Maksyutov, S., Marshall, J., Oda, T.,
3134 O'Dell, C. W., Oshchepkov, S., Palmer, P. I., Peylin, P., Poussi, Z., Reum, F., Takagi, H.,
3135 Yoshida, Y., and Zhuravlev, R. (2015). An intercomparison of inverse models for estimating
3136 sources and sinks of $CO_2$ using GOSAT measurements, *Journal of Geophysical Research*
3137 *Atmospheres*, **120**, 5253–5266. doi: 10.1002/2014JD022962

3138 Hubau, W., Lewis, S. L., Phillips O. L., Affum-Baffoe, Beeckman, K. H., Cuni-Sanchez, A.,
3139 Ewango, C. E. N., Fauset, S., Sheil, D., Sonké, B., Sullivan, M. J. P., Sunderland,T.,
3140 Thomas, S. C., Abernethy, K. A., Adu-Bredu, S., Amani C. A., Baker, T. R., Banin, L. F.,
3141 Baya, F., Begne, S. K., Bennett, A. C., Benedet, F., Bitariho, R., Bocko, Y. E., Boeckx, P.,
3142 Boundja, P., Brienen, R. J. W., Brncic, T., Chezeaux, E., Chuyong, G. B., Clark, C. J.,
3143 Collins, M., Comiskey, J. A., Coomes, D. A., Dargie, G. C., de Haulleville, T., Kamdem, M.
3144 N. D., Doucet, J. L., Esquivel-Muelbert, A., Feldpausch, T. R., Fofanah, A., Foli, E. G.,

Gilpin, M., Gloor, E., Gonmadje, C., Gourlet-Fleury, S., Hall, J. S., Hamilton, A. C., Harris, D. J., Hart, T. B., Hockemba, M. B. N., Hladik, A., Ifo, S. F., Jeffery, K. J., Jucker, T., Yakusu, E. K., Kearsley, E., Kenfack, D., Koch, A., Leal, M. E., Levesley, A., Lindsell, J. A., Lisingo, J., Lopez-Gonzalez, G., Lovett, J. C., Makana, J. R., Malhi, Y., Marshall, A. R., Martin, J., Martin, E. H., Mbayu, F. M., Medjibe, V. P., Mitchard, E. T. A., Moore, S., Munishi, P. K. T., Bengone, N. N., Ojo, L., Ondo, F. E., Peh, K. S., Pickavance, G. C., Poulsen, A. D., Poulsen, J. R., Qie, L., Reitsma, J., Rovero, F., Swaine, M. D., Talbot, J., Taplin J., Taylor, D. D., Thomas, D. W., Toirambe, B., Mukendi, J. T., Tuagben, D., Umunay, P. M., van der Heijden, G. M. F., Verbeeck, H., Vleminckx, J., Willcock, S., Wöll, H., Woods, J. T. and Zemagho, L. (2020). Asynchronous carbon sink saturation in African and Amazonian tropical forests. *Nature,* **579**, 80–87. doi:10.1038/s41586-020-2035-0

Huber, M. B. and Zanna, L. (2017). Drivers of uncertainty in simulated ocean circulation and heat uptake. *Geophysical Research Letters,* **44**, 1402-1413. doi:10.1002/2016GL071587

Humphrey, V., Zscheischler, J., Ciais, P., Gudmundsson, L., Sitch, S., & Seneviratne, S. I. (2018). Sensitivity of atmospheric $CO_2$ growth rate to observed changes in terrestrial water storage. *Nature*, **560**, 628. doi: 10.1038/s41586-018-0424-4

Humphrey, V., Berg, A., Ciais, P., Gentine, P., Jung, M., Reichstein, M., Seneviratne, S. I., and Frankenberg, C. (2021). Soil moisture–atmosphere feedback dominates land carbon uptake variability. *Nature*, **592**, 65-69. doi: 10.1038/s41586-021-03325-5

Hurtt, G. C., Chini, L., Sahajpal, R., Frolking, S., Bodirsky, B. L., Calvin, K., Doelman, J. C., Fisk, J., Fujimori, S., Klein Goldewijk, K., Hasegawa, T., Havlik, P., Heinimann, A., Humpenöder, F., Jungclaus, J., Kaplan, J. O., Kennedy, J., Krisztin, T., Lawrence, D., Lawrence, P., Ma, L., Mertz, O., Pongratz, J., Popp, A., Poulter, B., Riahi, K., Shevliakova, E., Stehfest, E., Thornton, P., Tubiello, F. N., van Vuuren, D. P. and Zhang, X. (2020). Harmonization of global land use change and management for the period 850–2100 (LUH2) for CMIP6. *Geoscientific Model Development*, **13**, 5425–5464. doi: 10.5194/gmd-13-5425-2020

Hwang, Y. Schlüter, S. Choudhury, T.; Um, J.-S. (2021). Comparative Evaluation of Top-Down GOSAT $XCO_2$ vs. Bottom-Up National Reports in the European Countries. *Sustainability*, **13**, 6700. doi: 10.3390/su1312670

Iida, T., Odate, T., Fukuchi, M. (2013). Long-Term Trends of Nutrients and Apparent Oxygen Utilization South of the Polar Front in Southern Ocean Intermediate Water from 1965 to 2008. *PLoS ONE,* **8**, e71766. doi:10.1371/journal.pone.0071766

IEA World Energy Balances, 2020 Edition. Available from https://www.iea.org/subscribe-to-data-services/world-energy-balances-and-statistics, last viewed on 30 November 2021.

IPCC 2006, 2006 IPCC Guidelines for National Greenhouse Gas Inventories, Prepared by the National Greenhouse Gas Inventories Programme, Eggleston H.S., Buendia L., Miwa K., Ngara T. and Tanabe K. (eds). Published: IGES, Japan.

IPCC 2014, Intergovernmental Panel on Climate Change. (2014). Climate change 2013: The physical science basis: Working Group I contribution to the Fifth Assessment Report of the Intergovernmental Panel on Climate Change. In T. F. Stocker, D. Qin, G.-K. Plattner, M. Tignor, S. K. Allen, J. Boschung, et al. (Eds.), Cambridge University Press. doi: 10.1017/CBO9781107415324

IPCC 2019, 2019 Refinement to the 2006 IPCC Guidelines for National Greenhouse Gas Inventories, Calvo Buendia, E., Tanabe, K., Kranjc, A., Baasansuren, J., Fukuda, M.,

Ngarize S., Osako, A., Pyrozhenko, Y., Shermanau, P. and Federici, S. (eds). Published: IPCC, Switzerland.

IPCC, 2021: Summary for Policymakers. In: Climate Change 2021: The Physical Science Basis. Contribution of Working Group I to the Sixth Assessment Report of the Intergovernmental Panel on Climate Change [Masson-Delmotte, V., P. Zhai, A. Pirani, S.L. Connors, C. Péan, S. Berger, N. Caud, Y. Chen, L. Goldfarb, M.I. Gomis, M. Huang, K. Leitzell, E. Lonnoy, J.B.R. Matthews, T.K. Maycock, T. Waterfield, O. Yelekçi, R. Yu, and B. Zhou (eds.)]. Cambridge University Press. In Press.

Ito, A. (2020). Constraining size-dependence of vegetation respiration rates, *Scientific Reports*, **10**, 4304. doi:10.1038/s41598-020-61239-0

Iudicone, D., Rodgers, K. B., Plancherel, Y., Aumont, O., Ito, T., Key, R. M., Madec, G. and Ishii, M. (2016). The formation of the ocean's anthropogenic carbon reservoir. *Scientific Reports*, **6**, 35473. doi:10.1038/srep35473

Jacobson, A. R., Mikaloff Fletcher, S. E., Gruber, N., Sarmiento, J. L. and Gloor, M. (2007). A joint atmosphere-ocean inversion for surface fluxes of carbon dioxide: 1. Methods and global-scale fluxes. *Global Biogeochemical Cycles*, **21**, 273. doi:10.1029/1999GL900363

Janssens-Maenhout, G., Crippa, M., Guizzardi, D., Muntean, M., Schaaf, E., Dentener, F., Bergamaschi, P., Pagliari, V., Olivier, J. G. J., Peters, J. A. H. W., van Aardenne, J. A., Monni, S., Doering, U., Petrescu, A. M. R., Solazzo, E. and Oreggioni, G. D. (2019). EDGAR v4.3.2 Global Atlas of the three major greenhouse gas emissions for the period 1970–2012. *Earth System Science Data*, **11**, 959-1002. doi:10.5194/essd-11-959-2019

Janssens-Maenhout, G., Pinty, B., Dowell, M., Zunker, H., Andersson, E., Balsamo, G., Bézy, J. L., Brunhes, T., Bösch, H., Bojkov, B., Brunner, D., Buchwitz, M., Crisp, D., Ciais, P., Counet, P., Dee, D., Denier van der Gon, H., Dolman, H., Drinkwater, M., Dubovnik O., Engelen, R., Fehr, T., Fernandez, V., Heimann, M., Holmlund, K., Houweling, S., Husband, R., Juvyns, O., Kentarchos, A., Landgraf, J., Lang, R., Löscher, A., Marshall, J., Meijer, Y., Nakajima, M., Palmer, P. I., Peylin, P., Rayner, P., Scholze, M., Sierk, B., Tamminen, J., Veefkind, P. (2020). Toward an operational anthropogenic $CO_2$ emissions monitoring and verification support capacity. *Bulletin of the American Meteorological Society*, **101**, E1439-E1451. doi:10.1175/BAMS-D-19-0017.1

Jeong, S.-J., Bloom, A. A., Schimel, D., Sweeney, C., Parazoo, N. C., Medvigy, D., Schaepman-Strub, G., Zheng, C., Schwalm, C. R., Huntzinger, D. N., Michalak, A. M., and Miller, C. E. (2018). Accelerating rates of Arctic carbon cycling revealed by long-term atmospheric $CO_2$ measurements. *Science Advances*, **4**. Eaao1167. doi: 10.1126/sciadv.aao1167

Jian, J., Vargas, R., Anderson-Teixeira, K., Stell, E., Herrmann, V., Horn, M., Kholod, N., Manzon, J., Marchesi, R., Paredes, D. and Bond-Lamberty, B. (2021). A restructured and updated global soil respiration database (SRDB-V5). *Earth System Science Data*, **13**, 255-267, doi: 10.5194/essd-13-255-2021

Jiang, C., and Ryu, Y. (2016). Multi-scale evaluation of global gross primary productivity and evapotranspiration products derived from Breathing Earth System Simulator (BESS). *Remote Sensing of Environment*, **186**, 528-547. doi: 10.1016/j.rse.2016.08.030

Johnson, K. S., Jannasch, H. W., Coletti, L. J., Elrod, V. A., Martz, T. R., Takeshita, Y., Carlson, R. J. and Connery, J. G. (2016). Deep-Sea DuraFET: A pressure tolerant pH sensor designed for global sensor networks. *Analytical Chemistry*, **88**, 3249-3256. doi:10.1021/acs.analchem.5b04653

3235 Joiner, J., Yoshida, Y., Zhang, Y., Duveiller, G., Jung, M., Lyapustin, A., Wang, Y., and Tucker C.
3236 J. (2018). Estimation of Terrestrial Global Gross Primary Production (GPP) with Satellite
3237 Data-Driven Models and Eddy Covariance Flux Data. Remote Sensing, 10, 1346, doi:
3238 10.3390/rs10091346
3239 Jones, C. D. Ciais, P., Davis, S. J., Friedlingstein, P., Gasser, T., Peters, G. P., Rogelj, J., van
3240 Vuuren, D. P., Canadell, J. G., Cowie, A., Jackson, R. B., Jonas, M., Kriegler, E., Littleton,
3241 E., Lowe, J. A., Milne, J., Shrestha, G., Smith, P., Torvanger, A., and Wiltshire, A. (2016).
3242 Simulating the Earth system response to negative emissions. *Environmental Research*
3243 *Letters,* **11**, 095012. doi: 10.1088/1748-9326/11/9/095012
3244 Joos, F., Bruno, M., Fink, R., Siegenthaler, U., Stocker, T. F., Le Quéré, C. and Sarmiento, J. L.
3245 (1996). An efficient and accurate representation of complex oceanic and biospheric models
3246 of anthropogenic carbon uptake. *Tellus B*, **48**, 397. doi:10.1034/j.1600-0889.1996.t01-2-
3247 00006.x
3248 Joos, F. and Spahni, R. (2008). Rates of change in natural and anthropogenic radiative forcing
3249 over the past 20,000 years, *Proceedings of the National Academy of Sciences, USA*, **105**,
3250 1425–1430. doi: 10.1073/pnas.0707386105
3251 Jung, M., Reichstein, M. and Bondeau, A. (2009). Towards global empirical upscaling of
3252 FLUXNET eddy covariance observations: validation of a model tree ensemble approach
3253 using a biosphere model. *Biogeosciences*, **6**, 2001–2013. doi:10.5194/bg-6-2001-2009
3254 Jung, M., Reichstein, M., Schwalm, C. R., Huntingford, C., Sitch, S., Ahlström, A., Arneth, A.,
3255 Camps-Valls, G., Ciais, P., Friedlingstein, P., Gans, F., Ichii, K., Jain, A. K., Kato, E.,
3256 Papale, D., Poulter, B., Raduly, B., Rödenbeck, C., Tramontana, G., Viovy, N., Wang, Y.-P.,
3257 Weber, U., Zaehle, S., and Zeng, N. (2017). Compensatory water effects link yearly global
3258 land $CO_2$ sink changes to temperature, *Nature*, **541**, 516–520. doi: 10.1038/nature20780
3259 Jung, M., Schwalm, C. Migliavacca, M., Walther, S., Camps-Valls, G., Koirala, S., Anthoni, P.,
3260 Besnard, S., Bodesheim, P., Carvalhais, N., Chevallier, F., Gans, F., Goll, D. S., Haverd, V.,
3261 Koehler, P., Ichii, K., Jain, A. K., Liu, J., Lombardozzi, D., Nabel, J. E. M. S., Nelson, J. A.,
3262 O'Sullivan, M., Pallandt, M., Papale, D., Peters, W., Pongratz, J., Roedenbeck, C., Sitch, S.,
3263 Tramontana, G., Walker, A., Weber, U. and Reichstein, M. (2020). Scaling carbon fluxes
3264 from eddy covariance sites to globe: synthesis and evaluation of the FLUXCOM approach.
3265 *Biogeosciences*, **17**, 1343–1365. doi: 10.5194/bg-17-1343-2020
3266 Kao, H.-Y. and Yu, J.-Y. (2009). Contrasting Eastern-Pacific and Central-Pacific Types of ENSO,
3267 *J. Clim*., 22, 615–632. doi: 10.1175/2008JCLI2309.1
3268 Kaminski, T., and Heimann, M. (2001). Inverse Modeling of Atmospheric Carbon Dioxide
3269 Fluxes. *Science*, **294**, 259a. doi: 10.1126/science.294.5541.259a
3270 Kaminski, T., Scholze, M., Vossbeck, M., Knorr, W., Buchwitz, M., & Reuter, M. (2017).
3271 Constraining a terrestrial biosphere model with remotely sensed atmospheric carbon
3272 dioxide. Remote Sensing of Environment, 203, 109–124. doi: 10.1016/j.rse.2017.08.017
3273 Karion, A., Sweeney, C., Tans, P. P. and Newberger, T. (2010). AirCore: An innovative
3274 atmospheric sampling system. *Journal of Atmospheric and Oceanic Technology*, **27**, 1839–
3275 1853. doi:10.1175/2010JTECHA1448.1
3276 Keeling, C. D. (1960). The concentration and isotopic abundances of carbon dioxide in the
3277 atmosphere. Tellus, 12, 200-203. doi: 10.1111/j.2153-3490.1960.tb01300.x

Keeling, C. D. (1973) *The Carbon Dioxide Cycle: Reservoir Models to Depict the Exchange of Atmospheric Carbon Dioxide with the Oceans and Land Plants*. In Chemistry of the Lower Atmosphere. Springer. doi: 10.1007/978-1-4684-1986-3_6

Keeling, C. D., Bacastow, R. B., Carter, A. F., Piper, S. C., Whorf, T. P., Heimann, M., Mook, W. G., and Roeloffzen, H. (1989). A Three-Dimensional Model of Atmospheric $CO_2$ Transport Based on Observed Winds: 1. Analysis of Observational Data. *Geophysical Monograph,* **55**, 165-236. doi: 10.1029/GM055p0165

Keeling, C., Whorf, T., Wahlen, M., and van der Plichtt, J. (1995). Interannual extremes in the rate of rise of atmospheric carbon dioxide since 1980. *Nature,* **375,** 666–670 (1995). doi: 10.1038/375666a0

Keeling, C. D., Chin, J. F. S., and Whorf, T. P. (1996). Increased activity of northern vegetation inferred from atmospheric $CO_2$ measurements. *Nature*, **382**, 146-149. doi: 10.1038/382146a0

Keeling, C. D., Piper, S. C., Bacastow, R. B., Wahlen, M., Whorf, T. P., Heimann, M., and Meijer, H. A. (2001). Exchanges of Atmospheric $CO_2$ and $^{13}CO_2$ with the Terrestrial Biosphere and Oceans from 1978 to 2000.I. Global Aspects, UC San Diego: Library – Scripps Digital Collection. Retrieved from https://escholarship.org/uc/item/09v319r9

Keeling, C. D., Piper, S. C., Bacastow, R. B., Wahlen, M., Wahlen, M., Whorf, T. P., Heinmann, M. and Meijer, H. A. (2005) 'Atmospheric $CO_2$ and $^{13}CO_2$ exchange with the terrestrial biosphere and oceans from 1978 to 2000: Observations and carbon cycle implications', in *A history of atmospheric $CO_2$ and its effects on plants, animals, and ecosystems*. Springer, pp. 83–113.

Keenan, T. F., and Riley, W. J. (2018). Greening of the land surface in the world's cold regions consistent with recent warming. *Nature Climate Change*, **8**, 825-828. doi: 10.1038/s41558-018-0258-y

Keenan, T. F., and Williams, C. A. (2018). The terrestrial carbon sink. *Annual Review of Environment and Resources*. **43**, 219-243. doi:10.1146/annurev-environ- 102017-030204

Keppler, L., Landschützer, P. (2019). Regional wind variability modulates the Southern Ocean carbon sink. *Scientific Reports,* **9**, 7384. doi:10.1038/s41598-019-43826-y

Key, R. M., Kozyr, A., Sabine, C. L., Lee, K., Wanninkhof, R., Bullister, J. L., Feely, R. A., Millero, F. J., Mordy, C. and Peng, T. H. (2004). A global ocean carbon climatology: Results from Global Data Analysis Project (GLODAP). *Global Biogeochemical Cycles*, **18**(4), GB4031. doi:10.1029/2004GB002247

Khatiwala, S., Primeau, F. and Hall, T. (2009). Reconstruction of the history of anthropogenic $CO_2$ concentrations in the ocean. *Nature,* **462,** 346–349. doi:10.1038/nature08526

Khatiwala, S., Tanhua, T., Mikaloff Fletcher, S., Gerber, M., Doney, C. S., Graven, H. D., Gruber, N., Mckinley, G. A., Murata, A. and Sabine, C. (2013). Global storage of anthropogenic carbon. *Biogeosciences,* **10**, 2169-2191, 2013. doi: 10.519/bg-10-2169-2013

Kiel, M., O'Dell, C. W., Fisher, B., Eldering, A., Nassar, R., MacDonald, C. G. and Wennberg, P. O. (2019). How bias correction goes wrong: measurement of $XCO_2$ affected by erroneous surface pressure estimates. *Atmospheric Measurement Techniques*, **12**, 2241-2259. doi: 10.5194/amt-12-2241-2019

King, A. W., Andres, R. J., Davis, K. J., Hafer, M., Hayes, D. J., Huntzinger, D. N., de Jong, B., Kurz, W. A., McGuire, A. D., Vargas, R., Wei, Y., West, T. O., and Woodall, C. W. (2015).

North America's net terrestrial CO2 exchange with the atmosphere 1990–2009. *Biogeosciences*, **12**, 399–414. doi: 10.5194/bg-12-399-2015

Knorr, W. (2009). Is the airborne fraction of anthropogenic $CO_2$ emissions increasing? *Geophysical Research Letters*, 36, L21710. doi:10.1029/2009GL040613

Kondo, M., Ichii, K., Takagi, H., & Sasakawa, M. (2015). Comparison of the data-driven top-down and bottom-up global terrestrial $CO_2$ exchanges: GOSAT $CO_2$ inversion and empirical eddy flux upscaling. Journal of Geophysical Research: Biogeosciences, 120(7), 1226–1245. doi: 10.1002/2014J G002866

Kondo, M., Patra, P. K., Sitch, S., Friedlingstein, P., Poulter, B., Chevallier, F., Ciais, P., Canadell, J. G., Bastos, A., Lauerwald, R., Calle, L., Ichii, K., Anthoni, P., Arneth, A., Haverd, V., Jain, A. K., Kato, E., Kautz, M., Law, R. M., Lienert, S., Lombardozzi, D., Maki, T., Nakamura, T., Peylin, P., Rödenbeck, C., Zhuravlev, R., Saeki, T., Tian, H., Zhu, D and Ziehn, T. (2020). State of the science in reconciling top-down and bottom-up approaches for terrestrial $CO_2$ budget. *Global Change Biology*, **26**, 1068–1084. doi: 10.1111/gcb.14917

Konings, A. G., Piles, M., Das, N., and Entekhabi, D.(2017). L-band vegetation optical depth and effective scattering albedo estimation from SMAP, *Remote Sensing of Environment*, **198**, 460-470. doi:10.1016/j.rse

Koren, G., van Schaik, E., Araujo, A. C., Boersma, K. F., Gartner, A., Killaars, L., Kooreman, M. L., Kruijt, B., van der Laan-Luijkx, I. T., von Randow, C., Smith, N. E., and Peters, W. (2018). Widespread reduction in sun-induced fluorescence from the Amazon during the 2015/2016 El Nino. *Philosophical Transactions of the Royal Society of London. Series B: Biological Sciences*, **373**, 20170408. doi:10.1098/rstb.2017.0408

Kuze, A., Suto, H., Nakajima, M., and Hamazaki, T. (2009). Thermal and near infrared sensor for carbon observation Fourier-transform spectrometer on the Greenhouse Gases Observing Satellite for greenhouse gases monitoring, *Applied Opt*ics, **48**, 6716–6733, doi:10.1364/AO.48.006716

Kuze, A., Suto, H., Shiomi, K., Kawakami, S., Tanaka, M., Ueda, Y., Deguchi, A., Yoshida, J., Yamamoto, Y., Kataoka, F., Taylor, T. E., and Buijs, H. L. (2016). Update on GOSAT TANSOFTS performance, operations, and data products after more than 6 years in space, *Atmospheric Measurment Technology*, **9**, 2445–2461. doi: 10.5194/amt-9-2445-2016

Kwon, E.Y., Devries, T., Galbraith, E.D., Hwang, J., Kim, G., and Timmermann, A. (2021). Stable carbon isotopes suggest large terrestrial carbon inputs to the global ocean. *Global Biogeochemical Cycles*, **35**, e2020GB006684. doi: 10.1029/2020GB006684

Lacroix, F., T. Ilyina, and J. Hartmann (2020). Oceanic $CO_2$ outgassing and biological production hotspots induced by pre-industrial river loads of nutrients and carbon in a global modeling approach. *Biogeosciences*, **17**(1), 55–88. doi:10.5194/bg-17-55-2020

Lamarche, C., Santoro, M., Bontemps, S., d'Andrimont, R., Radoux, J., Giustarini, L., Brockmann, C., Wevers, J., Defourny, P. and Arino, O. (2017). Compilation and validation of SAR and optical data products for a complete and global map of inland/ocean water tailored to the climate modeling community. *Remote Sensing*, **9**, 36. doi:10.3390/rs9010036

Landschützer, P., Gruber, N., Bakker, D. C. E., Schuster, U., Nakaoka, S., Payne, M. R., Sasse, T. P. and Zeng, J. (2013). A neural network-based estimate of the seasonal to inter-annual variability of the Atlantic Ocean carbon sink. *Biogeosciences,* **10**, 7793–7815. doi:10.5194/bg-10-7793-2013

3367 Landschützer, P., Gruber, N., Bakker, D. C. E. and Schuster, U. (2014). Recent variability of the
3368 global ocean carbon sink. *Global Biogeochemical Cycles*, **28**, 927–949.
3369 doi:10.1002/2014GB004853
3370 Landschützer, P., Gruber, N., Haumann, F. A., Rödenbeck, C., Bakker, D. C. E., van Heuven, S.,
3371 Hoppema, M., Metzl, N., Sweeney, C., Takahashi, T., Tilbrook, B. and Wanninkhof, R.
3372 (2015). The reinvigoration of the Southern Ocean carbon sink. *Science,* **349**, 1221–1224.
3373 doi:10.1126/science.aab2620
3374 Landschützer, P., Gruber, N., and Bakker, D. C. E. (2017). An updated observation-based global
3375 monthly gridded sea surface $pCO_2$ and air-sea $CO_2$ flux product from 1982 through 2015
3376 and its monthly climatology (NCEI Accession 0160558), Version 2.2, NOAA National
3377 Centers for Environmental Information, Dataset [2017-07-11].
3378 Landschützer, P., Laruelle, G. G., Roobaert, A. and Regnier, P. (2020). A uniform $pCO_2$
3379 climatology combining open and coastal oceans. *Earth System Science Data*, **12**, 2537–
3380 2553. doi:10.5194/essd-2020-90
3381 Langlais, C. E., Lenton, A., Matear, R., Monselesan, D., Legresy, B., Cougnon, E. and Rintoul,
3382 S. (2017). Stationary Rossby waves dominate subduction of anthropogenic carbon in the
3383 Southern Ocean. *Scientific Reports,* **7**, 17076. doi:10.1038/s41598-017-17292-3
3384 Laufkötter, C., Vogt, M., Gruber, N., Aita-Noguchi, M., Aumont, O., Bopp, L., Buitenhuis, E.,
3385 Doney, S. C., Dunne, J., Hashioka, T., Hauck, J., Hirata, T., John, J., Le Quéré, C., Lima,
3386 I.D., Nakano, H., Seferian, R., Totterdell, I., Vichi, M. and Völker, C. (2015). Drivers and
3387 uncertainties of future global marine primary production in marine ecosystem models.
3388 *Biogeosciences,* **12**, 6955–6984. doi:10.5194/bg-12-6955-2015
3389 Laufkötter, C., Vogt, M., Gruber, N., Aumont, O., Bopp, L., Doney, S.C., Dunne, J.P., Hauck, J.,
3390 John, J.G., Lima, I.D., Seferian, R. and Völker, C. (2016). Projected decreases in future
3391 marine export production: the role of the carbon flux through the upper ocean ecosystem.
3392 *Biogeosciences,* **13**, 4023–4047. doi:10.5194/bg-13-4023-2016
3393 Lauvset, S. K., Lange, N., Tanhua, T., Bittig, H. C., Olsen, A., Kozyr, A., Álvarez, M., Becker,
3394 S., Brown, P. J., Carter, B. R., Cotrim Da Cunha, L., Feely, R. A., van Heuven, S.,
3395 Hoppema, M., Ishii, M., Jeansson, E., Jutterström, S., Jones, S. D., Karlsen, M. K., Lo
3396 Monaco, C., Michaelis, P., Murata, A., Pérez, F. F., Pfeil, B., Schirnick, C., Steinfeldt, R.,
3397 Suzuki, T., Tilbrook, B., Velo, A., Wanninkhof, R., Woosley, R. J., and Key, R. M. (2021).
3398 An updated version of the global interior ocean biogeochemical data product,
3399 GLODAPv2.2021. *Earth System Science Data.* 13, 5565–5589. doi: 10.5194/essd-13-5565-
3400 2021
3401 Lei, R., Feng, S., Danjou, A., Broquet, G., Wu, D., Lin, J. C., O'Dell, C. W., and Lauvaux, T.
3402 (2021). Fossil fuel $CO_2$ emissions over metropolitan areas from space: A multi-model
3403 analysis of OCO-2 data over Lahore, Pakistan. *Remote Sensing of Environment*, **264**,
3404 112625. doi: 10.1016/j.rse.2021.112625
3405 Lenton, A. and Matear, R. J. (2007). Role of the Southern Annular Mode (SAM) in Southern
3406 Ocean $CO_2$ uptake. *Global Biogeochemical Cycles,* **21**, GB2016.
3407 doi:10.1029/2006GB002714
3408 Le Quéré, C., Rödenbeck, C., Buitenhuis, E. T., Conway, T. J., Langenfelds, R., Gomez, A.,
3409 Labuschagne, C., Ramonet, M., Nakazawa, T., Metzl, N., Gillett, N. and Heimann, M.
3410 (2007). Saturation of the Southern Ocean $CO_2$ Sink Due to Recent Climate Change.
3411 *Science,* **316**, 1735–1738. doi:10.1126/science.1136188

Le Quéré, C., Raupach, M. R., Canadell, J. G., Marland, G., Bopp, L., Ciais, P., Conway, T. J., Doney, S. C., Feely, R. A., Foster, P., Friedlingstein, P., Gurney, K., Houghton, R. A., House, J. I., Huntingford, C., Levy, P. E., Lomas, M. R., Majkut, J., Metzl, N., Ometto, J. P., Peters, G. P., Prentice, I. C., Randerson, J. T., Running, S. W., Sarmiento, J. L., Schuster, U., Sitch, S., Takahashi, T., Viovy, N., van der Werf, G. R. and Woodward, F. I. (2009). Trends in the sources and sinks of carbon dioxide. *Nature Geosciences,* **2**, 831–836. doi:10.1038/ngeo689

Le Quéré, C., Takahashi, T., Buitenhuis, E. T., Rödenbeck, C. and Sutherland, S. C. (2010). Impact of climate change and variability on the global oceanic sink of $CO_2$. *Global Biogeochemical Cycles,* **24**, GB4007. doi:10.1029/2009GB003599

Le Quéré, C., Andres, R. J., Boden, T., Conway, T., Houghton, R. A., House, J. I., Marland, G., Peters, G. P., van der Werf, G. R., Ahlström, A., Andrew, R. M., Bopp, L., Canadell, J. G., Ciais, P., Doney, S. C., Enright, C., Friedlingstein, P., Huntingford, C., Jain, A. K., Jourdain, C., Kato, E., Keeling, R. F., Klein Goldewijk, K., Levis, S., Levy, P., Lomas, M., Poulter, B., Raupach, M. R., Schwinger, J., Sitch, S., Stocker, B. D., Viovy, N., Zaehle and S. and Zeng, N. (2013). The global carbon budget 1959–2011. *Earth System Science Data,* **5**, 165–185. doi:10.5194/essd-5-165-2013

Le Quéré, C., Peters, G. P., Andres, R. J., Andrew, R. M., Boden, T. A., Ciais, P., Friedlingstein, P., Houghton, R. A., Marland, G., Moriarty, R., Sitch, S., Tans, P., Arneth, A., Arvanitis, A., Bakker, D. C. E., Bopp, L., Canadell, J. G., Chini, L. P., Doney, S. C., Harper, A., Harris, I., House, J. I., Jain, A. K., Jones, S. D., Kato, E., Keeling, R. F., Klein Goldewijk, K., Körtzinger, A., Koven, C., Lefèvre, N., Maignan, F., Omar, A., Ono, T., Park, G.-H., Pfeil, B., Poulter, B., Raupach, M.R., Regnier, P., Rödenbeck, C., Saito, S., Schwinger, J., Segschneider, J., Stocker, B.D., Takahashi, T., Tilbrook, B., van Heuven, S., Viovy, N., Wanninkhof, R., Wiltshire, A. and Zaehle, S. (2014). Global carbon budget 2013. *Earth System Science Data,* **6**, 235–263. doi:10.5194/essd-6-235-2014

Le Quéré, C., Moriarty, R., Andrew, R. M., Peters, G. P., Ciais, P., Friedlingstein, P., Jones, S. D., Sitch, S., Tans, P., Arneth, A., Boden, T. A., Bopp, L., Bozec, Y., Canadell, J. G., Chini, L. P., Chevallier, F., Cosca, C. E., Harris, I., Hoppema, M., Houghton, R. A., House, J. I., Jain, A. K., Johannessen, T., Kato, E., Keeling, R. F., Kitidis, V., Klein Goldewijk, K., Koven, C., Landa, C. S., Landschützer, P., Lenton, A., Lima, I. D., Marland, G., Mathis, J. T., Metzl, N., Nojiri, Y., Olsen, A., Ono, T., Peng, S., Peters, W., Pfeil, B., Poulter, B., Raupach, M. R., Regnier, P., Rödenbeck, C., Saito, S., Salisbury, J. E., Schuster, U., Schwinger, J., Séférian, R., Segschneider, J., Steinhoff, T., Stocker, B. D., Sutton, A. J., Takahashi, T., Tilbrook, B., van der Werf, G. R., Viovy, N., Wang, Y.-P., Wanninkhof, R., Wiltshire, A. and Zeng, N. (2015a). Global carbon budget 2014. *Earth System Science Data,* **7**, 47–85. doi:10.5194/essd-7-47-2015

Le Quéré, C., Moriarty, R., Andrew, R. M., Canadell, J. G., Sitch, S., Korsbakken, J. I., Friedlingstein, P., Peters, G. P., Andres, R.J., Boden, T. A., Houghton, R. A., House, J. I., Keeling, R. F., Tans, P., Arneth, A., Bakker, D. C. E., Barbero, L., Bopp, L., Chang, J., Chevallier, F., Chini, L. P., Ciais, P., Fader, M., Feely, R. A., Gkritzalis, T., Harris, I., Hauck, J., Ilyina, T., Jain, A. K., Kato, E., Kitidis, V., Klein Goldewijk, K., Koven, C., Landschützer, P., Lauvset, S. K., Lefèvre, N., Lenton, A., Lima, I. D., Metzl, N., Millero, F., Munro, D. R., Murata, A., Nabel, J. E. M. S., Nakaoka, S., Nojiri, Y., O'Brien, K., Olsen, A., Ono, T., Pérez, F. F., Pfeil, B., Pierrot, D., Poulter, B., Rehder, G., Rödenbeck, C., Saito, S., Schuster, U., Schwinger, J., Séférian, R., Steinhoff, T., Stocker, B. D., Sutton, A. J., Takahashi, T., Tilbrook, B., van der Laan-Luijkx, I. T., van der Werf, G. R., van Heuven, S.,

Vandemark, D., Viovy, N., Wiltshire, A., Zaehle, S. and Zeng, N. (2015b). Global Carbon Budget 2015. *Earth System Science Data,* **7**, 349–396. doi:10.5194/essd-7-349-2015

Le Quéré, C., Andrew, R. M., Canadell, J. G., Sitch, S., Korsbakken, J. I., Peters, G. P., Manning, A. C., Boden, T. A., Tans, P. P., Houghton, R. A., Keeling, R. F., Alin, S., Andrews, O. D., Anthoni, P., Barbero, L., Bopp, L., Chevallier, F., Chini, L. P., Ciais, P., Currie, K., Delire, C., Doney, S. C., Friedlingstein, P., Gkritzalis, T., Harris, I., Hauck, J., Haverd, V., Hoppema, M., Klein Goldewijk, K., Jain, A. K., Kato, E., Körtzinger, A., Landschützer, P., Lefèvre, N., Lenton, A., Lienert, S., Lombardozzi, D., Melton, J. R., Metzl, N., Millero, F., Monteiro, P. M. S., Munro, D. R., Nabel, J. E. M. S., Nakaoka, S., O'Brien, K., Olsen, A., Omar, A. M., Ono, T., Pierrot, D., Poulter, B., Rödenbeck, C., Salisbury, J., Schuster, U., Schwinger, J., Séférian, R., Skjelvan, I., Stocker, B. D., Sutton, A. J., Takahashi, T., Tian, H., Tilbrook, B., van der Laan-Luijkx, I. T., van der Werf, G. R., Viovy, N., Walker, A. P., Wiltshire, A. J. and Zaehle, S. (2016). Global Carbon Budget 2016. *Earth System Science Data,* **8**, 605–649. doi:10.5194/essd-8-605-2016

Le Quéré, C., Andrew, R. M., Friedlingstein, P., Sitch, S., Pongratz, J., Manning, A. C., Korsbakken, J. I., Peters, G. P., Canadell, J. G., Jackson, R. B., Boden, T. A., Tans, P. P., Andrews, O. D., Arora, V. K., Bakker, D. C. E., Barbero, L., Becker, M., Betts, R. A., Bopp, L., Chevallier, F., Chini, L. P., Ciais, P., Cosca, C. E., Cross, J., Currie, K., Gasser, T., Harris, I., Hauck, J., Haverd, V., Houghton, R. A., Hunt, C. W., Hurtt, G., Ilyina, T., Jain, A. K., Kato, E., Kautz, M., Keeling, R. F., Klein Goldewijk, K., Körtzinger, A., Landschützer, P., Lefèvre, N., Lenton, A., Lienert, S., Lima, I., Lombardozzi, D., Metzl, N., Millero, F., Monteiro, P. M. S., Munro, D. R., Nabel, J. E. M. S., Nakaoka, S., Nojiri, Y., Padin, X. A., Peregon, A., Pfeil, B., Pierrot, D., Poulter, B., Rehder, G., Reimer, J., Rödenbeck, C., Schwinger, J., Séférian, R., Skjelvan, I., Stocker, B. D., Tian, H., Tilbrook, B., Tubiello, F. N., van der Laan-Luijkx, I. T., van der Werf, G. R., van Heuven, S., Viovy, N., Vuichard, N., Walker, A. P., Watson, A. J., Wiltshire, A. J., Zaehle, S. and Zhu, D. (2018a). Global Carbon Budget 2017. *Earth System Science Data,* **10**, 405–448. doi:10.5194/essd-10-405-2018

Le Quéré, C., Andrew, R. M., Friedlingstein, P., Sitch, S., Hauck, J., Pongratz, J., Pickers, P. A., Korsbakken, J. I., Peters, G. P., Canadell, J. G., Arneth, A., Arora, V. K., Barbero, L., Bastos, A., Bopp, L., Chevallier, F., Chini, L.P., Ciais, P., Doney, S. C., Gkritzalis, T., Goll, D. S., Harris, I., Haverd, V., Hoffman, F. M., Hoppema, M., Houghton, R. A., Hurtt, G., Ilyina, T., Jain, A.K., Johannessen, T., Jones, C. D., Kato, E., Keeling, R. F., Goldewijk, K. K., Landschützer, P., Lefèvre, N., Lienert, S., Liu, Z., Lombardozzi, D., Metzl, N., Munro, D. R., Nabel, J. E. M. S., Nakaoka, S., Neill, C., Olsen, A., Ono, T., Patra, P., Peregon, A., Peters, W., Peylin, P., Pfeil, B., Pierrot, D., Poulter, B., Rehder, G., Resplandy, L., Robertson, E., Rocher, M., Rödenbeck, C., Schuster, U., Schwinger, J., Séférian, R., Skjelvan, I., Steinhoff, T., Sutton, A., Tans, P. P., Tian, H., Tilbrook, B., Tubiello, F. N., van der Laan-Luijkx, I. T., van der Werf, G. R., Viovy, N., Walker, A. P., Wiltshire, A. J., Wright, R., Zaehle, S. and Zheng, B. (2018b). Global Carbon Budget 2018. *Earth System Science Data,* **10**, 2141–2194. doi:10.5194/essd-10-2141-2018

Le Quéré, C., Jackson, R. B., Jones, M. W., Smith, A. J. P., Abernethy, S., Andrew, R. M., De-Gol, A. J., Willis, D. R., Shan, Y., Canadell, J. G., Friedlingstein, P., Creutzig, F. and Peters, G. P. (2020). Temporary reduction in daily global $CO_2$ emissions during the COVID-19 forced confinement. *Nature Climate Change* **10,** 647–653. doi: 10.1038/s41558-020-0797-x

Liang, M. C., Mahata, S., Laskar, A. H., Thiemens, M. H., and Newman, S. (2017). Oxygen isotope anomaly in tropospheric $CO_2$ and implications for $CO_2$ residence time in the

atmosphere and gross primary productivity. *Scientific Reports,* **7**, 13180. doi: 10.1038/s41598-017-12774-w

Liao, E., Resplandy, L., Liu, J. and Bowman, K. W. (2020). Amplification of the Ocean Carbon Sink During El Niños: Role of Poleward Ekman Transport and Influence on Atmospheric $CO_2$. *Global Biogeochemical Cycles* **34**, e2020GB006574. doi: 10.1029/2020GB006574

Liu, J., Bowman, K., Schimel, D., Parazoo, N., Jiang, Z., Lee, M., Bloom, A., Wunch, D., Gurney, K., Menemenlis, D., Girerach, M., Crisp, D. and Eldering A. (2017). Contrasting carbon cycle responses of the tropical continents to the 2015–2016 El Niño. *Science,* **358**, eaam5690. doi: 10.1126/science.aam5690

Liu, J., Wennberg, P. O., Parazoo, N. C., Yin, Y. and Frankenberg, C. (2020a). Observational constraints on the response of high-latitude northern forests to warming. *AGU Advances*, **2**, e2020AV000228. doi:10.1029/2020AV000228

Liu, Y. Y., de Jeu, R. A. M., McCabe, M. F., Evans, J. P., and van Dijk, A. I. J. M. (2011), Global long-term passive microwave satellite-based retrievals of vegetation optical depth, *Geophysical Research Letters*, **38**, L18402, doi:10.1029/2011GL048684.

Liu, Y. Y., Van Dijk, A. I., De Jeu, R. A., Canadell, J. G., McCabe, M. F., Evans, J. P., and Wang, G. (2015). Recent reversal in loss of global terrestrial biomass, *Nature Climate Change*, **5**, 470–474. doi: 10.1038/nclimate2581

Liu, Z., Ciais, P., Deng, Z., Lei, R., Davis, S. J., Feng, S., Zheng, B., Cui, D., Dou, X., Zhu, B., Guo, R., Ke, P., Sun, T., Lu, C., He, P., Wang, Y., Yue, X., Wang, Y., Lei, Y., Zhou, H., Cai, Z., Wu, Y., Guo, R., Han, T., Xue, J., Boucher, O., Boucher, E., Chevallier, F., Tanaka, K., Wei, Y., Zhong, H., Kang, C., Zhang, N., Chen, B., Xi, F., Liu, M., Bréon, F. M., Lu, Y., Zhang, Q., Guan, D., Gong, P., Kammen, D. M., He, K., and Schellnhuber, H. J. (2020b). Near-real-time monitoring of global $CO_2$ emissions reveals the effects of the COVID-19 pandemic, *Nature Communications*, **11**, 1–12. doi: 10.1038/s41467-020-18922-7

Long, M. C., Lindsay, K., Peacock, S., Moore, J. K., and Doney, S. C. (2013). Twentieth-century oceanic carbon uptake and storage in CESM1(BGC). *Journal of Climate*, **26**, 6775–6800. doi:10.1175/JCLI-D-12-00184.1

Lovenduski, N. S., Gruber, N., Doney, S. C. and Lima, I. D. (2007). Enhanced $CO_2$ outgassing in the Southern Ocean from a positive phase of the Southern Annular Mode. *Global Biogeochemical Cycles,* **21**, GB2026. doi:10.1029/2006GB002900

Lovenduski, N. S., Gruber, N. and Doney, S.C. (2008). Toward a mechanistic understanding of the decadal trends in the Southern Ocean carbon sink: Southern Ocean $CO_2$ flux trends. *Global Biogeochemical Cycles,* **22**(3), GB3016. doi:10.1029/2007GB003139

Lucht, W., Prentice, C., Myneni, R. B., Sitch, S., Friedlingstein, P., Cramer, W., Bousquet, P., Buermann, W. and Smith, B. (2002). Climatic control of the high-latitude vegetation greening trend and Pinatubo effect. *Science*, **296**, 1687–1689. doi:10.1126/science.1071828

Ma, X., Huete, A., Cleverly, J., Eamus, D., Chevallier, F., Joiner, J., Poulter, B., Zhang, Y., Guanter, L., Meyer, W., Xie, Z. and Ponce-Campos, G. (2016). Drought rapidly diminishes the large net $CO_2$ uptake in 2011 over semi-arid Australia. *Scientific Reports,* ***6***, 37747 (2016). doi: 10.1038/srep37747

Macbean, N., Maignan, F., Bacour, C., Lewis, P., Peylin, P., Guanter, L., Köhler, P., Gomez-Dans, J., and Disney, M. (2018). Strong constraint on modelled global carbon uptake using solar-induced chlorophyll fluorescence data. *Scientific Reports*, **8**, 1973. doi: 10.1038/s41598-018-20024-w

MacDougall, A. H., Frölicher, T. L., Jones, C. D., Rogelj, J., Matthews, H. D., Zickfeld, K., Arora, V. K., Barrett, N. J., Brovkin, V., Burger, F. A., Eby, M., Eliseev, A. V., Hajima, T., Holden, P. B., Jeltsch-Thömmes, A., Koven, C., Mengis, N., Menviel, L., Michou, M., Mokhov, I. I., Oka, A., Schwinger, J., Séférian, R., Shaffer, G., Sokolov, A., Tachiiri, K., Tjiputra, J., Wiltshire, A. and Ziehn, T. (2020). Is there warming in the pipeline? A multi-model analysis of the zero emissions commitment from $CO_2$. *Biogeosciences,* **17**, 2987–3016. doi:10.5194/bg-17-2987-2020

Maier-Reimer, E., Mikolajewicz, U. and Winguth, A. (1996). Future ocean uptake of $CO_2$: interaction between ocean circulation and biology. *Climate Dynamics*, 12, 711-721. doi: 10.1007/s003820050138

Maksyutov, S., Takagi, H., Valsala, V. K., Saito, M., Oda, T., Saeki, T., Belikov, D. A., Saito, R., Ito, A., Yoshida, Y., Morino, I., Uchino, O., Andres, R. J. and Yokota, T. (2013). Regional $CO_2$ flux estimates for 2009–2010 based on GOSAT and ground-based $CO_2$ observations. *Atmospheric Chemistry and Physics*, **13**, 2351-9373. doi: 1 0.5194/acp-13-9351-2013

Marsay, C.M., Sanders, R. J., Henson, S. A., Pabortsava, K., Achterberg, E. P. and Lampitt, R. S. (2015). Attenuation of sinking particulate organic carbon flux through the mesopelagic ocean. *Proceedings of the National Academy of Sciences,* **112**, 1089. doi:10.1073/pnas.1415311112

Marchant, R., Mumbi, C., Behera, S., and Yamagata, T. (2006). The Indian Ocean dipole – the unsung driver of climatic variability in East Africa. *African Journal_of Ecology*, **45**, 4-16. doi: 10.1111/j.1365-2028.2006.00707.x

Marrs, J. K., Reblin, J. S., Logan, B. A., Allen, D. W., Reinmann, A. B., Bombard, D. M., Tabachnik, D. and Hutyra, L. R. (2020). Solar-induced fluorescence does not track photosynthetic carbon assimilation following induced stomatal closure. *Geophysical Research Letters*, **47**, e2020GL087956. doi: 10.1029/2020GL087956

Marshall, G. J., Trends in the Southern Annular Mode from Observations and Reanalyses. *Journal of Climate*, **16**, 4134-4143. doi: 10.1175/1520-0442(2003)016<4134:TITSAM>2.0.CO;2

Mau, A. C., Reed, S. C., Wood, T. E. and Cavaleri, M. A. (2018). Temperate and tropical forest canopies are already functioning beyond their thermal thresholds for photosynthesis. *Forests*, **9**, 47. doi:10.3390/f9010047

McGuire, A. D., S. Sitch, J. S. Clein, R. Dargaville, G. Esser, J. Foley, M. Heimann, F. Joos, J. Kaplan, D. W. Kicklighter, R. A. Meier, J. M. Melillo, B. Moore, I. C. Prentice, N. Ramankutty, T. Reichenau, A. Schloss, H. Tian, L. J. Williams, and U. Wittenberg. (2001). Carbon balance of the terrestrial biosphere in the twentieth century: analyses of $CO_2$, climate and land use effects with four process-based ecosystem models. *Global Biogeochemical Cycles* **15**, 183-206. doi: 10.1029/2000GB001298

McKinley, G., Follows, M. & Marshall, J. (2004). Mechanisms of air-sea $CO_2$ flux variability in the equatorial Pacific and the North Atlantic. *Global Biogeochemical Cycles*, **18**, GB2011. doi:10.1029/2003GB002179

McKinley, G., Follows, M., and Marshall, J. (2004). Mechanisms of air-sea $CO_2$ flux variability in the equatorial Pacific and the North Atlantic. *Global Biogeochemical Cycles*, **18**, GB2011. doi:10.1029/2003GB002179

McKinley, G. A., Fay, A. R., Takahashi, T. and Metzl, N. (2011). Convergence of atmospheric and North Atlantic carbon dioxide trends on multidecadal timescales. *Nature Geosci,* **4**, 606–610. doi:10.1038/ngeo1193

McKinley, G. A., Pilcher, D. J., Fay, A. R., Lindsay, K., Long, M. C. and Lovenduski, N. S. (2016). Timescales for detection of trends in the ocean carbon sink. *Nature*, **530**, 469–472. doi:10.1038/nature16958

McKinley, G. A., Fay, A. R., Lovenduski, N. S. and Pilcher, D. J. (2017). Natural variability and anthropogenic trends in the ocean carbon sink. *Annual Review of Marine Science*, **9**, 125–150, doi:10.1146/annurev-marine-010816-060529

McKinley, G. A., Fay, A. R., Eddebbar, Y. A., Gloege L. and Lovenduski, N. S. (2020). External forcing explains recent decadal variability of the ocean carbon sink. *AGU Advances*, **1**, 1, e2019AV000149. doi:10.1029/2019AV000149

McPhaden, M. J., Zebiak, S. E., and Glantz, M. H. (2006). ENSO as an Integrating Concept in Earth Science, *Science*, **314**, 1740–1745. doi: 10.1126/science.1132588

Medlyn, B., Zaehle, S., De Kauwe, M., Walker, A. P., Dietze, M. C., Hanson, P. J., Hickler, T., Jain, A. K., Luo, Y., Parton, W., Prentice, I., C., Thornton, P. E., Wang, S., Wang, Y.-P., Weng, E., Iversen, C. M., McCarthy, H. R., Warren, J. M., Oren, R., and Norby, R. J. (2015). Using ecosystem experiments to improve vegetation models. *Nature Climate Change,* **5**, 528–534. doi: 10.1038/nclimate2621

Mercado, L.M., Medlyn, B. E., Huntingford, C., Oliver, R. J., Clark, D. B., Sitch, S., Zelazowski, P., Kattge, J., Harper, A. B. and Cox, P. M. (2018). Large sensitivity in land carbon storage due to geographical and temporal variation in the thermal response of photosynthetic capacity, *New Phytologist*, **218**, 1462-1477, doi: 10.1111/nph.15100.

Meroni, M., Rossini, M., Guanter, L., Alonso L., Rascher, U., Colombo, R., and Moreno, J. (2009). Remote sensing of solar-induced chlorophyll fluorescence: Review of methods and applications, *Remote Sensing of Environment*, **113**,2037-2051, ISSN 0034-4257, doi: 10.1016/j.rse.2009.05.003

Mikaloff Fletcher, S. E., Gruber, N., Jabobson, A. R., Doney, S., C., Sutkiewicz, S., Gerber, M., Follows, M., Joos, F., Lindsay, K., Menemenlis, D., Mouchet, A., Müller, S., A. and Sarmiento, J. L. (2006). Inverse estimates of anthropogenic $CO_2$ uptake, transport, and storage by the ocean, *Global Biogeochemical Cycles*, **20**, GB2002. doi:10.1029/2005GB002530

Miller, J. B., Lehman, S. J., Montzka, S. A., Sweeney, C., Miller, B. R., Karion, A., Wolak, C., Dlugokencky, E. J., Southon, J., Turnbull, J. C. and Tans, P. P. (2012). Linking emissions of fossil fuel $CO_2$ and other anthropogenic trace gases using atmospheric $^{14}CO_2$. *Journal of Geophysical Research: Atmospheres,* **117**, D08302. doi:10.1029/2011JD017048

Miller, J. B., Lehman, S. J., Verhulst, K. R., Miler, C., E., Duren, R. M., Yadav, V., Newman, S. and Sloop, C. D. (2020). Large and seasonally varying biospheric $CO_2$ fluxes in the Los Angeles megacity revealed by atmospheric radiocarbon. *Proceedings of the National Academy of Sciences*, **117**, 26681-26687. doi:10.1073/pnas.2005253117

Mohammed, G. H., Colombo, R., Middleton, E. M., Rascherd, U., van der Tol, C., Nedbal, L., Goulasf, Y., Pérez-Priego, O., Damm, A., Meroni, M., Joiner, J., Cogliati, S., Verhoef, W., Malenovský, Z., Gastellu-Etchegorry, J.-P., Miller, J. R., Guanter, L., Morenoo, J., Moya, I., Berry, J. A., Frankenberg, C., Zarco-Tejadaj, P. J. (2019). Remote sensing of solar-

induced chlorophyll fluorescence (SIF) in vegetation: 50 years of progress, *Remote Sensing of Environment*, **31** 111177. doi:10.1016/j.rse.2019.04.030

Molod, A., Takacs, L., Suarez, M., & Bacmeister, J. (2015). Development of the GEOS-5 atmospheric general circulation model: Evolution from MERRA to MERRA2. *Geoscientific Model Development*, **8**, 1339–1356. doi: 10.5194/gmd-8-1339-015.

Mongwe, N. P., Vichi, M. and Monteiro, P. M. S. (2018). The seasonal cycle of $pCO_2$ and $CO_2$ fluxes in the Southern Ocean: diagnosing anomalies in CMIP5 Earth system models. *Biogeosciences*, **15**, 2851–2872. doi:10.5194/bg-15-2851-2018

Monteil, G., Broquet, G., Scholze, M., Lang, M., Karstens, U., Gerbig, C., Koch, F.-T., Smith, N. E., Thompson, R. L., Luijkx, I. T., White, E., Meesters, A., Ciais, P., Ganesan, A. L., Manning, A., Mischurow, M., Peters, W., Peylin, P., Tarniewicz, J., Rigby, M., Rödenbeck, C., Vermeulen, A., and Walton, E. M. (2020). The regional European atmospheric transport inversion comparison, EUROCOM: first results on European-wide terrestrial carbon fluxes for the period 2006–2015, *Atmospheric Chemistry and Physics*, **20**, 12063–12091. doi: 10.5194/acp-20-12063-2020

Moore, J. K., Fu, W., Primeau, F., Britten, G. L., Lindsay, K., Long, M., Doney, S. C., Mahowald, N., Hoffman, F. and Randerson, J. T. (2018). Sustained climate warming drives declining marine biological productivity. *Science,* **359**, 1139–1143. doi:10.1126/science.aao6379

Müller, A., Tanimoto, H., Sugita, T., Machida, T., Nakaoka, S., Patra, P. K., Laughner, J., and Crisp, D. (2021).New approach to evaluate satellite-derived $XCO_2$ over oceans by integrating ship and aircraft observations, *Atmospheric Chemistry and Physics*, **21**, 8255–8271. doi: 10.5194/acp-21-8255-2021.

Myneni, R., Knyazikhin, Y., Park, T. (2015). MOD15A2H MODIS Leaf Area Index/FPAR 8-Day L4 Global 500m SIN Grid V006. NASA EOSDIS Land Processes DAAC. http://doi.org/10.5067/MODIS/MOD15A2H.006 (Last referenced 5 Dec 2021)

Nabuurs, G. J., Lindner, M., Verkerk, P., Gunia, K., Deda, Paola, Michalak, R. and Grassi, G. (2013). First signs of carbon sink saturation in European forest biomass. *Nature Climate Change,* **3**, 792–796. doi: 10.1038/nclimate1853

Nassar, R., Hill, T. G., McLinden, C. A., Wunch, D., Jones, D. B.A. and Crisp D. (2017). Quantifying $CO_2$ emissions from individual power plants from space. *Geophysical Research Letters*, **44**, 10045-10053. doi:10.1002/2017GL074702

Nassar, R., Mastrogiacomo, J.-P., Bateman-Hemphill, W., McCracken, C., MacDonald, C. G., Hill, T., O'Dell, C. W., Kiel, M., Crisp, D. (2021): Advances in quantifying power plant $CO_2$ emissions with OCO-2. *Remote Sensing of Environment,* **264**, 112579. doi: 10.1016/j.rse.2021.112579

Nemani, R. R., Keeling, C. D., Hashimoto, H., Jolly, W. M., Piper, S. C., Tucker, C. J., Myneni, R. B., and Running, S. W. (2003). Climate-Driven Increases in Global Terrestrial Net Primary Production from 1982 to 1999. *Science*, **300**, 1560-1563. doi: 10.1126/science.1082750

Norton, A. J., Rayner, P. J., Koffi, E. N., Scholze, M., Silver, J. D., and Wang, Y.-P. (2019). Estimating global gross primary productivity using chlorophyll fluorescence and a data assimilation system with the BETHY-SCOPE model. *Biogeosciences*, **16**, 3069–3093. doi: 10.5194/bg-16-3069-2019

Obermeier, W. A., Nabel, J. E. M. S., Loughran, T., Hartung, K., Bastos, A., Havermann, F., Anthoni, P., Arneth, A., Goll, D. S., Lienert, S., Lombardozzi, D., Luyssaert, S., McGuire, P. C., Melton, J. R., Poulter, B., Sitch, S., Sullivan, M. O., Tian, H., Walker, A. P., Wiltshire, A. J., Zaehle, S., and Pongratz, J. (2021). Modelled land use and land cover change emissions – a spatio-temporal comparison of different approaches, *Earth System Dynamics*, **12**, 635–670, doi: 10.5194/esd-12-635-2021

Oda, T., Maksyutov, S. and Andres, S. J. (2018). The Open-source Data Inventory for Anthropogenic Carbon dioxide ($CO_2$), version 2016 (ODIAC2016): A global, monthly fossil-fuel $CO_2$ gridded emission data product for tracer transport simulations and surface flux inversions. *Earth System Science Data,* **10**, 87-107. doi:10.5194/essd-10-87-2018

O'Dell, C. W., Eldering, A., Wennberg, P. O., Crisp, D., Gunson, M. R., Fisher, B., Frankenberg, C., Kiel, M., Lindqvist, H., Mandrake, L., Merrelli, A., Natraj, V., Nelson, R. R., Osterman, G. B., Payne, V. H., Taylor, T. E., Wunch, D., Drouin, B. J., Oyafuso, F., Chang, A., McDuffie, J., Smyth, M., Baker, D. F., Basu, S., Chevallier, F., Crowell, S. M. R., Feng, L., Palmer, P. I., Dubey, M., García, O. E., Griffith, D. W. T., Hase, F., Iraci, L. T., Kivi, R., Morino, I., Notholt, J., Ohyama, H., Petri, C., Roehl, C. M., Sha, M. K., Strong, K., Sussmann, R., Te, Y., Uchino, O. and Velazco, V. A. (2018). Improved retrievals of carbon dioxide from Orbiting Carbon Observatory-2 with the version 8 ACOS algorithm, *Atmospheric Measurement Techniques,* **11**: 6539–6576. doi:10.5194/amt-11-6539-2018

Olsen, A., Key, R. M., van Heuven, S., Lauvset, S. K., Velo, A., Lin, X. H., Schirnick, C., Kozyr, A., Tanhua, T.,Hoppema, M., Jutterstrom, S., Steinfeldt, R., Jeansson, E., Ishii, M., Perez, F. F., and Suzuki, T. (2016). The Global Ocean Data Analysis Project version 2 (GLODAPv2) - an internally consistent data product for the world ocean, *Earth System Science Data*, **8**, 297-323. doi: 10.5194/essd-8-297-2016

Olsen, A., Lange, N., Key, R. M., Tanhua, T., Bittig, H. C., Kozyr, A., Álvarez, M., Azetsu-Scott, K., Becker, S., Brown, P. J., Carter, B. R., Cotrim da Cunha, L., Feely, R. A., van Heuven, S., Hoppema, M., Ishii, M., Jeansson, E., Jutterström, S., Landa, C. S., Lauvset, S. K., Michaelis, P., Murata, A., Pérez, F. F., Pfeil, B., Schirnick, C., Steinfeldt, R., Suzuki, T., Tilbrook, B., Velo, A., Wanninkhof, R. and Woosley, R. J. (2020): An updated version of the global interior ocean biogeochemical data product, GLODAPv2.2020, *Earth System Science Data*, **12**, 3653-3678. doi: 10.5194/essd-12-3653-2020

Pacala, S. W., Hurtt, G. C., Baker, D., Peylin, P., Houghton, R. A., Birdsey, R. A., Heath, L., Sundquist, E. T., Stallard, R. F., Ciais, P., Moorcroft, P., Caspersen, J. P., Shevliakova, E., Moore, B., Kohlmaier, G., Holland, E., Gloor, M., Harmon, M. E., Fan, S.-M., Sarmiento, J. L., Goodale, C. L., Schimel, D. and Field, C. B. (2001), Consistent land- and atmosphere-based U.S. carbon sink estimates, *Science*, **292**, 2316– 2320, doi: 10.1126/science.1057320

Page. S. E., Siegert, F., Rieley, L. O., Boehm, H.-D. V., Jaya, A., and Limin, S. (2002). The amount of carbon released from peat and forest fires in Indonesia during 1997. *Nature,* **420**, 61–65. doi: 10.1038/nature01131

Palmer, P. I., Feng, L., Baker, D., Chevallier, F., Bösch, H. and Somkuti, P. (2019). Net carbon emissions from African biosphere dominate pan-tropical atmospheric $CO_2$ signal, *Nature Communications*, **10**, 3344. doi:10.1038/s41467-019-11097-w

Pan, Y., Birdsey, R. A., Fang, J., Houghton, R., Kauppi, P. E., Kurz, W. A., Phillips, O. L., Shvidenko, A., Lewis, S. L., Canadell, J. G., Ciais, P., Jackson, R. B., Pacala, S. W., McGuire, A. S., Piao, S., Rautiainen, A., Sitch, S. and Hayes, D. (2011). A large and

persistent carbon sink in the world's forests. *Science*, **333**, 988-993. doi:10.1126/science.1201609

Panassa, E., Santana-Casiano, J. M., González-Dávila, M., Hoppema, M., van Heuven, S. M. A. C., Völker, C., Wolf-Gladrow, D. and Hauck, J. (2018). Variability of nutrients and carbon dioxide in the Antarctic Intermediate Water between 1990 and 2014. *Ocean Dynamics,* **68**, 295–308. doi:10.1007/s10236-018-1131-2

Parazoo, N. C., Magney, T., Norton, A., Raczka, B., Bacour, C., Maignan, F., Baker, I., Zhang, Y., Qiu, B., Shi, M., MacBean, N., Bowling, D. R., Burns, S., Blanken, P. D., Stutz, J., Grossmann, K. and Frankenberg, C. (2020). Wide discrepancies in the magnitude and direction of modeled solar-induced chlorophyll fluorescence in response to light conditions. *Biogeosciences*, **17**, 3733–3755. doi:10.5194/bg-17-3733-2020

Pardo, P. C., Tilbrook, B., Langlais, C., Trull, T.W. and Rintoul, S. R. (2017). Carbon uptake and biogeochemical change in the Southern Ocean, south of Tasmania. *Biogeosciences,* **14**, 5217–5237. doi:10.5194/bg-14-5217-2017

Pearson, T. R. H., Brown, S., Murray, L. and Sidman, G. (2017). Greenhouse gas emissions from tropical forest degradation: an underestimated source. *Carbon Balance and Management*, **12**, 3. doi:10.1186/s13021-017-0072-2

Peiro, H., Crowell, S., Schuh, A., Baker, D. F., O'Dell, C., Jacobson, A. R., Chevallier, F., Liu, J., Eldering, A., Crisp, D., Deng, F., Weir, B., Basu, S., Johnson, M. S., Philip, S., and Baker, I. (2022). Four years of global carbon cycle observed from the Orbiting Carbon Observatory 2 (OCO-2) version 9 and in situ data and comparison to OCO-2 version 7, Atmos. Chem. Phys., 22, 1097–1130, doi: 10.5194/acp-22-1097-2022

Peng, B., Guan, K. Y., Zhou, W., Jiang, C. Y., Frankenberg, C., Sun, Y., He, L. Y. and Kohler, P. (2020). Assessing the benefit of satellite-based Solar-Induced Chlorophyll Fluorescence in crop yield prediction. *International Journal of Applied Earth Observation and Geoinformation*, **90**, 102126. doi:10.1016/j.jag.2020.102126

Peñuelas, J., Ciais, P., Canadell, J. G., Janssens, I. A., Fernández-Martínez, M., Carnicer, J., Obersteiner, M., Piao, S., Vautard, R, Sardans, J. (2017). Shifting from a fertilization-dominated to a warming-dominated period. *Nat Ecol Evol.* **1**, 1438-1445. doi: 10.1038/s41559-017-0274-8.

Peters, W., Miller, J. B., Whitaker, J., Denning, A. S., Hirsch, A., Krol, M. C., Zupanski, D., Bruhwiler, L., and Tan, P. P. (2005). An ensemble data assimilation system to estimate $CO_2$ surface fluxes from atmospheric trace gas observations, *Journal of Geophysical Research*, **110**, D24304, doi:10.1029/2005JD006157

Peters, W., Bastos, A., Ciais, P., and Vermeulen, A.(2020). A historical, geographical and ecological perspective on the 2018 European summer drought. *Philosophical Transactions of the Royal Society B: Biological Sciences*, **375**, 20190505, doi: 10.1098/rstb.2019.0505

Petrescu, A. M. R., Peters, G. P., Janssens-Maenhout, G., Ciais, P., Tubiello, F. N., Grassi, G., Nabuurs, G.-J., Leip, A., Carmona-Garcia, G., Winiwarter, W., Höglund-Isaksson, L., Günther, D., Solazzo, E., Kiesow, A., Bastos, A., Pongratz, J., Nabel, J. E. M. S., Conchedda, G., Pilli, R., Andrew, R. M., Schelhaas, M.-J. and Dolman, A. J. (2020). European anthropogenic AFOLU greenhouse gas emissions: a review and benchmark data. *Earth System Science Data*, **12**, 961–1001, doi:10.5194/essd-12-961-2020

Petrescu, A. M. R., McGrath, M. J., Andrew, R. M., Peylin, P., Peters, G. P., Ciais, P., Broquet, G., Tubiello, F. N., Gerbig, C., Pongratz, J., Janssens-Maenhout, G., Grassi, G., Nabuurs,

G.-J., Regnier, P., Lauerwald, R., Kuhnert, M., Balkovič, J., Schelhaas, M.-J., Denier van der Gon, H. A. C., Solazzo, E., Qiu, C., Pilli, R., Konovalov, I. B., Houghton, R. A., Günther, D., Perugini, L., Crippa, M., Ganzenmüller, R., Luijkx, I. T., Smith, P., Munassar, S., Thompson, R. L., Conchedda, G., Monteil, G., Scholze, M., Karstens, U., Brockmann, P., and Dolman, A. J. (2021). The consolidated European synthesis of $CO_2$ emissions and removals for the European Union and United Kingdom: 1990–2018, *Earth System Science Data*, **13**, 2363–2406, https://doi.org/10.5194/essd-13-2363-2021

Peylin, P., Bousquet, P., Le Quéré, C., Sitch, S., Friedlingstein, P., McKinley, G., Gruber, N., Rayner, P., and Ciais, P. (2005). Multiple constraints on regional $CO_2$ flux variations over land and oceans, *Global Biogeochemical Cycles*, **19**, GB1011. doi: 10.1029/2003GB002214

Peylin, P., Law, R. M., Gurney, K. R., Chevallier, F. Jacobson, A. R., Maki, T., Niwa, Y., Patra, P. K., Peters, W., Rayner, P. J., Rödenbeck, C., van der Laan-Luijkx, I. T., and Zhang, X. (2013). Global atmospheric carbon budget: results from an ensemble of atmospheric $CO_2$ inversions. *Biogeosciences*, **10**, 6699-6720. doi: 10.5194/bg-10-6699-2013

Pfeil, B., Olsen, A., Bakker, D. C. E., Hankin, S., Koyuk, H., Kozyr, A., Malczyk, J., Manke, A., Metzl, N., Sabine, C. L., Akl, J., Alin, S. R., Bates, N., Bellerby, R. G. J., Borges, A., Boutin, J., Brown, P. J., Cai, W.-J., Chavez, F. P., Chen, A., Cosca, C., Fassbender, A. J., Feely, R. A., González-Dávila, M., Goyet, C., Hales, B., Hardman-Mountford, N., Heinze, C., Hood, M., Hoppema, M., Hunt, C. W., Hydes, D., Ishii, M., Johannessen, T., Jones, S. D., Key, R. M., Körtzinger, A., Landschützer, P., Lauvset, S. K., Lefèvre, N., Lenton, A., Lourantou, A., Merlivat, L., Midorikawa, T., Mintrop, L., Miyazaki, C., Murata, A., Nakadate, A., Nakano, Y., Nakaoka, S., Nojiri, Y., Omar, A. M., Padin, X. A., Park, G.-H., Paterson, K., Perez, F. F., Pierrot, D., Poisson, A., Ríos, A. F., Santana-Casiano, J. M., Salisbury, J., Sarma, V. V. S. S., Schlitzer, R., Schneider, B., Schuster, U., Sieger, R., Skjelvan, I., Steinhoff, T., Suzuki, T., Takahashi, T., Tedesco, K., Telszewski, M., Thomas, H., Tilbrook, B., Tjiputra, J., Vandemark, D., Veness, T., Wanninkhof, R., Watson, A. J., Weiss, R., Wong, C. S. and Yoshikawa-Inoue, H. (2013). A uniform, quality controlled Surface Ocean $CO_2$ Atlas (SOCAT). *Earth System Science Data,* **5**, 125–143. doi:10.5194/essd-5-125-2013

Piao, S., Fang, J., Ciais, P., Peylin, P., Huang, Y., Sitch, S. and Wang T. (2009). The carbon balance of terrestrial ecosystems in China. *Nature,* **458**, 1009–1013. doi: 10.1038/nature07944

Piao, S., Liu, Z., Wang, Y., Ciais, P., Yao, Y., Peng, S., Chevallier, F., Friedlingstein, P., Janssens, I. A., Peñuelas, J., and Sitch, S. (2017). On the causes of trends in the seasonal amplitude of atmospheric $CO_2$. *Global Change Biology*, **24**, 608–616. doi: 10.1111/gcb.13909

Piao, S., Wang, X., Wang, K., Li, X., Bastos, A., Canadell, J. G., Ciais, P., Friedlingstein, P., and Sitch, S. (2020a). Interannual Variation of Terrestrial Carbon Cycle: Issues and Perspectives, *Global Change Biology*, **26**, 300–318. doi: 10.1111/gcb.14884

Piao, S., Wang, X., Park, T., Chen, C., Lian, X., He, Y. Bjerke, J. W., Chen, A., Ciais, P., Tommervik, H., Nemani, R. R. and Myneni, R. B. (2020b). Characteristics, drivers and feedbacks of global greening. *Nature Reviews Earth & Environment.,* **1**, 14–27. doi:10.1038/s43017-019-0001-x

Pongratz, J., Reick, C. H., Houghton, R. A. and House, J. I. (2014). Terminology as a key uncertainty in net land use and land cover change carbon flux estimates. *Earth System Dynamics*, **5**, 177–195, 2014. doi: 10.5194/esd-5-177-2014

Poulter, B., Frank, D., Ciais, P., Myneni, R. B., Andela, N., Bi, J., Broquet, G., Canadell, J. G., Chevallier, F., Liu, Y. Y., Running, S. W., Sitch, S. and van der Werf, G. R. (2014). Contribution of semi-arid ecosystems to interannual variability of the global carbon cycle. Nature, 509, 600-603. doi:10.1038/nature13376

Qin, Y. W. Xiao, X., Wigneron, J.-P., Ciais, P., Brandt, M., Fan, L., Li, X., Crowell, S., Wu, X., Doughty, R., Zhang, Y., Liu, F., Sitch, S., and Moore III, B. (2021). Carbon loss from forest degradation exceeds that from deforestation in the Brazilian Amazon, *Nature Climate Change*, **11**, 442-448. doi: 10.1038/s41558-021-01026-5, 2021.

Qiu, B., Ge, J., Guo, W. D., Pittman, A. J. and Mu, M. Y. (2020). Responses of Australian dryland vegetation to the 2019 heat wave at a sub daily scale. *Geophysical Research Letters,* **47**, e2019GL086569. doi:10.1029/2019GL086569

Quegan, S., Toan, L. T., Chave, J., Dall, J., Exbrayat, J. F., Minh, D. H. T., Lomas, M., D'Alessandro, M. M., Paillou, P., Papathanassiou, K., Rocca, F., Saatchi, S., Scipal, K., Shugart, H., Smallman, T. L., Soja, M. J., Tebaldini, S., Ulander, L., Villard, L. and Williams, M. (2019). The European Space Agency BIOMASS mission: measuring forest above-ground biomass from space. *Remote Sensing of the Environment,* **227**, 44–60. doi:10.1016/j.rse.2019.03.032

Quilcaille, Y., Gasser, T., Ciais, P., Lecocq, F., Janssens-Maenhout, G., and Mohr, S. (2018). Uncertainty in projected climate change arising from uncertain fossil-fuel emission factors. *Environmental Research Letters*, **13**, 044017. doi: 10.1088/1748-9326/aab304#references

Rabin, S. S., Melton, J. R., Lasslop, G., Bachelet, D., Forrest, M., Hantson, S., Kaplan, J. O., Li, F., Mangeon, S., Ward, D. S., Yue, C., Arora, V. K., Hickler, T., Kloster, S., Knorr, W., Nieradzik, L., Spessa, A., Folberth, G. A., Sheehan, T., Voulgarakis, A., Kelley, D. I., Prentice, I. C., Sitch, S., Harrison, S., and Arneth, A. (2017). The Fire Modeling Intercomparison Project (FireMIP), phase 1: experimental and analytical protocols with detailed model descriptions, *Geoscientific Model Development*, **10**, 1175–1197. doi: 10.5194/gmd-10-1175-2017.

Ramankutty N., Gibbs, H. K., Achard, F., Defries, R., Foley, J. A. and Houghton, R. A. (2007). Challenges to estimating carbon emissions from tropical deforestation. *Global Change Biology,* **13**, 51–66. doi: 10.1111/j.1365-2486.2006.01272.x

Randerson, J. T., Hoffman, F. M., Thornton, P. E., Mahowald, N. M., Lindsay, K., Lee, Y. H., Nevison, C. D. Doney, S. C., Bonan, G., Stöckli, R., Covey, C., Running, S. W. and Fung, I. Y. (2009). Systematic assessment of terrestrial biogeochemistry in coupled climate–carbon models. *Global Change Biology*, **15**, 2462-2484. doi: 10.1111/j.1365-2486.2009.01912.x

Randerson, J. T., Lindsay, K., Munoz, E., Fu, W., Moore, J. K., Hoffman, F. M., Mahowald, N. M. and Doney, S. C. (2015). Multi-century changes in ocean and land contributions to the climate-carbon feedback. *Global Biogeochemical Cycles*, **29**, 744-759. doi:10.1002/2014GB005079

Raupach, M. R., Canadell, J. G. and Le Quéré, C. (2008). Anthropogenic and biophysical contributions to increasing atmospheric $CO_2$ growth rate and airborne fraction. *Biogeosciences*, **5**, 1601–1613. doi:10.5194/bg-5-1601-2008

Raupach, M. R., Gloor, M., Sarmiento, J. L., Canadell, J. G., Frölicher, T. L., Gasser, T., Houghton, R. A., Le Quéré, C. and Trudinger, C. M. (2014). The declining uptake rate of atmospheric $CO_2$ by land and ocean sinks. *Biogeosciences*, **11**, 3453–3475. doi:10.1007/s10584-009-9596-0

Regnier, P., Friedlingstein, P., Ciais, P., Mackenzie, F. T., Gruber, N., Janssens, I. A., Laruelle, G. G., Lauerwald, R., Luyssaert, S., Andersson, A. J., Arndt, S., Arnosti, C., Borges, A. V., Dale, A. W., Gallego-Sala, A., Goddéris, Y., Goossens, N., Hartmann, J., Heinze, C., Ilyina, T., Joos, F., LaRowe, D. E., Leifeld, J., Meysman, F. J. R., Munhoven, G., Raymond, P. A., Spahni, R., Suntharalingam, P. and Thullner, M. (2013). Anthropogenic perturbation of the carbon fluxes from land to ocean. *Nature Geosciences,* **6**, 597–607. doi:10.1038/ngeo1830

Reichstein, M., Bahn, M., Ciais, P., Frank, D., Mahecha, M. D., Seneviratne, S. I., Zscheischler, J., Beer, C., Buchmann, N., Frank, D. C., Papale, D., Rammig, A., Smith, P., Thonicke, K., van der Velde, M., Vicca, S., Walz, A., and Wattenbach, M. (2013). Climate extremes and the carbon cycle, *Nature*, **500**, 287–295. doi: 10.1038/Nature12350, 2013

Remaud, M., Chevallier, F., Maignan, F., Belviso, S., Berchet, A., Parouffe, A., Abadie, C., Bacour, C., Lennartz, S., and Peylin, P. (2022). Plant gross primary production, plant respiration and carbonyl sulfide emissions over the globe inferred by atmospheric inverse modelling*, Atmos. Chem. Physics*, **22**, 2525-2552. doi: 10.5194/acp-22-2525-2022

Resplandy, L., Keeling, R. F., Rödenbeck, C.,. Stephens, B. B, Khatiwala, S., Rodgers, K. B., Long, M. C., Bopp, L. and. Tans, P. P. (2018). Revision of global carbon fluxes based on a reassessment of oceanic and riverine carbon transport. *Nature Geoscience*, **11**, 504–509. doi:10.1038/s41561-018-0151-3

Reuter, M., Buchwitz, M., Hilker, M., Heymann, J., Schneising, O., Pillai, D., Bovensmann, H., Burrows, J. P., Bösch, H., Parker, R., Butz, A., Hasekamp, O., O'Dell, C. W., Yoshida, Y., Gerbig, C., Nehrkorn, T., Deutscher, N. M., Warneke, T., Notholt, J., Hase, F., Kivi, R., Sussmann, R., Machida, T., Matsueda, H. and Sawa, Y. (2014). Satellite-inferred European carbon sink larger than expected. *Atmospheric Chemistry and Physics*, **14**, 13739-13753. doi: 10.5194/acp-14-13739-2014

Reuter, M., Buchwitz., M., Schneising, O., Krautwurst, S., O'Dell, C. W., Richter, A., Bovensmann, H. and Burrows, J. P. (2019). Towards monitoring localized $CO_2$ emissions from space: Co-located regional $CO_2$ and $NO_2$ enhancements observed by the OCO-2 and S5P satellites. *Atmospheric Chemistry and Physics*, **19**, 9371–9383. doi:10.5194/acp-19-9371-2019

Ridge, S. M. and McKinley, G. A. (2020). Advective controls on the North Atlantic anthropogenic carbon sink. *Global Biogeochemical Cycles*, **34**, 1138. doi:10.1029/2019GB006457

Ridge, S. M. and McKinley, G. A. (2021). Ocean carbon uptake under aggressive emission mitigation. *Biogeosciences* **18**, 2711–2725. doi: 10.5194/bg-18-2711-2021

Rödenbeck, C., Houweling, S., Gloor, M., and Heimann, M. (2003). $CO_2$ flux history 1982–2001 inferred from atmospheric data using a global inversion of atmospheric transport, *Atmospheric Chemistry and Physics*, **3**, 1919-1964. doi: 10.5194/acp-3-1919-2003, 2003.

Rödenbeck, C., Bakker, D. C. E., Metzl, N., Olsen, A., Sabine, C., Cassar N., Reum, F., Keeling, R. F and Heimann, M. (2014). Interannual sea-air $CO_2$ flux variability from an observation-driven ocean mixed-layer scheme. *Biogeosciences*, **11**, 4599–4613. doi:10.5194/bg-11-4599-2014

Rödenbeck, C., Bakker, D. C. E., Gruber, N., Iida, Y., Jacobson, A. R., Jones, S., Landschützer, P., Metzl, N., Nakaoka, S., Olsen, A., Park, G.-H., Peylin, P., Rodgers, K. B., Sasse, T. P., Schuster, U., Shutler, J. D., Valsala, V., Wanninkhof, R. and Zeng, J. (2015). Data-based estimates of the ocean carbon sink variability – first results of the Surface Ocean $pCO_2$

Mapping intercomparison (SOCOM). *Biogeosciences*, **12**, 7251–7278. doi:10.5194/bg-12-7251-2015

Rodgers, K. B., Schlunegger, S., Slater, R. D., Ishii, M., Frolicher, T. L., Toyama, K., Plancherel, Y., Aumont, O. and Fassbender, A. J. (2020). Reemergence of anthropogenic carbon into the ocean's mixed layer strongly amplifies transient climate sensitivity. *Geophysics Research Letters*, **47**, 130. doi:10.1002/2017GL073758

Rosan, T. M., Goldewijk, K. K., Ganzenmüller, R., O'Sullivan, M., Pongratz, J., Mercado, L. M., Aragao, L. E. O. C., Heinrich, V., von Randow, C., Wiltshire, A., Tubiello, F. N., Bastos, A., Friedlingstein, P, and Sitch, S. (2021). A multi-data assessment of land use and land cover emissions from Brazil during 2000–2019. Environmental Research Letters, 16, 074004. doi: 10.1088/1748-9326/ac08c3

Rosen, P., Hensley, S., Shaffer, S., Edelstein, W., Kim, Y., Kumar, R., Misra, T., Bhan, R., Satish, R. and Sagi, R. (2016). An update on the NASA-ISRO dual-frequency dbf SAR (NISAR) mission. *2016 IEEE International Geoscience and Remote Sensing Symposium*. IEEE, New York, pp. 2106–2108. doi:10.1109/IGARSS.2016.7729543

Rowland, L., da Costa, A. C., L., Galbraith, D. R., Oliveira, R. S., Binks, O. J., Oliveira, A. A. R., Pullen, A. M., Doughty, C. E., Metcalfe, D. B., Vsconcelos, S., S., Ferreia, L. V., Malhi, Y., Grace, J., Mencuccini, M., and Meir, P. (2015). Death from drought in tropical forests is triggered by hydraulics not carbon starvation. *Nature*, **528**, 119-122. doi: 10.1038/nature15539

Rubino, M., Etheridge, D. M., Thornton, D. P., Howden, R., Allison, C. E., Francey, R. J., Langenfelds, R. L., Steele, L. P., Trudinger, C. M., Spencer, D. A., Curran, M. A. J., van Ommen, T. D., and Smith, A. M.(2019). Revised records of atmospheric trace gases $CO_2$, CH4, N2O, and δ13C-CO2 over the last 2000 years from Law Dome, Antarctica, *Earth System Science Data*, **11**, 473–492. doi:10.5194/essd-11-473-2019

Rudnick, D. L. (2016). Ocean Research Enabled by Underwater Gliders. *Annual Review of Marine Science*, **8**, 519-541. doi:10.1146/annurev-marine-122414-033913

Saatchi, S. S., Harris, N. L., Brown, S., Lefsky, M., Mitchard, E. T. A., Salas, W., Zutta, B. R., Buermann, W., Lewis, S. L., Hagen, S., Petrova, S., White, L., Silman, M. and Morel, A. (2011). Benchmark map of forest carbon stocks in tropical regions across three continents. *Proceedings of the National Academy of Sciences*, **108**, 9899-9904. doi: 10.1073/pnas.1019576108

Sabine, C. L., Feely, R. A., Gruber, N., Key, R. M., Lee, K., Bullister, K. L., Wanninkhof, R. Wong, C. S., Wallace, D. W. R. Wallace, Tilbrook, B., Millero, F. J., Peng, T.-H., Kozyr, A., Ono, T. and Rois, A. F. (2004). The oceanic sink for anthropogenic $CO_2$. *Science,* **305**, 367–371. doi:10.1126/science.1097403

Sabine, C. L. and Tanhua, T. (2010). Estimation of anthropogenic $CO_2$ inventories in the ocean. *Annual Reviews of Marine Sciences,* **2**, 175-198. doi:10.1146/annurev-marine-120308-080947

Sabine, C., Sutton, A., McCabe, K., Lawrence-Slavas, N., Alin, S., Feely, R., Jenkins, R., Maenner, S., Meinig, C., Thomas, J., van Ooijen, E., Passmore, A. and Tilbrook, B. (2020). Evaluation of a new carbon dioxide system for autonomous surface vehicles. *J. Atmos. Ocean. Technol.*, **37**, 1305-1317. doi:10.1175/JTECH-D-20-0010.1

Sarmiento, J. L., and Sundquist E. T. (1992). Revised budget for the oceanic uptake of anthropogenic carbon dioxide, *Nature*, **356**, 589–593. doi:10.1038/356589a0

3950 Sarmiento, J. L. and Gruber, N. (2006). Ocean Biogeochemical Dynamics. Princeton University
3951 Press. ISBN: 0-691-01707-7. doi:10.1017/S0016756807003755
3952 Sarmiento, J. L., Gloor, M., Gruber, N., Beaulieu, C., Jacobson, A. R., Mikaloff Fletcher, S. E.,
3953 Pacala, S., and Rodgers, K. (2010). Trends and regional distributions of land and ocean
3954 carbon sinks. *Biogeosciences*, **7**, 2351-2367. doi: 10.5194/bg-7-2351-2010
3955 Scharlemann, J. P. W., Tanner, E. V. J., Hiederer, R. and Kapos, V. (2014). Global soil carbon:
3956 understanding and managing the largest terrestrial carbon pool. *Carbon Management*, **5**, 81-
3957 91. doi:10.4155/cmt.13.77
3958 Schepaschenko, D., Moltchanova, E., Shvidenko, A., Blyshchyk, V., Dmitriev, E., Martynenko,
3959 O., See, L. and Kraxner F. (2018). Improved estimates of biomass expansion factors for
3960 Russian forests. *Forests*, **9**, 312. doi:10.3390/f9060312
3961 Schimel, D., Stephens, B. B., and Fisher, J. B. (2015). Effect of increasing $CO_2$ on the terrestrial
3962 carbon cycle, *Proceeding of the National Academy of Sciences*, **112**, 436-441. doi:
3963 10.1073/pnas.1407302112
3964 Scholze, M., Kaminski, T., Knorr, W., Voßbeck, M., Wu, M., Ferrazzoli, P., Kerr, Y., Mialon, A.,
3965 Richaume, P., Rodríguez-Fernández, N., Vittucci, C., Wigneron, J. P., Mechlenburg, S. and
3966 Drusch, M. (2019). Mean European carbon sink over 2010–2015 estimated by simultaneous
3967 assimilation of atmospheric CO2, soil moisture, and vegetation optical depth. *Geophysical*
3968 *Research Letters*, **46**. doi:10. 1029/2019GL085725
3969 Schourup-Kristensen, V., Sidorenko, D., Wolf-Gladrow, D. A. and Völker, C. (2014). A skill
3970 assessment of the biogeochemical model REcoM2 coupled to the Finite Element Sea Ice–
3971 Ocean Model (FESOM 1.3). *Geoscientific Model Development*, **7**, 2769–2802.
3972 doi:10.5194/gmd-7-2769-2014
3973 Schuh, A., Jacobson, A. R., Basu, S., Weir, B., Baker, D., Bowman, K., Chevallier, F., Crowell,
3974 S., Davis, K., Deng, F., Denning, S., Feng, L., Jones, D., Liu, J., and Palmer, P. (2019).
3975 Quantifying the Impact of Atmospheric Transport Uncertainty on $CO_2$ Surface Flux
3976 Estimates, *Global Biogeochemical Cycles*, **33**, 484–500. doi: 10.1029/2018GB0060
3977 Schulze, E.-D., and M. Heimann. 1998. Carbon and water exchange of terrestrial ecosystems.
3978 Pages 145-161 in J. Galloway, and J. M. Melillo, editors. Asian change in the context of
3979 global change. Cambridge University Press, Cambridge, UK.
3980 Schwinger, J., Tjiputra, J. F., Heinze, C., Bopp, L., Christian, J. R., Gehlen, M., Ilyina, T., Jones,
3981 C. D., Salas-Mélia, D., Segschneider, J., Séférian, R. and Totterdell, I. (2014). Nonlinearity
3982 of ocean carbon cycle feedbacks in CMIP5 Earth system models. *Journal of Climate,* **27**,
3983 3869–3888. doi:10.1175/JCLI-D-13-00452.1
3984 Schwinger, J., Goris, N., Tjiputra, J. F., Kriest, I., Bentsen, M., Bethke, I., Ilicak, M., Assmann,
3985 K. M. and Heinze, C. (2016). Evaluation of NorESM-OC (versions 1 and 1.2), the ocean
3986 carbon-cycle stand-alone configuration of the Norwegian Earth System Model (NorESM1).
3987 *Geoscientific Model Development*, **9**, 2589–2622. doi:10.5194/gmd-9-2589-2016
3988 Schwinger, J. and Tjiputra, J. (2018). Ocean carbon cycle feedbacks under negative emissions.
3989 *Geophysical Research Letters*, **26**, 5289. doi:10.1088/1748-9326/11/5/055006
3990 Seelmann, K., Aßmann, S. and Körtzinger, A. (2019). Characterization of a novel autonomous
3991 analyzer for seawater total alkalinity: Results from laboratory and field tests. *Limnology and*
3992 *Oceanography: Methods*, **17**, 515-532. doi:10.1002/lom3.10329
3993 Séférian, R., Berthet, S., Yool, A., Palmieri, J., Bopp, L., Tagliabue, A., Kwaitkowski, L.,
3994 Aumont, O., Christian, J., Dunne, J., Gehlen, M., Ilyina, T., John, J. G., Li, H., Long, M. C.,

Luo, J. Y., Nakano, H., Romanou, A., Schwinger, J., Stock, C., Santana-Falcon, Y., Takano, Y., Tjiputra, J., Tsujino, H., Wantanabe, M., Wu, T., Wu, F. and Yamamoto, A. (2020). Tracking Improvement in Simulated Marine Biogeochemistry Between CMIP5 and CMIP6. *Curr. Clim. Change Rep.,* **6,** 95–119. doi: 10.1007/s40641-020-00160-0

Sellers, P. J., Schimel, D. S., Moore III, B., Liu, J. and Eldering, A. (2018). Observing Carbon Cycle-Climate Feedbacks from Space, *Proceedings of the National Academy of Sciences*, **115**, 7860-7868. doi:10.1073/pnas.1716613115

Sigman, D. M., Hain, M. P. and Haug, G. H. (2010). The polar ocean and glacial cycles in atmospheric $CO_2$ concentration. *Nature,* **466**, 47–55. doi:10.1038/nature09149

Sitch, S., Brovkin, V., von Bloh, W., van Vuuren, D., Eickhout, B. and Ganopolski, A. (2005). Impacts of future land cover changes on atmospheric $CO_2$ and climate. *Global Biogeochemical Cycles*, **19**, GB2013. doi: 10.1029/2004GB002311

Sitch, S., Friedlingstein, P., Gruber, N., Jones, S. D., Murray-Tortarolo, G., Ahlström, A., Doney, S. C., Graven, H., Heinze, C., Huntingford, C., Levis, S., Levy, P. E., Lomas, M., Poulter, B., Viovy, N., Zaehle, S., Zeng, N., Arneth, A., Bonan, G., Bopp, L., Canadell, J. G., Chevallier, F., Ciais, P., Ellis, R., Gloor, M., Peylin, P., Piao, S. L., Le Quéré, C., Smith, B., Zhu, Z. and Myneni, R. (2015). Recent trends and drivers of regional sources and sinks of carbon dioxide. *Biogeosciences*, **12**, 653–679. doi:10.5194/bg-12-653-2015

Sloyan, B. M., Wanninkhof, R., Kramp, M., Johnson, G. C., Talley, L. D., Tanhua, T., McDonagh, E., Cusack, C., O'Rourke, E., McGovern, E., Katsumata, K., Diggs, S., Hummon, J., Ishii, M., Azetsu-Scott, K., Boss, E., Ansorge, I., Perez, F. F., Mercier, H., Williams, M. J. M., Anderson, L., Lee, J. H., Murata, A., Kouketsu, S., Jeansson, E., Hoppema, M. & Campos, E. (2019). The Global Ocean Ship-Based Hydrographic Investigations Program (GO-SHIP): A Platform for Integrated Multidisciplinary Ocean Science. *Frontiers in Marine Science*, **6**, 445. doi: 10.3389/fmars.2019.00445

Smith, B., Prentice, I. C., and Sykes, M. T. (2001). Representation of vegetation dynamics in the modelling of terrestrial ecosystems comparing two contrasting approaches within European climate space, *Global Ecol. Biogeogr.*, **10**, 621–637. doi: 10.1046/j.1466-822X.2001.t01-1-00256.x

Smith P., Bustamante, M., Ahammad, H., Clark, H., Dong, H., Elsiddig, E. A., Haberl, H., Harper, R., House, J., Jafari M., Masera, O., Mbow, C., Ravindranath N. H., Rice C. W., Robledo Abad, C., Romanovskaya, A., Sperling, F. and Tubiello F. (2014). Agriculture, Forestry and Other Land Use (AFOLU). In: Climate Change 2014: Mitigation of Climate Change. Contribution of Working Group III to the Fifth Assessment Report of the Intergovernmental Panel on Climate Change [Edenhofer, O., R. Pichs-Madruga, Y. Sokona, E. Farahani, S. Kadner, K. Seyboth, A. Adler, I. Baum, S. Brunner, P. Eickemeier, B. Kriemann, J. Savolainen, S. Schlömer, C. von Stechow, T. Zwickel and J.C. Minx (eds.)]. Cambridge University Press, Cambridge, United Kingdom and New York, NY, USA.

Smith, W. K., Reed, S. C., Cleveland, C. C. Ballantyne, A. P., Anderegg, W. R. L., Wieder, W. R. Liu, Y. Y. and Running, S. (2015). Large divergence of satellite and Earth system model estimates of global terrestrial CO2 fertilization. *Nature Climate Change*, **6**, 306-310. doi:

Song, X.-P., Hansen, M. C., Stehman, S. V., Potapov, P. V., Tyukavina, A., Vermote, E. F. and Townshend, J. R. (2018). Global land change from 1982 to 2016. *Nature*, **560**, 639-343. doi:10.1038/s41586-018-0411-9

4039 Soong, J. L., Fuchslueger, L., Marañon-Jimenez, S., Torn, M. S., Janssens, I. A., Penuelas, J., and
4040 Richter, A. (2019). Microbial carbon limitation: The need for integrating microorganisms
4041 into our understanding of ecosystem carbon cycling. *Global Change Biology,* **26**, 1953–
4042 1961. doi:10.1111/gcb.14962
4043 Spawn, S. A., Sullivan, C. C., Lark, T. J. and Gibbs, H. K. (2020). Harmonized global maps of
4044 above and belowground biomass carbon density in the year 2010. *Scientific Data,* **7,** 112.
4045 doi:10.1038/s41597-020-0444-4
4046 Stamell, J., Rustagi, R. R., Gloege, L. and McKinley, G. A. (2020). Strengths and weaknesses of
4047 three Machine Learning methods for $pCO_2$ interpolation. *Geoscientific Model Development*
4048 *Discuss.* [preprint], doi:10.5194/gmd-2020-311, in review, 2020.
4049 Stock, C. A., Dunne, J. P., Fan, S., Ginoux, P., John, J., Krasting, J. P., Laufkötter, C., Paulot, F.
4050 and Zadeh, N. (2020). Ocean biogeochemistry in GFDL's Earth System Model 4.1 and its
4051 response to increasing atmospheric $CO_2$. *J. Adv. Model. Earth Syst.*, **12**, e2019MS002043.
4052 doi:10.1029/2019MS002043
4053 Sun, Y., Frankenberg, C., Jung, J., Joiner, J., Guanter, L., Köhler, P. and Magney, T. (2018).
4054 Overview of solar-Induced chlorophyll fluorescence (SIF) from the Orbiting Carbon
4055 Observatory-2: Retrieval, cross-mission comparison, and global monitoring for GPP.
4056 *Remote Sensing of Environment*, **209**, 808-823. doi:10.1016/j.rse.2018.02.016
4057 Sundquist, E.T., (1993). The global carbon dioxide budget. *Science,* **259**, 934–941.
4058 doi:10.1126/science.259.5097.934
4059 Sutton, A. J., Sabine, C. L., Maenner-Jones, S., Lawrence-Slavas, N., Meinig, C., Feely, R. A.,
4060 Mathis, J. T., Musielewicz, S., Bott, R., McLain, P. D., Fought, H. J. and Kozyr, A. (2014).
4061 A high-frequency atmospheric and seawater $pCO_2$ data set from 14 open-ocean sites using a
4062 moored autonomous system. *Earth System Science Data,* **6**, 353-366. doi:10.5194/essd-6-
4063 353-2014
4064 Sutton, A. J., Williams, N. L., & Tilbrook, B. (2021). Constraining Southern Ocean $CO_2$ Flux
4065 Uncertainty Using Uncrewed Surface Vehicle Observations. *Geophysical Research Letters*,
4066 **48**, e2020GL091748. doi:10.1029/2020gl091748
4067 Takahashi, T., Sutherland, S. C., Sweeney, C., Poisson, A., Metzl, N., Tilbrook, B., Bates, N.,
4068 Wanninkhof, R., Feely, R. A., Sabine, C., Olafsson, J., Nojiri, Y. (2002). Global sea–air $CO_2$
4069 flux based on climatological surface ocean $pCO_2$, and seasonal biological and temperature
4070 effects. *Deep Sea Research Part II: Topical Studies in Oceanography*, **49**, 9–10, 1601-1622.
4071 doi:10.1016/S0967-0645(02)00003-6
4072 Takahashi, T., Sutherland, S. C., Wanninkhof, R., Sweeney, C., Feely, R. A., Chipman, D. W.,
4073 Hales, B., Friederich, G., Chavez, F., Sabine, C., Watson, A., Bakker, D. C. E., Schuster, U.,
4074 Metzl, N., Yoshikawa-Inoue, H., Ishii, M., Midorikawa, T., Nojiri, Y., Körtzinger, A.,
4075 Steinhoff, T., Hoppema, M., Olafsson, J., Arnarson, T.S., Tilbrook, B., Johannessen, T.,
4076 Olsen, A., Bellerby, R., Wong, C. S., Delille, B., Bates, N. R. and de Baar, H. J. W. (2009).
4077 Climatological mean and decadal change in surface ocean $pCO_2$, and net sea–air $CO_2$ flux
4078 over the global oceans. *Deep Sea Research Part II: Topical Studies in Oceanography,* **56**,
4079 554–577. doi:10.1016/j.dsr2.2008.12.009
4080 Takeshita, Y., Johnson, K. S., Martz, T. R., Plant, J. N. and Sarmiento, J. L. (2018). Assessment
4081 of autonomous pH measurements for determining surface seawater partial pressure of $CO_2$.
4082 *Journal of Geophysical Research: Oceans,* **123**, 4003-4013. doi:10.1029/2017jc013387

Takeshita, Y., Johnson, K. S., Coletti, L., J., Jannasch, H. W., Walz, P. M. and Warren, J. W. (2020). Assessment of pH dependent errors in spectrophotometric pH measurements of seawater. *Marine Chemistry*, **223**, 103801. doi: 10.1016/j.marchem.2020.103801

Tanhua, T., van Heuven, S., Key, R. M., Velo, A., Olsen, A. and Schirnick, C. (2010). Quality control procedures and methods of the CARINA database. *Earth System Science Data* **2**, 35–49. doi:10.5194/essd-2-35-2010

Tanhua, T. and Keeling, R. F. (2012). Changes in column inventories of carbon and oxygen in the Atlantic Ocean. *Biogeosciences,* **9**, 4819-4833. doi:10.5194/bg-9-4819-2012

Tans, P. P., Fung, I. Y., and Takahashi, T. (1990). Observational constraints on the global atmospheric $CO_2$ budget, *Science*, **247**, 1431– 1438. doi: 10.1126/science.247.4949.1431

Teubner, I. E., Forkel, M., Jung, M., Liu, Y. Y., Miralles, D. G., Parinussa, R., van der Schalie, R., Vreugdenhil, M., Schwalm, C. R., Tramontana, G., Camps-Valls, G., and Dorigo, W. A. (2018). Assessing the relationship between microwave vegetation optical depth and gross primary production, *International Journal of Applied Earth Observation and Geoinformation*, **65**, 79–91. doi: 10.1016/j.jag.2017.10.006

Thomas, R. T., Prentice, I. C., Graven, H., Ciais, P., Fisher, J. B., Hayes, D. J., Huang, M., Huntzinger, D. N., Ito, A., Jain, A., and Mao, J. (2016). Increased light-use efficiency in northern terrestrial ecosystems indicated by $CO_2$ and greening observations, *Geophysical Research Letters*, **43**, 11339–11349. doi: 10.1002/2016GL070710

Tohjima, Y., Mukai, H., Machida, T., Hoshina, Y., and Nakaoka, S.-I. (2019). Global carbon budgets estimated from atmospheric $O_2/N_2$ and $CO_2$ observations in the western Pacific region over a 15-year period, *Atmospheric Chemistry and Physics*, **19**, 9269–9285, doi: 10.5194/acp-19-9269-2019

Torres, A. D., Keppel-Aleks, G., Doney, S. C., Fendrock, M., Luis, K., De Mazière, M., Hase, F., Petri, C., Pollard, D. F., Roehl, C. M., Sussmann, R., Velazco, V. A., Warneke, T. and Wunch D. (2019). A geostatistical framework for quantifying the imprint of mesoscale atmospheric transport on satellite trace gas retrievals. *Journal of Geophysical Research: Atmospheres*, **124**. doi: 10.1029/2018JD029933

Trenberth, K. E., and Smith, L. (2005). The mass of the atmosphere: A constraint on global analysis. *Journal of Climate*, **18**, 864-875. doi: 10.1175/JCLI-3299.1

Umezawa, T., Matsueda, H., Sawa, Y., Niwa, Y., Machida, T., and Zhou, L. (2018). Seasonal evaluation of tropospheric $CO_2$ over the Asia-Pacific region observed by the CONTRAIL commercial airliner measurements. *Atmospheric Chemistry and Physics*, **18**, 14851–14866, doi: 10.5194/acp-18-14851-2018

van der Laan-Luijkx, I. T., van der Velde, I. R., Krol, M. C., Gatti, L. V., Domingues, L. G., Correia, C. S. C., Miller, J. B., Gloor, M., van Leeuwen, T. T., Kaiser, J. W., Wiedinmyer, C., Basu, S., Clerbaux, C. and Peters, W. (2015). Response of the Amazon carbon balance to the 2010 drought derived with CarbonTracker South America, Global *Biogeochem. Cycles*, **29**, 1092– 1108. doi: 10.1002/2014GB005082

van der Velde, I. R., van der Werf, G. R., Houweling, S., Maasakkers, J. D., Borsdorff, T., Landgraf, J., Tol, P., van Kempen, T. A., van Hees, R., Hoogeveen, R., Veefkind, P. J., and Aben, A. (2021). Vast $CO_2$ release from Australian fires in 2019–2020 constrained by satellite. *Nature*, **597**, 366-369. doi: 10.1038/s41586-021-03712-y

van der Werf, G. R., Randerson, J. T., Giglio, L., van Leeuwen, T. T., Chen, Y., Rogers, B. M., Mu, M., van Marle, M. J. E., Morton, D. C., Collatz, G. J., Yokelson, R. J. and Kasibhatla,

P. S. (2017). Global fire emissions estimates during 1997–2016. *Earth System Science Data*, **9**, 697–720. doi:10.5194/essd-9-697-2017

Varon, D. J., Jacob, D. J., McKeever, J., Jervis, D., Durak, B. O. A., Xia, y., and Huang, Y. (2018). Quantifying methane point sources from fine-scale satellite observations of atmospheric methane plumes. *Atmospheric Measurement Technology*, **11**, 5673-5686. doi: 10.5194/amt-11-5673-2018

Verdy, A. Mazloff, M. R. (2017). A data assimilating model for estimating Southern Ocean biogeochemistry. *Journal of Geophysical Research: Oceans,* **122**, 6968–6988. doi:10.1002/2016JC012650

Vitousek, P. M., Porder, S., Houlton, B. Z., and Chadwick O. A. (2010). Terrestrial phosphorus limitation: mechanisms, implications, and nitrogen–phosphorus interactions. Ecological Applications, 20, 5-15. doi: 10.1890/08-0127.1

Walker, A. P., De Kauwe, M. G., Bastos, A., Belmecheri, S., Georgiou, K., Keeling, R. F., McMahon, S. M., Medlyn, B. E., Moore, D. J. P., Norby, R. J., Zaehle, S., Anderson-Teixeira, K. J., Battipaglia, G., Brienen, R. J. W., Cabugao, K. G., Cailleret, M., Campbell, E., Canadell, J. G., Ciais, P., Craig, M. E., Ellsworth, D. S., Farquhar, G. D., Fatichi, S., Fisher, J. B., Frank, D. C., Graven, H., Gu, L., Haverd, V., Heilman, K., Heimann, M., Hungate, B. A., Iversen, C. M., Joos, F., Jiang, M., Keenan, T. F., Knauer, J., Körner, C., Leshyk, V. O., Leuzinger, S., Liu, Y., MacBean, N., Malhi, Y., McVicar, T. R., Penuelas, J., Pongratz, J., Powell, A.S., Riutta, T., Sabot, M. E. B., Schleucher, J., Sitch, S., Smith, W. K., Sulman, B., Taylor, B., Terrer, C., Torn, M. S., Treseder, K. K., Trugman, A. T., Trumbore, S. E., van Mantgem, P. J., Voelker, S. L., Whelan, M. E. and Zuidema, P. A. (2021). Integrating the evidence for a terrestrial carbon sink caused by increasing atmospheric $CO_2$. *New Phytol.*, **229**, 2413-2445. doi: 10.1111/nph.16866

Wang, J., Wang, M., Kim, J.-S., Joiner, J., Zeng, N., Jiang, F., Wang, H., He, W., Wu, M., Chen, T., Ju, W. and Chen, J. M. (2021). Modulation of land photosynthesis by the Indian Ocean Dipole: Satellite-based observations and CMIP6 future projections. *Earth's Future*, **9**, e2020EF001942. doi: 10.1029/2020EF001942

Wang, S., Zhang, Y., Hakkarainen, J., Ju, W., Liu, Y., Jiang, F. and He, W. (2018). Distinguishing anthropogenic $CO_2$ emissions from different energy intensive industrial sources using OCO-2 observations: A case study in northern China. *Journal of Geophysical Research: Atmospheres*, **123**, 9462–9473. doi:10.1029/2018JD029005

Wanninkhof, R. (2014). Relationship between wind speed and gas exchange over the ocean revisited. *Limnology and Oceanography*, **12**, 351-362. doi: 10.4319/lom.2014.12.351

Watson, A. J., Schuster, U., Shutler, J. D., Holding, T., Ashton, I. G. C.,Landschützer, P., Woolf, D. K. and Goddijn-Murphy, L. (2020). Revised estimates of ocean-atmosphere $CO_2$ flux are consistent with ocean carbon inventory. *Nature Communications*, **11**, 4422. doi:10.1038/s41467-020-18203-3

Waugh, D. W., Hall, T. M., McNeil, B. I., Key, R. and Matear, R. J. (2006). Anthropogenic $CO_2$ in the oceans estimated using transit-time distributions. *Tellus,* **58B**, 376-389. doi:10.1111/j.1600-0889.2006.00222.x

Weir, B., Crisp, D., O'Dell, C. W., Basu, S., Chatterjee, A., Kolassa, J., Oda, T., Pawson, S., Poulter, B., Zhang, Z., Ciais, P., Davis, S. J., Liu, Z., and Ott, L. E. (2021). Regional impacts of COVID-19 on carbon dioxide detected worldwide from space. *Science Advances*, **7**, eabf9415. Doi: 10.1126/sciadv.abf9415

Welp, L., Keeling, R. and Meijer, H. A. J. (2011). Interannual variability in the oxygen isotopes of atmospheric $CO_2$ driven by El Niño. *Nature*, **477**, 579–582. doi:10.1038/nature10421

Wigneron, J.-P., Fan, L., Ciais, P., Bastos, A., Brandt, M., Chave, J., Saatchi, S., Baccini, A. and Fensholt, R. (2020). Tropical forests did not recover from the strong 2015–2016 El Niño event. *Science Advances*, **6**, eaay4603. doi:10.1126/sciadv.aay4603

Williams, N. L., Juranek, L. W., Feely, R. A., Johnson, K. S., Sarmiento, J. L., Talley, L. D., Dickson, A. G., Gray, A. R., Wanninkhof, R., Russell, J. L., Riser, S. C. and Takeshita, Y. (2017). Calculating surface ocean $pCO_2$ from biogeochemical Argo floats equipped with pH: An uncertainty analysis. *Global Biogeochemical Cycles*, **31**, 591-604. doi:10.1002/2016GB005541

Wohlfahrt, G., Gerdel, K., Migliavacca, M., Rotenberg, E., Tatarinov, F., M., Müller, J., Hammerle, A., Julitta, T., Spielmann, F. M., and Yakir, D. (2018). Sun-induced fluorescence and gross primary productivity during a heat wave. *Scientific Reports*, **8**, 14169. doi: 10.1038/s41598-018-32602-z

Wolf, S., Keenan, T. F., Fisher, J. B., Baldocchi, D. D., Desai, A. R., Richardson, A. D., Scott, R. L., Law, B. E., Litvak, M. E., Brunsell, N. A., Peters, W., and van der Laan-Luijkx, I. T. (2016). Warm spring reduced carbon cycle impact of the 2012 US summer drought, *Proc Natl Acad Sci USA*, **113**, 5880. doi: 10.1073/pnas.1519620113

Woolf, D. K., Shutler, J. D., Goddijn-Murphy, L., Watson, A. J., Chapron, B., Nightingale, P. D., Donlon, C. J., Piskozub, J., Yelland, M. J., Ashton, I., Holding, T., Schuster, U., Girard-Ardhuin, F., Grouazel, A., Piolle, J.-F., Warren, M., Wrobel-Niedzwiecka, I., Land, P. E., Torres, R., Prytherch, J., Moat, B., Hanafin, J., Ardhuin, F. and Paul, F. (2019). Key uncertainties in the recent air-sea flux of $CO_2$. *Global Biogeochemical Cycles*, **33**, 1548-1563. doi:10.1029/2018GB006041

Wu, D., Lin, J. C., Fasoli, B., Oda, T., Ye, X., Lauvaux, T., Yang, E. G. and Kort, E. A. (2018). A Lagrangian approach towards extracting signals of urban $CO_2$ emissions from satellite observations of atmospheric column $CO_2$ ($XCO_2$): X-Stochastic Time-Inverted Lagrangian Transport model ("X-STILT v1"). *Geoscientific Model Development*, **11**: 4843–4871. doi:10.5194/gmd-11-4843-2018

Wu, D. E., Lin, J. C., Oda, T. and Kort, E. A. (2020). Space-based quantification of per capita $CO_2$ emissions from cities, *Environmental Research Letters*, **15**, 035004. doi:10.1088/1748-9326/ab68eb

Wunch, D., Toon, G. C., Blavier, J.-F. L., Washenfelder, R. A., Notholt, J., Connor, B. J., Griffith, D. W., Sherlock, V., and Wennberg, P. O. (2011). The total carbon column observing network, *Philosophical Transactions of the Royal. Society A*, **369**, 2087–2112, doi:10.1098/rsta.2010.0240.

Wunch, D., Wennberg, P. O., Osterman, G., Fisher, B., Naylor, B., Roehl, C. M., O'Dell, C., Mandrake, L., Viatte, C., Griffith, D. W., Deutscher, N. M., Velazco, V. A., Notholt, J., Warneke, T., Petri, C., De Maziere, M., Sha, M. K., Sussmann, R., Rettinger, M., Pollard, D., Robinson, J., Morino, I., Uchino, O., Hase, F., Blumenstock, T., Kiel, M., Feist, D. G., Arnold, S. G., Strong, K., Mendonca, J., Kivi, R., Heikkinen, P., Iraci, L., Podolske, J., Hillyard, P. W., Kawakami, S., Dubey, M. K., Parker, H. A., Sepulveda, E., Rodriguez, O. E. G., Te, Y., Jeseck, P., Gunson, M. R., Crisp, D. and Eldering, A. (2017). Comparisons of the Orbiting Carbon Observatory-2 (OCO-2) $XCO_2$ measurements with TCCON, *Atmospheric Measurement Tech*niques, **10**, 2209–2238. doi: 10.5194/amt-10-2209-2017

Xiao, J., J. Chen, Davis, K. J. and Reichstein, M. (2012). Advances in upscaling of eddy covariance measurements of carbon and water fluxes. *Journal Geophysical Research: Biogeosciences*, **117**, G00J01. doi:10.1029/2011JG001889

Xiao, J., Chevallier, F., Gomez, C., Guanter, L., Hicke, J. A., Huete, A. R., Ichii, K., Ni, W., Pang, Y., Rahman, A. F. Sun, G., Yuan, W., Zhang, L. and Zhang, X. (2019). Remote sensing of the terrestrial carbon cycle: A review of advances over 50 years. *Remote Sensing of Environment*, **233**, 111383. doi:10.1016/j.rse.2019.111383

Xu, L., Saatchi, S. S., Yang, Y., Yu. Y., Pongratz, J., Bloom, A. A., Bowman, K., Worden, J., Liu, J., Yin, Y., Domke, G., McRoberts, R. E., Woodall, C., Nabuurs, G.-J., de-Miguel, S., Keller, M., Harris, N., Maxwell, S., and Schimel, D. (2021). Changes in global terrestrial live biomass over the 21st century. *Science Advances*, **7**, eabe9829. doi: 10.1126/sciadv.abe9829

Xue, L., Cai, W.-J., Takahashi, T., Gao, L., Wanninkhof, R., Wei, M., Li, K., Feng, L., and Yu, W. (2018). Climatic modulation of surface acidification rates through summertime wind forcing in the Southern Ocean. *Nature Communications*, **9**, 3240. doi: 10.1038/s41467-018-05443-7

Ye, X., Lauvaux, T., Kort, E.A., Oda, T., Feng, S., Lin, J. C., Yang, E. G., and Wu, D. (2020). Constraining fossil fuel $CO_2$ emissions from urban area using OCO-2 observations of total column $CO_2$. *Journal of Geophysical Research, Atmospheres*, **125**, e2019JD030528. doi: 10.1029/2019JD030528.

Yin, Y., Byrne, B., Liu, J., Wennberg, P., Davis, K. J., Magney, T., Koehler, P., He, L., Jeyaram, R., Humphrey, V., Gerken, T., Feng, S., Digangi, J. P. and Frankenberg, C. (2020). Cropland carbon uptake delayed and reduced by 2019 Midwest floods. *AGU Advances*, **1**, e2019AV000140. doi:10.1029/2019AV000140

Yoshida, Y., Ota, Y., Eguchi, N., Kikuchi, N., Nobuta, K., Tran, H., Morino, I., and Yokota, T. (2011). Retrieval algorithm for $CO_2$ and $CH_4$ column abundances from short-wavelength infrared spectral observations by the Greenhouse Gases Observing Satellite, *Atmospheric Measurment Technology*, **4**, 717–734. doi:10.5194/amt-4-717-2011

Yuan, W., Zheng, Y., Ciais, P., Lombardozzi, D., Wang, Y., Ryu, Y., Chen, G., Dong, W., Hu, Z., Jian, A. K., Jiang, C., Kato, E., Li, S., Lienert, S., Liu, S., Nabel, J. E. M. S., Qin, Z., Quine, T., Sitch, S., Smith, W. K., Wang, F., Wu, C., Xiao, Z, and Yang, S. (2019). Increased atmospheric vapor pressure deficit reduces global vegetation growth, *Science Advances*, **5**, eaax1396. doi: 10.1126/sciadv.aax1396

Zavarsky, A. and Marandino, C. A. (2019). The influence of transformed Reynolds number suppression on gas transfer parameterizations and global DMS and $CO_2$ fluxes. *Atmospheric Chemistry and Physics*, **19**, 1819-1834. doi:10.5194/acp-19-1819-2019

Zeebe, R. and Wolf-Gladrow, D. (2001). $CO_2$ in seawater: Equilibrium, kinetics, isotopes. *Elsevier Oceanogr. Ser.*, **65**, Elsevier, Amsterdam.

Zeng, N., Zhao, F., Collatz, G. J., Kalnay, E., Salawitch, R., West, T. O. and Guanter, L. (2014). Agricultural Green Revolution as a driver of increasing atmospheric $CO_2$ seasonal amplitude. *Nature,* **515**, 394–397. doi: 10.1038/nature13893

Zhang, Q., Li, M., Wang, M., Mizzi, A.P., Huang, Y., Wei, C., Jin, J., Gu, Q. (2021). $CO_2$ Flux over the Contiguous United States in 2016 Inverted by WRF-Chem/DART from OCO-2 $XCO_2$ Retrievals. *Remote Sens*., **13**, 2996. doi: 10.3390/rs13152996

Zhao, M., and Running, S. W. (2010). Drought-Induced Reduction in Global Terrestrial Net Primary Production from 2000 Through 2009. Science, 329, 940-943. doi: 10.1126/science.1192666

4263 Zhu, Z., Bi, J., Pan, Y., Ganguly, S., Anav, A., Xu, L., Samanta, A., Piao, S., Nemani, R. R., and
4264 Myneni, R. B. (2013). Global data sets of vegetation leaf area index (LAI)3g and fraction of
4265 Photosynthetically active radiation (FPAR)3g derived from global inventory modeling and
4266 mapping studies (GIMMS) normalized difference vegetation index (NDVI3g) for the period
4267 1981 to 2011. *Remote Sensing*, **5**, 927‑948. doi: 10.3390/rs5020927
4268 Zhu, Z., Piao, S., Myneni, R. B., Huang, M., Zeng, Z., Canadell, J. G., Ciais, P., Sitch, S.,
4269 Friedlingstein, P., Arneth, A., Cao, C., Cheng, L., Kato, E., Koven, C., Li, Y., Sian, X., Liu,
4270 Y., Liu, R., Mao, J., Pan, Y., Peng, S., Peñuelas, J., Poulter, B., Pugh, T. A. M., Stocker, B.
4271 D., Vlovy, N., Wang, X., Wang, Y., Xiao, Z., Yang, H., Zaehle, S., and Zeng, N. (2016).
4272 Greening of the Earth and its drivers. *Nature Climate Change*, **6**, 791–795. doi:
4273 10.1038/NCLIMATE3004
4274 Zhu, Z., Piao, S., Xu, Y., Bastos, A., Ciais, P., Peng, S. (2017). The effects of teleconnections on
4275 carbon fluxes of global terrestrial ecosystems. *Geophysical Research Letters*, **44**, 3209-
4276 3218. doi: 10.1002/2016GL071743
4277 Zickfeld, K., MacDougall, A. H., and Matthews, H. D. (2016). On the proportionality between
4278 global temperature change and cumulative $CO_2$ emissions during periods of net negative
4279 $CO_2$ emissions. *Environmental Research Letters*, **11**, 055006, doi:10.1088/1748-
4280 9326/11/5/055006
4281 Zscheischler, J., Michalak, A. M., Schwalm, C., Mahecha, M. D., Huntzinger, D. N., Reichstein,
4282 M., Berthier, G., Ciais, P., Cook, R. B. El-Masri, B., Huang, M., Ito, A., Jain, A., King, A.,
4283 Lei, H., Lu, C., Mao, J., Peng, S., Poulter, B., Ricciuto, D., Shi, X., Tao, B., Tian, H., Viovy,
4284 N., Wang, W., Wei, X., Yang, J., and Zeng, N. (2014). Impact of large-scale climate
4285 extremes on biospheric carbon fluxes: An inter-comparison based on MsTMIP data, *Global*
4286 *Biogeochem. Cycles*, **28**, 585–600, doi: 10.1002/2014GB004826